Tomas Bata University in Zlín
Centre of Polymer Systems

Thesis for state doctoral exam

Stimuli-responsive scaffolds

Stimuli-responsivní scaffoldy

Author: **Ing. Martina Martínková**

Degree programme: P3924 Material Sciences and Engineering

Degree course: 3911V040 Biomaterials and Biocomposites

Supervisor: prof. Ing. Petr Humpolíček, Ph.D.

Consultant: doc. Zdenka Víchová, Ph.D.

Zlín, November 2023

ACKNOWLEDGEMENT

First, I would like to express my deepest gratitude to my supervisor, prof. Ing. Petr Humpolíček, Ph.D. His exceptional leadership, investment of time, and unwavering patience have been instrumental in my academic journey. Under his mentorship, I have not only gained invaluable knowledge but also developed essential skills and qualities.

Additionally, I am sincerely thankful to my consultant, doc. Zdenka Víchová, Ph.D., for her invaluable guidance and support throughout my studies. Her expertise and insights have significantly contributed to my academic growth and development.

Moreover, I must also express my gratitude to Mgr. Jan Vícha, Ph.D. for sharing his immense knowledge with me. I would also like to express my sincere appreciation to doc. Ing. Věra Kašpárková, CSc., who enriched my academic experience. Also, I am thankful to Ing. Lukáš Münster, Ph.D. for willingness to share his knowledge and for help in the laboratories.

Lastly, I want to extend my thanks to all of my colleagues from Centre of Polymer Systems. Their support, collaboration, and shared experiences have created an enriching environment that has nurtured my academic pursuits. I am truly grateful for their presence and the sense of camaraderie we have fostered together.

I am extremely grateful for the immense support I received from my family, husband and close friends throughout my academic journey. Their unwavering presence and encouragement played a pivotal role in my success, and I cannot thank them enough. Their presence was a constant reminder that I was never alone on this educational path, and their belief in my abilities pushed me to reach new heights.

Finally, I would like to acknowledge the the Centre of Polymer Systems for financial support throughout my studies. The submitted disertation received support through the following projects: IGA/CPS/2019/004, IGA/CPS/2020/001, IGA/CPS/2021/001, IGA/CPS/2022/001 and IGA/CPS/2023/001. Financial support was also provided by the Czech Science Foundation through grants 19-16861S and 20-28732S. The financial support granted to my research work by the funding is also addressed and acknowledged in the published or submitted papers.

ABSTRACT

Tissue engineering (TE) is a multidisciplinary field that aims to preserve, restore, or enhance the physical and physiological properties of living tissues through combination of scaffolds and cells, engineering techniques, materials, and biochemical factors. Scaffolds for TE can be created from a variety of biomaterials, each with different properties suitable for specific applications. The biomaterial has to be selected with respect to the length of contact and the site of use in the biological system. Since several tissues in the body exhibit electrical activity, including brain tissues, cardiac muscle tissue, and skeletal muscles, a stimuli-responsive material is appropriate for TE of such tissues. Conducting polymers (CP) can be used to introduce stimuli-responsivity thanks to their electrical activity into a biomaterial. CP can be incorporated into composites or used to modify the surfaces of scaffolds made from other biomaterials, thereby providing specific bioactive properties. Especially combinations of CPs with natural polymers can be beneficial because they combine the electroactivity of CPs with the biocompatibility of biopolymers. In this work, different types of scaffolds suitable for modification with conducting polymers were prepared. Conducting polymers, specifically polyaniline and polypyrrole, were used to create conductive stimuli-responsive composites.

Key words: *Tissue Engineering, Cytocompatibility, Biomaterials, Conductive Polymers*

ABSTRAKT

Tkáňové inženýrství je multidisciplinární obor, jehož cílem je zachovat, obnovit nebo zlepšit fyzikální a fyziologické vlastnosti živých tkání pomocí kombinace scaffoldů a buněk, inženýrských technik, materiálů a biochemických faktorů. Scaffoldy pro tkáňové inženýrství lze vytvořit z různých biomateriálů, z nichž každý má jiné vlastnosti vhodné pro konkrétní aplikace. Biomateriál se vybírá s ohledem na délku kontaktu a místo použití v biologickém systému. Vzhledem k tomu, že několik tkání v těle vykazuje elektrickou aktivitu, včetně mozkové tkáně, srdeční svaloviny a kosterních svalů, je pro tkáňové inženýrství těchto tkání vhodný vodivě stimuli-responsivní materiál. K zavedení stimuli-responsivity (elektrické vodivosti) do biomateriálu lze použít například vodivé polymery. Ty mohou být začleněny do kompozitů nebo použity k modifikaci povrchu scaffoldů vyrobených z jiných biomateriálů, čímž získají specifické bioaktivní vlastnosti. Výhodné mohou být zejména kombinace vodivých polymerů s přírodními polymery, které kombinují elektroaktivitu vodivého polymeru s biokompatibilitou biopolymerů. V rámci této práci byly připraveny různé typy scaffoldů, vhodné pro modifikaci vodivými polymery. Pro vytvoření vodivých stimuli-responsivních kompozitů byly použity vodivé polmery, konkrétně polyanilin a polypyrrol.

Klíčová slova: *tkáňové inženýrství, cytokompatibilita, biomateriály, vodivé polymery*

TABLE OF CONTENT

1. INTRODUCTION

Tissue engineering (TE) has been explored in the last three decades. TE evolved from biomaterials development and its essence is the combination of biomaterials (e.g. in form of scaffolds), cells, biologically active molecules and physical signals into functional tissue-like structures. The main challenge is to modify the biomaterials used for this purpose so that their composition and/or structure mimic the native and physiological conditions for specific tissue cells. Advances in the knowledge and availability of stem cells, the emergence of new biomaterials as potential templates for tissue growth, improvements in bioreactor design, and a better understanding of healing processes are all contributing to the increasingly rapid development of this field.

This work deals with development of scaffolds, artificial implant structures, that support and control the growth of cells of the desired tissue. Supporting tissue growth is possible by selecting a suitable scaffold material, therefore the material is selected with respect to the site of application in the host tissue. For example, when designing scaffolds for hard TE (bone, cartilage and teeth), it is necessary to select a material that will have similar properties. Therefore, for bone TE, ceramics or polymeric materials such as polyetheretherketone (PEEK) can be considered. In the case of soft tissue, materials such as cellulose nanofibres can be used.

Various techniques can be used to obtain scaffolds with unique physical, chemical, mechanical, and biological properties. One of the possibilities of a simple and reproducible technological solution for scaffold preparation could be a manually hot-pressed technique. Another option for scaffold preparation is Powder Injection Molding technology (PIM). This technology could be beneficial in personalized medicine because it allows production with high precision. It is possible to obtain implants in various shapes with a defined pore size and overall porosity. All of these factors can affect implant acceptance. Another added value that will affect the instructive properties of cells is, for example, the electrical conductivity of biomaterials. This property is particularly important for electroactive tissues, because the electric field plays an important role in many biological processes. For this purpose, it is advisable to choose materials with combined electrical conductivity, appropriate candidates are conductive polymers.

Because most biological reactions take place at the interface between the biological system and the implant surface, the biointerface is a critical place. This is the reason why the surface properties of biomaterial are one of the main factors that affect its applicability *in vivo*. The chemical and physical characteristics of the biomaterial surface can affect many of cellular functions.

To reach the desired cell reaction, the surfaces could be functionalized. These are one of the main factors for the applicability of scaffolds in a real system.

2. TISSUE ENGINEERING

Tissue engineering (TE) is a multidisciplinary field that combines the targeted use of cells and biomaterials to maintain, restore or improve the function of living tissue (Langer and Vacanti, 1993). The term "tissue engineering" was defined by National Science Foundation in 1987. Nevertheless, TE approaches have been used since the seventies of the twentieth century (Ratner, 2013).

In particular, TE uses a combination of four key elements. 1) A suitable cell line, 2) the right environment such as a scaffold, 3) biomolecules (for example signalling molecules, growth factors, proteins) that keep cells productive, and finally, 4) external stimuli such as mechanical and electrical that affect cell behaviour. Figure 1 shows four key elements of TE.

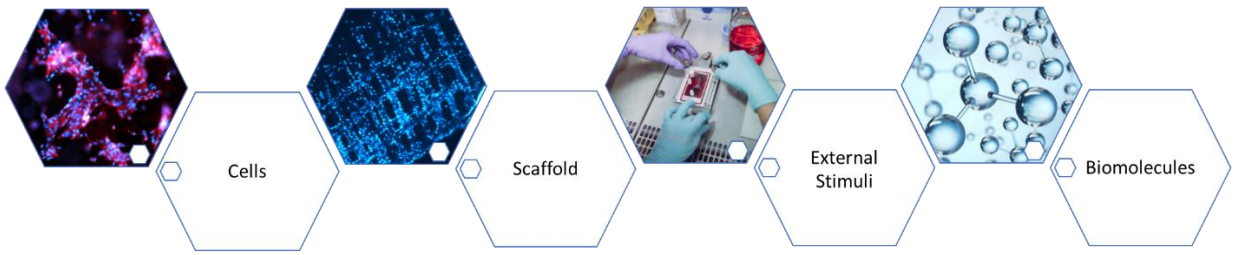

Fig. 1 Tissue engineering key elements

2.1 Scaffolds

TE relies on scaffolds as important components. The essential function of the scaffold is to provide support for the tissue structure, organ structure and to regulate primary cellular functions (cellular proliferation, growth). It is appropriate that the scaffold should mimic as closely as possible the environment of the tissue it will replace, thus the structure, architecture, and composition of the extracellular matrix (ECM).

The ECM is a three-dimensional architectural complex of proteins and polysaccharides that cooperate with each other (see Fig. 2) (Blitterswijk and Thomsen, 2008). This complex network consists of high molecular weight fibrous proteins such as collagen, laminin and fibronectin. Like proteins, the polysaccharide component is secreted and organized by the cells. Its exact composition varies from tissue to tissue. The molecules that make up the ECM, especially proteins, provide the mechanical strength needed for proper tissue function and serve as intermediary of exchanging information between cells and between cells and the ECM itself (Lee et al., 2016). The purpose of ECM is

to provide structural support to cells, but it can also serve as a physical barrier or as a selective filter for some soluble molecules. ECM acts as a structure for tissue and organ support, but also regulates many aspects of cell-instructive properties, including cell proliferation and growth, cell survival and change in cell shape, migration, and differentiation (Daley et al., 2008).

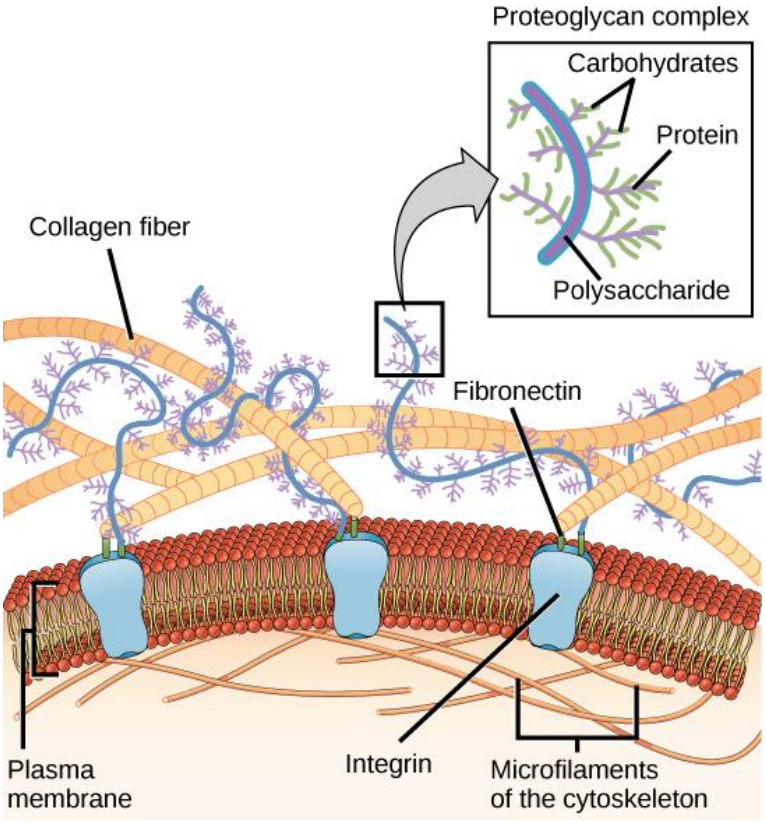

Fig. 2 Scheme of the extracellular matrix components and their connection to cytoskeleton (Bartee, 2018).

Scaffolds can be of natural origin or artificially made. By means of natural origin scaffold, the donor organ is used. The first great advances were made in the discovery of decellularization of organs. The materials from donor (as well as animal sources) have been used to make tissue replacements. Decellularized tissues and organs can be obtained by removing cells and immunogenic components from a tissue or organ. This preserves the composition of the extracellular matrix, which presents as a natural scaffold (Guruswamy Damodaran and Vermette, 2018). The most common use was in cardiovascular surgery of porcine heart valves. Other organs that are also often used to create and study decellularized replacements are, for example, the liver, lungs, pancreas, kidneys (Yu et al., 2016). However, all materials of animal origin must be specially chemically treated and further processed before they can be used (Berthiaume and Yarmush, 2003). One of the biggest limitations of decellularized scaffolds is the induction of an inflammatory response. Although scaffolds are decellularized and deprived of cellular components, cellular protein residues and

nuclear and mitochondrial DNA fragments may remain in the replacement (Bilodeau et al., 2020). There is also the problem of organ size and ethics. For this reason, artificial materials that could be used to make replacements, are being developed.

3. BIOMATERIALS

Materials used in contact with biological systems are referred as biomaterials. There are many definitions of the term biomaterial. One of the possible definitions is from the European Society for Biomaterials Consensus Conference II, where the term was defined as follows: "A biomaterial is a material intended to interface with biological systems to evaluate, treat, augment or replace any tissue, organ or function of the body" (Leali and Merolli, 2009). Since then, the term has been re-defined many times, but the definitions have always met in one point: biomaterial is a material that interacts with the human body.

3.1 Biological properties of biomaterials

The material in contact with the organism (directly or indirectly) can affected cellular functions. In order for a biomaterial to be used, it must meet a number of criteria. The most important is biocompatibility. The first commonly used definition of term biocompatibility comes from David F. Williams in 1987 "the ability of a material to perform with an appropriate host response in a specific situation" (Williams, D. F. and European Society for Biomaterials, 1987). Overall the material must elicit an appropriate biological response for the application in the body (O'Brien, 2011). Thus the material must be non-cytotoxic, non-carcinogenic and cannot cause immunological rejection, must not cause an inflammatory reaction and should contribute to a harmonious biological function. (Gad and Gad-McDonald, 2015).

Biocompatibility can be determined by several types of testing. The choice of testing depends on the endpoint of the biomaterial usage, the nature of body contact and the contact duration. The 2018 ISO 10993-1 standard on Biological evaluation of medical devices describes endpoints to be addressed in a biological risk assessment. The medical devices can be classified in terms of their location to: devices on the surface of the device, the external communication device and the implant. Surface devices can be distinguished in terms of contact with intact skin, mucosal membrane and breached or compromised surface. External communication devices are assessed according to whether they are in indirect contact with the blood path, the bloodstream or with tissue, bone, dentin. Implants are classified according to their contact with blood or tissue (bone). Depending on the duration of the contact, a distinction can be made between devices with a limited duration of up to 24 hours, a prolonged duration of more than 24 hours but less than 30 days, and a permanent duration of more than 30 days.

The diversity of medical devices implies that it is not necessary to test every material on all endpoints listed in the c biological risk assessment in the corresponding ISO standard. However, one of the tests compulsory for all bioapplications and conditions, is the determination of cytotoxicity (ISO 10993-1). More about cytotoxicity testing will be discussed in the chapter Biological testing.

The material must also possess suitable mechanical properties with regard to the application. In particular, these properties are important for orthopaedic applications. However, good vascularization is also essential for the production of bone and cartilage scaffolds. Therefore, attention must also be paid to porosity, pore distribution, exposed area and overall scaffold architecture (Carletti et al., 2011).

3.2 Material properties of biomaterials

Material properties are most often divided into two categories: surface properties and bulk properties.

3.2.1 Surface properties

Most biological reactions take place at the interface between the biological system and the surface of the biomaterial (biointerface) (Castner and Ratner, 2002). The surface properties of biomaterial are one of the main factors that affect its applicability in a real system. In TE, the chemical and physical characteristics of the biomaterial surface can affect cellular functions, such as proliferation, or migration, phenotype, differentiation and so on (Parisi et al., 2020).

The cellular response is manifested primarily in cell morphology, adhesion, migration, proliferation and differentiation. The determining factor in the level of cell adhesion to the surface is topography, surface chemistry (for example functional groups) and surface energy. The surface energy of the biomaterial affects the cell adhesion. This is related to the polar and dispersive components of surface free energy. It is believed that in order for the cells to adhere to the surface successfully, the total surface energy of the material is crucial. In fact, surface energy is closely related to surface wettability. A certain balance between hydrophobicity and hydrophilicity is desirable. Neither hydrophobic nor hydrophilic surface is suitable for biological applications. Nevertheless, protein absorption is easier on the hydrophobic surface (Ferrari et al., 2019; Wang et al., 2004). For measurement of surface wettability is commonly used an optical tensiometer and a contact angle is measured with the sessile drop method (see Fig. 3).

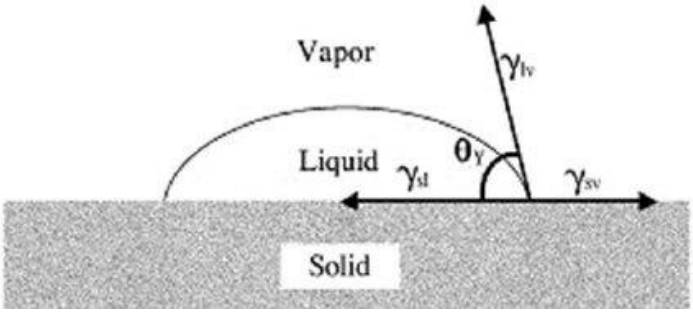

Fig. 3 Static contact angle measurement, method of the sessile drop (Lotfi et al., 2013)

The first reaction after contact of the biomaterial with the host system (body fluid) is the adhesion of proteins to the surface, which affects cell adhesion. Protein adsorption is faster than cell migration to a foreign surface, so the initial adsorbed protein layer is thought to be a critical factor in cell adhesion rate. Protein adsorption is affected by several aspects, for example physical and chemical properties of the material surface (Murphy et al., 2016). It is a complex process mainly influenced by various protein-surface physicochemical/intermolecular interactions such as Van der Waals, hydrophobic and electrostatic forces. The adsorption characteristics of a protein (e.g. the amount of protein adsorbed, the type of protein) are also influenced by the surface properties, such as its topography, roughness, surface energy and charge (Ma, 2014). The molecules within a mixture of proteins exhibit varying rates of diffusion towards a surface. Initially, the proteins with higher mobility, the smaller proteins (shown in green in the diagram in Fig. 4) with lower molecular weight and higher concentration tend to adsorb onto the surface first. However, these proteins may subsequently be displaced by larger proteins with a higher molecular weight (Hirsh et al., 2013). Vroman and Adams observed competitive protein exchange on surfaces, wherein proteins that had already adsorbed onto a surface from a protein mixture solution were displaced by subsequently arriving proteins (Vroman and Adams, 1969a; Vroman and Adams, 1969b).

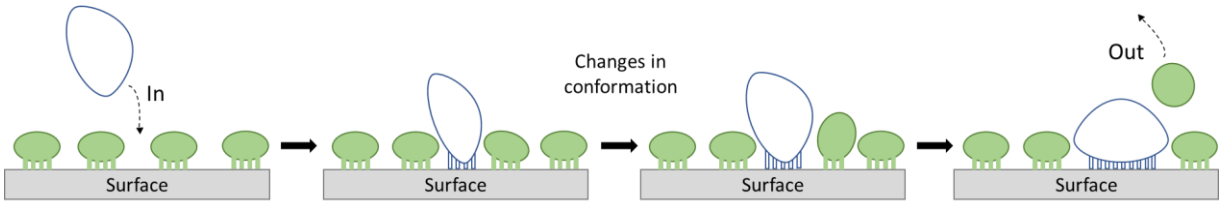

Fig. 4 Schematic representation of the competitive adsorption of proteins known as the Vroman effect

Irrespective of whether proteins are adsorbed on the surface of the biomaterial, cells can perceive and respond to the nanostructured surface, which in some cases may play a much more essential role than the surface chemistry itself (Webster et al., 2000). Thus the surface topography play a significant role on cell adhesion

and behaviour. The surface topography of biomaterials is a critical factor, especially in the field of hard TE, as it significantly impacts osseointegration. A well-designed topography has the potential to enhance the differentiation of cells adhering to the surface and promote the formation of a bone matrix (Dalby et al., 2007; Nagasawa et al., 2016). The surface topography is determined by roughness parameters describing amplitude of topography (such as feature size (Kearns et al., 2011), more rarely frequency parameters. The size of biological elements interacting with surfaces is another crucial parameter to consider. When comparing the reactions to the same surface topography, it is important to note that large cells, such as human primary bone cells (approximately 50 μm), will exhibit different responses compared to smaller cells like monocytes (approximately 10 μm) (Anselme et al., 2010). Another factor thaht has influence on cell attachment is organization of topography (Bettinger et al., 2009).

3.2.2 Bulk properties

In all cases the mechanical properties of a biomaterial must be as similar as possible to the characteristics of the tissue they will replace. Mechanical properties often analysed for most materials are its modulus of elasticity (Young modulus), tensile yield stress, fatigue strength, and toughness. Another property important for biomaterials is wear resistance, especially when abrasive fragments could trigger a cytotoxic response, even if the biomaterial in bulk form is biocompatible (Case et al., 1994). All these properties are assessed with respect to the mass density of the materials.

Body fluids contain a lot of dissolved oxygen and other oxidants causing unwanted material oxidation. The corrosive behaviour of some metals is undesirable due to the formation of toxic cations. Of course, this does not apply to noble metals such as gold, titanium, surgical steel, which is widely used in dental applications (Vrana et al., 2020).

Many of the materials used for bioapplications are non-porous. This can be justified by compliance with the required conditions for mechanical properties and as corrosion protection. It is caused by the fact, that the corrosion rate is faster near defects and accessible pores of a structure (Vrana et al., 2020). Also, the mechanical properties of porous scaffolds depend on the pore diameter and the overall porosity. When larger pores and overall pore interconnection correlate with lower mechanical strength due to higher void volume. Nevertheless, porosity, pore sizes, and pore shapes are important for some applications such as bone tissue reconstruction. The pore structure is one of the key factors in the development of scaffolds. Scaffolds should have an interconnected pore structure, i.e. open pores, and an overall high porosity to ensure cell penetration and a sufficiently large diffusion of nutrients into the cells within the scaffold. It is very important that the structure of the construction

material also allows the diffusion of waste and degradation substances from the scaffold, which are able to leave the body without interfering with the surrounding tissues and other organs (Murphy et al., 2010; O'Brien, 2011). Examples of different pore sizes, shapes, and biomaterials for scaffolds can be seen in Fig. 5.

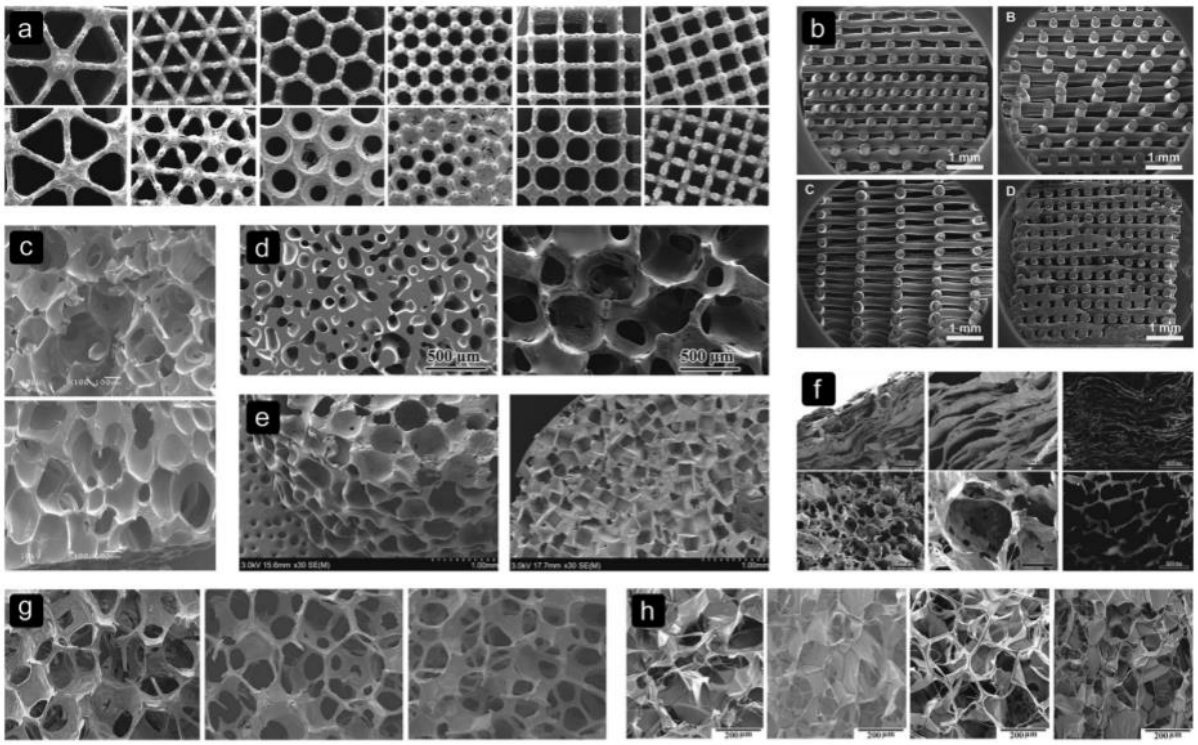

Fig. 5 Examples of different pore sizes, shapes, and biomaterials for scaffolds for tissue engineering. (a) Titanium (Ti6Al4V), (b) Starch poly(ε-caprolactone) (SPCL), (c) poly(lactide-coglycolide) (PLGA), (d) Bioactive glass (BG), (e) poly(propylene fumarate) (PPF), (f) collagen-apatite, (g) Mesoporous bioactive glass (MBG), and (h) Silk fibroin (SF) (Bobbert and Zadpoor, 2017).

The cellular behaviour is also determined by isotropy and anisotropy of materials. Material isotropy or anisotropy refers not only to the surface but also to the volume, since this disertation focuses on scaffolds, isotropy is included in the bulk properties. An isotropic structure is characterized by exhibiting the same properties or structure regardless of the viewing direction. On the other hand, anisotropy means dependence on directions (Tonndorf et al., 2021). Physiological and mechanical properties of most tissues possess a certain degree of anisotropy. Tissue anisotropy, in terms of bulk mechanical properties, can vary widely, ranging from high isotropy in tissues like the liver (Chen et al., 2019) to a high degree of anisotropy in tissues such as ligaments and tendons (Reid et al., 2021). Anisotropic material can have an effect on cell morphology and physiology (see Fig. 6) (Cabezas et al., 2019). The significance of anisotropy stems from the aforementioned understanding that cells can perceive anisotropy as cues influencing their behaviour.

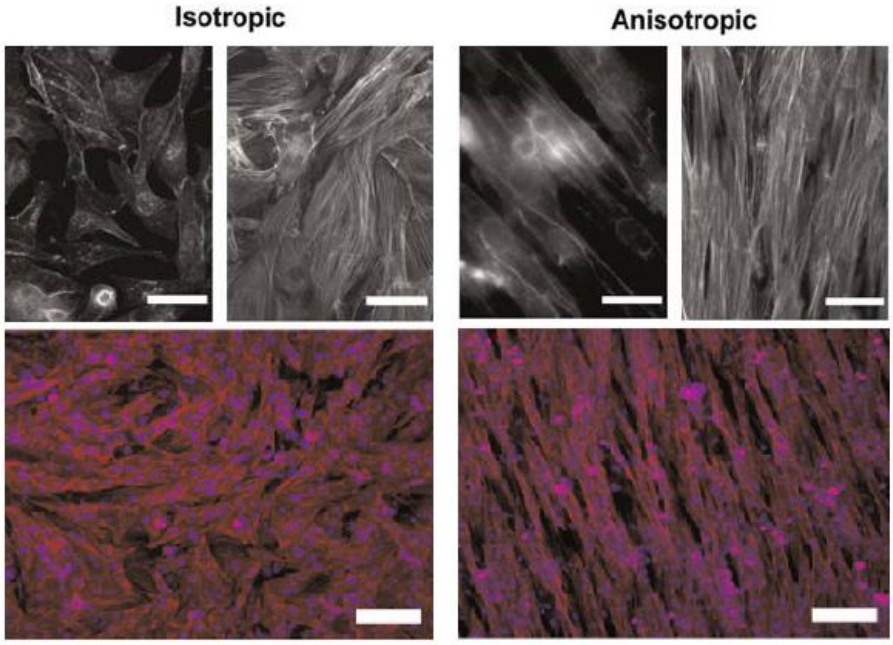

Fig. 6 Isotropic and anisotropic tissue scale bar = 100 μm edited from (Pong et al., 2011)

4. STIMULI-RESPONSIVE BIOMATERIALS

A special group of biomaterials, that can change their properties with the change of external stimuli (such light, pH, temperature, magnetic fields, or electricity), are the so-called stimuli-responsive biomaterials. External signals, that have the most impact, are electrical stimulation, photostimulation, ultrasound activation, and magnetic field stimulation (Gelmi and Schutt, 2021). Other options are temperature and pH-sensitive biomaterials. A specific example of a thermo-responsive polymer is poly(N-isopropyl acrylamide) (PNIPAAm). With increasing temperature the conformation changes and the surface of the material changes its hydrophilic/ hydrophobic properties (Nagase et al., 2018). This property can be exploited in a number of biomedical applications, such as drug delivery systems, "smart" cell culture setups, sensors, and separation technologies (Yang et al., 2020). For the drug delivery system pH-sensitive biomaterials can also be used. A system of targeted drug release based on pH change is a particular advantage because many diseased tissues are surrounded by an acidic microenvironment (Zhuo et al., 2020).

The next two chapters will be focused mainly on the application of electrical stimulation and piezoelectric stimulation, especially because bioelectricity and piezoelectricity are of great importance in the human body as well as in practical part of this disertation.

4.1 Electrical Stimulation

The meaning of an electric field in TE is mainly because of many excitable

tissues/organs, such as the brain, heart, and skeletal muscle. Every human sense uses ionic currents and electric fields in its transduction mechanism. Hearing, sight, touch, taste, and smell all of these senses have receptor systems enabling generate electrical signals to the brain (Pullar, 2011). The electrical phenomena that occur in living organism is called bioelectricity. Bioelectricity arises from the transmission of electrical signals *via* ion channels (ionic conductivity) and pumps located on or within the plasma membrane. The plasma membrane possesses the capacity to generate and sustain distinct charges on its opposing sides. This capability stems from disparities in ion concentrations between the cytosol and the external environment of the cell (Grimnes and Martinsen, 2015; Otero et al., 2012).

The heart is a prime example of where electrical stimuli plays a vital role. In order for the heart to contract regularly, it requires electrical signals. These signals originate from the sinoatrial node and occur at a frequency of about 60 – 100 times per minute. During diastolic depolarization, the action membrane potential starts approximately at –65 mV (Solazzo et al., 2019). In contrast, the maximum diastolic potential in pacemaking Purkinje cells is considerably more negative (approximately –85 mV) (Weiss, 1997). During the nodal action potential, the pacemaking Purkinje cells gradually depolarize spontaneously until they reach a threshold potential of –45 mV (Solazzo et al., 2019).

A lot of studies revealed the presence of electrical fields influence a variety of biological processes such as migration, proliferation, differentiation, orientation (Fig. 7), cytoskeletal organization, apoptosis and necrosis (Thrivikraman et al., 2018). It plays role in angiogenesis, mitosis, cell signalling (Murphy et al., 2010), formation of embryonic bodies or in the process of wound regeneration in injured tissues (McCaig et al., 2002). The reason is, that external electrical stimulation can help with modulation of cellular responses and this could lead to enhance tissue regeneration (Lee, 2013). Electric field can influence for example nerve regeneration (Zhu et al., 2019) reorganization of actin filaments or cell motility (Kumar et al., 2016).

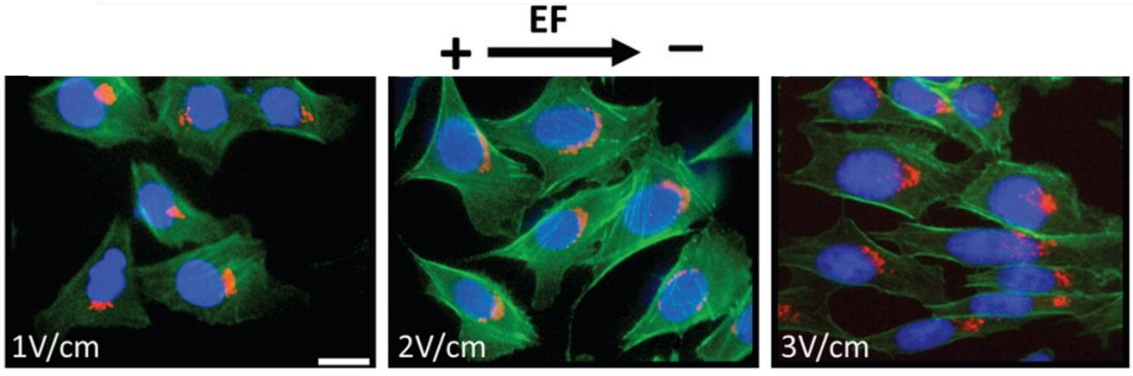

Fig. 7 Orientation of cells due to electric field, edited from (Pu et al., 2015)

Electrical conductivity refers to the ability of a material to carry electric current when subjected to an electric field. In solid conductors like metals and semiconductors, the movement of charge, is primarily attributed to the motion of electrons or electron-hole pairs. This form of conductivity is called electronic conductivity. In contrast, ionic conductivity arises in materials that contain mobile ions, such as certain liquids, molten salts, or solid-state electrolytes. In these cases, the electric current is carried by the motion of ions rather than electrons. When an electric field is present, the ions migrate through the material, facilitating the flow of charge. It's important to note that some materials exhibit a combination of both electronic and ionic conductivity (Miyamoto and Shibayama, 1973; Owen, 1989).

The majority of organic conjugated polymers lack inherent charge carriers. Consequently, in order to achieve conductivity in these polymers, external charge carriers must be introduced (Yi and Abidian, 2016). When it comes to ionic conductivity, various carriers can be involved, but the mobility of ions is generally much lower compared to the mobility of electrons typically observed in electronic conductivity (Miyamoto and Shibayama, 1973; Owen, 1989).

The electrical signal can be transferred *via* conductive biomaterials through two possible routes. The first is a series connection of conductive biomaterial and an electrical circuit. It follows the fact, that the electrical signal is transmitted by the biomaterial. This induces a local electrical field and its charge is not transferred from the biomaterial to the environing electrolyte. In the second case, the conductive biomaterial is used only as an electrode, which allows the transfer of charge by the surrounding electrolyte from the opposite electrode (Gelmi and Schutt, 2021).

Whole mechanisms of electrical stimulation of cell are uncertain. However, it is believed that the external electric field is able to change the distribution of the membrane receptors and intracellular levels of cell regulators. In addition, stimulation by electric field can lead to reducing the cell membrane potential and facilitate membrane depolarization to electrically excitable cells (such as neurons, cardiomyocytes, ...) (Lee, 2013).

4.2 Piezoelectric mediated electrical stimulation

Other smart materials for potential use in bioapplications is group of piezoelectric materials. These materials have ability to generate an electrical output as a response to applied mechanical stress (direct piezoelectric effect) (Mayeen and Kalarikkal, 2018). Piezoelectric crystals are for example Quartz, Berlinite, Topaz, Tourmaline or Cane sugar. Nevertheless, piezoelectric properties occur also in the human body. For instance, bone tissues show piezoelectricity. Human bones are directly affected by mechanical excitation (Singh et al., 2014). Another

naturally occurring materials are tendon, enamel, and dentin (Liboff and Shamos, 1971; Marino and Gross, 1989). Biocompatible piezoelectric materials include some synthetic polymers (such as poly(vinylidene fluoride) – PVDF, and poly-3-hydroxybutyrate-3-hydroxy valerate – PHBV), natural polymers (such as collagen, chitin and cellulose) and ceramics (barium titanate, zinc oxide) (Gelmi and Schutt, 2021).

5. TYPES OF BIOMATERIALS

Biomaterials are usually divided into three basic categories: metals, ceramics and polymers. Each of these groups is suitable for different applications and has its advantages and disadvantages. The work is mainly focused on polymeric materials. Therefore, in the following chapters the metal and ceramic group are briefly described and the polymer group is presented with its representatives.

5.1 Metals

Metals are inorganic materials bound by non-directional metallic bonds with highly mobile electrons, these electrons are not bound to particular atoms (Nouri and Wen, 2015). They are crystalline materials that are capable of forming many variations of crystal structures (Temenoff and Mikos, 2008). The main disadvantage of metal scaffolds is the lack of cells' biological recognition of the surface. Another limitation of metallic biomaterials is the possible release of toxic ions or particles due to corrosion or wear. These particles can lead to inflammation and allergic reactions. Overcoming these barriers is accomplished by surface modifications or surface coating. Proper surface treatment of parts made from selected metal compositions could increase biocompatibility and to a certain degree protect metallic biomaterial against wear and corrosion (Alvarez and Nakajima, 2009).

The properties of metallic materials arise from their structure, which is why metals are electrically and thermally conductive due to their free electrons. In terms of mechanical properties, it is important to note that metals are relatively strong but can be shaped. Metallic biomaterials used in TE can be either pure metals or alloys. Metals can be ductile (aluminium) or brittle (cast iron) and their properties are based on chemical composition (Santos, 2017). They can also achieve high strength and toughness with excellent corrosion resistance – Titanium alloys (de Viteri and Fuentes, 2013), high wear resistance – Cobalt-chromium alloys (Liu et al., 2015), stainless steels (Niinomi, 2002).

The most widely used applications of metals are in the field of cardiovascular as stent and artificial valves, then orthopaedic – bone fixation and artificial joints, dentistry – orthodontic wire and fillings, craniofacial – plate and screw, and otorhinolaryngology – artificial eardrum (Hermawan et al., 2011).

5.2 Ceramic

In general, ceramics are divided into groups based on the different reactions of ceramic materials to the biological environment (Ben-Nissan et al., 2019). The first group is bioinert ceramics and it is characterized mainly by the fact that the materials do not show any interaction with the surrounding tissue after implantation. This group includes for example alumina and zirconia. They have good biocompatibility, corrosion and wear resistance, mechanical strength and they are relatively biologically inactive (Boniecki et al., 2020; Huang and Best, 2014). Materials in this category are used for example as structural-support implants, such as bone devices and femoral heads (Pina et al., 2018).

Another group consists of bioactive ceramics, this category involves glass-ceramics and calcium phosphate ceramics (e.g. tricalcium phosphate, hydroxyapatite, …). The materials in this group must elicit specific biological activity. They interact with surrounding living tissues after implantation and form a bond between hard and soft tissues (Rahaman et al., 2011). As materials in this group are brittle they are mainly used as fillers for small bone defects and dental cavities (Dahiya et al., 2019). Ceramics in this group can also be bioresorbable.

Overall, ceramic materials are characteristic for their strength and good biocompatibility. Due to their structural similarity to native bone, they are suitable for bone TE (O'Brien, 2011). Ceramics are also used in orthopaedics, load-bearing applications, dentistry, and spinal surgery (Vaiani et al., 2023). The properties of ceramics and its microstructure depend mainly on the technology of production. One way to prepare ceramics for biomedical applications is powder injection molding (PIM) technology. This manufacturing technology could be beneficial in personalized medicine because it allows production with high precision. It is possible to obtain implants in various shapes with a defined pore size and overall porosity. All of these factors can affect implant acceptance. More about PIM technology is in the practical part of disertation.

5.3 Polymers

In general, polymers provide scaffolds with considerable processing flexibility, good biocompatibility or even biodegradability. It is the most common group from which scaffolds can be made. Polymer properties that determine the applicability of a polymer as a biomaterial include molecular weight, polymer structure, crystallinity, thermal and electrical properties. Polymers are divided into two groups, natural polymers and synthetic polymers, and each of these groups has its own advantages and disadvantages for use. Often used natural polymers are chitosan (Sukpaita et al., 2021), collagen (Jiang et al., 2018), alginate (Venkatesan et al., 2015), hyaluronic acid (Mohammadi et al., 2018),

cellulose (Torgbo and Sukyai, 2020) etc. Synthetic polymers include polyetheretherketone (PEEK) (Mavrogenis et al., 2014), polyurethane (Cooke et al., 2020), polylactide (Gregor et al., 2017) and many others. The next few subsections will describe mainly the materials that were used in the experimental part of the disertation.

5.3.1 Natural polymers

Natural biomaterials include materials with the protein or polysaccharide origin. Thus, these are natural polymers that take advantage of better cytocompatibility than for example synthetic polymers. Natural biopolymers such as collagen, fibrinogen, or hyaluronan, can provide biochemical stimuli to promote cell adhesion or differentiation. The main disadvantage of natural biopolymers isolated from natural sources is their less defined composition and also their susceptibility to biological contamination (Milne et al., 2003). Because their composition can be variable and thus the reproducibility of products becomes problematic.

5.3.1.1 Alginate

Alginate is a linear natural polymer obtained mainly from brown seaweed (Phaeophyta) or from soil bacteria. It is a block copolymer consisting of α-L-guluronic acid (G) and β-D-mannuronic acid (M) (Berthiaume and Yarmush, 2003). Its formula can be seen in figure 8. Alginates are constituted of tree types of blocks. The first option is alternating sequence of M and G blocks and thus form the most flexible part of the chain. Then there are the blocks of the GG itself and third type are MM blocks with polymerization degree greater than or equal to twenty (DP ≥ 20) (Rinaudo, 2008). Alginate is able to make a reversible hydrogel by the reaction of metal cations with functional carboxyl groups. Crosslinking of the alginate takes place ionically using bivalent cations (such as Ca^{2+}, Mg^{2+}, Ba^{2+}) in an aqueous solution (Blitterswijk and Thomsen, 2008).

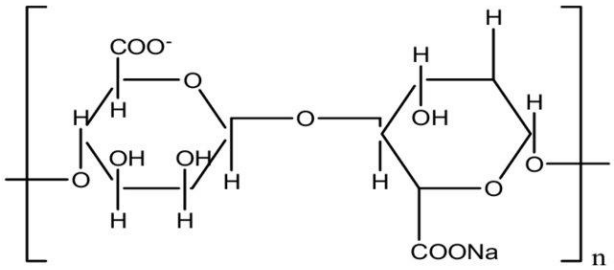

Fig. 8 Chemical structure of sodium alginate (Tamilisai et al., 2021)

Alginate is used for biomedical applications mainly due to its nontoxicity, good biocompatibility, biodegradability and easy gelation process (Sabu et al., 2018). Also, it facilitate wound healing (Davis and McLister, 2016). It is clear that it is

used for wound dressing (Varaprasad et al., 2020) and skin repairing. Alginate is one of the options for the production of soft tissue scaffolds (Yuan et al., 2017) and also for supporting connective tissue as cartilage (Klein et al., 2009). This polysaccharide is also used as a drug delivery system and as a cell encapsulation material (Hariyadi and Islam, 2020).

5.3.1.2 Cellulose

Cellulose is a linear homopolymer which consist of covalently bond units of D-anhydroglucopyranose established in chair conformation. The units are linked by β-1,4-glycosidic bonds and form cellobiose (see fig. 9). This biopolymer is found in plants and some other organism such as tunicates and bacteria (Sabu et al., 2018). Sources of cellulose from higher vascular plants include cotton, sisal, jute and the rigid cell walls of wood. Lower non-vascular plants containing cellulose are algae, lichen, and fungi (Sacui et al., 2014). Cellulose is possible to isolated in different forms such as cellulose nanocrystals (CNC) and cellulose nanofibrils (CNF) and both can be obtained by chemical and mechanical disintegration or enzymatic digestion methods (Sabu et al., 2018).

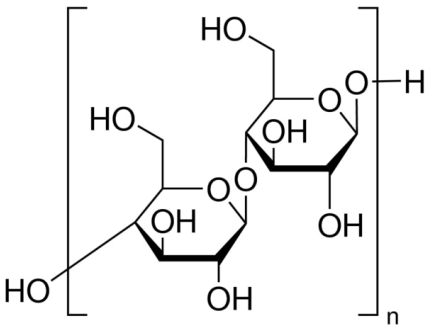

Fig. 9 Chemical structure of cellulose ("Cellulose C6288, Sigma-Aldrich,")

Cellulose is used for TE due to its tunable mechanical properties, high biocompatibility, ability to release drugs and retain moisture (Hickey and Pelling, 2019). In general, cellulose-based biomaterials are used for artificial skin (Vatankhah et al., 2014) and wound dressing (Liu et al., 2012; Rees et al., 2015). As already mentioned, cellulose has adjustable mechanical properties suitable even for rigid and mechanically demanding environments such as bones. It goes without saying that another use for cellulose is bone tissue (Zhang et al., 2015; Zhou et al., 2013). This natural polymer also finds use for neural applications (Yang et al., 2018) and blood vessels (Fink et al., 2011).

Derivates of cellulose

In order to achieve higher utilization of cellulose for bioapplications, various chemical treatments and functionalizations have been introduced and many cellulose derivatives are also used. The properties of the derivatives depend

on the degree of substitution and on the functionalization pattern (Seddiqi et al., 2021). Cellulose ethers, for example, are known to have a high-water retention and thermo-gelling ability. Their properties make them suitable for use in wound healing, e.g. carboxymethyl cellulose is used for wound dressing (Capanema et al., 2018). Other possible applications are in TE (Schütz et al., 2017) and drug delivery. Cellulose is insoluble in water and most solvents. However, cellulose esters are soluble in common solvents. They have the same biological uses as cellulose ethers (Mwesigwa and Basit, 2016; Schunck et al., 2005). The oxidation of cellulose by periodate salts leads to cellulose dialdehyde (DAC). Applications of DAC could be in TE (Li et al., 2009) and drug deliver carrier (Dash and Ragauskas, 2012).

5.3.1.3 Chitosan

Chitosan is a derivative of chitin, the second most common natural polysaccharide found mainly in crustacean shells, exoskeletons of insects and the cell wall of fungi. Chemically, chitin is formed by glucosamine molecules linked by a β (1→4) glycosidic bond (Shukla et al., 2013). It is thus a copolymer of D-glucosamine and N-acetyl-D-glucosamine units (Fig. 10). The solubility of chitosan is pH-dependent, but is also affected by several factors such as the degree of deacetylation and ion concentration.

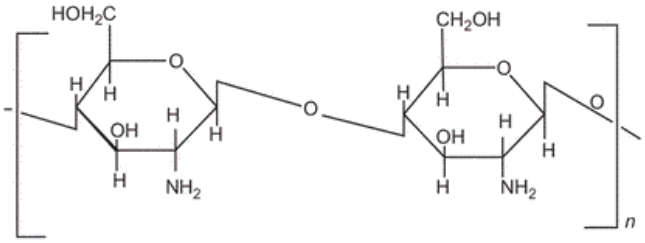

Fig. 10 Chemical structure of chitosan (Sabu et al., 2018)

Chitosan has been widely investigated for bioapplications due to its biodegradability (Vila et al., 2002), biocompatibility (Chellat et al., 2000) and wound healing properties (Adekogbe and Ghanem, 2005). Also, its structural similarity to glycosaminoglycans offers active sites for the binding of other molecules (e.g. growth factors) and increases cell adhesion, and induces beneficial responses within biological systems (Kumbar et al., 2014). Chitosan also has antibacterial and haemostatic properties. Moreover, chitosan positively affects formation of osteoblast. Therefore, chitosan is considered a suitable material for the regeneration of various tissues such as bone (Azaman et al., 2022; Moreira et al., 2019) or cartilage (Shen et al., 2021, 2015). Another possibility is its use in blood vessel (Chupa et al., 2000) and corneal regeneration (Rafat et al., 2008). Chitosan can be used in several form such as gels, films, membranes and fibers.

5.3.1.4 Hyaluronan

Hyaluronan (hyaluronic acid, HA) is a unique polysaccharide with great promise for TE. It occurs in epithelial, neural and connective tissues (Sabu et al., 2018). Hyaluronan belongs in to the family of glucosaminoglycans and it is present in ECM tissues and therefore shows high biocompatibility. It is also a polysaccharide that promotes cell proliferation and migration (Kumbar et al., 2014). Hyaluronan can be extracted from animal sources, but it is also produced in large quantities by *Streptococcus zooepidemicus* and *Streptococcus equiwit*, with good yield and high purity. In bacterial extraction, HA is isolated in the form of the sodium salt (Rinaudo, 2008).

HA is a copolymer composed of repeating monomeric units of β-(1,4)-D-glucuronic acid and β-(1,3)-N-acetyl-D-glucosamine (Fig. 11) (Sabu et al., 2018). Depending on the application, HA is used in different concentrations and molecular weights (Rinaudo, 2008).

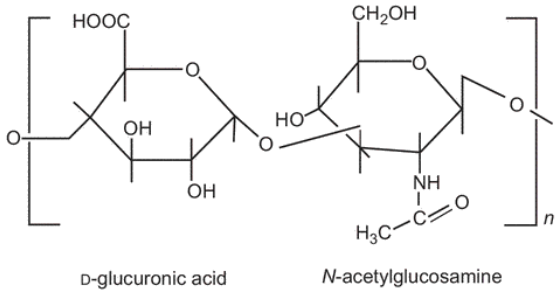

Fig. 11 Repeating monomers of hyaluronic acid (HA) (Sabu et al., 2018)

In regenerative medicine, HA finds use in the form of fibers, films and hydrogels (Ma, 2014). Due to the wide distribution of HA in the human body and its importance in certain body functions, it can be used in various field of medicine such as vascular (Zhu et al., 2014), cartilage (Matsiko et al., 2012), bone (Townsend et al., 2018), and skin TE (Monteiro et al., 2015) and cancer therapy as drug delivery (Trombino et al., 2019).

5.3.2 Conductive polymers

Another group of potentially suitable materials for TE from the category of polymers are electroactive biomaterials such as conductive polymers (CPs). As it is known, most polymers are electrical insulators and they are non-conductive due to their covalent bonding. On the other hand, CPs are synthetic organic polymers possessing conductivity up to 200 S/cm. Aromatic rings with conjugated π-orbitals and delocalized electrons occur in their formula, which allows electrical activity (Lee, 2013). The CPs are capable to transform the ionic conductivity to electronic conduction (Lindfors and Ivaska, 2002) and also have good optical properties (Balint et al., 2014). CPs can be synthesized using various

methods. The most common methods include electrochemical polymerization and chemical polymerization. In their pristine state, CPs have low electrical conductivity, but these can be enhanced by the use of dopants (K and Rout, 2021).

Overall their properties almost correspond to those of inorganic semiconductors. With relatively easy synthesis, CPs provide the desired electrical and optical properties. Thanks to that they can be used in a wide range of bioapplications, such as neural interfaces (Green et al., 2008), drug delivery systems (Chapman et al., 2020) or biosensors (Aydemir et al., 2016; Mawad et al., 2012). Overall, CPs are widely studied for regenerative medicine applications. One of the first CPs studied was polyacetylene, mainly due to its high electrical conductivity. Nonetheless, polyacetylene usually has a complex synthesis and is unstable in the air in the presence of humidity and other gases (Maity et al., 2021). Therefore, the materials as polypyrrole (PPy), polyaniline (PANI), Poly(3,4-ethylenedioxythiophene) (PEDOT) are increasingly being investigated.

For the synthesis of electroactive CPs films are usually used an electrochemical polymerization. This method is efficient due to its simplicity and reproducibility (Fomo et al., 2019). Electrochemical polymerization is usually performed using a three-electrode configuration (working, reading, and reference electrode) in a solution of monomer, a suitable solvent, and an electrolyte (dopant). When the correct voltage is applied to the working electrode, a polymer film immediately begins to form on the working electrode. This method allows the deposition of a thin polymer film with a well-controlled thickness (up to 20 nm) and morphology (Heinze et al., 2010). The product is sufficiently pure and does not necessarily need to be purified to remove any residual amounts of the original reaction mixture. The electrochemical polymerization method is burdened with certain disadvantages such as hydrolysis of the polymer chains and excessive oxidation, which can reduce the significant electroactivity and conductivity of synthesized polymer (Fomo et al., 2019; Inzelt, 2008).

The chemical method of synthesis involves the oxidation or reduction of monomers and their subsequent polymerization. The reaction is usually an oxidative polymerization. In the chemical oxidative polymerization of CPs, the monomer solution is mixed with a stoichiometric amount of oxidizing agent. This process yields the polymer in powder or film form and enables its mass production, making the method suitable for commercial applications (Inzelt, 2008). Through a chemical polymerization approach, the conjugated monomers react with an excess amount of oxidizing agent in a suitable solvent, in an acidic environment. The polymerization proceeds spontaneously and requires constant stirring as the reaction proceeds (Ghammami and Sajadi, 2005). Oxidants, oligomers and monomers remain in the product, so subsequent purification, for example by dialysis, is important. The main advantage of chemical polymerization is associated with mass reproducibility or scalability

at a reasonable cost (Ghosh and Majumdar, 2021; Umoren et al., 2022).

Enzymatic methods of CP synthesis are based on the application of oxidoreductases (often horseradish peroxidase (W. Liu et al., 2002)) and/or redox compounds formed by these enzymes. Enzymatic synthesis of CP can be carried out using redox enzymes (e.g., glucose oxidase and many other oxidases) which, during catalytic action, generate hydrogen peroxide which acts as an initiator of the polymerization reaction (e.g., pyrrole). Since enzymes are natural catalysts that are non-toxic, biodegradable, energy efficient and obtained from renewable sources, these reactions are more environmentally friendly (Loos, 2011; Ramanavicius and Ramanavicius, 2020; Sheldon and Van Pelt, 2013). Figure 12 shows the scheme of enzymatic polymerization of polypyrrole in the presence of the enzyme glucose oxidase, which generates hydrogen peroxide to initiate polymerization.

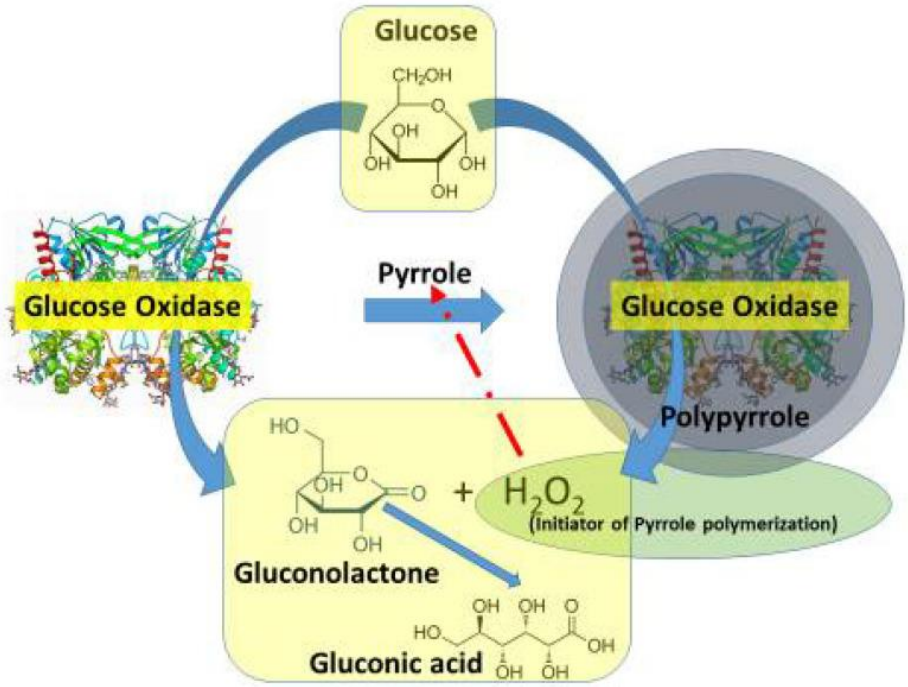

Fig. 12 Scheme of enzymatic polymerization of polypyrrole around enzyme glucose oxidase (Ramanavicius and Ramanavicius, 2020)

5.3.2.1 Polypyrrole

PPy (chemical structure in Fig. 13) is conjugated polymer which can be easy to synthesize. It could be prepared by electrochemical or chemical oxidation of pyrrole monomer. Reaction takes place at room temperature, and a variety of solvents can be used for preparation (Balint et al., 2014). Several different oxidants can be used in chemical oxidative polymerization, such as iron (III) chloride or ammonium persulfate. However, various oxidants and their concentrations can affect thermal stability, conductivity and morphology (Yussuf et al., 2018). The resulting intrinsic properties of PPy are determined

by the polymerization conditions. Overall, PPy powder or films has excellent mechanical and electrical properties and good *in vitro* biocompatibility. Thanks to its excellent properties that can respond to stimuli, PPy is a smart biomaterial that is allowed to dynamically control properties using an electric field application. Due to its stimuli-responsive characteristics, it is one of the most widely used CPs for biomedical applications (Khan et al., 2019). Its bioapplications are also aided by the fact that the pyrrole ring structure can be found in the aminoacids proline and hydroxyproline.

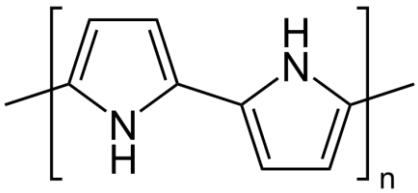

Fig. 13 Polypyrrole

There are studies that investigate PPy as biosensors (Pandey et al., 2018; Van Hao et al., 2018), scaffolds for TE (Naghavi Alhosseini et al., 2019), and drug delivery systems (Puiggalí-Jou et al., 2019; Shah et al., 2018).

5.3.2.2 Polyaniline

Polyaniline (PANI) or so called aniline black, could be easily synthesized by various methods. Chemical or electrochemical oxidation of the respective monomer is most often used for the PANI preparation (Pina and Falletta, 2022; Stejskal and Sapurina, 2005). The conductivity of PANI depends on the degree of its oxidation. Three redox forms are known. The first form is a completely reduced leucoemeraldine base (Fig. 14A). The second is a fully oxidized pernigraniline base (Fig. 14B) and the last is an emeraldine base (Fig. 14C), which consists of alternating units of oxidized and reduced forms (Qazi et al., 2014). The most conductive of these three forms is PANI emeraldine. This form is not inherently conductive, but the electrically conductive form can be transformed by doping to the emeraldine salt (Chiang and MacDiarmid, 1986). The advantage is good environmental stability and possibility of making PANI as a powder, thin film, hydrogel/cryogel or colloidal suspension (Humpolíček et al., 2018; Kašpárková et al., 2017; Kucekova et al., 2014). The morphology of polyaniline depends on the degree of oxidation, but it also depends on the reaction conditions. The growing interest in polyaniline for bioapplications is mainly due to its cytocompatibility with various cell lines, biocompatibility, adjustable conductivity, processability, and antibacterial efficacy (Kucekova et al., 2013; Qazi et al., 2014; Roshanbinfar et al., 2020). However, the main disadvantage of PANI is, that it exhibits pH-dependent conductivity. It loses its conductivity upon contact with physiologic pH (Lindfors and Ivaska, 2002). The potential of PANI applications lies in biosensors (for glucose sensing (Majumdar

and Mahanta, 2020; Zheng et al., 2020), cholesterol sensing (Li et al., 2015), Hepatitis virus sensing (Chowdhury et al., 2019) etc.), in drug delivery systems (Li et al., 2018) and TE (Massoumi et al., 2020; Roshanbinfar et al., 2020).

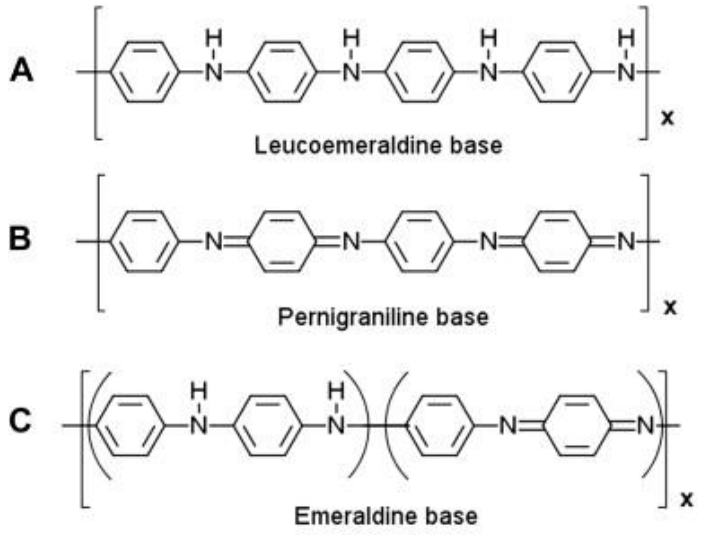

Fig. 14 Polyaniline forms, edited from (Qazi et al., 2014)

5.3.2.3 PEDOT

Poly(3,4-ethylenedioxythiophene) (Fig. 15) is a derivate of polythiophene (PTh). Its thermal stability and conductivity is better than PPy (Khan et al., 2019). PEDOT can be synthesized by electrochemical deposition or chemical oxidation. According to the chosen doping agent which will create strong charge capture centres and thus ensure electrical conductivity, the biological and physicochemical properties change (Zamora-Sequeira et al., 2018).

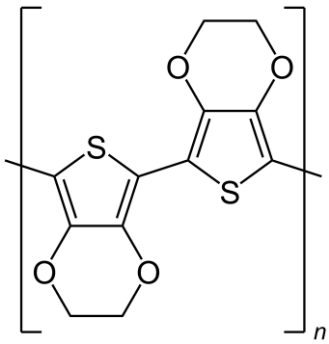

Fig. 15 Poly(3,4-ethylenedioxythiophene)

6. BIOLOGICAL TESTING

As mentioned at the beginning, in the chapter Biological properties of biomaterials, the cytotoxicity determination of a material is the first mandatory test in the evaluation of medical devices. In the following section the conditions for cytotoxicity determination according to the ISO standard will be summarised.

6.1 Cytotoxicity testing

In vitro cytotoxicity testing is given according to ISO standard 10993-5. The standard specifies three categories of cytotoxicity tests: extract test, direct contact test and indirect contact test (which includes agar diffusion and filter diffusion tests). The choice of the specific type of test depends mainly on the nature of the tested samples, and on their intended place of use and the nature of the application. At the end of the exposure period, an assessment of the presence and extent of the cytotoxic effect is evaluated. This part of the ISO standard leaves the choice of evaluation open. The methods frequently used in the determination of cytotoxicity can be divided into several categories. The most commonly used evaluation methods for in vitro cytotoxicity testing include colorimetric methods such as MTT, XTT or MTS. Other widely used methods are luminescence and fluorescence methods such as for example the ATP bioluminescence method. Or another option is to test cell viability using particle analysers.

6.2 Preparation of extracts from materials

Since medical devices are made of different materials (e.g polymers, metals, ceramics) it is usually not possible to define a specific quantity of the substances of interest. For most tests, the most appropriate technique to determine the biological reactivity of possible leachable chemicals from a material is to use fluid extracts of the device materials.

ISO 10993-12 describes the extraction methods and conditions on different types of test materials. If cytotoxicity is tested using an extract of the material, extraction conditions should simulate or be exaggerated from those in clinical use to define potential toxicological hazards. However, it is important that there are no significant changes in the material such as bonding, melting or change in chemical structure. Where testing is carried out on mammalian cells, the selected solvents that may be used are listed in the standard. For example, medium with or without serum or saline solution may be used as extraction media. Extraction must be performed in sterile, chemically inert, closed containers using aseptic techniques.

Temperature and time conditions of extraction can be seen in the table 1. Other conditions may be used, but these conditions must stimulate the extraction that occurs during clinical use or provide an appropriate level of potential risks. Any changes must be described and justified. *"Extraction is a complex process influenced by time, temperature, surface-area-to-volume ratio, the extraction vehicle and the phase equilibrium of the material"* (ISO standard 10993-12). If accelerated extraction or extraction under exaggerated conditions is used, the effects of higher temperatures or other conditions on the extraction kinetics

and the identity of the extracted substances must be acknowledged. For example, there are several concerns when using elevated temperatures; the energy of the elevated temperature may cause an increase in the crosslinking and/or degree of polymerization of the polymer, thus reducing the amount of free monomer that can migrate out of the polymer. Alternatively, the elevated temperature may lead to the formation of degradation materials that are not normally present in the finished medical device under the conditions of use.

Tab. 1 The extraction conditions (ISO standard 10993-12)

Temperature [°C]	**Time [h]**
37 ± 1	24 ± 2
37 ± 1	72 ± 2
50 ± 2	72 ± 2
70 ± 2	24 ± 2
121 ± 2	1± 0.1

7. TECHNIQUES OF CELL CULTIVATION

The cell cultivation techniques are different for suspension and adherent cells. Suspension cells are non-adhesive and are cultured in suspension. For their cultivation, specially treated culture flasks are not required. As their name suggests, adherent cells are attached to the substrate on which they proliferate. And the vessels for their cultivation is tissue-culture treated, on which the cells grow in monolayers (Sherr, 2004). Most cell types are adherent.

A typical approach to the cultivation of adherent cell culture is on 2D surfaces (Petri dishes, tissue plastic plates, ...) or in 3D systems such as scaffolds. For most of the initial assays described in the following chapter Properties of biomaterial, the cells are cultured in a monolayer in an incubator. However, this type of cultivation results in limited mass transfer. This is due to insufficient diffusion of metabolites, oxygen and carbon dioxide under static conditions. Bioreactors are used for higher nutrient transfer *in vitro*. The flow of the medium leads to continuous oxygen transport and waste disposal. In addition, dynamic conditions *in vitro* could mimic *in vivo* conditions to obtain a system that is subjected to dynamic and mechanical forces, mechanical stress, hydrostatic pressure, fluid shear stress and other environmental parameters such as pH, temperature (Hao et al., 2015; Salehi-Nik et al., 2013).

Cells respond to their physical surroundings through a process called mechanotransduction. This process involves the integration and conversion of various physical cues in the cell's microenvironment into biochemical signals within the cell. As a result, cellular behaviours such as adhesion, proliferation, morphology, migration, and differentiation can be influenced (Kaarj and Yoon,

2019). Despite the proven benefits of dynamic conditions in enhancing mechanotransduction effects, most in vitro studies are still conducted using static culture settings. However, specialized bioreactors have been developed to replicate the mechanical stimuli found in natural tissue environments. These bioreactors directly interact with the mechanosensitive compartments of cells, serving as active forces that guide cellular functions, including the differentiation of stem cells into specific lineages (Clementi et al., 2018). Mechanical forces affect cell instructive properties (e.g. proliferation and growth, cell migration, shape modulation, and differentiation) (Oliveira et al., 2017).

Bioreactors that control one or more important factors influencing cell behaviour can be used to mimic the in vivo environment/conditions. Due to the specificity of tissues and their culture requirements, there are several types of bioreactors that are designed to mimic in vivo conditions in a given tissue as closely as possible. Various specific conditions are imposed on bioreactors, such as shape, size, fluid dynamics, shear stress, etc. (Martin et al., 2004). Regarding the classification of tissue bioreactors, the reactors can be divided according to the main operating modes into perfusion systems, stirred vessels, and rotating wall vessels (Chaudhuri and Al-Rubeai, 2005). Typical bioreactors commonly used in TE are spinner flask, stirred (batch or continuous) vessels, airlift bioreactor, perfusion bioreactor, low gravity bioreactor, and membrane bioreactors (Annesini et al., 2016; Kim, 2014; Tapia et al., 2016). Figure 16 shows some of the culture vessels for static cultivation as well as for dynamic cultivation.

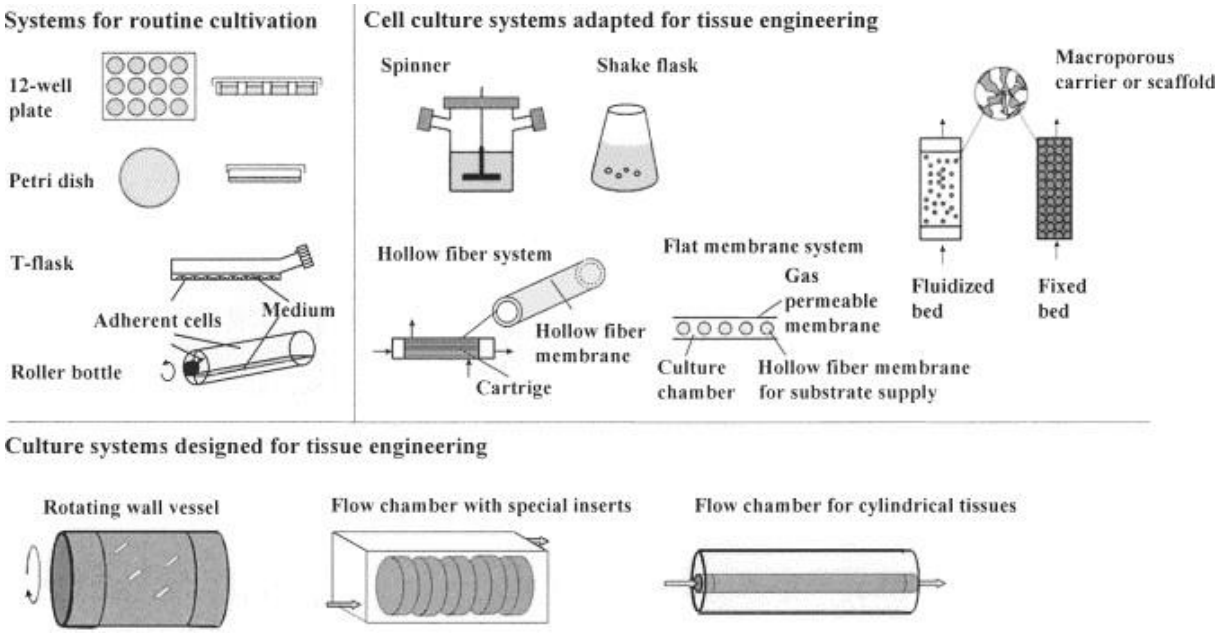

Fig. 16 Cell culture systems used in tissue engineering (Pörtner et al., 2005)

7.1 Perfusion Systems

Static cultivation may result in poor migration of cells into the internal environment of the scaffold. A cell shell will form on the surface of the scaffold, and the desired uniform distribution will not be established. In perfusion systems, weak cell growth can be overcome (Chen and Hu, 2006). The constant flow of medium through the pores and around the scaffold facilitates the transport of nutrients to the cells within the scaffold (Chaudhuri and Al-Rubeai, 2005). This causes orientation of cells in the direction of media flow, which is undesirable for some tissues. For example, in articular cartilage, the orientation of surface cells perpendicular to the flow is essential (Chen and Hu, 2006).

7.2 Stirred Vessels

The best known of the bioreactors with Stirred Vessels are Spinner Flasks. One of the most widespread applications of this type of bioreactor is the dynamic seeding of cells into a scaffold. The scaffold is placed in a culture medium that contains cells (Chaudhuri and Al-Rubeai, 2005). The Spinner Flask bioreactor was designed to generate hydrostatic forces that aid in mass transport. It consists of a cylindrical glass vessel and a mixing element that provides mixing of the culture medium. The stirring element can be, for example, a magnetic stirrer. This system promotes a uniform homogeneous distribution of cells and is mainly used for bone scaffolds. On the other hand, mixing the medium can cause turbulent flow (Ahmed et al., 2019) which may not be optimal because it causes higher shear stress (Chen and Hu, 2006).

7.3 Rotating Wall Vessel

The main purpose of rotary motion bioreactors is to increase the uniformity of cell distribution and to facilitate the transport of nutrients and waste products. The disadvantage of this type of bioreactors is the turbulent flow which results in high shear stress that could damage the cells (Ma, 2014). Although shear stress is necessary to modulate some of the mechanical properties of tissue scaffolds, high shear stress can lead to the formation of undesirable capsules surrounding the tissues (Chen and Hu, 2006).

8. AIMS OF DOCTORAL THESIS

The aim is to prepare and modify the biomaterials in the form of a scaffold and to determine the interactions between the prepared scaffolds and the cells. Overall, the aim is to prepare stimuli-responsive material enabling targeted interaction with the organism and cytocompatibility testing of prepared scaffolds. Another goal is to observe cellular behaviour on scaffolds using static and dynamic cultivation.

9. EXPERIMENTAL PART

The experimental part of the disertation was focused on the preparation and surface modification of scaffolds. Furthermore, the interactions between material and cells were investigated. Overall, routine tests for cytotoxicity and biocompatibility were performed in the cell laboratory. The MTT assay was used for cell quantification, evaluation was performed by spectrophotometry. NIH/3T3 (ECACC 93061524, England) mouse fibroblast lines were mostly used during the experiments. However, in some studies, the embryonic stem cell ES R1 line (Nagy et al., 1993) or cell line of mouse osteoblastic precursors (MC3T3-E1) obtained from the European Collection of Cell Culture (c.n. 99072810) were used. Furthermore, the effect of dynamic cultivation and electrical stimulation on cell cultures was investigated

A substantial part of this thesis deals with testing CPs as they are suitable for the preparation of stimuli-responsive scaffolds. From the theoretical part of the thesis, it can be understood that there are many material properties that affect cell behaviour. CPs were investigated for their conductivity because, as mentioned in the electrical stimulation subchapter, electrical signals affect cell fate. Of the CPs, PANI and PPy were used for the work mainly because of their relatively high conductivity and ease of synthesis. Interesting results were obtained when testing PANI films and coatings of ceramic substrate. In addition, these films and coatings were enriched with biopolymers that also affect cell behaviour. During the research, ceramic samples produced by powder injection technology (PIM) were investigated. Ceramic material has been studied primarily for its potential in bone TE. This was followed by the study of another material that could be used in TE of hard tissues. PEEK was studied for its elastic modulus similar to that of natural bone. Therefore, the cytocompatibility and bioactivity of PEEK grafts modified with farringtonite were investigated.

Another part of research focused on stimuli-responsive material suitable, for example, for soft TE. The study was aimed at preparation of PPy in combination with DAC, and combination of PPy with cotton modified with DAC, dialdehyde alginate (DAAL), or dialdehyde hyaluronate (DAH). To the authors' best knowledge, in this research, a completely new approach to template-controlled polymerization was used. Due to ongoing patent proceedings, the preparation and results of this study will only be described briefly.

9.1 Cell lines

Here, the cell lines that were used for the biological evaluation of the materials will be briefly introduced.

9.1.1 Mouse embryonic fibroblasts

The mouse fibroblasts NIH/3T3 cell line (ECACC 93061524, England) was used to test the biological properties of the scaffolds. It is a line of adherent mouse embryonic fibroblasts. The culture medium for this cell line consists of DMEM (Dulbecco's Modified Eagle Medium, Biosera) containing 10% Calf Sera (Biosera) and 1% Penicillin/Streptomycin (Biosera). For cultivation, TPP tissue-polystyrene bottles and dishes were used. Cultivation was carried out under constant conditions in an incubator (Heracell 150i, Thermo Scientific) at 37 °C, with a CO_2 concentration of 5% and a constant relative humidity of 90%.

9.1.2 Stem cells

Stem cells could play an essential role in regenerative medicine. They are unspecialized cells that can be found in most multicellular organisms. Those cells have the ability to convert into another cell type based on their purpose, also they can renew themselves (Bishop et al., 2002).

"The embryonic stem cell ES R1 line (Nagy et al., 1993) *was propagated in an undifferentiated state by culturing on gelatinized tissue culture dishes in complete media. The gelatinization was performed using 0.1% porcine gelatin in water. Complete medium with the following composition was used for the cultivation: Dulbecco's Modified Eagle's Medium (DMEM), 15% fetal calf serum, 100 U mL^{-1} penicillin, 0.1 mg mL^{-1} streptomycin, 100 mM non-essential amino acids solution (all from Thermo Fisher, Waltham, MA, USA), 0.05 mM 2-mercaptoethanol (Sigma, St. Louis, MO, USA) and 1000 U mL^{-1} of leukemia inhibitory factor (LIF) (Gibco, MA, USA)"*(Skopalová et al., 2021). Cultivation conditions in incubator are the same as for the NIH/3T3 line.

9.2 Samples preparation

The following part of the thesis briefly describes the methodology of preparation of the materials, which could have been prepared by myself or in collaboration with colleagues. Most of the tested materials were prepared in collaboration with other faculties or other universities. These methodologies are described in the articles.

9.2.1 Ceramic-based scaffold

Ceramic-based substrates (CBS) were prepared in collaboration with colleagues from department of production engineering Tomas Bata University by PIM technology. This method consists of four steps, where the first step is to create a homogeneous mixture that consists of powder material, polymer binder and space holder. *"The powder components of the PIM compound were aluminum*

oxide (Martinswerk – Huber Corporation, USA) (ρ = 3.98 g/cm^3, size range 0.1-3.0 μm) and a powder space holder (PSH), potassium chloride (KCl, Sigma Aldrich, Germany) (ρ = 1.98 g/cm^3, size range 125-500 μm). The powders were admixed into a partially water-soluble binder (Licomont EK 583, ρ = 1.08 g/cm^3, viscosity 1.5 mPa.s at 130 °C) in a batch mixer (Plasti-Corder, Brabender, Germany) with counter-rotating blades" (Martínková et al., 2022). The architecture of the scaffold and shape of pores is significantly influenced by the shape and size of PSH. Particles KCl of irregular shape were used.

The second step is the injection of the prepared mixture into the desired shape. Injection molding was performed on an injection molding machine (Allrounder 370S, Arburg, ARBURG GmbH + Co KG, Lössburg, Germany).

The third step is the removal of the binder by a suitable solvent or thermal decomposition and finally the sintering of the powder material to the final density. *"The water-soluble binder component and part of the PSH were removed by immersion in distilled water (60 °C) for 24h. The remaining binder (the backbone) was debound thermally (280 °C) at atmospheric pressure. Sintering was carried out in a PIM furnace (CLASIC CZ s.r.o., Revnice, Czech Republic) up to a maximum temperature of 1670 °C and for a holding time of 1h. The surfaces of CBS were inspected using SEM microscopy (VEGA, Tescan)"* (Martínková et al., 2022).

The surfaces of the CBS were functionalized by electrically-conductive polyaniline and polyaniline stabilized by biopolymer films prepared in a colloidal dispersion mode. Sodium alginate, sodium hyaluronate and chitosan were used, mainly due to their good biocompatibility. Subsequently, the cytocompatibility of the native ceramic substrate and bioactive coatings were investigated. Cytocompatibility was investigated under static and under dynamic conditions with electrical stimulation.

Surface functionalization of native substrate

The surface of a CBS prepared by powder injection molding was coated to become bioactive. For surface functionalization, four different coatings were designed. First of all, electroconductive PANI was used. However, several studies indicate the lack of cytocompatibility of PANI itself. Therefore, composite surfaces were further prepared. An innovative approach to the preparation, *in-situ* polymerization of aniline hydrochloride (AH; Sigma Aldrich, Germany) with oxidizing agent ammonium persulfate (APS; Sigma Aldrich, Germany) in the presence of stabilizers was used. This technique of colloidal dispersion mode of preparation was used for three biopolymer stabilizers – specifically, sodium hyaluronate (SH; Contipro a.s.), sodium alginate (SA; IPL, Czech Republic), and chitosan (CH; Sigma Aldrich). In this arrangement, biopolymers

provide cytocompatibility and the conducting polymer contribute with electroactivity. A schematic representation of the reaction is shown in Fig. 17. The methodology for each surface is given in the publication "Powder injection molded ceramic scaffolds: the role of pores size and surface functionalization on the cytocompatibility" (Martínková et al., 2022).

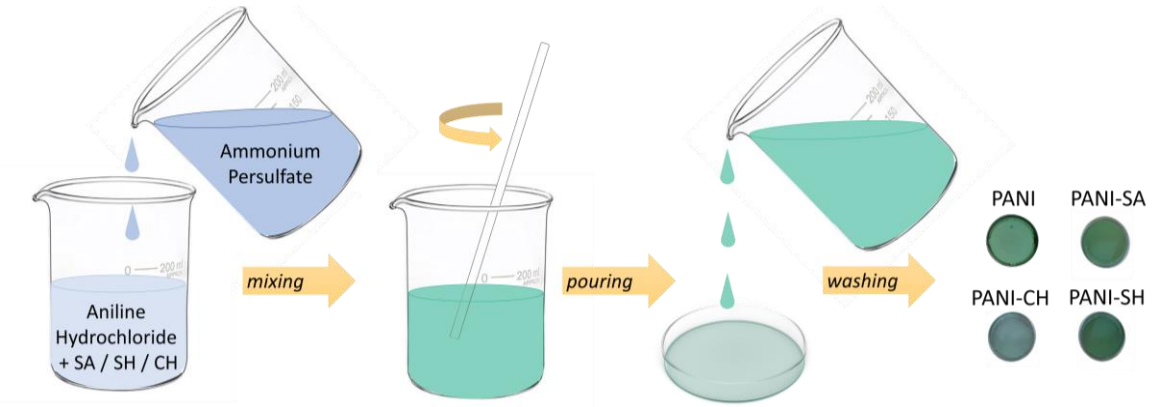

Fig. 17 Scheme for the preparation of PANI films in colloidal dispersion mode stabilized by SA, SH or CH

9.2.2 Preparation of dialdehyde cellulose nanofibrils with PPy (CNF-DAC PPy)

Solution in concentration of 0.5 wt% of Cellulose nanofibrils (CNF; 3 wt% in water, Cellulose lab, Canada) in ultra-pure water (UPW) was prepared. Then the solution was heated to 55 °C overnight under shaking. The solution was homogenized using a sonicator for 60 min.

Then the cellulose nanofibrils were oxidized from 10%. For oxidation was used periodate salt (sodium periodate $NaIO_4$; PENTA, Czech Republic). The reaction was carried out for 72 hours in the dark with stirring at 30 °C. After this time the reaction was terminated by the addition of ethylene glycol (PENTA, Czech Republic). Subsequently, dialysis of cellulose nanofibrils dialdehyde (CNF-DAC) against UPW was performed for 72 hours. The solution of CNF-DAC was investigated for the presence of residual oxidizing agents (periodate) by iodometric titration. The presence of iodine was detected in the sample, so the sample was purified by centrifugation and homogenization on a mechanical homogenizer. Then dialysis against 0.05 M NaCl (Sigma Aldrich Co.) using a 14 kDa MWCO membrane, until iodometric titration and XRF measurements confirmed complete removal of all oxidizing agents. Subsequently mass analysis was done.

To the solution of CNF-DAC, a pyrrole (Py; Sigma-Aldrich Co.) in different concentrations was added. To a CNF-DAC suspension of 0.5 wt% in UPW was added an amount of pyrrole corresponding to $n_{py} : n_{CHO}$ molar ratios of 1:1, 2:1, 4:1, and 8:1. This was followed by incubation for 24 hours on a shaker. Before polymerization, the solution was homogenized by ultrasonication for 10 minutes.

This was followed by the addition of an oxidizing agent to the solution (in mass ratio 1:4 Py : $FeCl_3$ Sigma-Aldrich Co.) under gentle shaking for 24h. After this time, the samples were filtered and washed with 0.2M hydrochloric acid (HCl; PENTA, Czech Republic), then with methanol (PENTA, Czech Republic) and finally with UPW. The samples were transferred into aqueous solution and lyophilized for SEM.

The different preparation procedure resulted in the formation of more rigid samples suitable for conductivity measurements. CNF-DAC dialysis was followed by filtration through a 0.4 μm pragopore filter. The pellet was dried between two vapor permeable membranes (Fig. 18) at 40 °C with a load of 1kg. The prepared CNF-DAC disks were consequently immersed in a solution of pyrrole (several different concentrations) and placed for 24h on an orbital shaker. Finally, iron (III) chloride was added four times the mass excess compared to pyrrole. After 24h, the samples were washed with UPW and then placed in an ultrasonic bath in 0.2 M HCl for 5 min. This was followed by washing with UPW, methanol, and finally 5 min in the ultrasonic bath with UPW. CNF-DAC PPy disk were dried between two vapor permeable membranes at 40 °C with a load of 1kg.

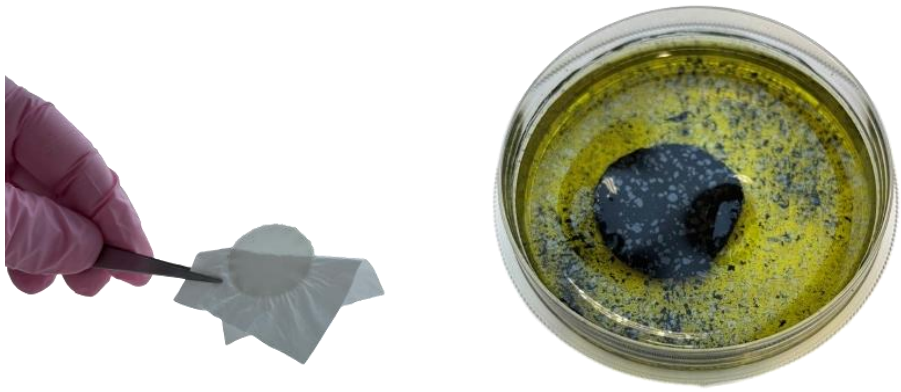

Fig. 18 CNF-DAC disk on vapor permeable membrane after drying (left), CNF-DAC PPy after polymerization before washing (right)

9.3 Biological properties

9.3.1 Cytotoxicity

In the theoretical part in the chapter biological testing the permitted conditions for testing according to ISO standard 10993-5 and 12 are given.

Extract preparation

The preparation of the extracts was carried out in accordance with the ISO standard 10993-12. If the material properties of the sample allow, the sample should be crushed or cut into small pieces for preparation in order to increase the surface area of the extracted material. The extraction ratio of the material

depends on the thickness, the preparation method and type of material. For example, in the case of the ceramic substrate prepared by the PIM method, the samples were crushed and extracted at a concentration of 0.2 g/mL of culture media. The extraction was carried out for 24 hours at 37 °C with stirring. Subsequently, the extracts were sterilized by filtration on syringe filter with a pore size of 0.22 μm (Merck, Darmstadt, Germany). The parent extracts (100 vol.%) were then diluted in culture medium to achieve the desired final concentration. In a second study testing the cytotoxicity of PEEK grafts, samples were extracted in concentration of 3 $cm^2 \cdot mL^{-1}$ of culture medium. Prior to extraction, samples were sterilized with ethanol for 1 hour, thus eliminating the need for filtration of extracts. All extracts were used within 24 hours. *In vitro* testing of cytotoxicity was performed according to the ISO 10993-5.

MTT assay

MTT (3-(4,5-dimethylthiazol-2-yl)-2,5-diphenyl tetrazolium bromid)) (Invitrogen Corporation, USA) in the form of a yellow solubilized solution is added to the cells. MTT is reduced in living and metabolically active cells by mitochondrial dehydrogenases and reducing agents to purple coloured formazan crystals (Freimoser et al., 1999; Y. Liu et al., 2002). Reduction of MTT to formazan is limited upon cytotoxic damage or destruction of the cell. A strong detergent is required to dissolve formazan. Dimethyl sulfoxide (DMSO) is considered the best solvent and is applied especially where large amounts of residual medium remain in the wells of the used microtiter plate (Twentyman and Luscombe, 1987). The absorbance is measured spectrophotometrically with an Infinite M200 Pro NanoQuant instrument (Tecan, Switzerland) at 570 nm. The degree of absorbance is directly proportional to the amount of formazan i.e. the number of living cells.

ATP assay

ATP assay is a method that can be used to evaluate cell viability. Adenosine triphosphate (ATP) serves as the main chemical energy carrier for living cells. When membrane integrity is disrupted, the cell loses its ability to synthesize ATP (Riss et al., 2004). Cellular ATP is one of the most sensitive indicators in measuring cell viability (Strehler and McElroy, 1957). This method is based on a reaction when the substrate D-luciferin is converted by enzyme luciferase to oxyluciferin. This conversion is driven by ATP in the presence of oxygen, magnesium ions and luciferase accompanied by visible light emissions (Lee et al., 2012). The resulting oxyluciferin produces a chemiluminescent signal whose intensity is directly proportional to the ATP concentration. The Cellular ATP Kit HTS (Invitrogen Corporation, USA) was used for ATP assessment in my co-authored research. Luminescence was measured on an Infinite Lumi luminometer (Tecan, Switzerland).

9.3.2 Cytocompatibility determination

The cytocompatibility of materials can be studied by determining cell adhesion, growth and proliferation. In cell adhesion assays, cells are seeded onto sterile samples at a concentration of 10^6 cells per 1 mL of culture medium. After 1 hour, unadhered cells were rinsed and the cell nuclei of adherent cells were visualized through nuclei counterstaining by Hoechst 33258 (Invitrogen, USA).

For the determination of cell proliferation, cells were seeded at a concentration of 10^5 cells per mL on the sample surface. Cultivation was carried out under standard incubation conditions for 48 h (can be extended if necessary). Subsequently, cells were fixed and stained by Hoechst 33258 and actin filaments were visualized through staining by ActinRed™ 555 (Thermo Fisher Scientific, USA).

Depending on previous results, the growth and ingrowth of cells under dynamic conditions with electrical stimulation can be further investigated. Cells were seeded on a scaffold at an initial concentration of 10^5 per mL and pre-cultivated for 72 h. The cell-seeded sample was then transferred to a bioreactor for 72 h. Electrical stimuli run 6 hours a day "*each successive hour-long period alternating between electrical stimulation and no stimulation. The medium flow was 54 RPM. The pulse had a rectangular waveform with a width of 3000 ms, and the voltage was set at 0.1 V."*(Martínková et al., 2022).

A number of tests with unsuccessful setups were performed before the correct electrical stimulation settings and testing times were achieved in the bioreactor.

10.SUMMARY OF RESULTS

The main focus of my doctoral study was to deepen the knowledge in the field of stimuli-responsive scaffolds. There are various materials available for creating a stimuli-responsive scaffold. However, many materials do not naturally respond to external stimuli but still possess appropriate characteristics for use in TE. Therefore, my research has also focused on modifying materials to enhance their bioactivity. The choice of material for the creation of scaffolds is made with regard to the intended use. For scaffolds to regenerate or restore soft tissues, materials from the polymer group are more likely to be used. For hard tissues such as bone, biomaterials need to have the required high degree of hardness and for this reason, ceramics are used. In the beginning, my research dealt with the preparation of ceramic-based biomaterials and functionalization of surfaces of sintered porous scaffolds by electrically-conducting polyaniline or polyaniline/biopolymer films prepared in a colloidal dispersion mode. CBS prepared by PIM technology has potential usage as bone scaffolds. However, there are also polymers such as PEEK that have suitable properties for use in bone TE. The research then moved on to another material that would be also suitable for bone TE and that was PEEK. The addition of farringtonite particles ($Mg_3(PO_4)_2$,) was introduced into the PEEK matrix to obtain physical-chemical and mechanical properties suitable for bone-related applications. In contrast, biomaterials suitable for soft TE should possess enhanced flexibility and mechanical properties that align with the specific functions of the tissues. For instance, load-bearing tissues like cartilage and tendons exhibit greater rigidity compared to nonload-bearing tissues like the brain. The utilization of conductive polymers holds promise in the development of electroactive soft tissues, including cardiac muscles, nerves, and skin. With this in mind, a comprehensive investigation was conducted on the combination of polypyrrole and cellulose as a potential approach. The theoretical portion of the thesis highlighted the various requirements that biomaterials must meet in order to be utilized in TE. Consequently, this thesis focused on the experimental evaluation of the prepared materials and their interactions with cells.

10.1 Scaffolds for hard TE

Hard tissue is calcified tissue in the human body, such as bones and teeth (tooth enamel, dentin and cementum). This mineralized tissue is mainly characterized by a firm intercellular matrix. The need for hard tissue surgery increases with the increasing lifespan of the population as the incidence of fractures increases. This is partially related to increased bone fragility. However, bone fractures and defects are a significant problem worldwide at any age. Bones are characterized by high compressive strength (cortical bone approximately 125 MPa along its longitudinal axis) (Kundu et al., 2014), of course in immature bones, where the mineralization process is still ongoing, this value is lower. In any

case, for bone TE, it is necessary to select a material that has high strength but is also flexible. Therefore, most of the materials that are brittle are not suitable, as the risk of failure increases (Zioupos et al., 2020). Biomaterials used for bone TE include metals, ceramics, natural or synthetic polymers and composites. On this basis, the experimental section was therefore divided into two parts according to the materials that were investigated in my research. One part will be dedicated to ceramic material and the other for polymer material.

1) *Ceramic scaffolds for bone TE applications* are ideal as ceramic combine good biocompatibility, osteoconductivity and corrosion resistance. However, hard and brittle ceramics limits its clinical use for TE. One of the representatives of ceramics is aluminium oxide. Alumina (Al_2O_3) is biocompatible, poses high hardness and good abrasion and corrosion resistance (Rahmati and Mozafari, 2019). The architecture of the scaffold is influenced by its manufacturing. The ability to produce individually design products with defined scaffold architecture is possible by additive technologies or here used PIM technology. It enables the production of personalized medical devices for hard TE. The pore size can be effectively controlled by the particle size of the space holder. Ceramic parts from alumina prepared by this technique was studied by Thomas-Vielma et al., 2008. However, this publication does not study the interaction of cells with material. The alumina parts prepared in this work are not porous and do not exhibit the defined porosity that is desirable for bone scaffolds.

Nevertheless, it is not only the bulk properties (porosity, thermal conductivity or elasticity) that are important for scaffold, but also the surface characteristics are critical. Since alumina is bioinert and does not interact with the surrounding bone tissue, it is possible to modified a surface with a biocompatible coating that will promote cell adhesion and proliferation. The study by Bertazzo et al., 2009 deals with bioactivation of alumina surface with low molecular weight dicarboxylic acid. The biocompatibility of this surface modification was proved by adhesion and viability of pre-osteoblasts. Such surface is bioactive, but does not allow the electrical stimuli-responsivity. Therefore, a surface treatment that makes scaffold electrically conductive is advantageous, especially for bone scaffolds because it promotes bone healing and regeneration. Ahmed El-Said et al., 2010 investigated cellular interaction on alumina substrate coated with PPy nanowire. They discovered that this surface modification exhibits better cell adhesion and proliferation of HeLa cancer cells and HMCF normal cells. In study of Jasenská et al., 2021, conductive composite films were presented. These films were prepared *via in-situ* polymerization of AH and SH or CH. From the available literature, it was found that this surface treatment approach in combination with a ceramic substrate has not yet been investigated.

To the author’s best knowledge, no study has been published on the combination of alumina substrate with a defined pore size for TE prepared by PIM technology.

Another innovative feature is surface modification by composite colloidal-based coating based on PANI and biopolymers. The article "*Powder injection molded ceramic scaffolds: The role of pores size and surface functionalization on the cytocompatibility"* by **Martínková M.**, Hausnerová B., Huba J., Martínek T., Káčerová S., Kašpárková V., Humpolíček P. published in Q1 journal Materials and Design (**ARTICLE I**) is one of the first to explore this issue. Initially, the cytotoxicity of native CBS prepared by PIM was investigated on cell line NIH/3T3. Native alumina substrates did not induce cytotoxicity. Further the porosity of CBS was visualized by SEM microphotographs. The architecture of CBS was influenced by different sizes of space holder and four different space holder *vs* powder volume ratios. There are conflicting reports in the available literature on the optimal average pore size for bone scaffolds. In work of Murphy et al., 2010 it was discovered that the highest cell viability was in the scaffold with a pore size of 325 μm and was therefore evaluated as the best pore size for bone TE. However, higher cell numbers were also observed for scaffolds with 120 μm pores. In **ARTICLE I**, the space holder in size of 125-250 μm and then 250-500 μm were used. In this study, it was confirmed that cell growth was better on samples with pore sizes greater than 250 μm (Fig. 19).

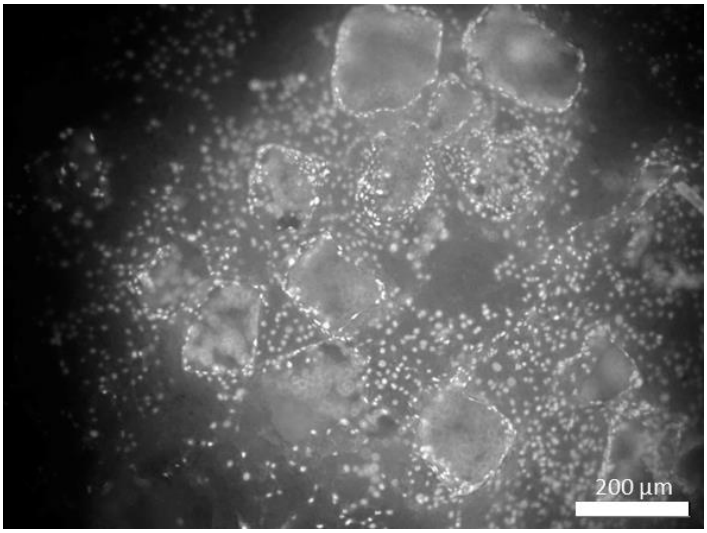

Fig. 19 Cell growth on native CBS with 30% of space holder with grain sizes greater than 250 μm

As mentioned above, the conductivity is important for bone grafts and scaffolds. The proper function of natural tissue is ensured by its ionic conductivity, therefore conductive polymers are a promising material for TE. The bioactive coatings by PANI films and PANI in combination with natural polymer stabilizers were prepared. Anyway, as reported in the study by Jasenská et al., 2021 pristine PANI does not provide an adequate cellular response. Addition of biopolymer stabilizers had a beneficial effect on cell adhesion, and proliferation. This was also confirmed in ARTICLE I, where the component of the extracellular matrix – sodium hyaluronate, or natural biopolymers such as sodium alginate and chitosan

were employed, and, subsequently, the cytocompatibility of the native and functionalized alumina scaffolds was determined. Interesting results were obtained in the determination of cytocompatibility on CBS modified with PANI films (Fig. 20). Cells on PANI film prepared on Petri dishes were unable to adhere, but PANI film on ceramic substrate allowed adhesion (Fig. 21 PANI). Overall cells could grow on the all surfaces and within the pores. However, the cell distribution on surfaces is uneven (Fig. 21).

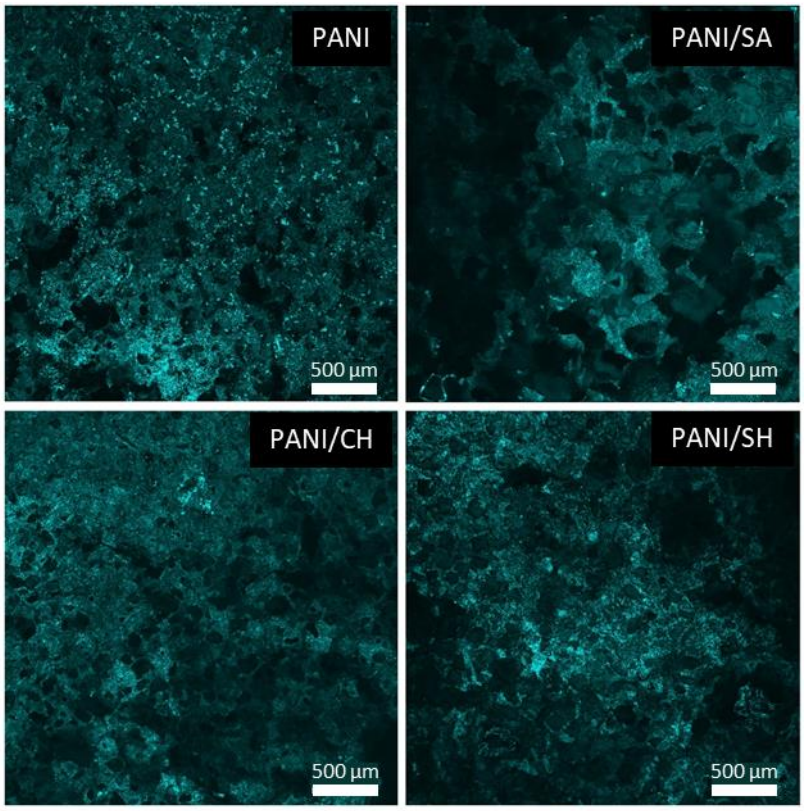

Fig. 20 Surfaces of modified CBS with 50% of space holder with grain sizes greater than 250 µm

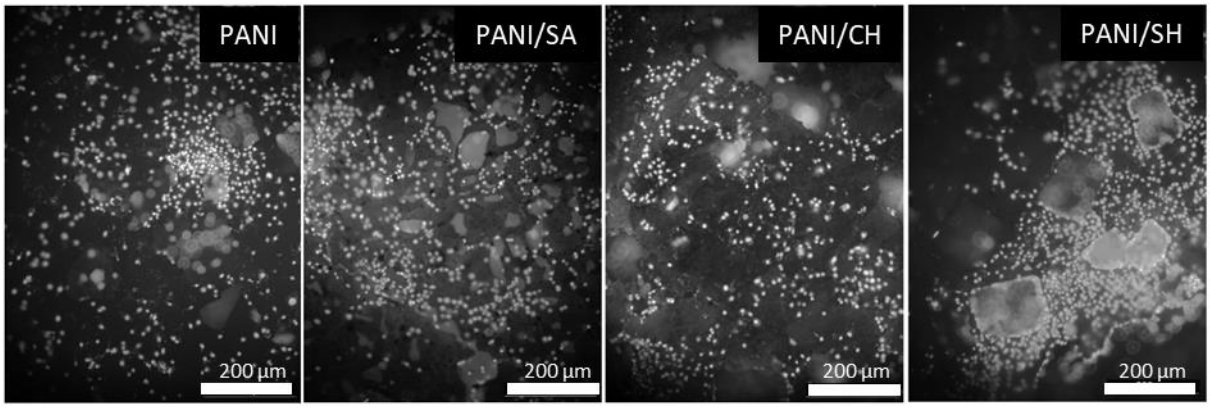

*Fig. 21 Cell grow on a modified ceramic scaffolds (CBS with 30% of space holder with grain sizes greater than 250 µm) under static cultivation (supplementary material of **ARTICLE I** (Martínková et al., 2022))*

Since the static cultivation has its limits, testing continued with dynamic cultivation in a bioreactor. Dynamic cultivation allows simulating the cell's surrounding microenvironment. It enhances mass transfer and mechanotransductive effects. The flow rate of the culture medium in the bioreactor is essential for bone scaffolds as it can promote bone regeneration. Furthermore, electrical stimulation also plays a major role in bone regeneration. A report by Kumar et al., 2016 investigated electric field-mediated cell growth to accelerate wound healing. In this research the direct current pulses with electric field intensity of 0.5-1 $V \cdot cm^{-1}$ were applied for 10 minutes (square waveform, 100 Hz frequency and 50% duty cycle). This study showed that cell growth under dynamic conditions with electrical field stimulation is higher than under static conditions with stimulation. Mobini et al., 2017 in their publication invastegated the effect of direct current electrical stimulation on rat mesenchymal stem cells. The cells were exposed to 0.01 $V \cdot cm^{-1}$ for 1 hour per day for 3, 7, and 14 days. The findings revealed that the ES changed expression patterns of certain osteogenic genes. The settings for electrical stimulation of cells vary in the literature, so this part of the study required a lot of time. For example, in article by Wen et al., 2013 MSC and cardiac myocytes coculture monolayer was stimulated by electric pulses current of power 40 μA, rectangular waveform 2 ms, frequency 2 Hz. These pulses were applied 3, 6 hours per day for 5days). Electric stimulation in neurogenesis were discussed in the research of Chang et al., 2011 used electrical stimulation with magnitude in range from 4 to 32 $\mu A/cm^2$ for 50 and 200 μs at 100 Hz. Study revealed that current density 8 $\mu A/cm^2$ for 200 μs at 100 Hz increased fetal NSC proliferation.

In the first few experiments, the bioreactor settings were too extreme and the cells did not proliferate under dynamic conditions. The morphology of the cells under simulated *in vivo* conditions with electric stimulation was not typically triangular (Fig. 22).

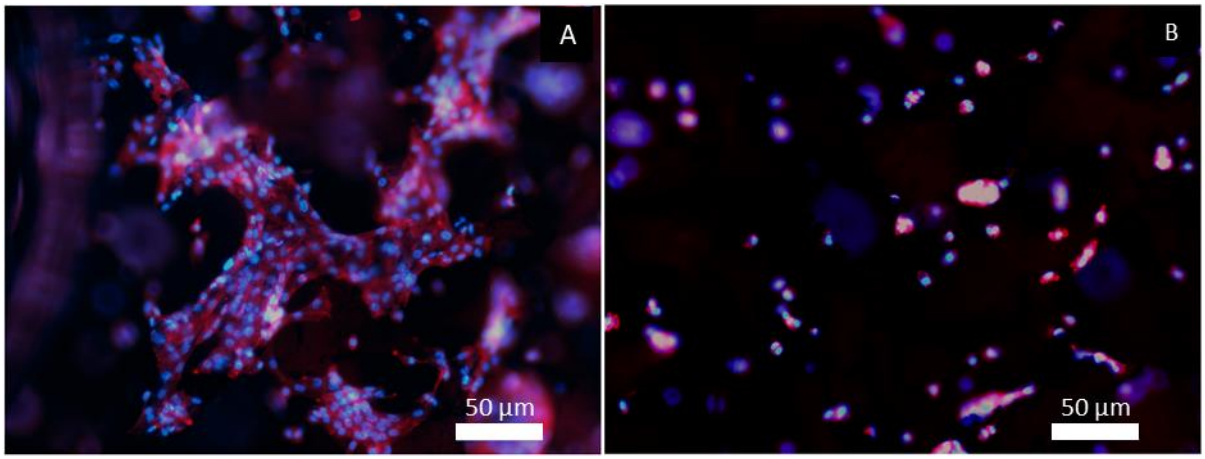

Fig. 22 Cell grow on CBS PANI-SH (CBS with 30% of space holder with grain sizes greater than 250 μm); (A) static cultivation; (B) dynamic cultivation

After a number of unsuccessful attempts, the settings of the medium flow and electrical pulses were optimized. The results were published in **ARTICLE I** and *"the electrical stimulation parameters were as follows: voltage 0.1V, pulse width 3000 ms, arrangement on square-wave "* (Martínková et al., 2022) with media flow 54 RPMI. Application of shear stress and external electrical stimulation resulted in a homogeneous cellular distribution. Both the absence of cytotoxicity and the cytocompatibility that were revealed demonstrate the application potential of these scaffolds.

2) *PEEK has high potential for use in bone TE* and connective tissue replacement. In particular, it is biocompatible, chemically stable and has an elastic modulus similar to that of natural bone (Gu et al., 2021). This material is widely studied for another numerous application such as dental implants (Sarot et al., 2010), orthopaedic (Ma et al., 2021), and spine implants (Mavrogenis et al., 2014). However, this material is bioinert and exhibits poor osteoconduction, which can lead to clinical failure. Another disadvantage is the poor antibacterial activity. These properties can be modified by additives or surface treatment. Since calcium phosphate occurs naturally in bone, many studies have focused on these materials for bone TE. For example, in research by Manzoor et al., 2021, hydroxyapatite was added to PEEK. The bioactivity was investigated and the formation of apatite was observed on the surfaces of samples. Other publications of Abdulkareem et al., 2019 focused on the antibacterial activity of chitosan-enriched PEEK-hydroxyapatite coatings. Based on this study, it was summarized that PEEK-chitosan-hydroxyapatite coatings have broad-spectrum antibacterial activity with potential for biomedical applications. However, the type of mineral additive can affect the determining the properties of the composites. As summarized in the study by Sikder et al., 2020, the addition of amorphous magnesium phosphate to PEEK enhanced biological activity and helped to significantly increase pre-osteoblast cellular response. This indicates that phosphate-based minerals such as farringtonite $Mg_3(PO_4)_2$ will positively affect the final properties of the biomaterial.

Most publications deal with the production of PEEK materials using 3D printing (Manzoor et al., 2021), extrusion (Tseng et al., 2018), or injection molding (Sagomonyants et al., 2008). Nevertheles, another option of manufacturing seems to be the manually hot-pressed technique. This method of preparation PEEK with farringtonite was used in our submitted paper by **Martínková M.**, Zárybnická L., Viani A., Killinger M., Mácová P., Sedláček T., Oralová V., Klepárník K. and Humpolíček P. entitled *"Polyetheretherketone Bioactivity Induced by Farringtonite: The Effect on Mineralization and Differentiation of Osteoblasts"* (**APPENDIX I**). Initially, the farringtonite material, which was synthesized from an analytical grade powder mixture, was characterized by XRPD. Then the particle mean diameter and specific surface area

of the powder was measured. The results were consistent with those from the farringtonite powder proposed for bioapplication. Main part of this work focused on characterization of physical-chemical and mechanical properties of grafts for bone TE. Fourier transform infrared (FTIR) maps were obtained to determine the distribution of farringtonite on the PEEK graft surface. The maps showed relatively homogeneous distribution of farringtonite in the PEEK matrix. Since this material is intended for use in bone TE, mechanical properties are important. Trabecular bone is estimated to have a modulus of elasticity around 5.4 GPa (Choi et al., 1990) to 14.8 GPa (Rho et al., 1993). There are studies that have measured a lower modulus of elasticity, approximately 1.3 GPa (Williams and Lewis, 1982). PEEK matrix had Young's modulus 5.8 GPa and as the concentration of the mineral additive increased, Young's modulus increased to 7.9 GPa (for more details see attached **APPENDIX I**). In order to determine whether osteoblasts affect grafts, the surface properties of grafts were tested before and after bioassays. As mentioned in the theoretical part of the thesis, the biomaterial surface influences cell adhesion and proliferation. The contact angle of the PEEK grafts was measured, which was approximately 75°. The results are consistent with the publication by Ren et al., 2018. Measurements after bioassays showed lower contact angle values, this could be due to protein binding to the surface.

One of the studies by Sikder et al., 2020 dealt with the preparation of PEEK with the additive amorphous magnesium phosphate. In this research, the material was processed using 3D printing. The research also confirmed that the incorporation of amorphous magnesium phosphate increased the bioactivity of PEEK and promoted a significant increase in the adhesion and proliferation of preosteoblasts. In our research (**APPENDIX I**) cytotoxicity was determined on a mouse fibroblast line. There was a slight decrease in cell viability below the cytotoxicity threshold. On the other hand, the results from cell adhesion and proliferation of osteoblast were comparable to the reference surfaces and even higher in the case of PEEK with 1% farringtonite. It was also found that the addition of farringtonite led to the mineralization process. Overall, the bone grafts made of PEEK and farringtonite was biocompatible, bioactive and could be used for treatement of bone defects and disiases. This material could also be further modifies using a surface coating to make it stimuli responsive.

10.1 Scaffolds for soft TE

Soft tissues play a crucial role in connecting, supporting, and enveloping various structures and organs within the body encompassing skeletal muscles, tendon vessels, and the nerves that supply them. Additionally, vital organs like the heart, brain, liver, and kidney are classified as soft tissues. Unfortunately, acute or chronic injuries can result in temporary or permanent damage to these organs and soft tissues. In cases of severe damage, the body's natural physiological repair

and restoration mechanisms may be insufficient. To address this, TE scaffolds have emerged as a promising clinical solution for repair or regeneration.

3) *Cellulose combined with conductive polypyrrole* has potential applications in biomedicine due to its unique mechanical, biochemical and physical properties. Cellulose is studied for its biocompatibility and possibility of tunable mechanical properties. Cellulose could be prepared in different forms such as nanocrystals (Abraham et al., 2017), nanofibrils (Olsson et al., 2010), hydrogels (Kundu et al., 2014) etc. When neural TE is considered, the addition of CPs is often studied. Publication by Zha et al., 2020 concerned with electrospun cellulose in combination of CPs (such as poly N-vinylpyrrole and Poly(3-hexylthiophene)) incorporated through *in situ* polymerization. *In vivo* cytocompatibility testing revealed that the scaffolds with CPs exhibited cell adhesion and proliferation. In research paper by Thunberg et al., 2015 *in situ* polymerization of PPy on electrospun cellulose nanofibers was described. During the investigation, it was found that no tested concentration of PPy does not cause cytotoxicity. Also, the results suggested that the addition of PPy helped cell adhesion and affected the differentiation of human neuroblastoma cell line. Nevertheless, this type of preparation often led to the inhomogeneous distribution of PPy in the matrix which caused inhomogeneous properties. In addition, PPy is often flaking off the surface. A stronger bond between the polypyrrole and the matrix could solve this problem.

However, none of the studies suggested the possibility of covalently binded PPy. This is possible due to condensation reaction between pyrrole cycles and aldehyde groups of dialdehydes of polysaccharides. For this reason, cellulose in our investigation was partily oxidized to create cellulose dialdehydes (SEM photographes of cellulose nanofibers see in Fig. 23). This idea is described in our patent that is currently under review.

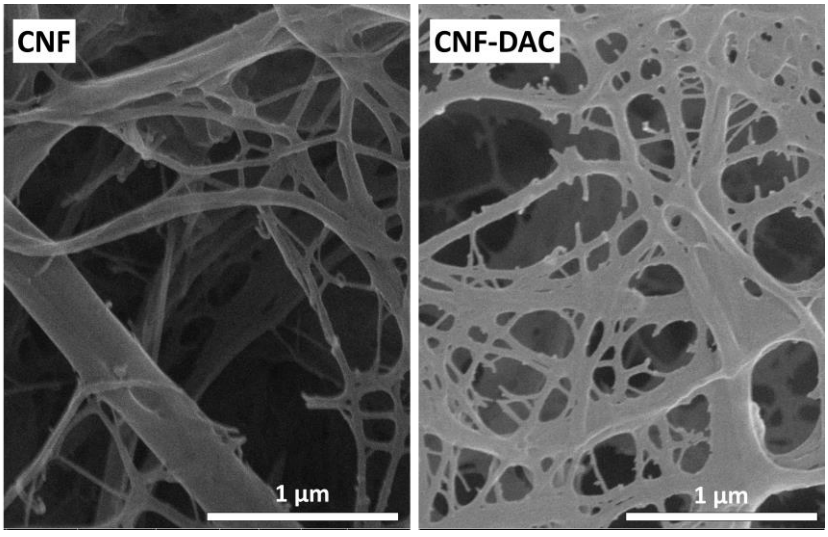

Fig. 23 SEM photographs of CNF and CNF-DAC suspensions

Subsequently, composites with covalently bound PPy were prepared. PPy was deposited on the CNF-DAC using template-controlled polymerization. SEM analysis revealed the presence of PPy grains on composites CNF-DAC-PPy in all samples, with the amount of deposited PPy increasing with increasing ratio of pyrrole to aldehyde groups during synthesis (Fig. 24).

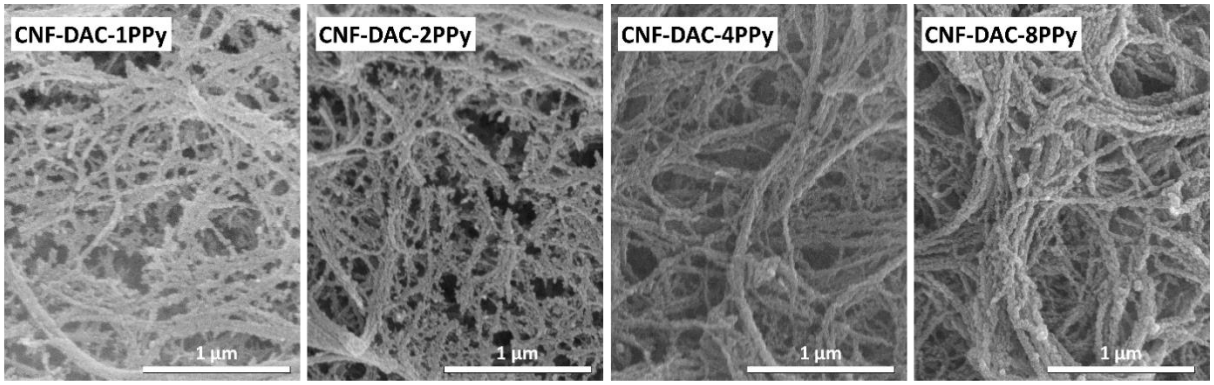

Fig. 24 SEM photographs of CNF-DAC with four different concentraion of PPy

CNF-DAC-2PPy and CNF-DAC-8PPy samples (n_{py} : n_{CHO} 2:1 and 8:1) were selected for further analysis. The conductivity was measured using the Van der Pauw four-electrode method (Keithley 6517B digital electrometer; Keithley 2410 voltage source; Keithley 7002 scanner). The specific conductivity of the CNF-DAC-2PPy sample was 0.708 mS/cm, while that of the 8PPy sample was 0.91 S/cm, which is due to the larger amount of deposited PPy.

To show the advantage of a stronger covalent bond, composites of unoxidized CNFs were also prepared in an analogous manner to the preparation of CNF-DAC-2PPy-8PPy. These samples are hereinafter referred to as CNF-2PPy-8PPy. These composites without cellulose dialdehydes had PPy attached by weak bonding interactions and thus were more susceptible to mechanical damage. CNF-DAC-2PPy-8PPy and CNF-2PPy-8PPy subjected to mechanical degradation in 30 min sonication using an MS 73 micro tip ultrasonicator with a Bandelin Sonopuls HD 2070. The composites prepared using unoxidized CNF fibers have lost a significant part of the deposited PPy layer. Especially in the CNF-2PPy samples where the PPy layer is almost completely absent, the PPy layer is still present in the CNF-DAC-2PPy and CNF-DAC-8PPy samples. The differences between the CNF and CNF-DAC samples are also apparent on a macroscopic scale, with much less fragmentation due to ultrasound in the CNF-DAC samples than in the CNF series. See details of the petri dishes in Fig. 25.

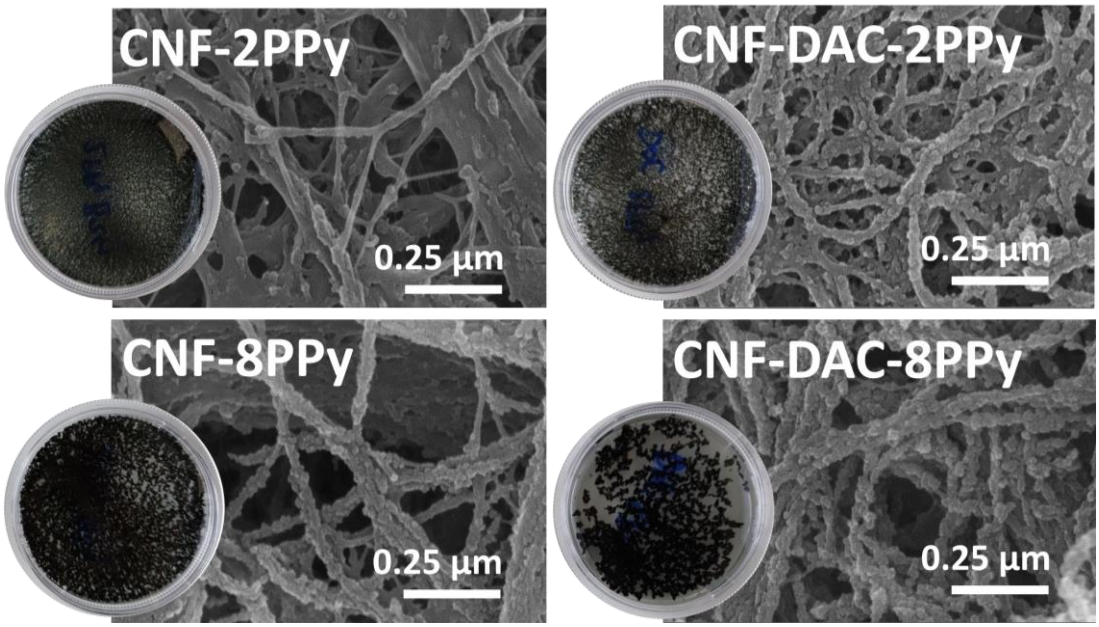

Fig. 25 SEM analysis of CNF-2PPy, CNF-DAC-2PPy, CNF-8PPy, CNF-DAC-8PPy after 30 min of sonication, demonstrating PPy layer damage in samples of the CNF-PPy series; Petri dishes with samples after sonication to compare fragmentation of samples after sonication

Thus, covalent anchoring leads to an increase in the coverage efficiency of the dialdehyde polysaccharide and an increase in the flaking resistance of the deposited polypyrrole layer from the matrix while maintaining the electrical conductivity of the as-prepared composites.

Furthermore, during my studies I was involved in testing the biological properties of conducting polymers. First co-authorship is in research by Skopalová K., Radaszkiewicz K.A., Kašpárková V., Stejskal J., Bober P., Junkar I., Mozetič M., Capáková Z., Lehocký M., **Kašparová M.**, Pacherník J., Humpolíček P., 2021. *Modulation of Differentiation of Embryonic Stem Cells by Polypyrrole: The Impact on Neurogenesis*. International Journal of Molecular Sciences 22, 501. Second publication by Gupta S., Acharya U., Pištěková H., Taboubi O., Morávková Z, **Kašparová M.**, Humpolíček P., Bober P., 2021. *Tuning the Conductivity, Morphology, and Capacitance with Enhanced Antibacterial Properties of Polypyrrole by Acriflavine Hydrochloride.* ACS Appl. Polym. Mater. 3, 6063–6069. In the third article the cytotoxicity of cryogels was tested together with the proliferation of the NIH 3T3 cell line. Milakin K.A., Morávková Z., Acharya U., **Kašparová M.**, Breitenbach S., Taboubi O., Hodan J., Hromádková J., Unterweger C., Humpolíček P., Bober P., 2021. *Enhancement of conductivity, mechanical and biological properties of polyaniline-poly(N-vinylpyrrolidone) cryogels by phytic acid*. Polymer 217, 123450.

Another paper where I tested cytotoxicity was by Musilová L., Achbergerová E., Vítková L., Kolařík R., **Martínková M.**, Minařík A., Mráček A., Humpolíček P., Pecha J., 2022. *Cross-Linked Gelatine by Modified Dextran as a Potential Bioink Prepared by a Simple and Non-Toxic Process*. Polymers 14, 391. In this research, the distribution of fixed and contrast-stained cells in a 3D printed structure was investigated.

11.CONTRIBUTION TO SCIENCE

Stimuli-responsive materials for tissue engineering are frequent subjects of research. Researchers are exploring a range of stimuli such as temperature, light, pH, magnetic fields, and electric fields with the aim of harnessing their potential to alter the properties, interactions, structure, and dimensions of materials. These stimuli-responsive materials hold great promise in the biomedical sector, field of TE, but also in drug delivery systems for diagnostics and treatment purposes. Despite a notable increase in the number of publications concerning stimuli-responsive biomaterials in recent years, there are still encountering challenges related to the fabrication methods and the composition of the material that would provide the cell-instructive potential.

Part of this work is focused on bones TE. The specificity of response to stimuli and the ability to respond to stimuli is essential for bone TE. When bone is mechanically deformed it generates a small electrical current that aids bone regeneration. Therefore, the possibility of electrical field stimulation is mainly investigated in this work, so this work also focuses on conducting polymers. However, mechanical fragility and poor processability of CPs limit their use. Therefore, here we come up with a solution based on a combination of materials that have suitable bulk properties (ceramic – ARTICLE I, PEEK - APPENDIX I) for bone TE with a thin conducting polymer film (pristine or prepared in colloidal dispersion mode ARTICLE I) on the surface of the material. The main contributions of this research to science include an innovative approach of surface modification by films of conductive polymers such as or prepared in colloidal dispersion mode. These modifications lead to different surface characteristics but also significantly change the cytocompatibility of materials. Coatings based on conductive polymers and biopolymers are electrically-conductive and cytocompatible.

Another achievement is in the new way of biomaterials preparation. This work introduces two manufacturing options that are not commonly used, yet enable the production of personalized medical devices. In our work (ARTICLE I) was declared that not only the architecture but also the porosity can be controlled using Powder injection molding technology moreover using an environmentally friendly approach. The second used fabrication method (APPENDIX I) was used for the bone graft of PEEK prepared by manually hot-pressed technique. This material is not stimuli-responsive but has suitable properties for bone TE. Due to the lack of time, it was not possible to finalize the surface modification or introduce the CP into the structure of PEEK grafts to be stimuli-responsive.

The last present study introduces a novel method for the preparation of conductive composites based on PPy and polysaccharide dialdehydes. Covalent bonding

of PPy on polysaccharide dialdehydes enhances the homogeneity of decoration efficiency, improves the resistance of the deposited polypyrrole layer against flaking from the matrix, and provides the electrical conductivity of the composites. To summarize the main contribution of this disertation to science is the extension of knowledge about the preparation of CPs based stimuli-responsive biomaterials.

REFERENCES

Abdulkareem, M.H., Abdalsalam, A.H., Bohan, A.J., 2019. Influence of chitosan on the antibacterial activity of composite coating (PEEK /HAp) fabricated by electrophoretic deposition. Progress in Organic Coatings 130, 251–259. https://doi.org/10.1016/j.porgcoat.2019.01.050

Abraham, E., Weber, D.E., Sharon, S., Lapidot, S., Shoseyov, O., 2017. Multifunctional Cellulosic Scaffolds from Modified Cellulose Nanocrystals. ACS Appl. Mater. Interfaces 9, 2010–2015. https://doi.org/10.1021/acsami.6b13528

Adekogbe, I., Ghanem, A., 2005. Fabrication and characterization of DTBP-crosslinked chitosan scaffolds for skin tissue engineering. Biomaterials 26, 7241–7250. https://doi.org/10.1016/j.biomaterials.2005.05.043

Ahmed El-Said, W., Yea, C.-H., Jung, M., Kim, H., Choi, J.-W., 2010. Analysis of effect of nanoporous alumina substrate coated with polypyrrole nanowire on cell morphology based on AFM topography. Ultramicroscopy 110, 676–681. https://doi.org/10.1016/j.ultramic.2010.02.031

Ahmed, S., Chauhan, V.M., Ghaemmaghami, A.M., Aylott, J.W., 2019. New generation of bioreactors that advance extracellular matrix modelling and tissue engineering. Biotechnol Lett 41, 1–25. https://doi.org/10.1007/s10529-018-2611-7

Alvarez, K., Nakajima, H., 2009. Metallic Scaffolds for Bone Regeneration. Materials 2, 790–832. https://doi.org/10.3390/ma2030790

Annesini, M.C., Marrelli, L., Piemonte, V., Turchetti, L., 2016. Artificial organ engineering. Springer Berlin Heidelberg, New York, NY.

Anselme, K., Ploux, L., Ponche, A., 2010. Cell/Material Interfaces: Influence of Surface Chemistry and Surface Topography on Cell Adhesion. Journal of Adhesion Science and Technology 24, 831–852. https://doi.org/10.1163/016942409X12598231568186

Aydemir, N., Malmström, J., Travas-Sejdic, J., 2016. Conducting polymer based electrochemical biosensors. Phys. Chem. Chem. Phys. 18, 8264–8277. https://doi.org/10.1039/C5CP06830D

Azaman, F.A., Zhou, K., Blanes-Martínez, M. del M., Brennan Fournet, M., Devine, D.M., 2022. Bioresorbable Chitosan-Based Bone Regeneration Scaffold Using Various Bioceramics and the Alteration of Photoinitiator Concentration in an Extended UV Photocrosslinking Reaction. Gels 8, 696. https://doi.org/10.3390/gels8110696

Balint, R., Cassidy, N.J., Cartmell, S.H., 2014. Conductive polymers: Towards a smart biomaterial for tissue engineering. Acta Biomaterialia 10, 2341–2353. https://doi.org/10.1016/j.actbio.2014.02.015

Bartee, L., 2018. General Biology I: Survey of Cellular Biology.

Ben-Nissan, B., Cazalbou, S., Choi, A.H., 2019. Bioceramics, in: Encyclopedia of Biomedical Engineering. Elsevier, pp. 16–33. https://doi.org/10.1016/B978-0-12-801238-3.99867-2

Bertazzo, S., Zambuzzi, W.F., Da Silva, H.A., Ferreira, C.V., Bertran, C.A., 2009. Bioactivation of alumina by surface modification: a possibility for improving the applicability of alumina in bone and oral repair. Clinical Oral Implants Research 20, 288–293. https://doi.org/10.1111/j.1600-0501.2008.01642.x

Berthiaume, F., Yarmush, M.L., 2003. Tissue Engineering, in: Encyclopedia of Physical Science and Technology. Elsevier, pp. 817–842. https://doi.org/10.1016/B0-12-227410-5/00783-3

Bettinger, C.J., Langer, R., Borenstein, J.T., 2009. Engineering Substrate Topography at the Micro- and Nanoscale to Control Cell Function. Angew. Chem. Int. Ed. 48, 5406–5415. https://doi.org/10.1002/anie.200805179

Bilodeau, C., Goltsis, O., Rogers, I.M., Post, M., 2020. Limitations of recellularized biological scaffolds for human transplantation. J Tissue Eng Regen Med 14, 521–538. https://doi.org/10.1002/term.3004

Bishop, A.E., Buttery, L.D.K., Polak, J.M., 2002. Embryonic stem cells. J. Pathol. 197, 424–429. https://doi.org/10.1002/path.1154

Blitterswijk, C.A. van, Thomsen, P., 2008. Tissue engineering, 1st ed. ed, Academic Press series in biomedical engineering. Academic Press, London Burlington, MA.

Bobbert, F.S.L., Zadpoor, A.A., 2017. Effects of bone substitute architecture and surface properties on cell response, angiogenesis, and structure of new bone. J. Mater. Chem. B 5, 6175–6192. https://doi.org/10.1039/C7TB00741H

Boniecki, M., Sadowski, T., Gołębiewski, P., Węglarz, H., Piątkowska, A., Romaniec, M., Krzyżak, K., Łosiewicz, K., 2020. Mechanical properties of alumina/zirconia composites. Ceramics International 46, 1033–1039. https://doi.org/10.1016/j.ceramint.2019.09.068

Cabezas, M.D., Meckes, B., Mirkin, C.A., Mrksich, M., 2019. Subcellular Control over Focal Adhesion Anisotropy, Independent of Cell Morphology, Dictates Stem Cell Fate. ACS Nano 13, 11144–11152. https://doi.org/10.1021/acsnano.9b03937

Capanema, N.S.V., Mansur, A.A.P., de Jesus, A.C., Carvalho, S.M., de Oliveira, L.C., Mansur, H.S., 2018. Superabsorbent crosslinked carboxymethyl cellulose-PEG hydrogels for potential wound dressing applications. International Journal of Biological Macromolecules 106, 1218–1234. https://doi.org/10.1016/j.ijbiomac.2017.08.124

Carletti, E., Motta, A., Migliaresi, C., 2011. Scaffolds for Tissue Engineering and 3D Cell Culture, in: Haycock, J.W. (Ed.), 3D Cell Culture, Methods in Molecular Biology. Humana Press, Totowa, NJ, pp. 17–39. https://doi.org/10.1007/978-1-60761-984-0_2

Case, C., Langkamer, V., James, C., Palmer, M., Kemp, A., Heap, P., Solomon, L., 1994. Widespread dissemination of metal debris from implants. The

Journal of Bone and Joint Surgery. British volume 76-B, 701–712. https://doi.org/10.1302/0301-620X.76B5.8083255
Castner, D.G., Ratner, B.D., 2002. Biomedical surface science: Foundations to frontiers. Surface Science 500, 28–60. https://doi.org/10.1016/S0039-6028(01)01587-4
Cellulose C6288, Sigma-Aldrich [WWW Document], n.d. . MERCK. URL http://www.sigmaaldrich.com/ (accessed 5.18.23).
Chang, K.-A., Kim, J.W., Kim, J.A., Lee, S., Kim, S., Suh, W.H., Kim, H.-S., Kwon, S., Kim, S.J., Suh, Y.-H., 2011. Biphasic Electrical Currents Stimulation Promotes both Proliferation and Differentiation of Fetal Neural Stem Cells. PLoS ONE 6, e18738. https://doi.org/10.1371/journal.pone.0018738
Chapman, C.A.R., Cuttaz, E.A., Goding, J.A., Green, R.A., 2020. Actively controlled local drug delivery using conductive polymer-based devices. Applied Physics Letters 116, 010501. https://doi.org/10.1063/1.5138587
Chaudhuri, J., Al-Rubeai, M. (Eds.), 2005. Bioreactors for tissue engineeering: principles, design and operation. Springer, Dordrecht ; [London].
Chellat, F., Tabrizian, M., Dumitriu, S., Chornet, E., Magny, P., Rivard, C.-H., Yahia, L., 2000. In vitro andin vivo biocompatibility of chitosan-xanthan polyionic complex. J. Biomed. Mater. Res. 51, 107–116. https://doi.org/10.1002/(SICI)1097-4636(200007)51:1<107::AID-JBM14>3.0.CO;2-F
Chen, H.-C., Hu, Y.-C., 2006. Bioreactors for tissue engineering. Biotechnol Lett 28, 1415–1423. https://doi.org/10.1007/s10529-006-9111-x
Chen, J., Patnaik, S.S., Prabhu, R.K., Priddy, L.B., Bouvard, J.-L., Marin, E., Horstemeyer, M.F., Liao, J., Williams, L.N., 2019. Mechanical Response of Porcine Liver Tissue under High Strain Rate Compression. Bioengineering 6, 49. https://doi.org/10.3390/bioengineering6020049
Chiang, J.-C., MacDiarmid, A.G., 1986. 'Polyaniline': Protonic acid doping of the emeraldine form to the metallic regime. Synthetic Metals 13, 193–205. https://doi.org/10.1016/0379-6779(86)90070-6
Choi, K., Kuhn, J.L., Ciarelli, M.J., Goldstein, S.A., 1990. The elastic moduli of human subchondral, trabecular, and cortical bone tissue and the size-dependency of cortical bone modulus. Journal of Biomechanics 23, 1103–1113. https://doi.org/10.1016/0021-9290(90)90003-L
Chowdhury, A.D., Takemura, K., Li, T.-C., Suzuki, T., Park, E.Y., 2019. Electrical pulse-induced electrochemical biosensor for hepatitis E virus detection. Nat Commun 10, 3737. https://doi.org/10.1038/s41467-019-11644-5
Chupa, J.M., Foster, A.M., Sumner, S.R., Madihally, S.V., Matthew, H.W.T., 2000. Vascular cell responses to polysaccharide materials: Biomaterials 21, 2315–2322. https://doi.org/10.1016/S0142-9612(00)00158-7

Clementi, A., Egger, D., Charwat, V., Kasper, C., 2018. Cell Culture Conditions: Cultivation of Stem Cells Under Dynamic Conditions, in: Gimble, J.M., Marolt, D., Oreffo, R., Redl, H., Wolbank, S. (Eds.), Cell Engineering and Regeneration. Springer International Publishing, Cham, pp. 1–33. https://doi.org/10.1007/978-3-319-37076-7_58-1

Cooke, M.E., Ramirez-GarciaLuna, J.L., Rangel-Berridi, K., Park, H., Nazhat, S.N., Weber, M.H., Henderson, J.E., Rosenzweig, D.H., 2020. 3D Printed Polyurethane Scaffolds for the Repair of Bone Defects. Front. Bioeng. Biotechnol. 8, 557215. https://doi.org/10.3389/fbioe.2020.557215

Dahiya, M.S., Tomer, V.K., Duhan, S., 2019. Bioactive glass/glass ceramics for dental applications, in: Applications of Nanocomposite Materials in Dentistry. Elsevier, pp. 1–25. https://doi.org/10.1016/B978-0-12-813742-0.00001-8

Dalby, M., Gadegaard, N., G. Curtis, A., C. Oreffo, R., 2007. Nanotopographical Control of Human Osteoprogenitor Differentiation. CSCR 2, 129–138. https://doi.org/10.2174/157488807780599220

Daley, W.P., Peters, S.B., Larsen, M., 2008. Extracellular matrix dynamics in development and regenerative medicine. Journal of Cell Science 121, 255–264. https://doi.org/10.1242/jcs.006064

Dash, R., Ragauskas, A.J., 2012. Synthesis of a novel cellulose nanowhisker-based drug delivery system. RSC Adv. 2, 3403. https://doi.org/10.1039/c2ra01071b

Davis, J., McLister, A., 2016. Passive and Interactive Dressing Materials, in: Smart Bandage Technologies. Elsevier, pp. 93–144. https://doi.org/10.1016/B978-0-12-803762-1.00004-7

de Viteri, V.S., Fuentes, E., 2013. Titanium and Titanium Alloys as Biomaterials, in: Gegner, J. (Ed.), Tribology - Fundamentals and Advancements. InTech. https://doi.org/10.5772/55860

Ferrari, M., Cirisano, F., Morán, M.C., 2019. Mammalian Cell Behavior on Hydrophobic Substrates: Influence of Surface Properties. Colloids and Interfaces 3, 48. https://doi.org/10.3390/colloids3020048

Fink, H., Hong, J., Drotz, K., Risberg, B., Sanchez, J., Sellborn, A., 2011. An in vitro study of blood compatibility of vascular grafts made of bacterial cellulose in comparison with conventionally-used graft materials. J. Biomed. Mater. Res. 97A, 52–58. https://doi.org/10.1002/jbm.a.33031

Fomo, G., Waryo, T., Feleni, U., Baker, P., Iwuoha, E., 2019. Electrochemical Polymerization, in: Jafar Mazumder, M.A., Sheardown, H., Al-Ahmed, A. (Eds.), Functional Polymers, Polymers and Polymeric Composites: A Reference Series. Springer International Publishing, Cham, pp. 105–131. https://doi.org/10.1007/978-3-319-95987-0_3

Freimoser, F.M., Jakob, C.A., Aebi, M., Tuor, U., 1999. The MTT [3-(4,5-Dimethylthiazol-2-yl)-2,5-Diphenyltetrazolium Bromide] Assay Is a Fast and Reliable Method for Colorimetric Determination of Fungal Cell

Densities. Appl Environ Microbiol 65, 3727–3729. https://doi.org/10.1128/AEM.65.8.3727-3729.1999
Gad, S.C., Gad-McDonald, S., 2015. Biomaterials, Medical Devices, and Combination Products: Biocompatibility Testing and Safety Assessment, 0 ed. CRC Press. https://doi.org/10.1201/b19086
Gelmi, A., Schutt, C.E., 2021. Stimuli-Responsive Biomaterials: Scaffolds for Stem Cell Control. Adv. Healthcare Mater. 10, 2001125. https://doi.org/10.1002/adhm.202001125
Ghammami, S., Sajadi, S., 2005. Tetrabutylammonium fluorochromate(VI)(TBFAC): A mild and efficient reagent for oxidation of organic substrates. J Serb Chem Soc 70, 1243–1248. https://doi.org/10.2298/JSC0511243G
Ghosh, S., Majumdar, D., 2021. Chemical Synthesis of Conducting Polymers Nanostructures, in: Ghosh, S. (Ed.), Conjugated Polymer Nanostructures for Energy Conversion and Storage Applications. Wiley, pp. 43–83. https://doi.org/10.1002/9783527820115.ch2
Green, R.A., Lovell, N.H., Wallace, G.G., Poole-Warren, L.A., 2008. Conducting polymers for neural interfaces: Challenges in developing an effective long-term implant. Biomaterials 29, 3393–3399. https://doi.org/10.1016/j.biomaterials.2008.04.047
Gregor, A., Filová, E., Novák, M., Kronek, J., Chlup, H., Buzgo, M., Blahnová, V., Lukášová, V., Bartoš, M., Nečas, A., Hošek, J., 2017. Designing of PLA scaffolds for bone tissue replacement fabricated by ordinary commercial 3D printer. J Biol Eng 11, 31. https://doi.org/10.1186/s13036-017-0074-3
Grimnes, S., Martinsen, Ø.G., 2015. History of Bioimpedance and Bioelectricity, in: Bioimpedance and Bioelectricity Basics. Elsevier, pp. 495–504. https://doi.org/10.1016/B978-0-12-411470-8.00011-8
Gu, X., Sun, X., Sun, Y., Wang, J., Liu, Y., Yu, K., Wang, Y., Zhou, Y., 2021. Bioinspired Modifications of PEEK Implants for Bone Tissue Engineering. Front. Bioeng. Biotechnol. 8, 631616. https://doi.org/10.3389/fbioe.2020.631616
Guruswamy Damodaran, R., Vermette, P., 2018. Tissue and organ decellularization in regenerative medicine. Biotechnol. Prog. 34, 1494–1505. https://doi.org/10.1002/btpr.2699
Hao, J., Zhang, Y., Jing, D., Shen, Y., Tang, G., Huang, S., Zhao, Z., 2015. Mechanobiology of mesenchymal stem cells: Perspective into mechanical induction of MSC fate. Acta Biomaterialia 20, 1–9. https://doi.org/10.1016/j.actbio.2015.04.008
Hariyadi, D.M., Islam, N., 2020. Current Status of Alginate in Drug Delivery. Advances in Pharmacological and Pharmaceutical Sciences 2020, 1–16. https://doi.org/10.1155/2020/8886095

Heinze, J., Frontana-Uribe, B.A., Ludwigs, S., 2010. Electrochemistry of Conducting Polymers—Persistent Models and New Concepts. Chem. Rev. 110, 4724–4771. https://doi.org/10.1021/cr900226k

Hermawan, H., Ramdan, D., P. Djuansjah, J.R., 2011. Metals for Biomedical Applications, in: Fazel, R. (Ed.), Biomedical Engineering - From Theory to Applications. InTech. https://doi.org/10.5772/19033

Hickey, R.J., Pelling, A.E., 2019. Cellulose Biomaterials for Tissue Engineering. Front. Bioeng. Biotechnol. 7, 45. https://doi.org/10.3389/fbioe.2019.00045

Hirsh, S.L., McKenzie, D.R., Nosworthy, N.J., Denman, J.A., Sezerman, O.U., Bilek, M.M.M., 2013. The Vroman effect: Competitive protein exchange with dynamic multilayer protein aggregates. Colloids and Surfaces B: Biointerfaces 103, 395–404. https://doi.org/10.1016/j.colsurfb.2012.10.039

Huang, J., Best, S., 2014. Ceramic biomaterials for tissue engineering, in: Tissue Engineering Using Ceramics and Polymers. Elsevier, pp. 3–34. https://doi.org/10.1533/9780857097163.1.3

Humpolíček, P., Radaszkiewicz, K.A., Capáková, Z., Pacherník, J., Bober, P., Kašpárková, V., Rejmontová, P., Lehocký, M., Ponížil, P., Stejskal, J., 2018. Polyaniline cryogels: Biocompatibility of novel conducting macroporous material. Sci Rep 8, 135. https://doi.org/10.1038/s41598-017-18290-1

Inzelt, G., 2008. Chemical and Electrochemical Syntheses of Conducting Polymers, in: Conducting Polymers, Monographs in Electrochemistry. Springer Berlin Heidelberg, Berlin, Heidelberg, pp. 123–148. https://doi.org/10.1007/978-3-540-75930-0_4

ISO 10993-1:2018, Biological evaluation of medical devices — Part 1: Evaluation and testing within a risk management process

ISO 10993-5:2009, Biological evaluation of medical devices — Part 5: Tests for in vitro cytotoxicity

ISO 10993-12:2009, Biological evaluation of medical devices — Part 12: Sample preparation and reference materials

Jasenská, D., Kašpárková, V., Radaszkiewicz, K.A., Capáková, Z., Pacherník, J., Trchová, M., Minařík, A., Vajďák, J., Bárta, T., Stejskal, J., Lehocký, M., Truong, T.H., Moučka, R., Humpolíček, P., 2021. Conducting composite films based on chitosan or sodium hyaluronate. Properties and cytocompatibility with human induced pluripotent stem cells. Carbohydrate Polymers 253, 117244. https://doi.org/10.1016/j.carbpol.2020.117244

Jiang, L.-B., Su, D.-H., Liu, P., Ma, Y.-Q., Shao, Z.-Z., Dong, J., 2018. Shape-memory collagen scaffold for enhanced cartilage regeneration: native collagen versus denatured collagen. Osteoarthritis Cartilage 26, 1389–1399. https://doi.org/10.1016/j.joca.2018.06.004

K, N., Rout, C.S., 2021. Conducting polymers: a comprehensive review on recent advances in synthesis, properties and applications. RSC Adv. 11, 5659–5697. https://doi.org/10.1039/D0RA07800J

Kaarj, Yoon, 2019. Methods of Delivering Mechanical Stimuli to Organ-on-a-Chip. Micromachines 10, 700. https://doi.org/10.3390/mi10100700

Kašpárková, V., Humpolíček, P., Capáková, Z., Bober, P., Stejskal, J., Trchová, M., Rejmontová, P., Junkar, I., Lehocký, M., Mozetič, M., 2017. Cell-compatible conducting polyaniline films prepared in colloidal dispersion mode. Colloids and Surfaces B: Biointerfaces 157, 309–316. https://doi.org/10.1016/j.colsurfb.2017.05.066

Kearns, V.R., Mcmurray, R.J., Dalby, M.J., 2011. Biomaterial surface topography to control cellular response: technologies, cell behaviour and biomedical applications, in: Surface Modification of Biomaterials. Elsevier, pp. 169–201. https://doi.org/10.1533/9780857090768.1.169

Khan, M., Cantù, E., Tonello, S., Serpelloni, M., Lopomo, N., Sardini, E., 2019. A Review on Biomaterials for 3D Conductive Scaffolds for Stimulating and Monitoring Cellular Activities. Applied Sciences 9, 961. https://doi.org/10.3390/app9050961

Kim, W.-S., 2014. Cell Culture Bioreactors: Controls, Measurements, and Scale-Down Model, in: Baltz, R.H., Davies, J.E., Demain, A.L., Bull, A.T., Junker, B., Katz, L., Lynd, L.R., Masurekar, P., Reeves, C.D., Zhao, H. (Eds.), Manual of Industrial Microbiology and Biotechnology. ASM Press, Washington, DC, USA, pp. 676–684. https://doi.org/10.1128/9781555816827.ch48

Klein, T.J., Malda, J., Sah, R.L., Hutmacher, D.W., 2009. Tissue Engineering of Articular Cartilage with Biomimetic Zones. Tissue Engineering Part B: Reviews 15, 143–157. https://doi.org/10.1089/ten.teb.2008.0563

Kucekova, Z., Humpolicek, P., Kasparkova, V., Perecko, T., Lehocký, M., Hauerlandová, I., Sáha, P., Stejskal, J., 2014. Colloidal polyaniline dispersions: Antibacterial activity, cytotoxicity and neutrophil oxidative burst. Colloids and Surfaces B: Biointerfaces 116, 411–417. https://doi.org/10.1016/j.colsurfb.2014.01.027

Kucekova, Z., Kasparkova, V., Humpolicek, P., Sevcikova, P., Stejskal, J., 2013. Antibacterial properties of polyaniline-silver films. Chemical Papers 67. https://doi.org/10.2478/s11696-013-0385-x

Kumar, A., Nune, K.C., Misra, R.D.K., 2016. Electric field-mediated growth of osteoblasts – the significant impact of dynamic flow of medium. Biomater. Sci. 4, 136–144. https://doi.org/10.1039/C5BM00350D

Kumbar, S., Laurencin, C., Deng, M. (Eds.), 2014. Natural and synthetic biomedical polymers, First edition. ed. Elsevier, Amsterdam ; Boston.

Kundu, J., Pati, F., Shim, J.-H., Cho, D.-W., 2014. Rapid prototyping technology for bone regeneration, in: Rapid Prototyping of Biomaterials. Elsevier, pp. 289–314. https://doi.org/10.1016/B978-0-08-102663-2.00012-5

Langer, R., Vacanti, J.P., 1993. Tissue Engineering. Science 260, 920–926. https://doi.org/10.1126/science.8493529

Leali, P.T., Merolli, A., 2009. Fundamentals of Biomaterials, in: Merolli, Antonio, Joyce, T.J. (Eds.), Biomaterials in Hand Surgery. Springer Milan, Milano, pp. 1–11. https://doi.org/10.1007/978-88-470-1195-3_1

Lee, J.Y., 2013. Electrically Conducting Polymer-Based Nanofibrous Scaffolds for Tissue Engineering Applications. Polymer Reviews 53, 443–459. https://doi.org/10.1080/15583724.2013.806544

Lee, M.-S., Park, W.-S., Kim, Y., Ahn, W., Kwon, S.-H., Her, S., 2012. Intracellular ATP Assay of Live Cells Using PTD-Conjugated Luciferase. Sensors 12, 15628–15637. https://doi.org/10.3390/s121115628

Lee, S.J., Atala, A., Yoo, J.J. (Eds.), 2016. In situ tissue regeneration: host cell recruitment and biomaterial design. Academic Press is an imprint of Elsevier, London, United Kingdom ; San Diego, CA, USA.

Li, J., Wan, Y., Li, L., Liang, H., Wang, J., 2009. Preparation and characterization of 2,3-dialdehyde bacterial cellulose for potential biodegradable tissue engineering scaffolds. Materials Science and Engineering: C 29, 1635–1642. https://doi.org/10.1016/j.msec.2009.01.006

Li, L., Wang, Y., Pan, L., Shi, Ye, Cheng, W., Shi, Yi, Yu, G., 2015. A Nanostructured Conductive Hydrogels-Based Biosensor Platform for Human Metabolite Detection. Nano Lett. 15, 1146–1151. https://doi.org/10.1021/nl504217p

Li, S., Jasim, A., Zhao, W., School of Mechanical and Electronic Engineering, Wuhan University of Technology, Wuhan 430070, PR China, Fu, L., Ullah, M.W., Shi, Z., Yang, G., 2018. Fabrication of pH-electroactive Bacterial Cellulose/Polyaniline Hydrogel for the Development of a Controlled Drug Release System. ES Mater.Manuf. https://doi.org/10.30919/esmm5f120

Liboff, A.R., Shamos, M.H., 1971. Piezoelectric Effect in Dentin. J Dent Res 50, 516–516. https://doi.org/10.1177/00220345710500027901

Lindfors, T., Ivaska, A., 2002. pH sensitivity of polyaniline and its substituted derivatives. Journal of Electroanalytical Chemistry 531, 43–52. https://doi.org/10.1016/S0022-0728(02)01005-7

Liu, C., Matsunami, C., Shirosaki, Y., Miyazaki, T., 2015. Bioactive Co-Cr alloy for biomedical applications prepared by surface modification using self-assembled monolayers and poly-γ-glutamic acid. Dental Materials Journal 34, 707–712. https://doi.org/10.4012/dmj.2015-064

Liu, W., Kumar, J., Tripathy, S., Samuelson, L.A., 2002. Enzymatic Synthesis of Conducting Polyaniline in Micelle Solutions. Langmuir 18, 9696–9704. https://doi.org/10.1021/la0206357

Liu, X., Lin, T., Gao, Y., Xu, Z., Huang, C., Yao, G., Jiang, L., Tang, Y., Wang, X., 2012. Antimicrobial electrospun nanofibers of cellulose acetate and polyester urethane composite for wound dressing. J. Biomed. Mater. Res. 100B, 1556–1565. https://doi.org/10.1002/jbm.b.32724

Liu, Y., Peterson, D.A., Kimura, H., Schubert, D., 2002. Mechanism of Cellular 3-(4,5-Dimethylthiazol-2-yl)-2,5-Diphenyltetrazolium Bromide (MTT) Reduction. Journal of Neurochemistry 69, 581–593. https://doi.org/10.1046/j.1471-4159.1997.69020581.x

Loos, K. (Ed.), 2011. Biocatalysis in polymer chemistry. Wiley-VCH Verlag, Weinhem.

Lotfi, M., Nejib, M., Naceur, M., 2013. Cell Adhesion to Biomaterials: Concept of Biocompatibility, in: Pignatello, R. (Ed.), Advances in Biomaterials Science and Biomedical Applications. InTech. https://doi.org/10.5772/53542

Ma, H., Suonan, A., Zhou, J., Yuan, Q., Liu, L., Zhao, X., Lou, X., Yang, C., Li, D., Zhang, Y., 2021. PEEK (Polyether-ether-ketone) and its composite materials in orthopedic implantation. Arabian Journal of Chemistry 14, 102977. https://doi.org/10.1016/j.arabjc.2020.102977

Ma, P.X., 2014. Biomaterials and regenerative medicine.

Maity, S., Singha, K., Pandit, P., 2021. Advanced applications of green materials in electromagnetic shielding, in: Applications of Advanced Green Materials. Elsevier, pp. 265–292. https://doi.org/10.1016/B978-0-12-820484-9.00011-8

Majumdar, S., Mahanta, D., 2020. Deposition of an ultra-thin polyaniline coating on a TiO_2 surface by vapor phase polymerization for electrochemical glucose sensing and photocatalytic degradation. RSC Adv. 10, 17387–17395. https://doi.org/10.1039/D0RA01571G

Manzoor, F., Golbang, A., Jindal, S., Dixon, D., McIlhagger, A., Harkin-Jones, E., Crawford, D., Mancuso, E., 2021. 3D printed PEEK/HA composites for bone tissue engineering applications: Effect of material formulation on mechanical performance and bioactive potential. Journal of the Mechanical Behavior of Biomedical Materials 121, 104601. https://doi.org/10.1016/j.jmbbm.2021.104601

Marino, A.A., Gross, B.D., 1989. Piezoelectricity in cementum, dentine and bone. Archives of Oral Biology 34, 507–509. https://doi.org/10.1016/0003-9969(89)90087-3

Martin, I., Wendt, D., Heberer, M., 2004. The role of bioreactors in tissue engineering. Trends in Biotechnology 22, 80–86. https://doi.org/10.1016/j.tibtech.2003.12.001

Martínková, M., Hausnerová, B., Huba, J., Martínek, T., Káčerová, S., Kašpárková, V., Humpolíček, P., 2022. Powder injection molded ceramic scaffolds: The role of pores size and surface functionalization on the cytocompatibility. Materials & Design 224, 111274. https://doi.org/10.1016/j.matdes.2022.111274

Massoumi, B., Abbasian, M., Jahanban-Esfahlan, R., Mohammad-Rezaei, R., Khalilzadeh, B., Samadian, H., Rezaei, A., Derakhshankhah, H., Jaymand, M., 2020. A novel bio-inspired conductive, biocompatible, and adhesive

terpolymer based on polyaniline, polydopamine, and polylactide as scaffolding biomaterial for tissue engineering application. International Journal of Biological Macromolecules 147, 1174–1184. https://doi.org/10.1016/j.ijbiomac.2019.10.086

Matsiko, A., Levingstone, T.J., O'Brien, F.J., Gleeson, J.P., 2012. Addition of hyaluronic acid improves cellular infiltration and promotes early-stage chondrogenesis in a collagen-based scaffold for cartilage tissue engineering. Journal of the Mechanical Behavior of Biomedical Materials 11, 41–52. https://doi.org/10.1016/j.jmbbm.2011.11.012

Mavrogenis, A.F., Vottis, C., Triantafyllopoulos, G., Papagelopoulos, P.J., Pneumaticos, S.G., 2014. PEEK rod systems for the spine. Eur J Orthop Surg Traumatol 24, 111–116. https://doi.org/10.1007/s00590-014-1421-4

Mawad, D., Stewart, E., Officer, D.L., Romeo, T., Wagner, P., Wagner, K., Wallace, G.G., 2012. A Single Component Conducting Polymer Hydrogel as a Scaffold for Tissue Engineering. Advanced Functional Materials 22, 2692–2699. https://doi.org/10.1002/adfm.201102373

Mayeen, A., Kalarikkal, N., 2018. Development of ceramic-controlled piezoelectric devices for biomedical applications, in: Fundamental Biomaterials: Ceramics. Elsevier, pp. 47–62. https://doi.org/10.1016/B978-0-08-102203-0.00002-0

McCaig, C.D., Rajnicek, A.M., Song, B., Zhao, M., 2002. Has electrical growth cone guidance found its potential? Trends in Neurosciences 25, 354–359. https://doi.org/10.1016/S0166-2236(02)02174-4

Milne, I., Ritchie, R.O., Karihaloo, B.L. (Eds.), 2003. Comprehensive structural integrity, 1st ed. ed. Elsevier/Pergamon, Amsterdam ; Boston.

Miyamoto, T., Shibayama, K., 1973. Free-volume model for ionic conductivity in polymers. Journal of Applied Physics 44, 5372–5376. https://doi.org/10.1063/1.1662158

Mobini, S., Leppik, L., Thottakkattumana Parameswaran, V., Barker, J.H., 2017. *In vitro* effect of direct current electrical stimulation on rat mesenchymal stem cells. PeerJ 5, e2821. https://doi.org/10.7717/peerj.2821

Mohammadi, F., Mohammadi Samani, S., Tanideh, N., Ahmadi, F., 2018. Hybrid Scaffolds of Hyaluronic Acid and Collagen Loaded with Prednisolone: an Interesting System for Osteoarthritis. Adv Pharm Bull 8, 11–19. https://doi.org/10.15171/apb.2018.002

Monteiro, I.P., Shukla, A., Marques, A.P., Reis, R.L., Hammond, P.T., 2015. Spray-assisted layer-by-layer assembly on hyaluronic acid scaffolds for skin tissue engineering: Layer-By-Layer Assembly on Hyaluronic Acid Scaffolds for Skin Tissue Engineering. J. Biomed. Mater. Res. 103, 330–340. https://doi.org/10.1002/jbm.a.35178

Moreira, C.D.F., Carvalho, S.M., Florentino, R.M., França, A., Okano, B.S., Rezende, C.M.F., Mansur, H.S., Pereira, M.M., 2019. Injectable chitosan/gelatin/bioactive glass nanocomposite hydrogels for potential

bone regeneration: In vitro and in vivo analyses. International Journal of Biological Macromolecules 132, 811–821. https://doi.org/10.1016/j.ijbiomac.2019.03.237
Murphy, C.M., Haugh, M.G., O'Brien, F.J., 2010. The effect of mean pore size on cell attachment, proliferation and migration in collagen–glycosaminoglycan scaffolds for bone tissue engineering. Biomaterials 31, 461–466. https://doi.org/10.1016/j.biomaterials.2009.09.063
Murphy, W., Black, J., Hastings, G. (Eds.), 2016. Handbook of Biomaterial Properties.
Mwesigwa, E., Basit, A.W., 2016. An investigation into moisture barrier film coating efficacy and its relevance to drug stability in solid dosage forms. International Journal of Pharmaceutics 497, 70–77. https://doi.org/10.1016/j.ijpharm.2015.10.068
Nagasawa, M., Cooper, L.F., Ogino, Y., Mendonca, D., Liang, R., Yang, S., Mendonca, G., Uoshima, K., 2016. Topography Influences Adherent Cell Regulation of Osteoclastogenesis. J Dent Res 95, 319–326. https://doi.org/10.1177/0022034515616760
Nagase, K., Yamato, M., Kanazawa, H., Okano, T., 2018. Poly(N-isopropylacrylamide)-based thermoresponsive surfaces provide new types of biomedical applications. Biomaterials 153, 27–48. https://doi.org/10.1016/j.biomaterials.2017.10.026
Naghavi Alhosseini, S., Moztarzadeh, F., Karkhaneh, A., Dodel, M., Khalili, M., Eslami Arshaghi, T., Elahirad, E., Mozafari, M., 2019. Improved cellular response on functionalized polypyrrole interfaces. Journal Cellular Physiology 234, 15279–15287. https://doi.org/10.1002/jcp.28173
Nagy, A., Rossant, J., Nagy, R., Abramow-Newerly, W., Roder, J.C., 1993. Derivation of completely cell culture-derived mice from early-passage embryonic stem cells. Proc. Natl. Acad. Sci. U.S.A. 90, 8424–8428. https://doi.org/10.1073/pnas.90.18.8424
Niinomi, M., 2002. Recent metallic materials for biomedical applications. Metall and Mat Trans A 33, 477–486. https://doi.org/10.1007/s11661-002-0109-2
Nouri, A., Wen, C., 2015. Introduction to surface coating and modification for metallic biomaterials, in: Surface Coating and Modification of Metallic Biomaterials. Elsevier, pp. 3–60. https://doi.org/10.1016/B978-1-78242-303-4.00001-6
O'Brien, F.J., 2011. Biomaterials & scaffolds for tissue engineering. Materials Today 14, 88–95. https://doi.org/10.1016/S1369-7021(11)70058-X
Oliveira, N.M., Reis, R.L., Mano, J.F., 2017. Open Fluidics: A Cell Culture Flow System Developed Over Wettability Contrast-Based Chips. Adv. Healthcare Mater. 6, 1700638. https://doi.org/10.1002/adhm.201700638
Olsson, R.T., Azizi Samir, M.A.S., Salazar-Alvarez, G., Belova, L., Ström, V., Berglund, L.A., Ikkala, O., Nogués, J., Gedde, U.W., 2010. Making flexible magnetic aerogels and stiff magnetic nanopaper using cellulose nanofibrils

as templates. Nature Nanotech 5, 584–588. https://doi.org/10.1038/nnano.2010.155
Otero, T.F., Martinez, J.G., Arias-Pardilla, J., 2012. Biomimetic electrochemistry from conducting polymers. A review. Electrochimica Acta 84, 112–128. https://doi.org/10.1016/j.electacta.2012.03.097
Owen, J., 1989. Ionic Conductivity, in: Comprehensive Polymer Science and Supplements. Elsevier, pp. 669–686. https://doi.org/10.1016/B978-0-08-096701-1.00058-6
Pandey, A.K., Pandey, P.C., Agrawal, N.R., Das, I., 2018. Synthesis and characterization of dendritic polypyrrole silver nanocomposite and its application as a new urea biosensor: Research Article. J. Appl. Polym. Sci. 135, 45705. https://doi.org/10.1002/app.45705
Parisi, L., Toffoli, A., Ghezzi, B., Mozzoni, B., Lumetti, S., Macaluso, G.M., 2020. A glance on the role of fibronectin in controlling cell response at biomaterial interface. Japanese Dental Science Review 56, 50–55. https://doi.org/10.1016/j.jdsr.2019.11.002
Pina, C.D., Falletta, E., 2022. Advances in Polyaniline for Biomedical Applications. CMC 29, 329–357. https://doi.org/10.2174/0929867328666210419135519
Pina, S., Reis, R.L., Oliveira, J.M., 2018. Ceramic biomaterials for tissue engineering, in: Fundamental Biomaterials: Ceramics. Elsevier, pp. 95–116. https://doi.org/10.1016/B978-0-08-102203-0.00004-4
Pong, T., Adams, W.J., Bray, M.-A., Feinberg, A.W., Sheehy, S.P., Werdich, A.A., Parker, K.K., 2011. Hierarchical architecture influences calcium dynamics in engineered cardiac muscle. Exp Biol Med (Maywood) 236, 366–373. https://doi.org/10.1258/ebm.2010.010239
Pörtner, R., Nagel-Heyer, S., Goepfert, C., Adamietz, P., Meenen, N.M., 2005. Bioreactor design for tissue engineering. Journal of Bioscience and Bioengineering 100, 235–245. https://doi.org/10.1263/jbb.100.235
Pu, J., Cao, L., McCaig, C.D., 2015. Physiological extracellular electrical signals guide and orient the polarity of gut epithelial cells. Tissue Barriers 3, e1037417. https://doi.org/10.1080/21688370.2015.1037417
Puiggalí-Jou, A., Del Valle, L.J., Alemán, C., 2019. Drug delivery systems based on intrinsically conducting polymers. Journal of Controlled Release 309, 244–264. https://doi.org/10.1016/j.jconrel.2019.07.035
Pullar, C.E. (Ed.), 2011. The physiology of bioelectricity in development, tissue regeneration, and cancer, Biological effects of electromagnetics series. CRC Press, Boca Raton.
Qazi, T.H., Rai, R., Boccaccini, A.R., 2014. Tissue engineering of electrically responsive tissues using polyaniline based polymers: A review. Biomaterials 35, 9068–9086. https://doi.org/10.1016/j.biomaterials.2014.07.020

Rafat, M., Li, F., Fagerholm, P., Lagali, N.S., Watsky, M.A., Munger, R., Matsuura, T., Griffith, M., 2008. PEG-stabilized carbodiimide crosslinked collagen–chitosan hydrogels for corneal tissue engineering. Biomaterials 29, 3960–3972. https://doi.org/10.1016/j.biomaterials.2008.06.017

Rahaman, M.N., Day, D.E., Sonny Bal, B., Fu, Q., Jung, S.B., Bonewald, L.F., Tomsia, A.P., 2011. Bioactive glass in tissue engineering. Acta Biomaterialia 7, 2355–2373. https://doi.org/10.1016/j.actbio.2011.03.016

Rahmati, M., Mozafari, M., 2019. Biocompatibility of alumina-based biomaterials–A review. J Cell Physiol 234, 3321–3335. https://doi.org/10.1002/jcp.27292

Ramanavicius, S., Ramanavicius, A., 2020. Conducting Polymers in the Design of Biosensors and Biofuel Cells. Polymers 13, 49. https://doi.org/10.3390/polym13010049

Ratner, B.D. (Ed.), 2013. Biomaterials science: an introduction to materials in medicine, 3rd ed. ed. Elsevier/Academic Press, Amsterdam ; Boston.

Rees, A., Powell, L.C., Chinga-Carrasco, G., Gethin, D.T., Syverud, K., Hill, K.E., Thomas, D.W., 2015. 3D Bioprinting of Carboxymethylated-Periodate Oxidized Nanocellulose Constructs for Wound Dressing Applications. BioMed Research International 2015, 1–7. https://doi.org/10.1155/2015/925757

Reid, J.A., Dwyer, K.D., Schmitt, P.R., Soepriatna, A.H., Coulombe, K.L., Callanan, A., 2021. Architected fibrous scaffolds for engineering anisotropic tissues. Biofabrication 13, 045007. https://doi.org/10.1088/1758-5090/ac0fc9

Ren, Y., Sikder, P., Lin, B., Bhaduri, S.B., 2018. Microwave assisted coating of bioactive amorphous magnesium phosphate (AMP) on polyetheretherketone (PEEK). Materials Science and Engineering: C 85, 107–113. https://doi.org/10.1016/j.msec.2017.12.025

Rho, J.Y., Ashman, R.B., Turner, C.H., 1993. Young's modulus of trabecular and cortical bone material: Ultrasonic and microtensile measurements. Journal of Biomechanics 26, 111–119. https://doi.org/10.1016/0021-9290(93)90042-D

Rinaudo, M., 2008. Main properties and current applications of some polysaccharides as biomaterials. Polym. Int. 57, 397–430. https://doi.org/10.1002/pi.2378

Riss, T.L., Moravec, R.A., Niles, A.L., Duellman, S., Benink, H.A., Worzella, T.J., Minor, L., 2004. Cell Viability Assays, in: Markossian, S., Grossman, A., Brimacombe, K., Arkin, M., Auld, D., Austin, C., Baell, J., Chung, T.D.Y., Coussens, N.P., Dahlin, J.L., Devanarayan, V., Foley, T.L., Glicksman, M., Gorshkov, K., Haas, J.V., Hall, M.D., Hoare, S., Inglese, J., Iversen, P.W., Kales, S.C., Lal-Nag, M., Li, Z., McGee, J., McManus, O., Riss, T., Saradjian, P., Sittampalam, G.S., Tarselli, M., Trask, O.J., Wang, Y., Weidner, J.R., Wildey, M.J., Wilson, K., Xia, M., Xu, X. (Eds.),

Assay Guidance Manual. Eli Lilly & Company and the National Center for Advancing Translational Sciences, Bethesda (MD).

Roshanbinfar, K., Vogt, L., Ruther, F., Roether, J.A., Boccaccini, A.R., Engel, F.B., 2020. Nanofibrous Composite with Tailorable Electrical and Mechanical Properties for Cardiac Tissue Engineering. Adv. Funct. Mater. 30, 1908612. https://doi.org/10.1002/adfm.201908612

Sabu, T., Balakrishnan, P., Sreekala, Meyyarappallil Sadasivan, Sreekala, M. S. (Eds.), 2018. Fundamental biomaterials: polymers, Woodhead Publishing series in biomaterials. Woodhead Publishing (an imprint of Elsevier), Duxford Cambridge Kidlington.

Sacui, I.A., Nieuwendaal, R.C., Burnett, D.J., Stranick, S.J., Jorfi, M., Weder, C., Foster, E.J., Olsson, R.T., Gilman, J.W., 2014. Comparison of the Properties of Cellulose Nanocrystals and Cellulose Nanofibrils Isolated from Bacteria, Tunicate, and Wood Processed Using Acid, Enzymatic, Mechanical, and Oxidative Methods. ACS Appl. Mater. Interfaces 6, 6127–6138. https://doi.org/10.1021/am500359f

Sagomonyants, K.B., Jarman-Smith, M.L., Devine, J.N., Aronow, M.S., Gronowicz, G.A., 2008. The in vitro response of human osteoblasts to polyetheretherketone (PEEK) substrates compared to commercially pure titanium. Biomaterials 29, 1563–1572. https://doi.org/10.1016/j.biomaterials.2007.12.001

Salehi-Nik, N., Amoabediny, G., Pouran, B., Tabesh, H., Shokrgozar, M.A., Haghighipour, N., Khatibi, N., Anisi, F., Mottaghy, K., Zandieh-Doulabi, B., 2013. Engineering Parameters in Bioreactor's Design: A Critical Aspect in Tissue Engineering. BioMed Research International 2013, 1–15. https://doi.org/10.1155/2013/762132

Santos, G.A. dos, 2017. The Importance of Metallic Materials as Biomaterials. ATROA 3. https://doi.org/10.15406/atroa.2017.03.00054

Sarot, J.R., Contar, C.M.M., Cruz, A.C.C.D., De Souza Magini, R., 2010. Evaluation of the stress distribution in CFR-PEEK dental implants by the three-dimensional finite element method. J Mater Sci: Mater Med 21, 2079–2085. https://doi.org/10.1007/s10856-010-4084-7

Schunck, M., Neumann, C., Proksch, E., 2005. Artificial Barrier Repair in Wounds by Semi-Occlusive Foils Reduced Wound Contraction and Enhanced Cell Migration and Reepithelization in Mouse Skin. Journal of Investigative Dermatology 125, 1063–1071. https://doi.org/10.1111/j.0022-202X.2005.23890.x

Schütz, K., Placht, A.-M., Paul, B., Brüggemeier, S., Gelinsky, M., Lode, A., 2017. Three-dimensional plotting of a cell-laden alginate/methylcellulose blend: towards biofabrication of tissue engineering constructs with clinically relevant dimensions: 3D plotting of a cell-laden alginate/methylcellulose blend. J Tissue Eng Regen Med 11, 1574–1587. https://doi.org/10.1002/term.2058

Seddiqi, H., Oliaei, E., Honarkar, H., Jin, J., Geonzon, L.C., Bacabac, R.G., Klein-Nulend, J., 2021. Cellulose and its derivatives: towards biomedical applications. Cellulose 28, 1893–1931. https://doi.org/10.1007/s10570-020-03674-w

Shah, S., Firlak, M., Berrow, S., Halcovitch, N., Baldock, S., Yousafzai, B., Hathout, R., Hardy, J., 2018. Electrochemically Enhanced Drug Delivery Using Polypyrrole Films. Materials 11, 1123. https://doi.org/10.3390/ma11071123

Sheldon, R.A., Van Pelt, S., 2013. Enzyme immobilisation in biocatalysis: why, what and how. Chem. Soc. Rev. 42, 6223–6235. https://doi.org/10.1039/C3CS60075K

Shen, Y., Xu, Y., Yi, B., Wang, X., Tang, H., Chen, C., Zhang, Y., 2021. Engineering a Highly Biomimetic Chitosan-Based Cartilage Scaffold by Using Short Fibers and a Cartilage-Decellularized Matrix. Biomacromolecules 22, 2284–2297. https://doi.org/10.1021/acs.biomac.1c00366

Shen, Z.-S., Cui, X., Hou, R.-X., Li, Q., Deng, H.-X., Fu, J., 2015. Tough biodegradable chitosan–gelatin hydrogels via in situ precipitation for potential cartilage tissue engineering. RSC Adv. 5, 55640–55647. https://doi.org/10.1039/C5RA06835E

Sherr, C.J., 2004. Principles of Tumor Suppression. Cell 116, 235–246. https://doi.org/10.1016/S0092-8674(03)01075-4

Shukla, S.K., Mishra, A.K., Arotiba, O.A., Mamba, B.B., 2013. Chitosan-based nanomaterials: A state-of-the-art review. International Journal of Biological Macromolecules 59, 46–58. https://doi.org/10.1016/j.ijbiomac.2013.04.043

Sikder, P., Ferreira, J.A., Fakhrabadi, E.A., Kantorski, K.Z., Liberatore, M.W., Bottino, M.C., Bhaduri, S.B., 2020. Bioactive amorphous magnesium phosphate-polyetheretherketone composite filaments for 3D printing. Dental Materials 36, 865–883. https://doi.org/10.1016/j.dental.2020.04.008

Singh, J., Rani, S., Rohini, Parida, A., 2014. Generation of piezoelectricity from the human body, in: 2014 Annual International Conference on Emerging Research Areas: Magnetics, Machines and Drives (AICERA/ICMMD). Presented at the 2014 Annual International Conference on Emerging Research Areas: Magnetics, Machines and Drives (AICERA/iCMMD), IEEE, Kottayam, pp. 1–5. https://doi.org/10.1109/AICERA.2014.6908277

Skopalová, K., Radaszkiewicz, K.A., Kašpárková, V., Stejskal, J., Bober, P., Junkar, I., Mozetič, M., Capáková, Z., Lehocký, M., Kašparová, M., Pacherník, J., Humpolíček, P., 2021. Modulation of Differentiation of Embryonic Stem Cells by Polypyrrole: The Impact on Neurogenesis. International Journal of Molecular Sciences 22, 501. https://doi.org/10.3390/ijms22020501

Solazzo, M., O'Brien, F.J., Nicolosi, V., Monaghan, M.G., 2019. The rationale and emergence of electroconductive biomaterial scaffolds in cardiac tissue engineering. APL Bioengineering 3, 041501. https://doi.org/10.1063/1.5116579

Stejskal, J., Sapurina, I., 2005. Polyaniline: Thin films and colloidal dispersions (IUPAC Technical Report). Pure and Applied Chemistry 77, 815–826. https://doi.org/10.1351/pac200577050815

Strehler, B.L., McElroy, W.D., 1957. [122] Assay of adenosine triphosphate, in: Methods in Enzymology. Elsevier, pp. 871–873. https://doi.org/10.1016/S0076-6879(57)03466-7

Sukpaita, T., Chirachanchai, S., Pimkhaokham, A., Ampornaramveth, R.S., 2021. Chitosan-Based Scaffold for Mineralized Tissues Regeneration. Marine Drugs 19, 551. https://doi.org/10.3390/md19100551

Tamilisai, R., Palanisamy, P.N., Selvasekarapandian, S., Maheshwari, T., 2021. Sodium alginate incorporated with magnesium nitrate as a novel solid biopolymer electrolyte for magnesium-ion batteries. J Mater Sci: Mater Electron 32, 22270–22285. https://doi.org/10.1007/s10854-021-06713-9

Tapia, F., Vázquez-Ramírez, D., Genzel, Y., Reichl, U., 2016. Bioreactors for high cell density and continuous multi-stage cultivations: options for process intensification in cell culture-based viral vaccine production. Appl Microbiol Biotechnol 100, 2121–2132. https://doi.org/10.1007/s00253-015-7267-9

Temenoff, J.S., Mikos, A.G., 2008. Biomaterials: the Intersection of biology and materials science, Pearson Prentice Hall bioengineering. Pearson/Prentice Hall, Upper Saddle River, N.J.

Thomas-Vielma, P., Cervera, A., Levenfeld, B., Várez, A., 2008. Production of alumina parts by powder injection molding with a binder system based on high density polyethylene. Journal of the European Ceramic Society 28, 763–771. https://doi.org/10.1016/j.jeurceramsoc.2007.08.004

Thrivikraman, G., Boda, S.K., Basu, B., 2018. Unraveling the mechanistic effects of electric field stimulation towards directing stem cell fate and function: A tissue engineering perspective. Biomaterials 150, 60–86. https://doi.org/10.1016/j.biomaterials.2017.10.003

Thunberg, J., Kalogeropoulos, T., Kuzmenko, V., Hägg, D., Johannesson, S., Westman, G., Gatenholm, P., 2015. In situ synthesis of conductive polypyrrole on electrospun cellulose nanofibers: scaffold for neural tissue engineering. Cellulose 22, 1459–1467. https://doi.org/10.1007/s10570-015-0591-5

Tonndorf, R., Aibibu, D., Cherif, C., 2021. Isotropic and Anisotropic Scaffolds for Tissue Engineering: Collagen, Conventional, and Textile Fabrication Technologies and Properties. IJMS 22, 9561. https://doi.org/10.3390/ijms22179561

Torgbo, S., Sukyai, P., 2020. Biodegradation and thermal stability of bacterial cellulose as biomaterial: The relevance in biomedical applications. Polymer Degradation and Stability 179, 109232. https://doi.org/10.1016/j.polymdegradstab.2020.109232

Townsend, J.M., Andrews, B.T., Feng, Y., Wang, J., Nudo, R.J., Van Kampen, E., Gehrke, S.H., Berkland, C.J., Detamore, M.S., 2018. Superior calvarial bone regeneration using pentenoate-functionalized hyaluronic acid hydrogels with devitalized tendon particles. Acta Biomaterialia 71, 148–155. https://doi.org/10.1016/j.actbio.2018.02.013

Trombino, S., Servidio, C., Curcio, F., Cassano, R., 2019. Strategies for Hyaluronic Acid-Based Hydrogel Design in Drug Delivery. Pharmaceutics 11, 407. https://doi.org/10.3390/pharmaceutics11080407

Tseng, J.-W., Liu, C.-Y., Yen, Y.-K., Belkner, J., Bremicker, T., Liu, B.H., Sun, T.-J., Wang, A.-B., 2018. Screw extrusion-based additive manufacturing of PEEK. Materials & Design 140, 209–221. https://doi.org/10.1016/j.matdes.2017.11.032

Twentyman, P., Luscombe, M., 1987. A study of some variables in a tetrazolium dye (MTT) based assay for cell growth and chemosensitivity. Br J Cancer 56, 279–285. https://doi.org/10.1038/bjc.1987.190

Umoren, S.A., Solomon, M.M., Saji, V.S., 2022. Conducting polymers, in: Polymeric Materials in Corrosion Inhibition. Elsevier, pp. 443–466. https://doi.org/10.1016/B978-0-12-823854-7.00002-3

Vaiani, L., Boccaccio, A., Uva, A.E., Palumbo, G., Piccininni, A., Guglielmi, P., Cantore, S., Santacroce, L., Charitos, I.A., Ballini, A., 2023. Ceramic Materials for Biomedical Applications: An Overview on Properties and Fabrication Processes. JFB 14, 146. https://doi.org/10.3390/jfb14030146

Van Hao, P., Xuan, C.T., Thanh, P.D., Thuat, N.-T., Hai, N.H., Tuan, M.A., 2018. Detection analysis limit of nonlinear characteristics of DNA sensors with the surface modified by polypyrrole nanowires and gold nanoparticles. Journal of Science: Advanced Materials and Devices 3, 129–138. https://doi.org/10.1016/j.jsamd.2018.04.002

Varaprasad, K., Jayaramudu, T., Kanikireddy, V., Toro, C., Sadiku, E.R., 2020. Alginate-based composite materials for wound dressing application:A mini review. Carbohydrate Polymers 236, 116025. https://doi.org/10.1016/j.carbpol.2020.116025

Vatankhah, E., Prabhakaran, M.P., Jin, G., Mobarakeh, L.G., Ramakrishna, S., 2014. Development of nanofibrous cellulose acetate/gelatin skin substitutes for variety wound treatment applications. J Biomater Appl 28, 909–921. https://doi.org/10.1177/0885328213486527

Venkatesan, J., Bhatnagar, I., Manivasagan, P., Kang, K.-H., Kim, S.-K., 2015. Alginate composites for bone tissue engineering: A review. International Journal of Biological Macromolecules 72, 269–281. https://doi.org/10.1016/j.ijbiomac.2014.07.008

Vila, A., Sánchez, A., Tobío, M., Calvo, P., Alonso, M.J., 2002. Design of biodegradable particles for protein delivery. Journal of Controlled Release 78, 15–24. https://doi.org/10.1016/S0168-3659(01)00486-2

Vrana, N.E., Knopf-Marques, H., Barthes, J. (Eds.), 2020. Biomaterials for organ and tissue regeneration: new technologies and future prospects, Woodhead Publishing series in biomaterials. Woodhead Publishing, Oxford ; Cambridge, MA.

Vroman, Leo, Adams, A.L., 1969a. Identification of rapid changes at plasma-solid interfaces. J. Biomed. Mater. Res. 3, 43–67. https://doi.org/10.1002/jbm.820030106

Vroman, L., Adams, A.L., 1969b. Findings with the recording ellipsometer suggesting rapid exchange of specific plasma proteins at liquid/solid interfaces. Surface Science 16, 438–446. https://doi.org/10.1016/0039-6028(69)90037-5

Wang, Y.-X., Robertson, J.L., Spillman, Jr., W.B., Claus, R.O., 2004. Effects of the Chemical Structure and the Surface Properties of Polymeric Biomaterials on Their Biocompatibility. Pharm Res 21, 1362–1373. https://doi.org/10.1023/B:PHAM.0000036909.41843.18

Webster, T.J., Ergun, C., Doremus, R.H., Siegel, R.W., Bizios, R., 2000. Specific proteins mediate enhanced osteoblast adhesion on nanophase ceramics. J. Biomed. Mater. Res. 51, 475–483. https://doi.org/10.1002/1097-4636(20000905)51:3<475::AID-JBM23>3.0.CO;2-9

Weiss, J.N., 1997. Ion Channels in Cardiac Muscle, in: The Myocardium. Elsevier, pp. 81–142. https://doi.org/10.1016/B978-012436570-4/50005-4

Wen, L., Zhang, C., Nong, Y., Yao, Q., Song, Z., 2013. Mild Electrical Pulse Current Stimulation Upregulates S100A4 and Promotes Cardiogenesis in MSC and Cardiac Myocytes Coculture Monolayer. Cell Biochem Biophys 65, 43–55. https://doi.org/10.1007/s12013-012-9402-x

Williams, J.L., Lewis, J.L., 1982. Properties and an Anisotropic Model of Cancellous Bone From the Proximal Tibial Epiphysis. Journal of Biomechanical Engineering 104, 50–56. https://doi.org/10.1115/1.3138303

Yang, J., Du, M., Wang, L., Li, S., Wang, G., Yang, X., Zhang, L., Fang, Y., Zheng, W., Yang, G., Jiang, X., 2018. Bacterial Cellulose as a Supersoft Neural Interfacing Substrate. ACS Appl. Mater. Interfaces 10, 33049–33059. https://doi.org/10.1021/acsami.8b12083

Yang, L., Fan, X., Zhang, J., Ju, J., 2020. Preparation and Characterization of Thermoresponsive Poly(N-Isopropylacrylamide) for Cell Culture Applications. Polymers 12, 389. https://doi.org/10.3390/polym12020389

Yi, N., Abidian, M.R., 2016. Conducting polymers and their biomedical applications, in: Biosynthetic Polymers for Medical Applications. Elsevier, pp. 243–276. https://doi.org/10.1016/B978-1-78242-105-4.00010-9

Yu, Y., Alkhawaji, A., Ding, Y., Mei, J., 2016. Decellularized scaffolds in regenerative medicine. Oncotarget 7, 58671–58683. https://doi.org/10.18632/oncotarget.10945

Yuan, L., Wu, Y., Fang, J., Wei, X., Gu, Q., El-Hamshary, H., Al-Deyab, S.S., Morsi, Y., Mo, X., 2017. Modified alginate and gelatin cross-linked hydrogels for soft tissue adhesive. Artificial Cells, Nanomedicine, and Biotechnology 45, 76–83. https://doi.org/10.3109/21691401.2015.1129622

Yussuf, A., Al-Saleh, M., Al-Enezi, S., Abraham, G., 2018. Synthesis and Characterization of Conductive Polypyrrole: The Influence of the Oxidants and Monomer on the Electrical, Thermal, and Morphological Properties. International Journal of Polymer Science 2018, 1–8. https://doi.org/10.1155/2018/4191747

Zamora-Sequeira, R., Ardao, I., Starbird, R., García-González, C.A., 2018. Conductive nanostructured materials based on poly-(3,4-ethylenedioxythiophene) (PEDOT) and starch/κ-carrageenan for biomedical applications. Carbohydrate Polymers 189, 304–312. https://doi.org/10.1016/j.carbpol.2018.02.040

Zha, F., Chen, W., Hao, L., Wu, C., Lu, M., Zhang, L., Yu, D., 2020. Electrospun cellulose-based conductive polymer nanofibrous mats: composite scaffolds and their influence on cell behavior with electrical stimulation for nerve tissue engineering. Soft Matter 16, 6591–6598. https://doi.org/10.1039/D0SM00593B

Zhang, C., Salick, M.R., Cordie, T.M., Ellingham, T., Dan, Y., Turng, L.-S., 2015. Incorporation of poly(ethylene glycol) grafted cellulose nanocrystals in poly(lactic acid) electrospun nanocomposite fibers as potential scaffolds for bone tissue engineering. Materials Science and Engineering: C 49, 463–471. https://doi.org/10.1016/j.msec.2015.01.024

Zheng, H., Liu, M., Yan, Z., Chen, J., 2020. Highly selective and stable glucose biosensor based on incorporation of platinum nanoparticles into polyaniline-montmorillonite hybrid composites. Microchemical Journal 152, 104266. https://doi.org/10.1016/j.microc.2019.104266

Zhou, C., Shi, Q., Guo, W., Terrell, L., Qureshi, A.T., Hayes, D.J., Wu, Q., 2013. Electrospun Bio-Nanocomposite Scaffolds for Bone Tissue Engineering by Cellulose Nanocrystals Reinforcing Maleic Anhydride Grafted PLA. ACS Appl. Mater. Interfaces 5, 3847–3854. https://doi.org/10.1021/am4005072

Zhu, C., Fan, D., Wang, Y., 2014. Human-like collagen/hyaluronic acid 3D scaffolds for vascular tissue engineering. Materials Science and Engineering: C 34, 393–401. https://doi.org/10.1016/j.msec.2013.09.044

Zhu, R., Sun, Z., Li, C., Ramakrishna, S., Chiu, K., He, L., 2019. Electrical stimulation affects neural stem cell fate and function in vitro. Experimental Neurology 319, 112963. https://doi.org/10.1016/j.expneurol.2019.112963

Zhuo, S., Zhang, F., Yu, J., Zhang, X., Yang, G., Liu, X., 2020. pH-Sensitive Biomaterials for Drug Delivery. Molecules 25, 5649. https://doi.org/10.3390/molecules25235649

Zioupos, P., Kirchner, H.O.K., Peterlik, H., 2020. Ageing bone fractures: The case of a ductile to brittle transition that shifts with age. Bone 131, 115176. https://doi.org/10.1016/j.bone.2019.115176

LIST OF FIGURES

LIST OF ABBREVIATIONS AND SYMBOLS

Alphabetically ordered

AH	Aniline hydrochloride
APS	Amonium persulfate
CBS	Ceramic-based substrate
CH	Chitosan
CPs	Conductive polymers
CNF	Cellulose nanofibrils
CNF-DAC	Cellulose nanofibrils dialdehyde
CNF-DAC PPy	Cellulose nanofibrils dialdehyde with polypyrrole
CNF/PPy	Cellulose nanofibrils with polypyrrole
DAAL	Dialdehyde alginate
DAC	Dialdehyde cellulose
DAH	Dialdehyde hyaluronate
ECM	Extracellular matrix
HA	Hyaluronic acid
PANI	Polyaniline
PEDOT	Poly(3,4-ethylenedioxythiophene)
PEEK	Polyetheretherketone
PHBV	Poly-3-hydroxybutyrate-3-hydroxy valerate
PHS	Powder space holdes
PIM	Powder Incjecton Molding
PTh	Polythiophene
PVDF	Poly(vinylidene fluoride)
PNIPAAm	Poly(N-isopropyl acrylamide
PPy	Polypyrrole
SA	Sodium alginate
SH	Sodium hyaluronate
TE	Tissue engineering
UPW	Ultra-pure water

CURRICULUM VITAE

Personal information	Name: Martina Martínková, Ing. Birth name: Kašparová Contact: martinkova@utb.cz Sex: Female | Nationality: Czech

Education

2019 – present	*Ph.D. study* Centre of polymer systems, Tomas Bata University in Zlín (Czech Republic) **Biomaterials and Biocomposites**
2017 – 2019	*Master´s degree* Faculty of Technology, Tomas Bata University in Zlín (Czech Republic) **Polymer Engineering**
2014 – 2017	*Bachelor´s degree* Faculty of Technology, Tomas Bata University in Zlín (Czech Republic) **Polymeric Materials and Technology**

Research projects

2023	Project IGA/CPS/2023/001, Development of advanced biomaterials and their future application Member of project team
2022	Project IGA/CPS/2022/001, Preparation of advanced biomaterials and their application Member of project team
2020-2022	Project OP RDE Junior Grants of TBU in Zlín, JUNG-2020-001, Smart biomaterials based on conducting polymers Member of project team
2021	Project IGA/CPS/2021/001, Biocompatibility of material Member of project team
2020 – 2021	Project GAČR 20-28732S, Colloidal systems for topical formulations. Pickering emulsions and polymer based colloids. Member of project team

2020	Project IGA/CPS/2020/001, Biocompatibility and antimicrobial activity of materials Investigator
2019	Project IGA/CPS/2019/004, Biological properties of materials Member of project team
2019	Project GAČR 19-16861S, Interactions between materials and stem cells in simulated *in vivo* conditions Member of project team

Conferences and seminars

04/09/2022 – 09/09/2022	*36th European Colloid & Interface Society Conference* Chania, Crete, Greece Poster title "Conducting film prepared in colloidal dispersion mode, the efficient way of surface functionalization"
28/06/2022 – 01/07/2022	*Tissue Engineering and Regenerative Medicine International Society (TERMIS) European Chapter Conference 2022* Krakow, Poland Poster title "Conducting polyaniline films prepared in colloidal dispersion mode in presence of bioactive polysaccharides"
08/11/2021 – 12/11/2021	*Fellowship on Institute of Biophysics of the CAS* Institute of Biophysics of the CAS, Brno Practical training of isolation and manipulation of mouse Caco-2 cell line

Pedagogic activities

Student training in laboratories

Mentoring the bachelor thesis:
Exosomes

LIST OF PUBLICATIONS

Articles published in journals indexed on Web of Science:

Martínková M., Hausnerová B., Huba J., Martínek T., Káčerová S., Kašpárková V., Humpolíček P., 2022. Powder injection molded ceramic scaffolds: The role of pores size and surface functionalization on the cytocompatibility. Materias and Design 224. ISSN 02641275. DOI 10.1016/j.matdes.2022.111274

Musilová L., Achbergerová E., Vítková L., Kolařík R., **Martínková M.**, Minařík A., Mráček A., Humpolíček P., Pecha J., 2022. Cross-Linked Gelatine by Modified Dextran as a Potential Bioink Prepared by a Simple and Non-Toxic Process. Polymers 14, 391. DOI 10.3390/polym14030391

Gupta S., Acharya U., Pištěková H., Taboubi O., Morávková Z, **Kašparová M.**, Humpolíček P., Bober P., 2021. Tuning the Conductivity, Morphology, and Capacitance with Enhanced Antibacterial Properties of Polypyrrole by Acriflavine Hydrochloride. ACS Applied Polymer Materials. 3, 6063–6069. DOI 10.1021/acsapm.1c00775

Milakin K.A., Morávková Z., Acharya U., **Kašparová M.**, Breitenbach S., Taboubi O., Hodan J., Hromádková J., Unterweger C., Humpolíček P., Bober P., 2021. Enhancement of conductivity, mechanical and biological properties of polyaniline-poly(N-vinylpyrrolidone) cryogels by phytic acid. Polymer 217, 123450. DOI 10.1016/j.polymer. 2021.123450

Skopalová K., Radaszkiewicz K.A., Kašpárková V., Stejskal J., Bober P., Junkar I., Mozetič M., Capáková Z., Lehocký M., **Kašparová M.**, Pacherník J., Humpolíček P., 2021. Modulation of Differentiation of Embryonic Stem Cells by Polypyrrole: The Impact on Neurogenesis. International Journal of Molecular Sciences 22, 501. DOI 10.3390/ijms22020501

Submitted article to the editors of international journals with an impact factor:

Martínková M., Zárybnická L., Viani A., Killinger M., Mácová P., Sedláček T., Oralová V., Klepárník K. and Humpolíček P., Polyetheretherketone Bioactivity Induced by Farringtonite: The Effect on Mineralization and Differentiation of Osteoblasts

ARTICLE 1

Martínková M., Hausnerová B., Huba J., Martínek T., Káčerová S., Kašpárková V., Humpolíček P., 2022. *Powder injection molded ceramic scaffolds: The role of pores size and surface functionalization on the cytocompatibility*. Materias and Design 224. ISSN 02641275. DOI 10.1016/j.matdes.2022.111274

Materials & Design 224 (2022) 111274

Contents lists available at ScienceDirect

Materials & Design

journal homepage: www.elsevier.com/locate/matdes

Powder injection molded ceramic scaffolds: The role of pores size and surface functionalization on the cytocompatibility

Martina Martínková [a,*], Berenika Hausnerová [a,b], Jakub Huba [b], Tomáš Martínek [c], Simona Káčerová [a], Věra Kašpárková [a,b], Petr Humpolíček [a,b,*]

[a] Tomas Bata University in Zlin, Centre of Polymer Systems, tr. Tomase Bati 5678, Zlin 76001, Czech Republic
[b] Tomas Bata University in Zlin, Faculty of Technology, Vavreckova, 275, Zlin 76001, Czech Republic
[c] Tomas Bata University in Zlin, Faculty of Applied Informatics, Nad Stranemi, 4511, Zlin 76005, Czech Republic

GRAPHICAL ABSTRACT

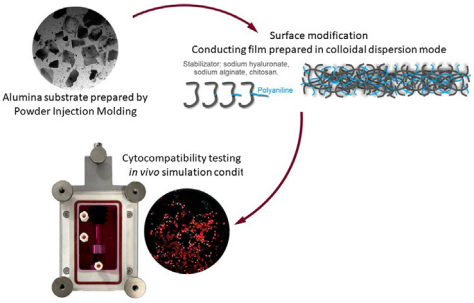

ARTICLE INFO

Article history:
Received 6 April 2022
Revised 5 October 2022
Accepted 19 October 2022
Available online 20 October 2022

Keywords:
Powder Injection Molding
Surface Modification
Polyaniline
Alumina
Tissue Engineering
Cytocompatibility

ABSTRACT

The alumina-based scaffolds prepared by powder injection molding can be preferentially used for preparation of bone grafts. Here, the final architecture of alumina scaffolds was efficiently controlled by powder space holder size and volume ratio. The alumina is not intrinsically cell-instructive material and thus the coating with electrically-conducting polyaniline or polyaniline/biopolymer films prepared in a colloidal dispersion mode was used to provide this advanced property. The component of the extracellular matrix, sodium hyaluronate, or natural biopolymers (sodium alginate or chitosan) were employed, and, subsequently, the cytocompatibility of the native and functionalized alumina scaffolds were determined. Both the absence of cytotoxicity and the cytocompatibility that were revealed demonstrate the application potential of these composites. The scaffolds with pore size greater than 250 μm were more cytocompatibility than those with pores size between 125 and 250 μm. The cytocompatibility was confirmed under *in vivo*-mimicking dynamic cultivation conditions which further improve the cell distribution and growth.

1. Introduction

Personalized medical devices such as dental prostheses, bone grafts or personalised medical devices often require the preparation of precisely designed scaffolds. While 3D printing techniques are applicable for polymer-based scaffolds, Powder Injection Molding (PIM) allows the preparation of precisely designed ceramics-

Abbreviations: CBS, ceramic-based scaffold; CH, chitosan; SA, sodium alginate; SH, sodium hyaluronate; AH, aniline hydrochloride; APS, ammonium persulfate.

* Corresponding authors.
E-mail addresses: martinkova@utb.cz (M. Martínková), hausnerova@utb.cz (B. Hausnerová), jhuba@utb.cz (J. Huba), tmartinek@utb.cz (T. Martínek), s_kacerova@utb.cz (S. Káčerová), vkasparova@utb.cz (V. Kašpárková), humpolicek@utb.cz (P. Humpolíček).

https://doi.org/10.1016/j.matdes.2022.111274
0264-1275/

based products made. The precise design together with homogeneous chemical composition [1] is considered as main advantages of PIM made materials. PIM allow to fabricate the personalised medical devices made of ceramics which can be especially advantageous in bone or dental engineering. The resulting porous PIM structures have a different internal structure to those fabricated by additive manufacturing plus allows to control the porosity [2].

Aluminum oxide (alumina) has good biocompatibility [3], excellent corrosion resistance, high wear resistance and strength, and is chemically bioinert [4]. In addition, its price is substantially lower in comparison to, for example, titanium alloys. It should also be mentioned that the production of porous alumina structures is not as demanding as in the case of titanium and its alloys, which are highly reactive and thus must be mixed, molded, and also debound/sintered carefully under protective atmospheres.

Both, the bulk and surface properties must be considered when the cytocompatibility of scaffolds are considered. From the bulk properties, the pore shape is known to affect cell behavior, as in the bone tissue regeneration process, the size and interconnection of pores affect the cell migration, proliferation, and ingrowth into the scaffold [5]. Another bulk properties such porosity [6], thermal conductivity [7], and elasticity [8] is not limited the ceramic-based scaffolds (CBS) application, but the surface characteristics are. Thus, the composites combining the appropriate bulk characteristics with stimuli-responsive surface coatings seems to be the most appropriate way for preparation of desired cell-instructive scaffolds.

One of the most suitable materials for the preparation of stimuli-responsive, and thus cell-instructive coatings is polyaniline (PANI) [5]. PANI is a widely studied conducting polymer that possesses some unique properties. For example, the coating by PANI itself is not adequately cytocompatible, but can be combined with a variety of biomolecules, by the preparation of thin films based on colloidal dispersions, to produce cytocompatible films [9,10]. PANI also intrinsically combines electronic and ionic conductivities, which is advantageous for material/cell communication. As mentioned, PANI can be stabilized by biopolymers that influence the cellular physiology [11,12]. The following compounds can be used as stabilizers: sodium hyaluronate, which can provide final material-specific bioactivity, especially changes in stem cell gene expression [13]; chitosan, which is well known for its antibacterial properties [14]; and alginate, which is widely used in a variety of biomedical applications including tissue engineering [15].

There have been studies devoted to the space-holder-assisted PIM of metal powders such as 316 L stainless steel and several titanium alloys, but there has hitherto been no report on aluminum oxide. Considering the shape of the pores, polymethyl methacrylate (PMMA) was used as a spherical space-holder for 316 L stainless steel [16,17] and Ti6Al4V [18], while sodium chloride (NaCl) and potassium chloride (KCl) have been employed in cases where an irregular shape of particles or fibers with a high L/D ratio is desired. Thus, one of the novelties of presented study is the use of KCl as space holder for aluminium oxide. Another innovative feature of the approach used in the present study is the colloidal-based coating of surfaces. Concretely, the surfaces of a substrate were coated with various films based on polyaniline (PANI) stabilized by biopolymers – in this case, sodium hyaluronate, chitosan, and sodium alginate. Using these biopolymers, cell compatibility, or more generally the biocompatibility of materials, might be controlled.

2. Materials and methods

2.1. Preparation of native ceramic-based substrates

The powder components of the PIM compound were aluminum oxide (Martinswerk – Huber Corporation, USA) (ρ = 3.98 g/cm^3, size range 0.1–3.0 μm) and a powder space holder (PSH), potassium chloride (KCl, Sigma Aldrich, Germany) (ρ = 1.98 g/cm^3, size range 125–500 μm). The powders were admixed into a partially water-soluble binder (Licomont EK 583, ρ = 1.08 g/cm^3, viscosity 1.5 mPa.s at 130 °C) in a batch mixer (Plasti-Corder, Brabender, Germany) with counter-rotating blades. The powder content was kept at 60 vol%, the powder: PSH ratio varied from 20:40 to 50:10, and two size ranges of the PSH were tested, see Table 1 (samples marked as CBS – Ceramic Based Substrates).

Injection molding was performed on an injection molding machine (Allrounder 370S, Arburg, ARBURG GmbH + Co KG, Lössburg, Germany) with a universal tooling frame. The inserts for test samples were made by machining EN AW 7022 aluminum alloy. The test geometry consisted of a round plate (diameter 45 mm) with a highly-drafted angle due to the absence of an ejector system. The molding pressures were optimized to obtain defect-free samples, (see Table 1).

Afterwards, the water-soluble binder component and part of the PSH were removed by immersion in distilled water (60 °C) for 24 h. The remaining binder (the backbone) was debound thermally (280 °C) at atmospheric pressure. Sintering was carried out in a PIM furnace (CLASIC CZ s.r.o., Revnice, Czech Republic) up to a maximum temperature of 1670 °C and for a holding time of 1 h. The surface of CBS were inspected using SEM microscopy (VEGA, Tescan).

2.2. Surface functionalization of native substrate

The surface of native CBS was further coated to become bioactive. Four different compositions of the coating were tested. Firstly, polyaniline (PANI) was used for coating. This coating can provide electroactivity but according to previous studies does not provide adequate cytocompatibility. Another three coatings were therefore prepared *via* the innovative *in-situ* polymerization of aniline hydrochloride in the presence of stabilizers – concretely, sodium hyaluronate (SH), sodium alginate (SA), and chitosan (CH) [11]. The final composite coating is denominated either as PANI/SH, PANI/SA, or PANI/CH. In all cases, aniline hydrochloride (AH, Sigma Aldrich, Germany) and ammonium persulfate (APS, Sigma Aldrich, Germany) were used for the preparation of each coating.

Preparation of PANI coating. PANI films were prepared by mixing 0.2 M AH and 0.25 M APS solutions and then pouring the reaction mixture over samples and into Petri dishes. After 1 h of polymerization, the surfaces were washed with 0.2 M HCl (Penta, Czech Republic) and rinsed with methanol (Penta, Czech Republic).

Preparation of PANI/SH coating. For the preparation of PANI with SH, 0.2 M AH, 0.1 M APS, and 1 % SH (Contipro a.s., Czech Republic) were used. SH in demineralized water was shaken at 55 °C overnight. Then, the AH solution was added, followed by the APS solution. The reaction mixture was poured over samples and into Petri dishes, and polymerization carried out for 4 h.. As before, this step was followed by washing with 0.2 M HCl and rinsing with methanol.

Preparation of PANI/SA coating. PANI film stabilized with sodium alginate (IPL, Czech Republic) was prepared using 0.2 M AH, 0.25 M APS, and 2 % SA. The solution of SA was made in demineralized water and shaken at 37 °C overnight. Afterward, AH was added, followed by APS; thereafter, samples and the Petri dishes were coated with the PANI/SA mixture. The polymer films were allowed to polymerize for 4 h. The last step was the fixation of films with 0.2 M HCl and methanol.

Preparation of PANI/CH coating. This surface modification was made with 0.2 M AH, 0.01 M APS, and 2 % chitosan (Sigma Aldrich, Germany). Firstly, a solution of CH was prepared by dissolving it in 1 M HCl and shaking the solution at 55 °C overnight. After filtration of the solution, AH was added, followed by APS. The surfaces were

Table 1
Composition of mixture and parameters of powder injection moulding process. Two ranges of PSH grain sizes were used in this study, firstly grains in the size range of 125–250 ($^{\leq 250}$) μm and grains of 250–500 μm ($^{\geq 250}$).

Abbreviation	Powder Space Holder		Powder	Pressure [bar]	
	size [μm]	[vol.%]	[vol.%]	Injection	Holding
$CBS^{\geq 250\_A}$	250–500	20	40	2100	1650
$CBS^{\geq 250\_B}$		30	30	1500	1200
$CBS^{\geq 250\_C}$		40	20	1900	1500
$CBS^{\geq 250\_D}$		50	10	2100	1650
$CBS^{\leq 250\text{-}E}$	125–250	20	40	2100	1650
$CBS^{\leq 250\text{-}F}$		30	30	1500	1200
$CBS^{\leq 250\text{-}G}$		40	20	1900	1500
$CBS^{\leq 250\text{-}H}$		50	10	2100	1650

covered with the resulting mixture and the film was left to polymerize for 12 h. Subsequently, the films were washed with 0.2 M HCl and rinsed with methanol.

2.3. Cytotoxicity determination

In the tests, a mouse embryonic fibroblast cell line (ATCC CRL-1658 NIH/3T3, USA) was used. The cultivation medium consisted of Dulbecco's Modified Eagle's Medium (PAA Laboratories GmbH, Austria) containing 10 % bovine calf serum (BioSera, France) and 1 % of Penicillin/Streptomycin (GE Healthcare HyClone, United Kingdom). The test was repeated twice, each with five repetitions per sample. Cells were incubated at 37 °C in 5 % CO_2 in humidified air.

Cytotoxicity of the native substrate. Native CBS were crushed and extracted according to ISO standard 10993–12 in media with a concentration of 0.2 g/mL. The tested samples were extracted in a culture medium for 24 h at 37 °C with stirring. The parent extracts (100 vol%) were then diluted in the culture medium to achieve final concentrations of 75, 50, 25, 10, and 1 vol%. All extracts were used within 24 h.

Cytotoxicity testing itself was performed according to ISO protocol 10 993–5. Cells were preincubated in 96 well plates (TPP, Switzerland) at a concentration of 10^5 cells per mL. The extracts were added to pre-cultivated cells for another 24 h. All tests were performed in quadruplicates. The evaluation of cell viability at the end of exposure was performed using Tetrazolium (MTT cell proliferation assay kit, Duchefa Biochemie, Netherlands). The absorbance was measured at 570 nm with an Infinite M200 Pro NanoQuant instrument (Tecan, Switzerland) and the reference wavelength was adjusted to 690 nm. The results are presented as the cell viability (%) in NIH/3T3 culture compared to that in medium without PIM extracts (reference cell viability corresponds to 1). The morphology of cells from the culture plates was assessed after their cultivation in CBS extracts by using an inverted Olympus IX 81 phase contrast microscope (Olympus, Germany).

2.4. Cytocompatibility determination

The cytocompatibility study began with the determination of cell adhesion, growth, and proliferation on (1) native CBS and (2) the films used for its functionalization. The results from these initial steps allowed us to design and perform (3) bioactivity studies in which cell growth and ingrowth under static or dynamic conditions with electrical stimulation were investigated.

The cultivation conditions for experiments 1 and 2 were the same: the cells were incubated at 37 °C in humidified air with 5 % CO_2 for 2 days. The differences were in the concentrations of seeded cells: 2×10^5 per mL for experiment 1, and half that concentration (10^5 per mL) for experiment 2. The experimental setup and cultivation conditions for experiment 3 were adjusted as follows: A concentration of 2×10^5 cells per mL was seeded on substrates with a functionalized surface. After 3 days of proliferation, samples were transferred to a bioreactor enabling electrical stimulation. The bioreactor was run for 6 h per day for a total run-time of 72 h, each successive hour-long period alternating between electrical stimulation and no stimulation. The medium flow was 54 RPM. The pulse had a rectangular waveform with a width of 3000 ms, and the voltage was set at 0.1 V. Cells were visualised through nuclei counterstaining by Hoechst 33,258 (Invitrogen, USA) and actin filaments were visualized by counterstaining with ActinRed™ 555 (Thermo Fisher Scientific, USA).

3. Results and discussion

3.1. Space holder size and volume determine the architecture of CBS

Substrate composition, architecture, pore size, and porosity all play important roles in the context of designing materials for use within biomedicine. Here, we used different sizes of space holder, different space holder *vs* powder ratios, and different processing parameters. Scaffold porosity increases with increasing additions of the powder space holder. In addition, the shape of the pores can be influenced by the shape of the PSH grains. As can be clearly seen in Fig. 1, the critical parameter determining the material properties is the space holder size and its ratio to powder, while processing parameters seems to be less important. Using these two components, the architecture, porosity, and especially the pore size can be easily controlled.

3.2. Native CBS do not induce cytotoxicity

The level of cytotoxicity predetermines any application of a material in biomedicine. Here, the ISO procedure was used to determine the cytotoxicity of the native substrate. The cytotoxicity evaluation is based on the determination of effect of soluble impurities leaching from the material, thus the cytotoxicity of substrates with functionalized surfaces was not determined, as the volume ratio of coatings was very low and could not thus induce cytotoxicity. The surface functionalization can however influence the cytocompatibility due to receptor-based interaction with cells. This issue is determined and discussed further.

As presented in Fig. 2, the native CBS did not induce cytotoxicity. Only in the case of two samples, $CBS^{\geq 250\_B,}$ $CBS^{\leq 250\text{-}F}$ marked as B and F, the cell viability slightly decreased bellow the 70 %, and thus approach the cytotoxicity threshold. If the standard deviations and cytotoxicity of higher concentrations (in case of sample B) are considered, the cytotoxicity of those concentrations was not clearly proved. It can thus be concluded that native CBS are applicable in biomedicine and can be further functionalized to become bioactive.

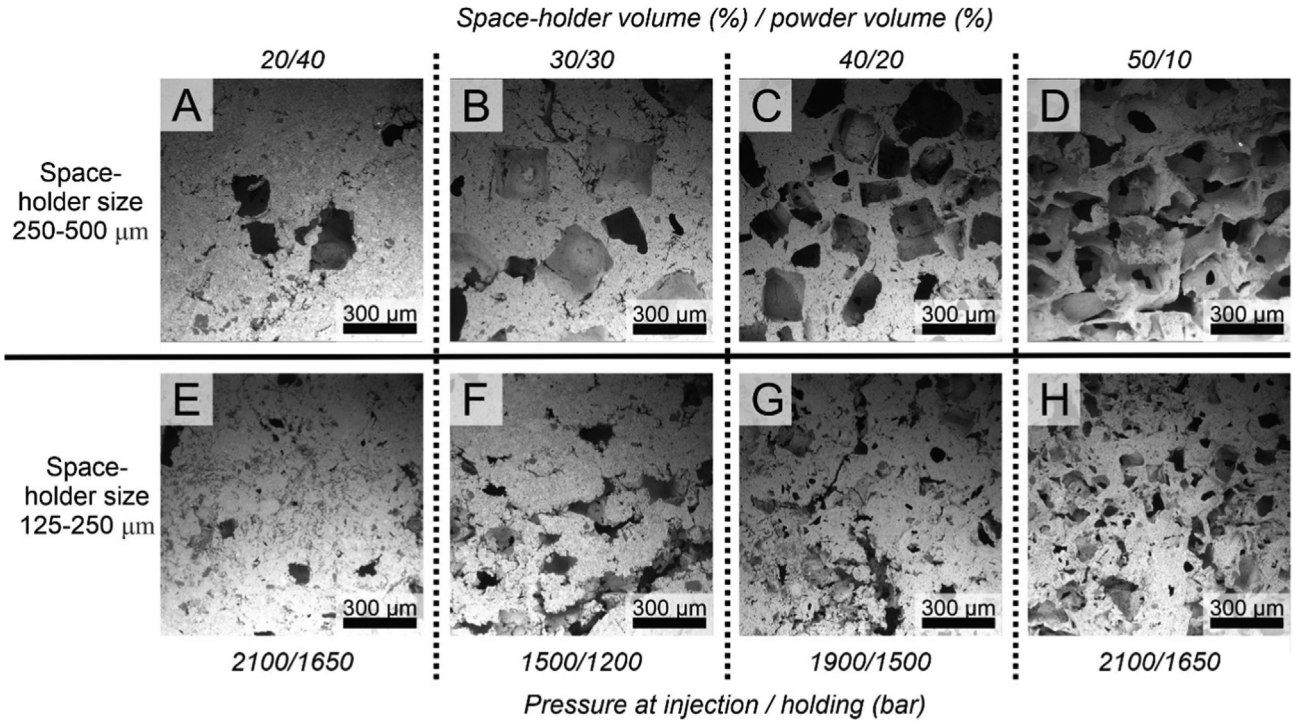

Fig. 1. SEM images of the structure of native CBS prepared using different compositions and preparation parameters. The effect of the size of the space-holder as well as the ratio between space and powder volume on the final structure of the substrate can be clearly seen. The pore size is highly correlated to the size of space holder, while the space holder / powder volume ration predetermine the porosity and pore interconnection. A = $CBS^{\geq 250\_A}$ B = $CBS^{\geq 250\_B}$, C = $CBS^{\geq 250\_C}$, D = $CBS^{\geq 250\_D}$, E = $CBS^{\leq 250\text{-}E}$, F = $CBS^{\leq 250\text{-}F}$, G = $CBS^{\leq 250\text{-}G}$, H = $CBS^{\leq 250\text{-}H.}$

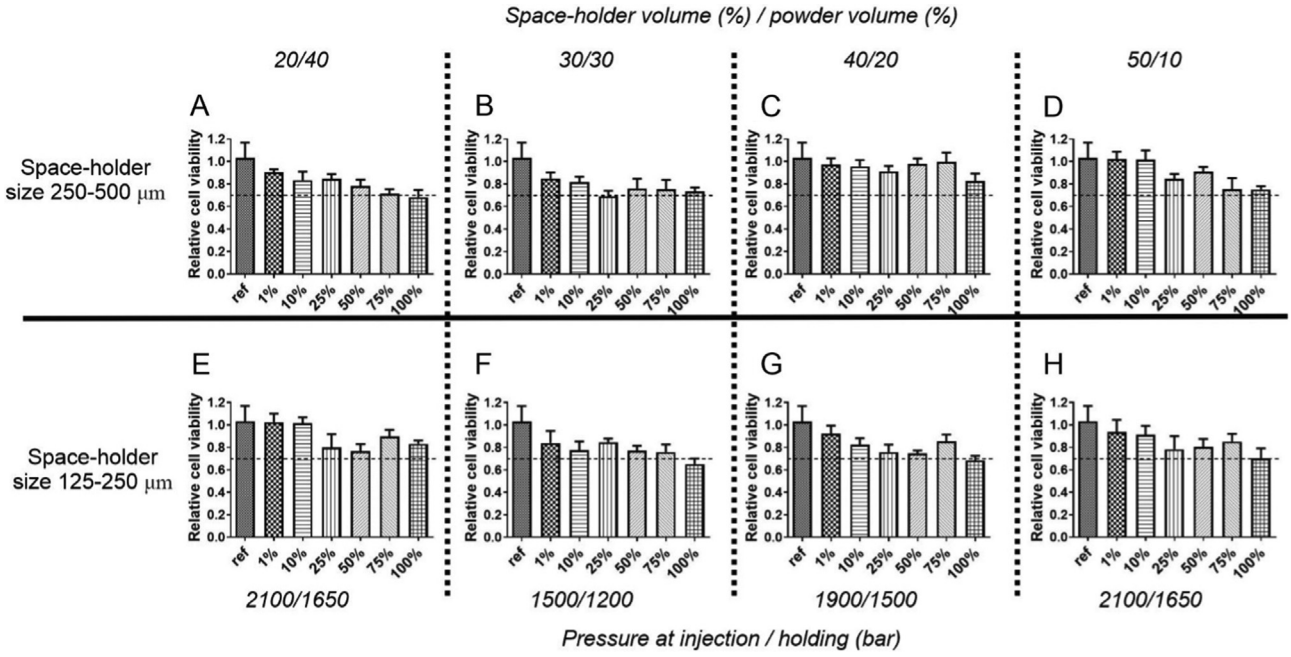

Fig. 2. The cytotoxicity of native CBS determined by a decrease in cell viability compared to the reference (data were converted to a percentage of the control and expressed as the mean ± standard deviation, n = 5). The ISO 10–993 procedure, concretely the testing of extracts, was used. The cytotoxicity threshold is marked by dashed lines; when the viability falls below 70 %, samples are considered to induce cytotoxicity. None of the tested native substrates induced cytotoxicity. A = $CBS^{\geq 250\_A}$; B = $CBS^{\geq 250\_B}$, C = $CBS^{\geq 250\_C}$, D = $CBS^{\geq 250\_D}$, E = $CBS^{\leq 250\text{-}E}$, F = $CBS^{\leq 250\text{-}F}$, G = $CBS^{\leq 250\text{-}G}$, H = $CBS^{\leq 250\text{-}H.}$

3.3. Bioactive coatings prepared in colloidal dispersion mode are cytocompatible

The conductivity is one of the crucial properties when the bioactivity of bone scaffolds and grafts are considered [19]. The conductivity can be achieved by incorporation of conducting polymers. It was, however, previously determined that native PANI does not provide an adequate cell response, which was also confirmed by this study (see Fig. 3B). Functionalization was therefore performed by means of an innovative procedure combining the

synthetic conducting polymer (providing stimuli-responsivity) with biopolymers (providing cytocompatibility). The procedure is based on the preparation of thin films in colloidal dispersion mode [10]. The final composite coating can thus provide both bioactivity and cytocompatibility.

To confirm the cytocompatibility of the surface functionalization employed here, cells were seeded onto surfaces and their proliferation and morphology were determined. The quantification of cells on the individual surfaces was not determined due to both the interaction of films with reagents used for cell viability evaluation (especially the MTT assay results can be biased) and due to the fact, that cell quantity does not provide relevant information about the real cytocompatibility which depends on cell physiology and morphology. It is clearly shown that cells on the PANI films were not capable of proliferation (see Fig. 3B). From the study [11], it is known that the addition of biocompatible polysaccharides to colloidal films changes the surface energy and surface topography, which can also lead to a change in cytocompatibility. Fig. 3C show that the number of cells on the surface modified with PANI/SA was smaller than the numbers of cells on the surfaces modified with PANI/SH (Fig. 3E) and PANI/CH (Fig. 3D) film. Also, on PANI/SA (Fig. 3C), round cells could be observed that were capable of adhering onto the surface, but they could not proliferate. The number of cells on the surface stabilized by alginate was smaller in comparison to the other stabilized films. Fig. 3E shows the cell on the surface coated with PANI/SH are present in higher quantity and especially their morphology is more physiological. This could be because of SH, which can support not only cell adhesion and proliferation but mainly their physiological state according to the type of adhered cells. The actin cytoskeleton of cells on this film was more fibrous compared to the reference sample (Fig. 3A). The proliferation rate on the PANI/CH film (Fig. 3D) was similar to that on the PANI/SH film and also the morphology of actin fibers was similar in these two cases. It can be clearly seen that the best cytocompatibility was offered by the PANI/SH and PANI/CH coatings. From those, the PANI/SH was later chosen as the most promising treatment for the determination of bioactivity under dynamic cultivation conditions. Sodium hyaluronate was chosen with regard to bioactivity related to stem cell differentiation [20].

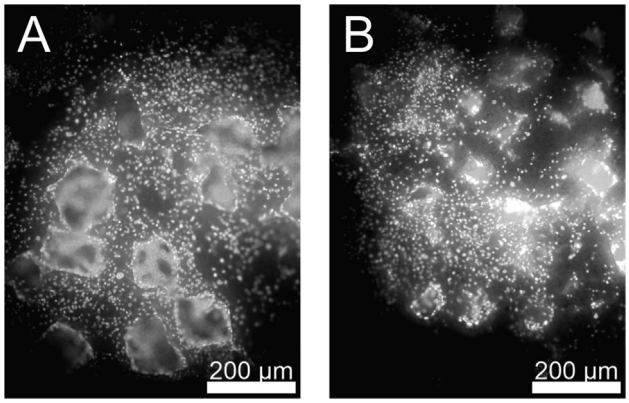

Fig. 4. Cell growth on the surface and within the pores of native $CBS^{\geq 250\_B}$ (A) and $CBS^{\leq 250\_F}$ (B) prepared with 30 vol% of space holder. The cells were seeded in a concentration of 2×10^5 cells per mL and cultivated for 2 days. Individual cells were visualised through nuclei counterstaining by Hoechst (white). There were no significant differences between any of native CBS. The $CBS^{\geq 250\_D}$ were chosen as the most appropriate for other experiments.

3.4. Cells can grow on the surface and within the pores of CBS under static cultivation conditions

In addition, cell growth on the surface of the sample, as well as cell ingrowth into the pores were investigated on native as well functionalized CBS. Cells were able to attach to, and subsequently grow on all mentioned samples.

Fig. 4 provides a detailed view of the surface of the native CBS without any surface treatment and with different pores sizes (A 250 μm and more, B 125–250 μm). Overall, the growth of cells was better on samples with a pore size greater than 250 μm than on samples with a pore size between 125 and 250 μm. The lowest viability was observed for CBS functionalized with PANI. In contrast, functionalization by films prepared in colloidal dispersion mode improved cell growth on PIM samples in the case of all stabilizers. Also, there were no significant differences in cell growth between $CBS^{PANI/SH}$, $CBSP^{PANI/SA}$, and $CBS^{PANI/CH}$. Moreover, the cell

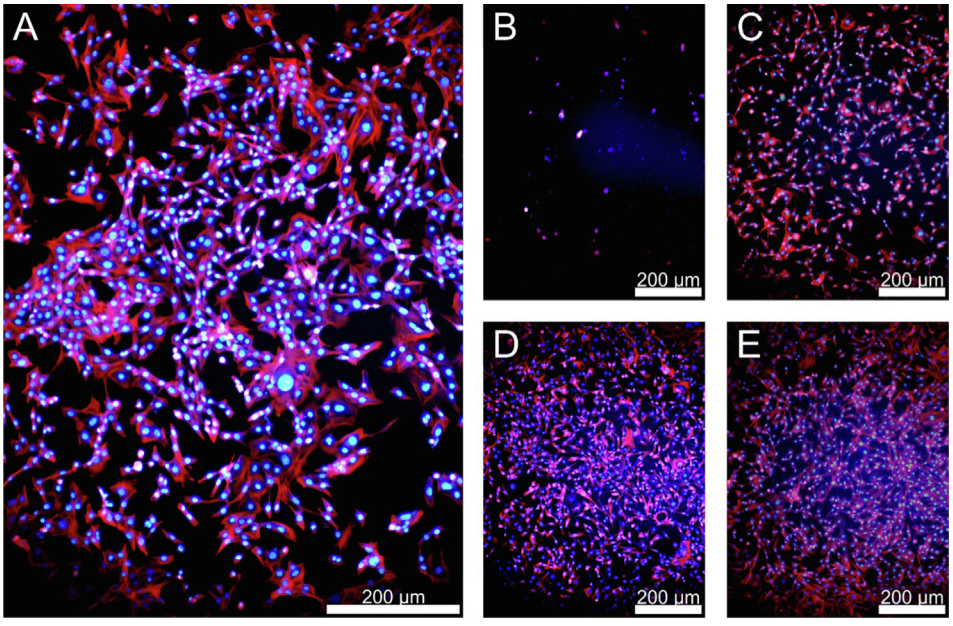

Fig. 3. Cell proliferation on reference – the cell culture polystyrene without surface modification (A); PANI (B), PANI/SA (C); PANI/CH (D); and PANI/SH (E). Cells were seeded in a concentration of 10^5 cells per mL and cultivated for 2 days. Cell nuclei were visualized by counterstaining with Hoechst; actin filaments were visualized by counterstaining with ActinRed™ 555 The appropriate cytocompatibility was observed in the case of the PANI/CH and PANI/SH coating.

quantity was very similar to that observed for pure PIM samples. Based on microscopic observations it can be concluded, that cells were able to ingrowth deeper into the pores in all of the samples.

Due to the best cytocompatibility of CBS with pores higher than 250 μm and most promising properties of PANI/SH based coating the only CBS$^{\geq 250_D_PANI/SH}$ was used for further experiments.

3.5. Dynamic conditions and electrical stimulation improve cytocompatibility

The final goal of the here presented study was to prepare a CBS which is not only cytocompatible but also possess stimuli-responsive and thus even cell-instructive potential. The importance of *in vivo* occurred dynamic condition is often omitted within the cytocompatibility study. In this context, the mechanotransduction which integrates various physical cues from a cell's surrounding microenvironment and converts them into biochemical intracellular signaling responses are most important. The flow of cultivation medium (shear stress) is main part of mechanotransduction when the bone scaffolds are considered. Here we apply the media flow 54 RPMI. Except of mechanotransduction, the instructive role of electroconductivity is obviously of great importance. Especially in case of bone tissue, the role of electroconductivity of materials is discussed [21].

There are no generally accepted protocols used for the electrical stimulation of cells, the set-ups vary not only in the applied voltage (from ~ 4–5 mV to 150 mV) but also pulse duration (mostly from 2 ms to 200 ms), frequency (mostly between 2 and 6 Hz), and waveform (e.g. monophasic, square) [19,22,23]. In here presented experiments the commercial equipment was used and the electrical stimulation parameters were as follows: voltage 0.1 V, pulse width 3000 ms, arrangement on square-wave.

As mentioned, the CBS with a pore size above 250 μm was chosen for the experiments under dynamic conditions. The preferential cytocompatibility of materials with pore size of about 200 to 300 μm is generally considered as ideal for bone tissue replacements [24] and was confirmed even on the CBS (see Fig. 4A). The coating with PANI/SH was chosen as the most promising, mainly due to the bioactivity of SH.

Both described cell-stimuli external factors, shear stress and external electrical stimuli, were applied together, and the results are presented in Fig. 5. It is obvious that application of shear stress and external electrical stimulation has an important effect on few cellular parameters (please compare the Fig. 5A and 5B versus 5C and 5D). Firstly, the cell quantity is higher on the surfaces exposed to dynamic conditions, and more importantly the cell distribution is more homogeneous. This is critical for the scaffold acceptance after implantation [25]. In addition, a slightly different cell morphology and structure of cytoskeleton can be observed under dynamic conditions with electrical pulses than under static conditions. This can be connected to both the applied shear stress and electrostimulation [26,27].

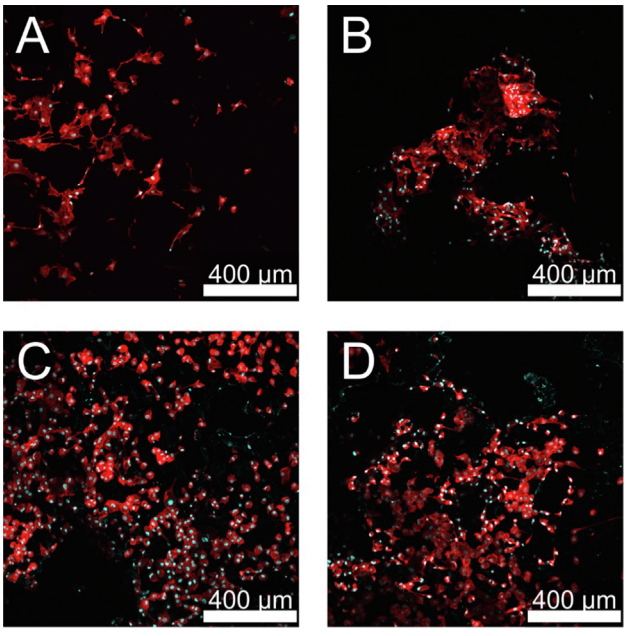

Fig. 5. Cell distribution and cell morphology on CBS$^{\geq 250_D_PANI/SH}$ under static (A,B) or dynamic (C,D) cultivation conditions. Cells were seeded in a concentration of 2 × 10^5 cells per mL and precultivated in static conditions for 3 days and subsequently cultivated in dynamic conditions for another 3 days. Cell nuclei are visualized by counterstaining with Hoechst, actin filaments are visualized by counterstaining with ActinRed. Parameters of dynamic conditions: Media flow 54 RPMI, pulse width 3000 ms, square waveform, voltage 0.1 V.

4. Conclusion

Ceramic-based scaffolds prepared by Powder Injection Molding are promising candidates for use as medical scaffolds, especially in bone regeneration and restoration. The composition of the PIM mixture as well as the processing parameters were tested to reveal their impact on the architecture of the porous material. It was found that the final architecture can be efficiently controlled by the powder space holder size and the volume ratio. However, alumina itself does not provide adequate cytocompatibility, or, especially, bioactivity. None of the prepared ceramic-based scaffolds induced cytotoxicity, and more importantly, cells were able to grow on their surface and ingrowth into the pores. The scaffolds surfaces were therefore subsequently functionalized by stimuli-responsive polyaniline-based films. To improve the cytocompatibility, coatings were innovatively prepared in colloidal dispersion mode and combined the synthetic conducting polymer with biopolymer stabilizers (sodium hyaluronate, chitosan, and sodium alginate). This functionalization further significantly improved the cytocompatibility of the ceramic-based scaffolds. The bioactivity of the prepared scaffolds was confirmed by an improvement in cytocompatibility when dynamic cultivation conditions and electrical impulses were applied. The *in vivo* mimicking conditions improve the cytocompatibility of scaffolds, especially in context of cell distribution and growth.

Data availability

Data will be made available on request.

Declaration of Competing Interest

The authors declare that they have no known competing financial interests or personal relationships that could have appeared to influence the work reported in this paper.

Acknowledgements

The work was supported within the project OP RDE Junior Grants of TBU in Zlin, Reg. No. CZ.02.2.69/0.0/0.0/19_073/0016941 (JUNG-2020-001), Czech Science Foundation (20-28732S) and Ministry of Education, Youth and Sports of the Czech Republic – DKRVO (RP/CPS/2022/001 and RP/CPS/2022/003).

Appendix A. Supplementary material

Supplementary data to this article can be found online at https://doi.org/10.1016/j.matdes.2022.111274.

References

[1] G. Matula, A. Szatkowska, K. Matus, B. Tomiczek, M. Pawlyta, Structure and properties of Co-Cr-Mo alloy manufactured by powder injection molding method, Materials 14 (8) (Apr. 2021) 2010, https://doi.org/10.3390/ma14082010.

[2] D. Zhao et al., Surface topography and cytocompatibility of metal injection molded Ti–22Nb alloy as biomaterial, Trans. Nonferrous Metals Soc. China 28 (7) (Jul. 2018) 1342–1350, https://doi.org/10.1016/S1003-6326(18)64772-7.

[3] M. Rahmati, M. Mozafari, Biocompatibility of alumina-based biomaterials–a review, J. Cell Physiol. 234 (4) (Apr. 2019) 3321–3335, https://doi.org/10.1002/jcp.27292.

[4] D.F. Heaney, J.D. Gurosik, C. Binet, Isotropic forming of porous structures via metal injection molding, J. Mater. Sci. 40 (4) (Feb. 2005) 973–981, https://doi.org/10.1007/s10853-005-6516-1.

[5] Y. Arteshi, A. Aghanejad, S. Davaran, Y. Omidi, Biocompatible and electroconductive polyaniline-based biomaterials for electrical stimulation, Eur. Polym. J. 108 (Nov. 2018) 150–170, https://doi.org/10.1016/j.eurpolymj.2018.08.036.

[6] J.L. Hernandez, K.A. Woodrow, Medical Applications of Porous Biomaterials: Features of Porosity and Tissue-Specific Implications for Biocompatibility, Adv Healthcare Materials 11 (9) (May 2022) 2102087, https://doi.org/10.1002/adhm.202102087.

[7] M.S. Zafar et al., "Properties of dental biomaterials", in *Advanced Dental Biomaterials*, Elsevier (2019) 7–35, https://doi.org/10.1016/B978-0-08-102476-8.00002-5.

[8] A.M.J. Coenen, K.V. Bernaerts, J.A.W. Harings, S. Jockenhoevel, S. Ghazanfari, Elastic materials for tissue engineering applications: Natural, synthetic, and hybrid polymers, Acta. Biomater. 79 (Oct. 2018) 60–82, https://doi.org/10.1016/j.actbio.2018.08.027.

[9] P. Bober, P. Humpolíček, J. Pacherník, J. Stejskal, T. Lindfors, Conducting polyaniline based cell culture substrate for embryonic stem cells and embryoid bodies, RSC Adv. 5 (62) (2015) 50328–50335, https://doi.org/10.1039/C5RA07504A.

[10] V. Kašpárková et al., Cell-compatible conducting polyaniline films prepared in colloidal dispersion mode, Colloids Surf., B 157 (Sep. 2017) 309–316, https://doi.org/10.1016/j.colsurfb.2017.05.066.

[11] D. Jasenská et al., Conducting composite films based on chitosan or sodium hyaluronate. Properties and cytocompatibility with human induced pluripotent stem cells, Carbohydr. Polym. 253 (Feb. 2021), https://doi.org/10.1016/j.carbpol.2020.117244 117244.

[12] V. Kašpárková et al., Polyaniline colloids stabilized with bioactive polysaccharides: Non-cytotoxic antibacterial materials, Carbohydr. Polym. 219 (Sep. 2019) 423–430, https://doi.org/10.1016/j.carbpol.2019.05.038.

[13] M. Hemshekhar, R.M. Thushara, S. Chandranayaka, L.S. Sherman, K. Kemparaju, K.S. Girish, Emerging roles of hyaluronic acid bioscaffolds in tissue engineering and regenerative medicine, Int. J. Biol. Macromol. 86 (May 2016) 917–928, https://doi.org/10.1016/j.ijbiomac.2016.02.032.

[14] F. Croisier, C. Jérôme, Chitosan-based biomaterials for tissue engineering, Eur. Polym. J. 49 (4) (Apr. 2013) 780–792, https://doi.org/10.1016/j.eurpolymj.2012.12.009.

[15] J. Sun, H. Tan, Alginate-Based Biomaterials for Regenerative Medicine Applications, Materials 6 (4) (Mar. 2013) 1285–1309, https://doi.org/10.3390/ma6041285.

[16] H.Ö. Gülsoy, R.M. German, Production of micro-porous austenitic stainless steel by powder injection molding, Scr. Mater. 58 (4) (Feb. 2008) 295–298, https://doi.org/10.1016/j.scriptamat.2007.10.004.

[17] K. Nishiyabu, S. Matsuzaki, S. Tanaka, Net-Shape Manufacturing of Micro Porous Metal Components by Powder Injection Molding, MSF 534–536 (Jan. 2007) 981–984, https://doi.org/10.4028/www.scientific.net/MSF.534-536.981.

[18] G. Engin, B. Aydemir, H.Ö. Gülsoy, Injection molding of micro-porous titanium alloy with space holder technique, Rare Met. 30 (6) (Dec. 2011) 565–571, https://doi.org/10.1007/s12598-011-0430-2.

[19] L. Leppik et al., Combining electrical stimulation and tissue engineering to treat large bone defects in a rat model, Sci. Rep. 8 (1) (Dec. 2018) 6307, https://doi.org/10.1038/s41598-018-24892-0.

[20] M.B. Asparuhova, V. Chappuis, A. Stähli, D. Buser, A. Sculean, Role of hyaluronan in regulating self-renewal and osteogenic differentiation of mesenchymal stromal cells and pre-osteoblasts, Clin. Oral. Invest. 24 (11) (Nov. 2020) 3923–3937, https://doi.org/10.1007/s00784-020-03259-8.

[21] D.T. Dixon, C.T. Gomillion, Conductive Scaffolds for Bone Tissue Engineering: Current State and Future Outlook, JFB 13 (1) (Dec. 2021) 1, https://doi.org/10.3390/jfb13010001.

[22] K. Ronaldson-Bouchard et al., Advanced maturation of human cardiac tissue grown from pluripotent stem cells, Nature 556 (7700) (Apr. 2018) 239–243, https://doi.org/10.1038/s41586-018-0016-3.

[23] Z. Zhao et al., Optimization of Electrical Stimulation for Safe and Effective Guidance of Human Cells, Bioelectricity 2 (4) (Dec. 2020) 372–381, https://doi.org/10.1089/bioe.2020.0019.

[24] C.M. Murphy, M.G. Haugh, F.J. O'Brien, The effect of mean pore size on cell attachment, proliferation and migration in collagen–glycosaminoglycan scaffolds for bone tissue engineering, Biomaterials 31 (3) (Jan. 2010) 461–466, https://doi.org/10.1016/j.biomaterials.2009.09.063.

[25] C. Kleinhans et al., A perfusion bioreactor system efficiently generates cell-loaded bone substitute materials for addressing critical size bone defects, Biotechnol. J. 10 (11) (Sep. 2015) 1727–1738, https://doi.org/10.1002/biot.201400813.

[26] C. Chen, X. Bai, Y. Ding, I.-S. Lee, Electrical stimulation as a novel tool for regulating cell behavior in tissue engineering, Biomater. Res. 23 (1) (Dec. 2019) 25, https://doi.org/10.1186/s40824-019-0176-8.

[27] J. Hansmann, F. Groeber, A. Kahlig, C. Kleinhans, H. Walles, Bioreactors in tissue engineering-principles, applications and commercial constraints, Biotechnol. J. 8 (3) (Mar. 2013) 298–307, https://doi.org/10.1002/biot.201200162.

Supplementary material

Powder injection molded ceramic scaffolds: the role of pores size and surface functionalization on the cytocompatibility

Martina Martínková et al.[1]

[1] *Centre of Polymer Systems and Faculty of Technology, Tomas Bata University in Zlin, 760 01 Zlin, Czech Republic*

SM 3.3 Cells can grow on the surface and within the pores of CBS under static cultivation conditions

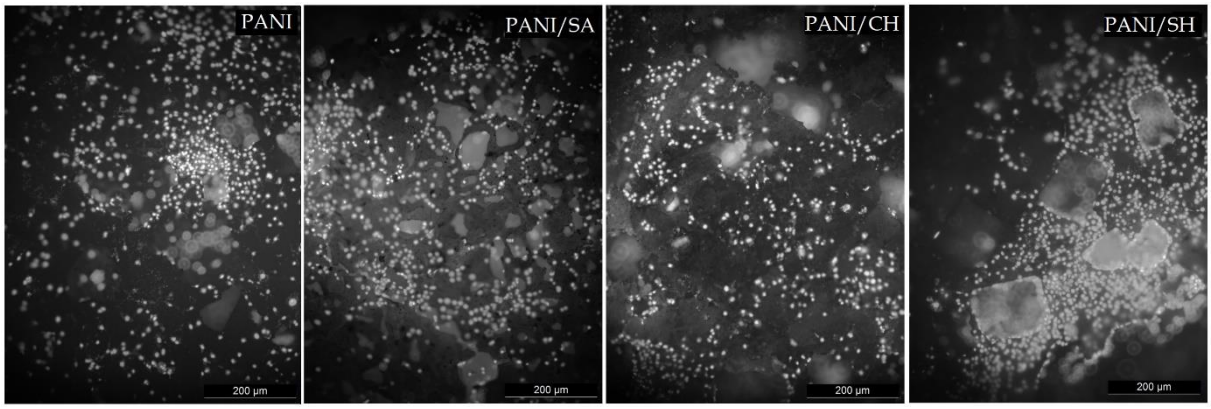

Fig. 1 Cell growth on a ceramic scaffolds ($CBS^{\leq 250\text{-}F}$) with all types of surface modifications.

From the photograph of the ceramic scaffold surface modified with pristine PANI, it can be seen that the cells are capable of adhesion and proliferation. On the surface modified with PANI/CH, there appear to be fewer cells, however, the cells ingrow into the scaffold's internal environment. As this is testing under static conditions, the cells are not evenly distributed on the surfaces.

ARTICLE 2

Skopalová K., Radaszkiewicz K.A., Kašpárková V., Stejskal J., Bober P., Junkar I., Mozetič M., Capáková Z., Lehocký M., **Kašparová M.**, Pacherník J., Humpolíček P., 2021. *Modulation of Differentiation of Embryonic Stem Cells by Polypyrrole: The Impact on Neurogenesis.* International Journal of Molecular Sciences 22, 501. DOI 10.3390/ijms22020501

International Journal of
Molecular Sciences

MDPI

Article

Modulation of Differentiation of Embryonic Stem Cells by Polypyrrole: The Impact on Neurogenesis

Kateřina Skopalová [1], Katarzyna Anna Radaszkiewicz [2], Věra Kašpárková [1,3], Jaroslav Stejskal [4], Patrycja Bober [4], Ita Junkar [5], Miran Mozetič [5], Zdenka Capáková [1], Marián Lehocký [1,3], Martina Kašparová [1], Jiří Pacherník [2,*] and Petr Humpolíček [1,3,*]

1 Centre of Polymer Systems, Tomas Bata University in Zlín, 760 01 Zlín, Czech Republic; skopalova@utb.cz (K.S.); vkasparkova@utb.cz (V.K.); capakova@utb.cz (Z.C.); lehocky@utb.cz (M.L.); m3_kasparova@utb.cz (M.K.)
2 Department of Experimental Biology, Faculty of Science, Masaryk University, 625 00 Brno, Czech Republic; 432029@mail.muni.cz
3 Faculty of Technology, Tomas Bata University in Zlín, 760 01 Zlín, Czech Republic
4 Institute of Macromolecular Chemistry, Academy of Sciences of the Czech Republic, 162 06 Prague 6, Czech Republic; stejskal@imc.cas.cz (J.S.); bober@imc.cas.cz (P.B.)
5 Department of Surface Engineering, Jožef Stefan Institute, Jamova cesta 39, SI-1000 Ljubljana, Slovenia; ita.junkar@ijs.si (I.J.); miran.mozetic@ijs.si (M.M.)
* Correspondence: jipa@sci.muni.cz (J.P.); humpolicek@utb.cz (P.H.)

Abstract: The active role of biomaterials in the regeneration of tissues and their ability to modulate the behavior of stem cells in terms of their differentiation is highly advantageous. Here, polypyrrole, as a representantive of electro-conducting materials, is found to modulate the behavior of embryonic stem cells. Concretely, the aqueous extracts of polypyrrole induce neurogenesis within embryonic bodies formed from embryonic stem cells. This finding ledto an effort to determine the physiological cascade which is responsible for this effect. The polypyrrole modulates signaling pathways of Akt and ERK kinase through their phosphorylation. These effects are related to the presence of low-molecular-weight compounds present in aqueous polypyrrole extracts, determined by mass spectroscopy. The results show that consequences related to the modulation of stem cell differentiation must also be taken into account when polypyrrole is considered as a biomaterial.

Keywords: conducting polymer; polypyrrole; biocompatibility; neurogenesis; stem cells

Citation: Skopalová, K.; Radaszkiewicz, K.A.; Kašpárková, V.; Stejskal, J.; Bober, P.; Junkar, I.; Mozetič, M.; Capáková, Z.; Lehocký, M.; Kašparová, M.; et al. Modulation of Differentiation of Embryonic Stem Cells by Polypyrrole: The Impact on Neurogenesis. *Int. J. Mol. Sci.* **2021**, *22*, 501. https://doi.org/10.3390/ijms22020501

Received: 9 December 2020
Accepted: 29 December 2020
Published: 6 January 2021

1. Introduction

The conjugated structure of conducting polymers (CPs) is, among other factors, mainly responsible for their unique properties, such as high electron affinity, low energy optical transmission, and low ionization potential [1]. Another advantageous aspect of utilizing CPs, especially in biomedicine, is their intrinsically combined electron and ionic conductivity. As a result, CPs are able to convert electrical signals to ionic ones and vice versa. This is a crucial factor for the efficient exchange of signals and stimuli between living objects (e.g., cells or tissues) and conducting materials [2]. Therefore, CPs are excellent materials for tissue engineering with respect to stimulating nerve cells and tissues [3], as electrical stimulation increases neurite outgrowth in vitro and promotes nerve regeneration in vivo [4]. Electric stimuli also affect the differentiation of embryonic stem cells (ESCs). In contrast to cells differentiated by growth factors, ESCs stimulated by electric current are able to differentiate into more specific types [5].

Polypyrrole (PPy) is one of the most studied CPs in the context of tissue engineering applications. It can be synthesized by chemical or electrochemical polymerization [6,7]. The electrochemical method is relatively expensive, and, moreover, a conducting substrate is required for the polymerization. The chemical synthesis of PPy can be accomplished

using oxidative polymerization, admicellar polymerization, and layer-by-layer deposition [8], giving rise to PPy in the conducting form of a salt, which can be converted by alkali treatment to a non-conducting base [9,10]. PPy polycation is prepared in the form of thin films or powders, and negatively charged counter-ions can be incorporated into its structure during polymerization. By changing the counter-ions, also called "dopants", the physical properties of the polymer can be controlled [11].

In tissue engineering, the application of electrical stimuli through PPy not only increases neurite outgrowth but also regulates the shape and function of endothelial cells, and enhances the proliferation of smooth muscle cells. PPy also exhibits interesting potential with respect to its application in controlled drug release. If a suitable dopant is incorporated in the polymer, it can be released into the surrounding environment by electrical stimulation [12]. For example, Richardson et al. [13] prepared cochlear implant electrodes coated with a combination of PPy, *p*-toluene sulfonate, and nerve growth factor neurotrophin-3 (NT3). The release of NT3 was controlled by electrical stimuli and neurite outgrowth increased. However, PPy is not only suitable for the cell stimulation by electrical signals, but also exhibits antimicrobial activity. Such antimicrobial activity was, for example, confirmed in a study by Milakin et al. [14], who demonstrated the antimicrobial effect of cryogel scaffolds combining PPy and gelatin.

The abovementioned studies clearly demonstrate the unique properties of PPy itself; however, PPy is also interesting due to the properties of its main precursor, heterocyclic pyrrole. The pyrrole molecule is contained in a broad range of therapeutic substances and natural products as one of the main constituents, such as porphyrins. Thus, this heterocyclic compound and its derivatives can serve as the source of a number of pharmacologically active substances. For example, Kang et al. reported on pyrrole-3-carboxamide, which was evaluated as an antidepressant drug [15], and pyrrole derivatives with a sulfonamide group were reported to exhibit antitumor activity [16]. PPy derivatives are also known for their neuroprotectivity. Aiello et al. [17] investigated the natural pyrrole containing product daminin, which showed neuroprotective ability against Parkinson's and Alzheimer's diseases. In general, pyrrole derivatives can also act as anti-inflammatory, antituberculous, antiviral, antimalarial, and insecticidal agents [18]. In summary, the above facts suggest that pyrrole and its derivatives affect intracellular signaling pathways. Thanks to the promising application potential of conducting polymers in tissue engineering, the investigation of their biological properties has been at the center of attention for several years. In addition to their basic characteristics, such as cytotoxicity, adhesion, and the ability to enhance cell growth, neurogenesis has remained at the center of efforts towards developing new, smart materials. To the best of our knowledge, no previous study has investigated the effect of PPy, PPy oligomers (Figure 1), low-molecular-weight by-products, or residual impurities present in PPy after its synthesis on the neurogenesis of stem cells. The biological activity of pyrrole and a large number of its derivatives has led the authors to question the role of these low-molecular-weight substances in the control of cellular fate. Therefore, the aim of this paper was to determine the impact of aqueous PPy extracts containing the pyrrole-based substances on the neurogenesis of ESCs.

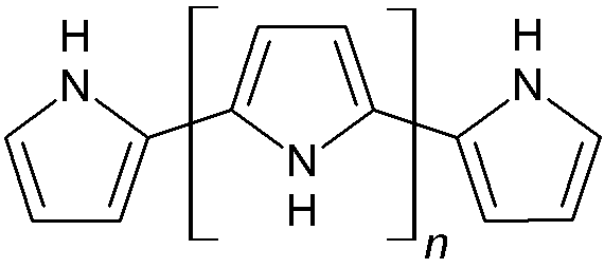

Figure 1. The formula of pyrrole oligomer. n = 0, 1, 2, ...

2. Materials and Methods

2.1. Preparation of PPy Powders

Polypyrrole salt was synthetized by oxidizing 0.2 M pyrrole (Sigma-Aldrich, China) with 0.5 M iron-(III) chloride hexahydrate (Sigma-Aldrich, Germany) in an aqueous environment. The oxidant-to-pyrrole mole ratio was 2.5. The mixture was left to polymerize at room temperature for 12 h. The precipitated black PPy was collected on a filter, rinsed with 0.2 M hydrochloric acid followed by acetone, and dried at room temperature over silica gel [19]. Preliminary tests conducted in this laboratory demonstrated that the effect of PPy base (formed via the deprotonation of PPy salt with ammonia [10]) on neurogenesis was insignificant; therefore, the present study applies only to PPy hydrochloride (hereinafter referred to as PPy) and the preparation of PPy base is not reported.

2.2. Preparation of Extracts

Samples of PPy were extracted according to ISO 10993-12 with the following modification: 0.05 g PPy per 1 mL of cultivation medium was used instead of the ISO-defined ratio of 0.2 g polymer per 1 mL. The extraction was conducted in chemically inert closed containers using aseptic techniques at 37 ± 1 °C under stirring for 24 h. Subsequently, the extract was separated from the polymer powder by centrifugation at 1000 g for 15 min followed by the second centrifugation of supernatant under the same conditions. The parent extracts (100%) were used for the testing of cytotoxicity according to the ISO 10 993-5 protocol. The parent 100% extracts were diluted in complete medium to obtain a series of dilutions. All extracts were used within 24 h. Prior to in vitro testing, the extracts the extracts were sterilized by sterile filtration through a 0.22 µm Millex GV filter (Merck, Darmstadt, Germany). All tests were performed in four separate sets.

2.3. Culture of Embryonic Stem Cells

The embryonic stem cell ES R1 line [20] was propagated in an undifferentiated state by culturing on gelatinized tissue culture dishes in complete media. The gelatinization was performed using 0.1% porcine gelatin in water. Complete medium with the following composition was used for the cultivation: Dulbecco's Modified Eagle's Medium (DMEM), 15% fetal calf serum, 100 U mL^{-1} penicillin, 0.1 mg mL^{-1} streptomycin, 100 mM non-essential amino acids solution (all from Thermo Fisher, Waltham, MA, USA), 0.05 mM 2-mercaptoethanol (Sigma, St. Louis, MO, USA) and 1000 U mL^{-1} of leukemia inhibitory factor (LIF) (Gibco, MA, USA) [21,22].

2.4. Cytotoxicity

The cytotoxicity testing of extracts of PPy was performed according to the ISO 10 993-5 protocol. Samples were extracted according to ISO 10993-12 in the ratio of 0.2 g per 1 mL of DMEM media. Extraction was performed in chemically inert closed containers using aseptic techniques at 37 ± 1 °C under stirring for 24 h. The parent extracts (100%) were then diluted in a complete medium to obtain a series of dilutions with concentrations of 25, 10, 5 and 1%. All extracts were used within 24 h. For proliferation testing, cells were seeded at a density of 5000 cells per cm^2 24 h before treatment. As a reference giving 100% cell proliferation, cells cultivated in the complete medium without extract added were used. In addition, the proliferation of cells differentiating in the presence of extracts but without the presence of LIF in the cultivation medium was also tested. Cells were treated with extracts for 48 h and, to assess cytotoxic effects, the mass of viable cells was determined as the level of ATP using Cellular ATP Kit HTS (Biothema, Handen, Sweden). Samples were prepared and analyzed according to Konopka et al. [23]. Before lyses, the morphology of the cells was observed and documented using an inverted Olympus phase contrast microscope (Olympus IX51, Tokyo, Japan) supplemented with a digital camera (Olympus E-450, Tokyo, Japan). All tests were performed in four separate sets. Statistical significance was determined by ANOVA with post hoc Tukey's Multiple Comparison test; * $p < 0.05$.

2.5. ESCs Differentiation

The ESC differentiation was induced through the formation of embryoid bodies (EBs) by hanging drop techniques (400 cells per one 35 µL drop) in LIF-free complete medium [24]. Pictures of growing EBs were captured by digital camera using an Olympus binocular microscope (Olympus SZX7, Tokyo, Japan). The diameter of five-day-old EBs was measured and the number of EBs with expanding neuronal cells was also determined. The EBs were treated with 1, 5, and 25% extract of PPy for 5 days. Consequently, the number of expanding EBs in adherent culture with visible neurites was determined on days 7 and 11 after the seeding of 5-day-old EBs (12 and 16 days of ESC differentiation in total).

In the next step, the 5-day-old EBs were transferred to a gelatinized 24-well plate (one EB per well) and cultivated in serum-free DMEM-F12 media (1:1) containing 100 U mL^{-1} penicillin, 0.1 mg mL^{-1} streptomycin and insulin–transferrin–selen (ITS) supplement (all from Thermo Fisher, Waltham, MA, USA) for the next 11 days. The medium was replaced with fresh medium every 2 days of cell culture. Differentiating cells were observed using an inverted Olympus phase contrast microscope (Olympus IX51, Tokyo, Japan) and documented with a digital camera (Olympus E-450, Tokyo, Japan) [21]. All tests were performed in four separate sets. Data are reported as the mean and standard deviations from a minimum of four independent experiments. ANOVA with post hoc Tukey's Multiple Comparison test was applied to determine any statistical differences between the samples. p values of ≤ 0.05 were considered statistically significant. Design of experiment leading to formation of EBs in the presence or absence of PPy extracts is given in Figure 2.

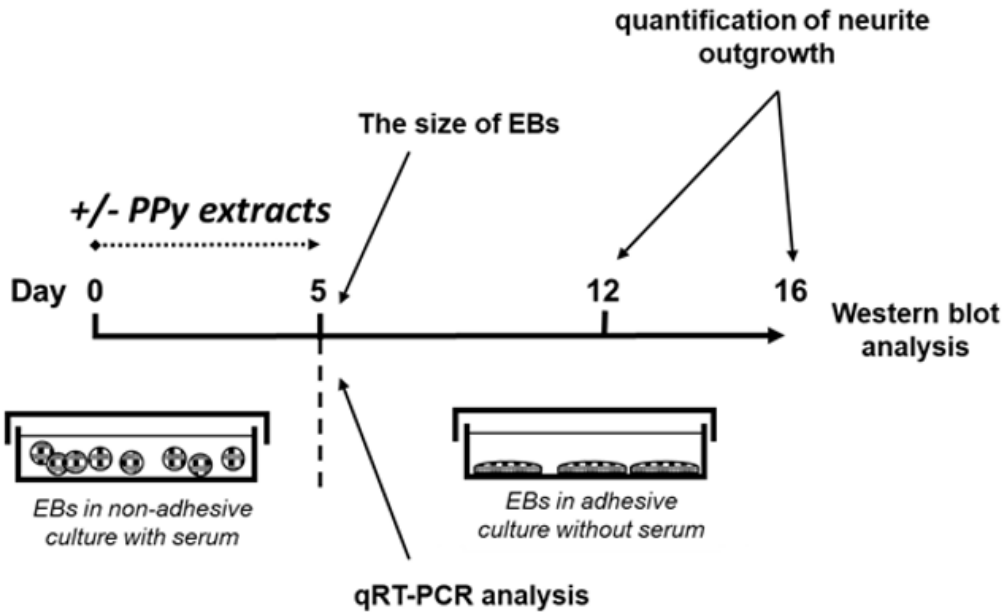

Figure 2. Design of experiment: formation of embryoid bodies in the presence or absence of PPy extracts.

2.6. Expressions of Neural Markers by Quantitative RT-PCR

Total RNA was extracted by Qiagen RNeasy Mini Kit (Qiagen, Hilden, Germany). Complementary DNA was synthesized according to the manufacturer' instructions for RevertAid Reverse Transcriptase reverse transcriptase kit (Thermo Fisher, Waltham, MA, USA). Real-time PCR of neural cell phenotype markers was performed in a Roche 480 Light-Cycler using Light Cycler®480 DNA SYBR Green I Master (Roche, Basel, Switzerland). Primers and annealing conditions are listed in Table 1. GAPDH was used as a reference gene [24–26]. Data are presented as the differences between reference and samples treated with PPy extracts after normalization to the reference gene by the $2^{-(Cq(target)-Cq(reference))}$ method [27,28]. All tests were performed in four separate sets. Data are reported as

the mean and standard deviations from a minimum of four independent experiments. Statistical significance was determined by ANOVA with post hoc Tukey's Multiple Comparison test; * $p < 0.05$. (*) and (#) mark statistically significant differences compared to ESCs and to EBs without PPy treatment, respectively.

Table 1. Primer sequences for target and reference genes used in qRT-PCR assays; F = forward primer (5′–3′), R = reverse primer (3′–5′).

Gene	Primer Sequence	T annealing (°C)	Product Size (pb)
Pax 6	F TGCCCTTC-CATCTTTGCTTG R TCTGCCCGTTCAA-CATCCTTAG	60	178
Sox 1	F CCAGCCTCCA-GAGCCCGACT R GGCATCGC-CTCGCTGGGTTT	62	258
Mash 1	F GGTCTCGTCC-TACTCCTCCG R GCTGCCATCCT-GCTTCCAAA	62	137
Gapdh	F AAGGGCTCAT-GACCACAGTC R CATACTTG-GCAGGTTTCTCCA	62	252

2.7. Western Blot

Western blot assay of the expressions of the neuron-specific proteins N-cadherin, N-CAM, β III tubulin, and doublecortin [29–33] in non-differentiating ESCs and in differentiating ESCs with and without PPy treatment (reference (REF)) on Day 16 of differentiation was performed. The level of β-actin was used as a control of protein loading [34]. Cells were directly lysed using 100 mM Tris/HCl (pH 6.8), 20% glycerol, 1% sodium dodecyl sulfate, 0.01% bromophenol blue, and 1% 2-mercaptoethanol. Western blotting was performed according to the manufacturer's instructions with minor modifications. Concretely, the SDS-PAGE was run at 110 V and the transfer onto polyvinylidine fluoride membrane was conducted for 1 h at 100 V (Mini-Protean III; Bio-Rad, Hercules, CA, USA). Membranes were blocked in 5% non-fat dry milk solution in TBS-Tween 20 buffer (TBST) for 30 min and subsequently incubated overnight at 4 °C with the following primary antibodies: N-CAM (Sigma, St. Louis, MO, USA), N-cadherin (BD Biosciences, Franklin Lakes, NJ, USA, 610920), doublecortin (Abcam, Cambridge, United Kingdom, 18723), β-III-tubulin (Sigma, St. Louis, MO, USA, T5076), p-Akt (phospho-S473; Cell Signaling, 4060), Akt (Cell Signaling Technology, Beverly, MA, USA, 4691), p-ERK1/2 (phospho-T202/Y204; Cell Signaling Technology, Beverly, MA, USA, 8544), ERK1/2 (Cell Signaling Technology, Beverly, MA, USA, 4695), p-GSK3 (phospho-S9; Cell Signaling Technology, Beverly, MA, USA, 9336), and β-actin (Santa Cruz Biotechnology, Dallas, TX, USA, SC47778). The membranes were washed in TBST and incubated with horse radish peroxidase-conjugated secondary antibodies (Sigma, St. Louis, MO, USA). Immunoreactive bands were detected using ECL detection reagent kit (Sigma, St. Louis, MO, USA) and the FusionSL chemiluminescence documentation system (Vilber-Lourmat, Collégien, France). Results were quantified by the densitometric analysis of Western blot bands using the Fiji distribution of ImageJ. All tests were performed in four separate sets. Data are presented as mean and standard deviation from a minimum of four independent experiments. Statistical significance was determined by ANOVA with post hoc Tukey's Multiple Comparison test; * $p < 0.05$. (*) and (#) mark statistically significant differences compared to ESCs and to EBs without PPy treatment, respectively.

2.8. Characterization of Extracts

PPy extracts were analyzed with a 1260 Series liquid chromatography system coupled to a 6520 Accurate-Mass Q-TOF mass spectrometer (both Agilent Technologies, Santa Clara, CA, USA). A dual-spray electrospray ionization source was employed. A sample volume of 5 µL was infused into a continuous flow of mobile phase with no column installed. Samples were eluted with a flow rate of 0.3 mL min^{-1} using 1% (v/v) aqueous formic acid at 30 °C.

Mass spectroscopy analyses were conducted on PPy extracts prepared using the procedure described above, with deionized water as the extraction liquid. The positive ion mode mass spectrometry conditions were as follows: gas temperature, 300 °C; fragmentor voltage, 75 V; capillary voltage, 3 kV; nozzle voltage, 2 kV; scan range m/z, 50 to 1700; 1 $scan^{-1}$. The internal mass reference ions m/z 922.009798 and 121.050873 were used to keep mass axis calibration stable during the analysis.

2.9. Statistical Analysis

Statistical significance was determined by ANOVA with post hoc Tukey's Multiple Comparison test. More detailed information and values of significance are provided in individual chapters in the methodology.

3. Results and Discussion

The effect of the electrical conductivity of the material is particularly interesting with respect to excitable tissues and cells, such as cardiac or nerve cells, represented here by neuronal lines derived from ESCs. A prerequisite for using any material in contact with cells and tissues is the absence of its cytotoxicity, which concerns also materials based on PPy. In studies by Humpolíček et al. [19] and Capákova et al. [35], the cytotoxic properties of two PPy forms were tested, namely protonated PPy salt and deprotonated PPy base, which were prepared by various techniques.

As the effect of PPy base on neurogenesis proved to be insignificant, the current study reports only on the investigation of neurogenesis induced by extracts of PPy salt (hereinafter referred to as PPy). As described in the work by Humpolíček et al. [19], PPy extract loses its cytotoxic effect at 5% concentration. In the case of the embryotoxicity of PPy, erythroid cluster formation and beating foci completely disappeared in the presence of 25% extract.

The cytotoxic effect of PPy extracts (1, 5 and 25%) on ESCs was also determined in the present study. Cytotoxicity was tested not only on undifferentiated ESCs in the presence of leukemia inhibitory factor (LIF) but also on cells that differentiated spontaneously due to LIF depletion. The results are presented in Figure 3, demonstrating a correlation between relative cellularity, PPy extract concentration and cell phenotype. For undifferentiated cells cultured in the presence of LIF, a cytotoxic effect was observed at the highest tested concentration of PPy extract (25%). The results are comparable with those reported by Humpolíček et al. [19]. The ability of ESCs cultured in the absence of LIF to undergo spontaneous differentiation has already been reported by Smith et al. [36]. In the case of cells that underwent differentiation (Figure 3B), the relative cellularity was reduced by almost 50% already in the presence of the lowest concentration of PPy extract (1%), in comparison with the reference. Therefore, cells cultured under normal conditions, in which they retain their ability to self-renew, and in an undifferentiated state exhibit higher resistance to environmental changes.

The work described here, which extends the abovementioned study by Humpolíček et al. [19], concentrates on testing the toxicity impact on EBs. Cells were exposed to extracts during the induction and maintenance of EBs for a period of 5 days. In principle, EBs mimic the development of embryos and the cells differentiate into all three embryonic germ layers [37]. The cytotoxic effect of PPy extract on the size of growing EBs is shown in Figure 4A. Significant reductions in EBs sizes were found only in the case of cultivation with 25% extract. Here, the cells differentiated into many types and formed abundant

intercellular interactions (Figure 4B). The influence of lower tested concentrations of PPy extract (1 and 5%) did not negatively influence EB dimensions, demonstrating thus no harmful effect on the part of the studied substance.

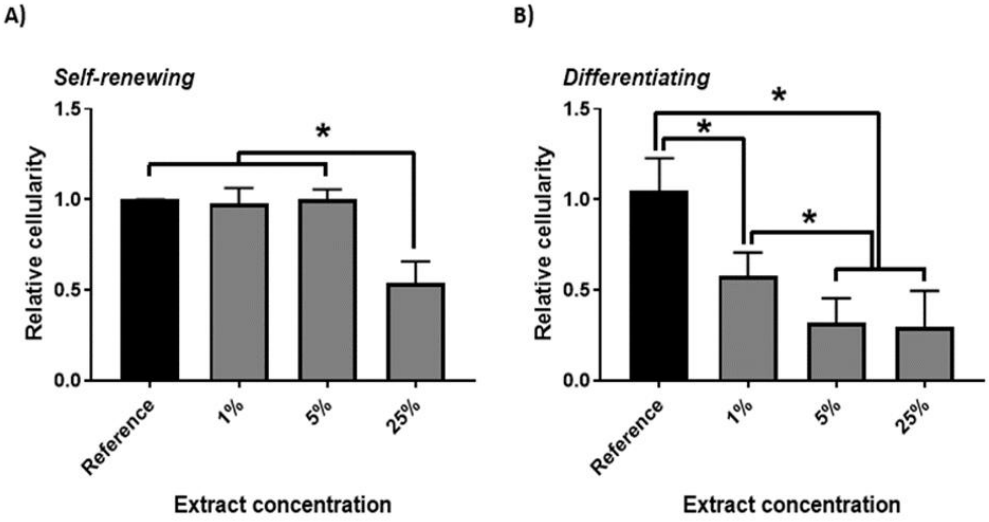

Figure 3. Cytotoxic effect of polypyrrole (PPy) extract on embryonic stem cells (ESCs) after treatment with 1, 5, and 25% extract in self-renewing media (**A**), and in media enabling their spontaneous differentiation (**B**) after 48 h in comparison with reference. Data are reported as the mean and standard deviations from a minimum of four independent experiments. ANOVA with post hoc Tukey's Multiple Comparison test was applied to determine any statistical differences between the samples. p values of ≤ 0.05 were considered statistically significant and are labeled with (*).

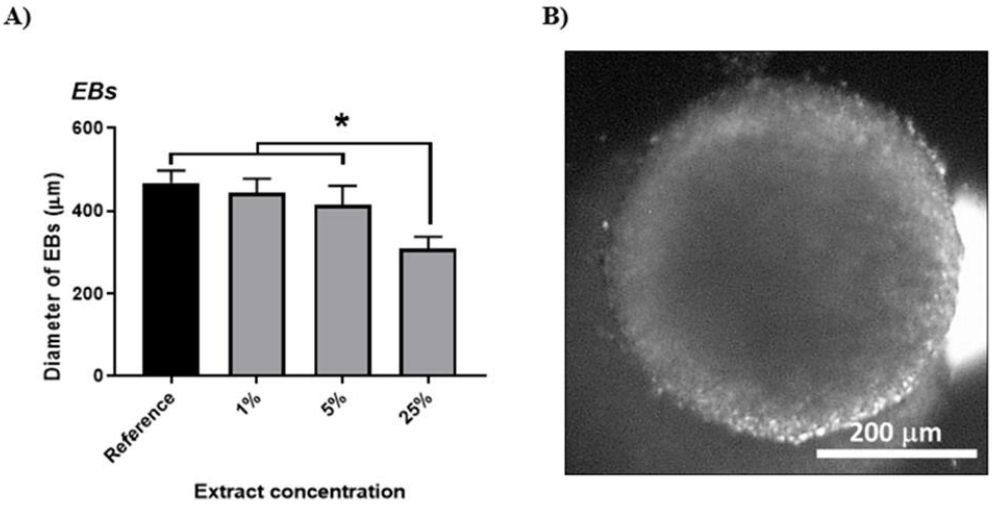

Figure 4. (**A**) Cytotoxic effect of PPy extract on embryoid bodies (EBs). The size of EBs determined on Day 5 of culture. (**B**) Embryonic body. Data are reported as the mean and standard deviations from a minimum of four independent experiments. Statistical significance was determined by ANOVA with post hoc Tukey's Multiple Comparison test; * $p < 0.05$.

Due to its conductivity, PPy can serve as smart material influencing cell differentiation and promoting the proliferation of various types of nerve cells. However, additional external factors, such as the presence of signaling molecules or an electric current are needed for successful cell differentiation. Therefore, the use of PPy formulated as a scaffold, which can combine all these factors, enhances the ability of cells to differentiate. A recent study by Granato et al. [38] investigated the differentiation of the murine Neuro2a cell line on poly (butylene adipate-*co*-terephthalate) (PBAT) fibers blended with PPy. The cells were cultured on the material for three days in the presence of media promoting neurodifferentiation.

On a substrate containing 2% PPy, the occurrence of neurites was higher in comparison with neat PBAT. The presence of PPy in the blend also increased its hydrophilicity, resulting in improved cell adhesion. In another work, Stewart et al. [39] investigated the effect of PPy on the differentiation of human neural stem cells (hNSCs) in the presence of an electric field. The conducting PPy substrate promoted differentiation into neurons under the influence of electric current, in contrast to the reference (a glass-based substrate with protein laminin). Biocompatibility with Schwann cells is also very important for the use of materials in neural tissue engineering. This was demonstrated in a study conducted by Wang et al. [40], who reported on the absence of cytotoxic effects even in the case of 50% PPy extract. Moreover, Schwann cells were able to proliferate on the PPy membrane. Comparable results were published by Sun et al. [41]. Here, a PPy coated composite of poly (L-lactic acid-*co*-ε-caprolactone) with silk fibroin (PLCL/SF) was used as the test material. In comparison with the reference (non-coated PLCL/SF), Schwann cells manifested better proliferation on PPy-coated PLCL/SF. The authors also used this conducting polymer to induce the differentiation of neuroblastic cells in the absence of nerve growth factor in the culture medium by applying only an electric field. However, they observed that the conducting polymer was not able to induce differentiation without stimulation by the electrical current. On the basis of the findings reported in the above publications, it can be stated that all the mentioned factors playing a role in neurogenesis are mutually supportive.

However, to date, no studies have been published on the effect of PPy extracts on the neurogenesis of ESCs. Here, EBs were formed by the hanging drop method in the presence of 1, 5 and 25% PPy extracts for 5 days. Then, EBs were cultivated on adherent plastic in the absence of serum in the culture medium. Neurogenesis was evaluated on days 7 and 11 of culture (12 and 16 days of overall differentiation, respectively) as the percentage of bodies with visible neurites (Figure 5B). Compared to reference cells, extract-treated EBs developed earlier and more frequent neuronal processes. The 5% PPy extract exerted the greatest effect on the formation of neurites (Figure 5A). In the light of these results, the expressions of early neurogenic transcripts were evaluated in 5-day-old EBs growing in the presence of 5% PPy extract. For comparison, expression was also assessed in undifferentiated ESCs and EBs formed without extract. PAX6 [42], SOX1 [43] and MASH1 [44] are factors important for neurogenic processes and are expressed primarily at the beginning of neuron development. As expected, the expression levels of these transcripts in ESCs were very low. EBs cultured in the absence of extract increased the expression of all genes due to spontaneous differentiation. However, the highest level of expression was observed in EBs in the presence of 5% PPy extract (Figure 5C).

Neurogenesis was also determined through the protein level by means of Western blot assay. The neuron-specific proteins were carefully chosen on the basis of their properties and action during neurogenesis. N-cadherin was one of the neuroproteins tested in the present study. N-cadherin has an important function for cell adhesion and also for cell interactions under the development of the central nervous system (CNS) [29]. N-CAM (also known as CD56), the neural cell adhesion molecule, was chosen as another marker of neurogenesis. This immunoglobulin occurs on the cell surface in the central and peripheral nervous systems. Along with N-cadherin, it is involved both in cell adhesion and in synaptogenesis [30]. A protein that is also involved in neurogenesis is β-III-tubulin (or TUJ1). It is predominantly expressed in the cytoskeleton of neuroblasts [31]. Another protein detectable under the development of embryonic neural systems is doublecortin (doublin), which belongs to the family of microtubule-associated proteins (MAPs) and is mainly involved in neuronal migration [32,33]. It is commonly used in experiments as one of the markers of neurogenesis.

In the present study, the expressions of the abovementioned neurospecific proteins (N-cadherin, N-CAM, β-III-tubulin, and doublecortin) were studied, with beta-actin used as a reference protein. Expression was determined after 16 days of cultivation both in undifferentiated ESCs and in differentiated cells in the absence and presence of 5% PPy extract. The results of the assay, summarized in Figure 6, show a significant increase in the

expressions of all the tested neuroproteins in PPy-treated cells, these being higher by 50% or more than in the samples with PPy extract absent. The presented observations, therefore, indicate that PPy extracts contain compounds that positively affect cell neurogenesis.

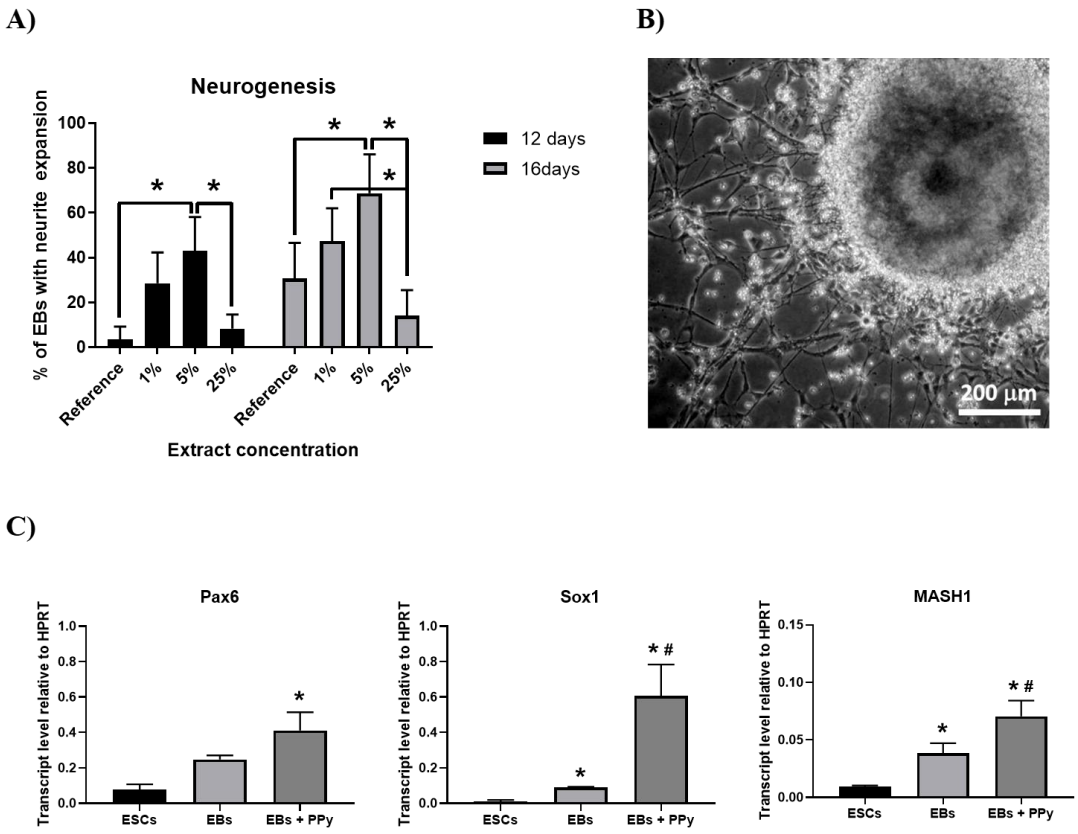

Figure 5. Influence of PPy extracts on neurogenesis. (**A**) Formation of EBs with neurite expansion after treatment with PPy extracts. (**B**) Microscopic visualization of expanded EB with neurites. (**C**) the expression of early neurogenic transcripts (Pax6, Sox1, and MASH1) in non-differentiating ESCs and in 5-day-old EBs growing in the absence (EBs) or in the presence of 5% PPy extract (EBs + PPy). Data are reported as the mean and standard deviations from a minimum of four independent experiments. Statistical significance was determined by ANOVA with post hoc Tukey's Multiple Comparison test; * $p < 0.05$. (*) and (#) mark statistically significant differences compared to ESCs and to EBs without PPy treatment, respectively.

Akt (or PBK) is a serine/threonine kinase involved in a variety of processes such as the regulation of cell growth, proliferation, migration, protein synthesis, and differentiation. The disruption of Akt kinase-mediated signal transduction leads to neurodegenerative diseases, such as Alzheimer's, Parkinson's, and Huntington's disease. Akt occurs in the organism in three forms (Akt1, Akt2 and Akt3) that share a highly conserved structure. All isoforms are abundantly expressed in the CNS and their activation is affected by various growth factors, insulin, or cell stress. Akt activity is determined as the ratio of phosphorylated Akt at Ser473 to total Akt [45,46]. Through the PI3K signaling pathway, Akt is involved in neuronal survival and growth [47,48]. GSK-3 (glycogen synthase kinase-3) is one of the most important physiological substrates for Akt [49,50]. The activity of this signaling molecule is usually inhibited by Akt phosphorylation, following a response to stimulation by a certain factor [51,52].

To discover possible molecular mechanisms underlying the influence of PPy extract on neurogenesis, the status of selected signaling proteins was determined (Figure 7). Various pyrrole-containing compounds have the ability to inhibit the activity of GSK3 [53–55]. Other kinases, such as Akt (or PKB) and/or ERK can phosphorylate and thus also modify the activity of GSK3 [56,57]. The ability of PPy extract to inhibit the phosphorylation of the mentioned kinases was also determined within this study. Concretely, the ESCs

were seeded 24 h before treatment with 10% PPy extract and subsequently exposed to extract for 15 and 60 min. Cells were lysed and analyzed by the Western blot technique. PPy extract significantly attenuated the level of phosphorylated Akt kinase at both tested time points. In contrast to Akt, the level of phosporylated ERK increased; however, a significant increase was observed only in the sample treated for 15 min. No changes were observed in the phosphorylation of GSK3 in cells treated by PPy extract (Figure 7). As already mentioned above, it was reported that various pyrrole-containing compounds inhibited the activity of GSK3 [53–55]. GSK3 plays an important role in a myriad of cellular processes including the regulation of neurogenesis and neuronal function in the developing and adult brain [57]. The phosphorylation status of GSK3 Ser9 was unchanged in cells exposed to PPy extract. Accordingly, we believe that the activity of GSK3 was not modified by extract of PPy. Unexpectedly, here, downregulation of the phosphorylation of GSK3 upstream kinase Akt (Ser473) was observed, which reflects the inhibition of Akt activity. In contrast, the phosphorylation of ERK (another important upstream kinase of GSK3) was slightly downregulated. This reciprocal phospho status of Akt and ERK kinases corresponds to mutual competition between their signaling pathways [58]. The stimulation of ESC neurogenesis by the inhibition of Akt kinase activity was described previously [59]. Moreover, many growth factors activate Akt signaling in many cell types. On the other hand, growth factor depletion, which also leads to the inhibition of Akt activity, provides the initiation of neurogenesis in ESCs [60,61]. On the basis of these facts, we assume that the promotion of neurogenesis in ESCs by PPy extract is connected with the PPy extract-mediated modulation of Akt signaling pathway activity.

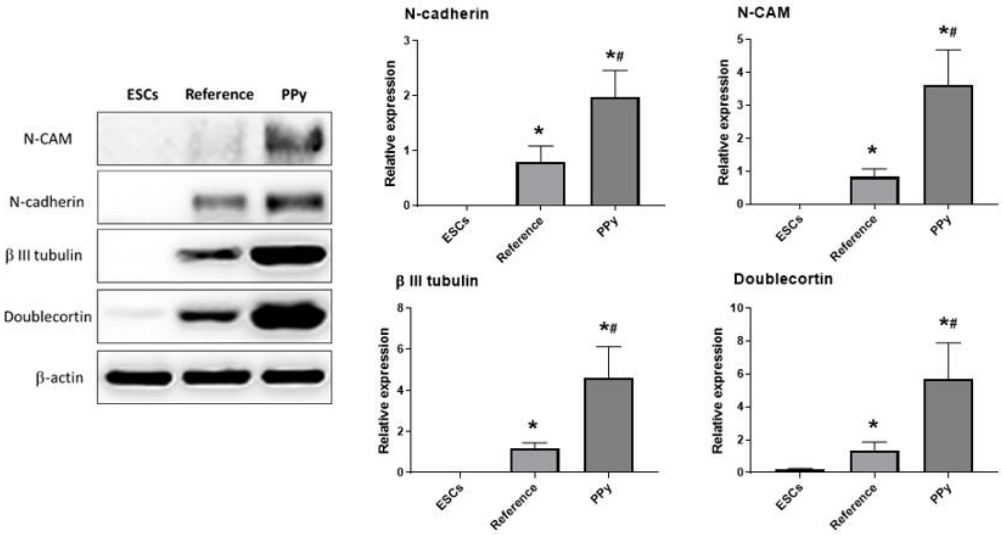

Figure 6. Western blot assay of the expression of neuron-specific proteins N-cadherin, N-CAM, β-III-tubulin, and doublecortin in non-differentiating ESCs and in differentiating ESCs with PPy treatment (PPy) and without PPy treatment (Reference) on day 16 of differentiation. The level of β-actin was used as a control of protein loading. Data are reported as the mean and standard deviations from a minimum of four independent experiments. Statistical significance was determined by ANOVA with post hoc Tukey's Multiple Comparison test; * $p < 0.05$. (*) and (#) mark statistically significant differences compared to ESCs and to Reference, respectively.

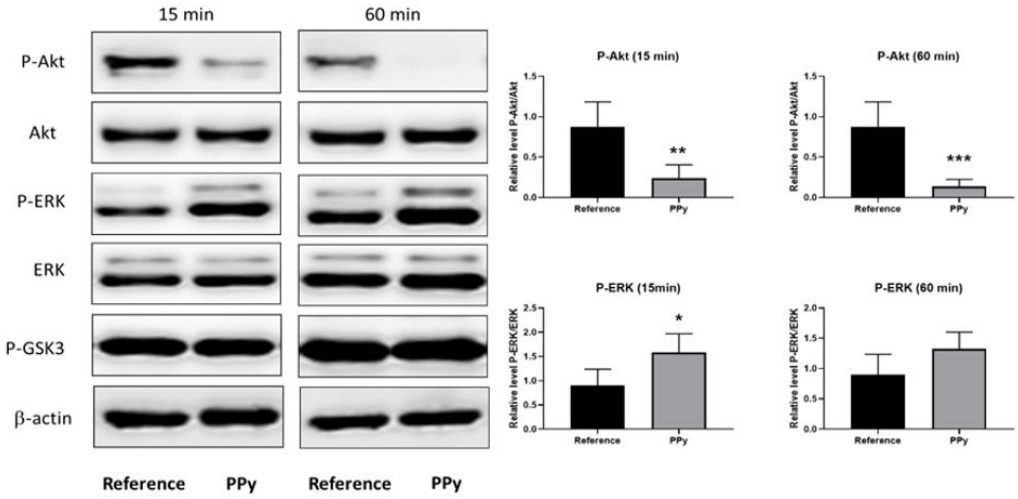

Figure 7. PPy extract inhibits Akt kinase phosphorylation. ESCs were either exposed or not exposed (reference) to 10% PPy extract (PPy) for 15 and 60 min. The levels of active, phosphorylated forms of Akt, ERK and GSK3 kinases, and the level of β-actin were determined by Western blot techniques. The level of β-actin was used as a control of protein loading. Representative Western blot and quantified data from four independent experiments are shown. Statistical significance was determined by *t*-test; * $p < 0.05$; ** $p < 0.01$; *** $p < 0.001$.

Work undertaken to determine the reasons for the cytotoxicity of polyaniline was previously published by Stejskal et al. [62] and Kašpárková et al. [63]. On the basis of their findings, it can be assumed that such cytotoxic effects are mainly connected with the presence of low-molecular-weight impurities. In order to look into the composition of PPy extracts and to identify any low-molecular-weight products and oligomers that might induce neurogenesis, electrospray mass spectrometry (MS) analyses of the samples were conducted.

Mass spectrometry, with the exception of pyrolysis MS, has not frequently been used as an analytical tool for the characterization of PPy. This is mainly due to the extremely poor solubility of PPy in common solvents suitable for MS. However, the studied aqueous PPy extracts, which are assumed to contain low-molecular-mass fractions/impurities of the polymer, can be accessible for analysis. A representative mass spectrum of the studied PPy extract is shown in Figure 8A, and, from this, it is obvious that within the studied m/z region, the sample comprises one main dominating molecular ion (M + H) + m/z = 325.2. Higher masses are also present at significantly lower intensities, with a pattern typical for oligomers. The interpretation of the recorded MS spectra is not, however, straightforward and, surprisingly, very limited information on the occurrence or structure of PPy oligomers and impurities exists in the literature [64,65]. Nevertheless, the mass of the main molecular ion with m/z = 325.2 can be assigned to PPy pentamer. Higher masses can then correspond to oligomers and/or their adducts, and may comprise oxygen and oxygen containing by-products. Taking into consideration the presence of Cl^-dopant anions originating from $FeCl_3$ oxidant, the presence of adducts containing chlorine can also be expected. Interestingly, the higher masses present in the spectrum are separated by a mass of about Δm/z ~125 Da. A similar observation was reported by Appel et al., who studied oligomers soluble in a PPy reaction mixture using UV–Vis and GPC techniques [64]. In their work, PPy was synthetized in two ways: (1) from *p*-toluene sulfonic acid and pyrrole in acetonitrile via oxidation by oxygen in the surrounding air, and (2) electropolymerization from the same system. The authors concluded that, in both cases, there are some preferred oligomers formed with n = 3, 4, 7, 12 and 19, and that oligomers up to n = 30 were present. This is an indication of the formation of larger oligomers by combinations of smaller ones. In addition, Fermin and Scharifker [65] studied oligomers under elctropolymeration with aqueous KNO_3 or KCl as electrolytes and observed soluble oligomers with up to nine pyrrole units in the electrolyte solutions, together with polypyrrole gradually depositing

onto the electrode surface. Though neither of the reported procedures can be compared with oxidation using $FeCl_3$, it is quite obvious that the presence of different oligomer types will depend on the polymerization procedure and oxidation agent, as well as the reaction system. The interpretation of the spectra is also complicated because of the known shortcomings of ESI-MS—namely, the fact that analytes with higher molecular masses may acquire several electrostatic charges during the ESI process. A series of multiply charged species are consequently produced, including adducts with impurities, water, and components of mobile phase [66]. Unambiguous deconvolution of the spectra recorded for PPy extract in our work is, therefore, difficult and is beyond the scope of the current study.

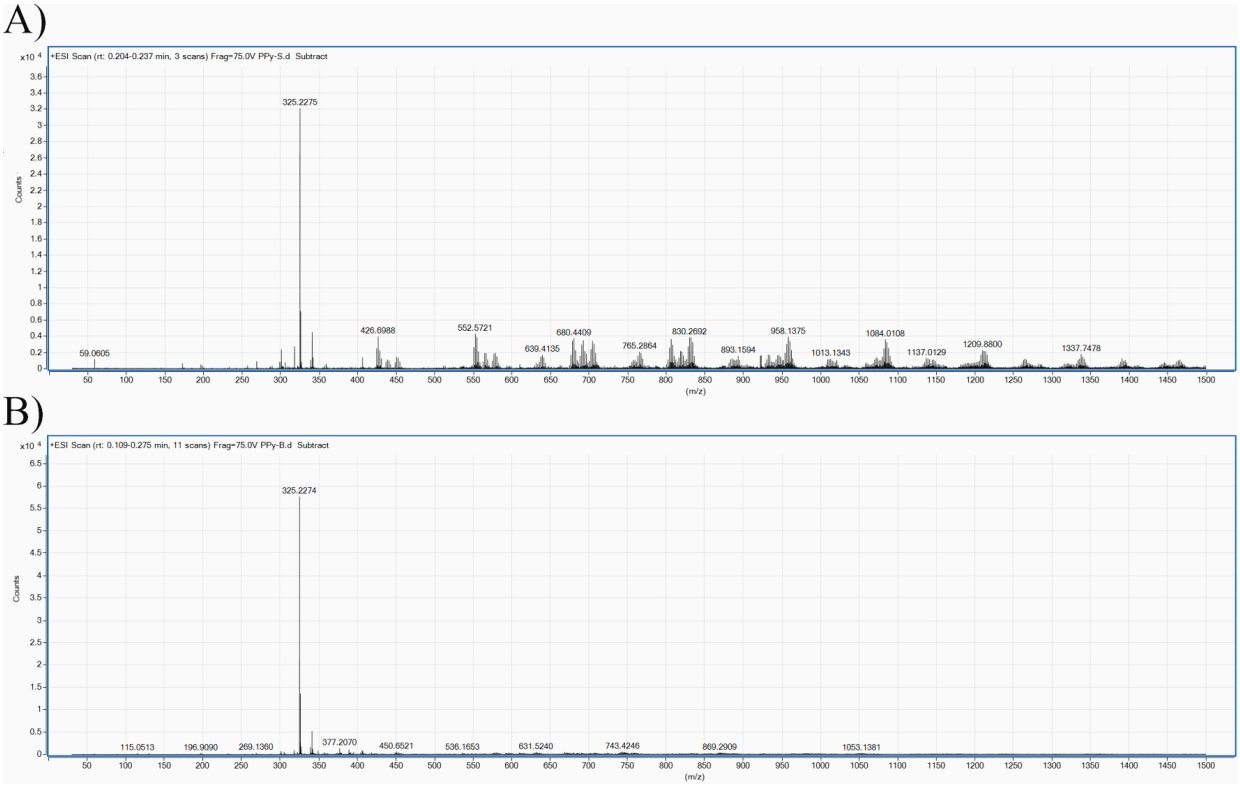

Figure 8. Positive-ion ESI-MS spectrum of polypyrrole extract; (**A**) polypyrrole salt, (**B**) polypyrrole base.

Combining the results from MS analysis and cytotoxicity testing, it can be concluded that neither of the detected substances exhibit severe cytotoxicity to EBs, as shown by their insignificant size reduction after treatment with 5% PPy extract. Neurogenesis, however, is induced by species with m/z higher than 325.5, as this pentamer is still present in the deprotonated PPy base (Figure 8B), which, in the present study, have not induced neurogenesis. The oligomers with higher masses are absent or detected in substantially lower amounts. The absence of higher oligomers in the PPy base is due to the deprotonation process transforming PPy from salt to base form, which serves as a purification procedure. There are a number of substances which can be present as by-products of PPy synthesis and can regulate stem cell behavior. In this respect, the work of Park et al. [67] can be mentioned. In this study, the influence of extract of dried Euphoria longan, which has been used in ancient Chinese medicine for the treatment of forgetfulness, was tested. The extract was tested in vivo in mice and it was shown that it regulates neurogenesis and promotes memory. A pyrrole-lactone-based natural alkaloid named longanlactone was later isolated from Euphoria seeds [68]. This pyrrole-lactone is responsible for the promotion of neurogenesis, as confirmed in a recent study by Reddy et al. [69], in which various synthetic derivatives of longanlactone have also been tested.

4. Conclusions

The conjugated structure of conducting polymers (CPs) is, among other factors, mainly responsible for their unique properties.

Polypyrrole, an example of a conducting polymer, is one of the most attractive materials within this group for applications in tissue engineering. It finds application not only because of its good level of biocompatibility, but also due to its intrinsic combination of electronic and ionic conductivity. These characteristics are mainly advantageous when preparing biointerfaces, and controlling and regulating cell fate. PPy itself, as a chemical substance, exhibits no known effects on the differentiation of stem cells. However, the question remains whether and to what extent any of the low-molecular-weight products and residual impurities present in PPy affect cell physiology. In the present study, the cytotoxicity of aqueous PPy extracts and their effects on the differentiation of embryonic bodies formed from mouse embryonic stem cells (ES R1 line) were investigated. Cytotoxic effects on undifferentiated cells cultured in the presence of leukemia inhibitory factor were first observed at the highest tested concentration of PPy extract (i.e., 25%). On the other hand, in cells that underwent differentiation, relative cellularity decreased by ~50% relative to the reference already after treatment with the lowest extract concentration (i.e., 1%).

With regard to neurogenesis, EBs cultured in the presence of PPy extracts (especially those with 5% concentration) formed nerve processes and amplified neurite expansion more abundantly than non-treated EBs (reference). In the light of these findings, the expressions of genes associated with early neurogenesis (specifically Pax6, Sox1, and MASH1) were measured in EBs formed in the presence of 5% PPy extract and found to be higher than in the reference EBs. Similarly, the expressions of neurospecific proteins (N-cadherin, N-CAM, β-III-tubulin, doublecortin) increased in comparison with the reference. The 10% PPy extract then exerted an effect on the modulation of Akt and ERK kinase signaling pathways. This effect is also associated with neurogenesis. The observed induction of neurogenesis in EBs could be related to the presence of PPy oligomers in the extract, which were determined by mass spectrometry. The cellular behavior is likely influenced by these low-molecular-weight compounds; however, the exact determination of which of these compounds causes this effect is beyond the scope of this study.

Author Contributions: Conceptualization, J.P., J.S., and P.H.; methodology, K.S., K.A.R., V.K. and P.B.; formal analysis, K.A.R., P.B., Z.C., K.S., I.J., M.M. and M.K.; writing—original draft preparation, K.S., J.P., P.H. and M.L.; writing—review and editing, V.K., P.H. and J.P.; supervision, P.H. and J.P. All authors have read and agreed to the published version of the manuscript.

Funding: This work was supported by Czech Science Foundation (19-16861S). Author J.P. thanks to Czech Science Foundation (Project 17-05466S). Author K.S. thanks the internal grant agency of Tomas Bata University in Zlín (IGA/CPS/2021/001). Authors I.J. and M.M. thank to Slovenian Research Agency (grant P2-0082). This work was supported by the Ministry of Education, Youth and Sports of the Czech Republic—DKRVO (RP/CPS/2020/001).

Institutional Review Board Statement: Not applicable.

Informed Consent Statement: Not applicable.

Data Availability Statement: The data presented in this study are available on request from the corresponding author.

Acknowledgments: Authors thank to Tomáš Šopík and Pavel Kucharczyk for technical support.

Conflicts of Interest: The authors declare no conflict of interest. The funders had no role in the design of the study; in the collection, analyses, or interpretation of data; in the writing of the manuscript, or in the decision to publish the results.

Abbreviations

CPs	conducting polymers
ESCs	embryonic stem cells
PPy	polypyrrole
NT3	neurotrophin-3
LIF	leukemia inhibitory factor
EBs	embryoid bodies
ITS	Insulin–transferrin–selen
REF	reference
PBAT	butylene adipate-*co*-terephthalate
hNSCs	human neural stem cells
PLCL/SF	composite of poly (L-lactic acid-*co*-ε-caprolactone) with silk fibroin
CNS	central nervous system
MAPs	microtubule-associated proteins
GSK-3	glycogen synthase kinase-3
MS	mass spectrometry

References

1. Ateh, D.; Navsaria, H.; Vadgama, P. Polypyrrole-based conducting polymers and interactions with biological tissues. *J. R. Soc. Interface* **2006**, *3*, 741–752. [CrossRef]
2. Kim, S.Y.; Kim, K.-M.; Hoffman-Kim, D.; Song, H.-K.; Palmore, G.T.R. Quantitative Control of Neuron Adhesion at a Neural Interface Using a Conducting Polymer Composite with Low Electrical Impedance. *ACS Appl. Mater. Interfaces* **2011**, *3*, 16–21. [CrossRef] [PubMed]
3. Gomez, N.; Schmidt, C.E. Nerve growth factor-immobilized polypyrrole: Bioactive electrically conducting polymer for en-hanced neurite extension. *J. Biomed. Mater. Res. Part A* **2007**, *81*, 135–149. [CrossRef] [PubMed]
4. Mittnacht, U.; Hartmann, H.; Hein, S.; Oliveira, H.; Dong, M.; Pêgo, A.P.; Kjems, J.; Howard, K.A.; Schlosshauer, B. Chitosan/siRNA Nanoparticles Biofunctionalize Nerve Implants and Enable Neurite Outgrowth. *Nano Lett.* **2010**, *10*, 3933–3939. [CrossRef] [PubMed]
5. Yamada, M.; Tanemura, K.; Okada, S.; Iwanami, A.; Nakamura, M.; Mizuno, H.; Ozawa, M.; Ohyama-Goto, R.; Kitamura, N.; Kawano, M.; et al. Electrical Stimulation Modulates Fate Determination of Differentiating Embryonic Stem Cells. *Stem Cells* **2006**, *25*, 562–570. [CrossRef] [PubMed]
6. Fonner, J.M.; Forciniti, L.; Nguyen, H.; Byrne, J.D.; Kou, Y.F.; Syeda-Nawaz, J.; Schmidt, C.E. Biocompatibility implications of polypyrrole synthesis techniques. *Biomed. Mater.* **2008**, *3*, 034124. [CrossRef] [PubMed]
7. Vernitskaya, T.V.; Efimov, O.N. Polypyrrole: A conducting polymer; its synthesis, properties and applications. *Russ. Chem. Rev.* **1997**, *66*, 443–457. [CrossRef]
8. Castano, H.; O'Rear, E.A.; McFetridge, P.S.; Sikavitsas, V.I. Polypyrrole Thin Films Formed by Admicellar Polymeriza-tion Support the Osteogenic Differentiation of Mesenchymal Stem Cells. *Macromol. Biosci.* **2004**, *4*, 785–794. [CrossRef]
9. Omastová, M.; Trchová, M.; Kovářová, J.; Stejskal, J. Synthesis and structural study of polypyrroles prepared in the presence of surfactants. *Synth. Met.* **2003**, *138*, 447–455. [CrossRef]
10. Stejskal, J.; Trchová, M.; Bober, P.; Morávková, Z.; Kopecký, D.; Vrňata, M.; Prokeš, J.; Varga, M.; Watzlová, E. Polypyrrole salts and bases: Superior conductivity of nanotubes and their stability towards the loss of conductivity by depro-tonation. *RSC Adv.* **2016**, *6*, 88382–88391. [CrossRef]
11. Lee, J.-W.; Serna, F.; Nickels, A.J.; Schmidt, C.E. Carboxylic Acid-Functionalized Conductive Polypyrrole as a Bioactive Platform for Cell Adhesion. *Biomacromolecules* **2006**, *7*, 1692–1695. [CrossRef] [PubMed]
12. Gilmore, K.J.; Kita, M.; Han, Y.; Gelmi, A.; Higgins, M.J.; Moulton, S.E.; Clark, G.M.; Kapsa, R.; Wallace, G.G. Skeletal muscle cell proliferation and differentiation on polypyrrole substrates doped with extracellular matrix components. *Biomaterials* **2009**, *30*, 5292–5304. [CrossRef] [PubMed]
13. Richardson, R.T.; Thompson, B.; Moulton, S.E.; Newbold, C.; Lum, M.G.; Cameron, A.; Wallace, G.G.; Kapsa, R.; Clark, G.; O'Leary, S. The effect of polypyrrole with incorporated neurotrophin-3 on the promotion of neurite outgrowth from auditory neurons. *Biomaterials* **2007**, *28*, 513–523. [CrossRef] [PubMed]
14. Milakin, K.A.; Capáková, Z.; Acharya, U.; Vajďák, J.; Morávková, Z.; Hodan, J.; Humpolíček, P.; Bober, P. Bio-compatible and antibacterial gelatin-based polypyrrole cryogels. *Polymer* **2020**, *197*, 122491. [CrossRef]
15. Kang, S.Y.; Park, E.J.; Park, W.K.; Kim, H.J.; Jeong, D.; Jung, M.E.; Song, K.S.; Lee, S.H.; Seo, H.J.; Kim, M.J.; et al. Arylpiperazine-containing pyrrole 3-carboxamide derivatives targeting serotonin 5-HT2A, 5-HT2C, and the serotonin transporter as a potential antidepressant. *Bioorganic Med. Chem. Lett.* **2010**, *20*, 1705–1711. [CrossRef] [PubMed]
16. Bavadi, M.; Niknam, K.; Shahraki, O. Novel pyrrole derivatives bearing sulfonamide groups: Synthesis in vitro cytotoxicity evaluation, molecular docking and DFT study. *J. Mol. Struct.* **2017**, *1146*, 242–253. [CrossRef]

17. Aiello, A.; D'Esposito, M.; Fattorusso, E.; Menna, M.; Müller, W.E.G.; Perović-Ottstadt, S.; Tsuruta, H.; Gulder, T.A.M.; Bringmann, G. Daminin, a bioactive pyrrole alkaloid from the Mediterranean sponge Axinella damicornis. *Tetrahedron* **2005**, *61*, 7266–7270. [CrossRef]
18. Ahmad, S.; Alam, O.; Naim, M.J.; Shaquiquzzaman, M.; Alam, M.M.; Iqbal, M. Pyrrole: An insight into recent pharmacological advances with structure activity relationship. *Eur. J. Med. Chem.* **2018**, *157*, 527–561. [CrossRef]
19. Humpolíček, P.; Kašpárková, V.; Pacherník, J.; Stejskal, J.; Bober, P.; Capáková, Z.; Radaszkiewicz, K.A.; Junkar, I.; Lehocký, M. The biocompatibility of polyaniline and polypyrrole: A comparative study of their cytotoxicity, em-bryotoxicity and impurity profile. *Mater. Sci. Eng. C* **2018**, *91*, 303–310. [CrossRef]
20. Nagy, A.; Rossant, J.; Abramow-Newerly, W.; Roder, J.C. Derivation of completely cell culture-derived mice from early-passage embryonic stem cells. *Proc. Natl. Acad. Sci. USA* **1993**, *90*, 8424–8428. [CrossRef]
21. Humpolíček, P.; Radaszkiewicz, K.A.; Kašpárková, V.; Stejskal, J.; Trchová, M.; Kuceková, Z.; Vičarová, H.; Pacherník, J.; Lehocký, M.; Minařík, A. Stem cell differentiation on conducting polyaniline. *RSC Adv.* **2015**, *5*, 68796–68805. [CrossRef]
22. Bober, P.; Humpolíček, P.; Pacherník, J.; Stejskal, J.; Lindfors, T. Conducting polyaniline based cell culture substrate for embryonic stem cells and embryoid bodies. *RSC Adv.* **2015**, *5*, 50328–50335. [CrossRef]
23. Konopka, R.; Hýzdalová, M.; Kubala, L.; Pacherník, J. New luminescence-based approach to measurement of luciferase gene expression reporter activity and adenosine triphosphate-based determination of cell viability. *Folia Biol.* **2010**, *56*, 66–71.
24. Willems, E.; Mateizel, I.; Kemp, C.; Cauffman, G.; Sermon, K.; Leyns, L. Selection of reference genes in mouse embryos and in differentiating human and mouse ES cells. *Int. J. Dev. Biol.* **2006**, *50*, 627–635. [CrossRef]
25. Abranches, E.; Silva, M.; Pradier, L.; Schulz, H.; Hummel, O.; Henrique, D.; Bekman, E. Neural Differentiation of Embryonic Stem Cells In Vitro: A Road Map to Neurogenesis in the Embryo. *PLoS ONE* **2009**, *4*, e6286. [CrossRef]
26. Večeřa, J.; Kudová, J.; Kučera, J.; Kubala, L.; Pacherník, J. Neural Differentiation Is Inhibited through HIF1α/β-Catenin Signaling in Embryoid Bodies. *Stem Cells Int.* **2017**, *2017*, 8715798. [CrossRef]
27. Kučera, J.; Binó, L.; Štefková, K.; Jaroš, J.; Vašíček, O.; Večeřa, J.; Kubala, L.; Pacherník, J. Apocynin and Diphe-nyleneiodonium Induce Oxidative Stress and Modulate PI3K/Akt and MAPK/Erk Activity in Mouse Embryonic Stem Cells. *Oxidative Med. Cell. Longev.* **2016**, *2016*, 7409196. [CrossRef]
28. Binó, L.; Veselá, I.; Papežíková, I.; Procházková, J.; Vašíček, O.; Štefková, K.; Kučera, J.; Hanáčková, M.; Ku-bala, L.; Pacherník, J. The depletion of p38alpha kinase upregulates NADPH oxidase 2/NOX2/gp91 expression and the pro-duction of superoxide in mouse embryonic stem cells. *Arch. Biochem. Biophys.* **2019**, *671*, 18–26. [CrossRef]
29. Chen, J.; Zacharek, A.; Li, Y.; Li, A.; Wang, L.; Katakowski, M.; Roberts, C.; Lu, M.; Chopp, M. N-cadherin me-diates nitric oxide-induced neurogenesis in young and retired breeder neurospheres. *Neuroscience* **2006**, *140*, 377–388. [CrossRef]
30. Fiszbein, A.; Schor, I.E.; Kornblihtt, A.R. Fundamentals of NCAM Expression, Function, and Regulation of Alternative Splicing in Neuronal Differentiation. In *Neural Surface Antigens*; Pruszak, J., Ed.; Academic Press: Boston, MA, USA, 2015; pp. 131–140.
31. Fanarraga, M.L.; Avila, J.; Zabala, J.C. Expression of unphosphorylated class III beta-tubulin isotype in neuroepithelial cells demonstrates neuroblast commitment and differentiation. *Eur. J. Neurosci.* **1999**, *11*, 516–527. [CrossRef]
32. Gleeson, J.G.; Lin, P.T.; Flanagan, L.A.; Park, P.J. Doublecortin Is a Microtubule-Associated Protein and Is Expressed Widely by Migrating Neurons. *Neuron* **1999**, *23*, 257–271. [CrossRef]
33. Fourniol, F.; Perderiset, M.; Houdusse, A.; Moores, C. Chapter 3—Structural Studies of the Doublecortin Family of MAPs. In *Methods in Cell Biology*; Correia, J.J., Wilson, L., Eds.; Academic Press: Boston, MA, USA, 2013; Volume 115, pp. 27–48.
34. She, X.; Rohl, C.A.; Castle, J.C.; Kulkarni, A.; Johnson, J.M.; Chen, R. Definition, conservation and epigenetics of housekeeping and tissue-enriched genes. *BMC Genom.* **2009**, *10*, 269. [CrossRef] [PubMed]
35. Capáková, Z.; Radaszkiewicz, K.A.; Acharya, U.; Truong, T.H.; Pacherník, J.; Bober, P.; Kašpárková, V.; Stejskal, J.; Pfleger, J.; Lehocký, M.; et al. The biocompatibility of polyaniline and polypyrrole 211.Doping with organic phosphonates. *Mater. Sci. Eng. C* **2020**, *113*, 110986. [CrossRef] [PubMed]
36. Smith, A.; Nichols, J.; Robertson, M.; Rathjen, P.D. Differentiation inhibiting activity (DIA/LIF) and mouse development. *Dev. Biol.* **1992**, *151*, 339–351. [CrossRef]
37. Cerdan, C.; Hong, S.H.; Bhatia, M. Formation and Hematopoietic Differentiation of Human Embryoid Bodies by Suspen-sion and Hanging Drop Cultures. *Curr. Protoc. Stem Cell Biol.* **2007**, *3*, 1D.2.1–1D.2.16. [CrossRef]
38. Granato, A.E.C.; Ribeiro, A.C.; Marciano, F.R.; Rodrigues, B.V.M.; Lobo, A.O.; Porcionatto, M. Polypyrrole in-creases branching and neurite extension by Neuro2A cells on PBAT ultrathin fibers. *Nanomed. Nanotechnol. Biol. Med.* **2018**, *14*, 1753–1763. [CrossRef]
39. Stewart, E.; Kobayashi, N.R.; Higgins, M.J.; Quigley, A.F.; Jamali, S.C.; Moulton, S.E.; Kapsa, R.; Wallace, G.G.; Crook, J.M. Electrical Stimulation Using Conductive Polymer Polypyrrole Promotes Differentiation of Human Neural Stem Cells: A Biocompatible Platform for Translational Neural Tissue Engineering. *Tissue Eng. Part C Methods* **2015**, *21*, 385–393. [CrossRef]
40. Wang, X.; Gu, X.; Yuan, C.; Chen, S.; Zhang, P.; Zhang, T.; Yao, J.; Chen, F.; Chen, G. Evaluation of biocompat-ibility of polypyrrole in vitro and in vivo. *J. Biomed. Mater. Res. Part A* **2004**, *68*, 411–422. [CrossRef]
41. Sun, B.; Wu, T.; Wang, J.; Li, D.; Wang, J.; Gao, Q.; Bhutto, M.A.; El-Hamshary, H.; Al-Deyab, S.S.; Mo, X. Polypyrrole-coated poly(l-lactic acid-co-ε-caprolactone)/silk fibroin nanofibrous membranes promoting neural cell proliferation and differentiation with electrical stimulation. *J. Mater. Chem. B* **2016**, *4*, 6670–6679. [CrossRef]
42. Simpson, T.I.; Price, D.J. Pax6: A pleiotropic player in development. *BioEssays* **2002**, *24*, 1041–1051. [CrossRef]

43. Pevny, L.H.; Sockanathan, S.; Placzek, M.; Lovell-Badge, R. A role for SOX1 in neural determination. *Development* **1998**, *125*, 1967–1978. [PubMed]
44. Lo, L.; Tiveron, M.C.; Anderson, D.J. MASH1 activates expression of the paired homeodomain transcription factor Phox2a, and couples pan-neuronal and subtype-specific components of autonomic neuronal identity. *Development* **1998**, *125*, 609–620. [PubMed]
45. Kumar, N.; Afeyan, R.; Sheppard, S.; Harms, B.; Lauffenburger, D.A. Quantitative analysis of Akt phosphorylation and activity in response to EGF and insulin treatment. *Biochem. Biophys. Res. Commun.* **2007**, *354*, 14–20. [CrossRef] [PubMed]
46. Kučera, J.; Netušilová, J.; Sladeček, S.; Lánová, M.; Vašíček, O.; Štefková, K.; Navrátilová, J.; Kubala, L.; Pacherník, J. Hypoxia Downregulates MAPK/ERK but Not STAT3 Signaling in ROS-Dependent and HIF-1-Independent Manners in Mouse Embryonic Stem Cells. *Oxidative Med. Cell. Longev.* **2017**, *2017*, 1–16. [CrossRef] [PubMed]
47. Rai, S.N.; Dilnashin, H.; Birla, H.; Singh, S.S.; Zahra, W.; Rathore, A.S.; Singh, B.K.; Singh, S.P. The Role of PI3K/Akt and ERK in Neurodegenerative Disorders. *Neurotox. Res.* **2019**, *35*, 775–795. [CrossRef] [PubMed]
48. Burke, R.E. Inhibition of mitogen-activated protein kinase and stimulation of Akt kinase signaling pathways: Two approaches with therapeutic potential in the treatment of neurodegenerative disease. *Pharmacol. Ther.* **2007**, *114*, 261–277. [CrossRef] [PubMed]
49. Cross, D.A.E.; Alessi, D.R.; Cohen, P.; Andjelkovich, M.; Hemmings, B.A. Inhibition of glycogen synthase kinase-3 by insulin mediated by protein kinase B. *Nat. Cell Biol.* **1995**, *378*, 785–789. [CrossRef]
50. McCubrey, J.A.; Steelman, L.S.; Bertrand, F.E.; Davis, N.M.; Sokolosky, M.; Abrams, S.L.; Montalto, G.; D'Assoro, A.B.; Libra, M.; Nicoletti, F.; et al. GSK-3 as potential target for therapeutic intervention in cancer. *Oncotarget* **2014**, *5*, 2881–2911. [CrossRef]
51. Eldar-Finkelman, H.; Martinez, A. GSK-3 Inhibitors: Preclinical and Clinical Focus on CNS. *Front. Mol. Neurosci.* **2011**, *4*, 32. [CrossRef]
52. Pap, M.; Cooper, G.M. Role of Glycogen Synthase Kinase-3 in the Phosphatidylinositol 3-Kinase/Akt Cell Survival Pathway. *J. Biol. Chem.* **1998**, *273*, 19929–19932. [CrossRef]
53. Coghlan, M.P.; Culbert, A.A.; Cross, D.A.E.; Corcoran, S.L.; Yates, J.W.; Pearce, N.J.; Rausch, O.L.; Mur-phy, G.J.; Carter, P.S.; Roxbee Cox, L.; et al. Selective small molecule inhibitors of glycogen synthase kinase-3 modulate glycogen metab-olism and gene transcription. *Chem. Biol.* **2000**, *7*, 793–803. [CrossRef]
54. Kramer, T.; Schmidt, B.; Monte, F.L. Small-Molecule Inhibitors of GSK-3: Structural Insights and Their Application to Alzheimer's Disease Models. *Int. J. Alzheimer's Dis.* **2012**, *2012*, 1–32. [CrossRef] [PubMed]
55. Desai, M.C.; Ng, S.; Ni, Z.J.; Pfister, K.B.; Ramurthy, S.; Subramanian, S.; Wagman, A.S. Pyrrole Based Inhibitors of Glycogen Synthase Kinase 3. U.S. Patent No. 7,250,443, 31 July 2007.
56. Beurel, E.; Grieco, S.F.; Jope, R.S. Glycogen synthase kinase-3 (GSK3): Regulation, actions, and diseases. *Pharmacol. Ther.* **2015**, *148*, 114–131. [CrossRef] [PubMed]
57. Seira, O.; del Río, J.A. Glycogen Synthase Kinase 3 Beta (GSK3β) at the Tip of Neuronal Development and Regeneration. *Mol. Neurobiol.* **2014**, *49*, 931–944. [CrossRef] [PubMed]
58. Manning, B.D.; Toker, A. AKT/PKB Signaling: Navigating the Network. *Cell* **2017**, *169*, 381–405. [CrossRef]
59. Kotasová, H.; Veselá, I.; Kučera, J.; Houdek, Z.; Procházková, J.; Králičková, M.; Pacherník, J. Phosphoinositide 3-kinase inhibition enables retinoic acid-induced neurogenesis in monolayer culture of embryonic stem cells. *J. Cell. Biochem.* **2012**, *113*, 563–570. [CrossRef]
60. Wataya, T.; Ando, S.; Muguruma, K.; Ikeda, H.; Watanabe, K.; Eiraku, M.; Kawada, M.; Takahashi, J.; Hashimoto, N.; Sasai, Y. Minimization of exogenous signals in ES cell culture induces rostral hypothalamic differentiation. *Proc. Natl. Acad. Sci. USA* **2008**, *105*, 11796–11801. [CrossRef]
61. Pacherník, J.; Esner, M.; Bryja, V.; Dvořak, P.; Hampl, A. Neural differentiation of mouse embryonic stem cells grown in monolayer. *Reprod. Nutr. Dev.* **2003**, *42*, 317–326. [CrossRef]
62. Stejskal, J.; Hajná, M.; Kašpárková, V.; Humpolíček, P.; Zhigunov, A.; Trchová, M. Purification of a conducting polymer, polyaniline, for biomedical applications. *Synth. Met.* **2014**, *195*, 286–293. [CrossRef]
63. Kašpárková, V.; Humpolíček, P.; Stejskal, J.; Kopecká, J.; Kuceková, Z.; Moučka, R. Conductivity, impurity profile, and cytotoxicity of solvent-extracted polyaniline. *Polym. Adv. Technol.* **2016**, *27*, 156–161. [CrossRef]
64. Appel, G.; Schmeißer, D.; Bauer, J.; Bauer, M.; Egelhaaf, H.J.; Oelkrug, D. The formation of oligomers in the electrolyte upon polymerization of pyrrole. *Synth. Met.* **1999**, *99*, 69–77. [CrossRef]
65. Fermin, D.; Scharifker, B. Products in solution during electrodeposition of polypyrrole. *J. Electroanal. Chem.* **1993**, *357*, 273–287. [CrossRef]
66. Ozeki, Y.; Omae, M.; Kitagawa, S.; Ohtani, H. Electrospray ionization-ion mobility spectrometry-high resolution tandem mass spectrometry with collision-induced charge stripping for the analysis of highly multiply charged intact polymers. *Analyst* **2019**, *144*, 3428–3435. [CrossRef] [PubMed]
67. Park, S.J.; Park, N.H.; Kim, N.H.; Lee, S.; Yoon, B.H.; Jung, W.Y.; Lee, K.-T.; Cheong, J.H.; Ryu, J.H. The memory-enhancing effects of Euphoria longan fruit extract in mice. *J. Ethnopharmacol.* **2010**, *128*, 160–165. [CrossRef] [PubMed]

68. Zheng, G.; Wei, X.; Xu, L.; Li, Z.; Liu, G.; Zhang, X. A New Natural Lactone from Dimocarpus longan Lour. Seeds. *Molecules* **2012**, *17*, 9421–9425. [CrossRef]
69. Reddy, C.R.; Tukaram, A.G.; Mohammed, S.Z.; Dilipkumar, U.; Babu, B.N.; Chakravarty, S.; Bhattacharya, D.; Joshi, P.; Gree, R. Synthesis and biological evaluation of longanlactone analogues as neurotrophic agents. *Bioorganic Med. Chem. Lett.* **2018**, *28*, 673–676. [CrossRef] [PubMed]

ARTICLE 3

Gupta S., Acharya U., Pištěková H., Taboubi O., Morávková Z, **Kašparová M.**, Humpolíček P., Bober P., 2021. *Tuning the Conductivity, Morphology, and Capacitance with Enhanced Antibacterial Properties of Polypyrrole by Acriflavine Hydrochloride.* ACS Applied Polymer Materials. 3, 6063–6069. DOI 10.1021/acsapm.1c00775

ACS APPLIED POLYMER MATERIALS

pubs.acs.org/acsapm Article

Tuning the Conductivity, Morphology, and Capacitance with Enhanced Antibacterial Properties of Polypyrrole by Acriflavine Hydrochloride

Sonal Gupta, Udit Acharya, Hana Pištěková, Oumayma Taboubi, Zuzana Morávková, Martina Kašparová, Petr Humpolíček, and Patrycja Bober*

Cite This: *ACS Appl. Polym. Mater.* 2021, 3, 6063−6069

Read Online

ACCESS | Metrics & More | Article Recommendations

ABSTRACT: In this study, a simple one-step preparation of polypyrrole (PPy) assisted by an organic dye, acriflavine hydrochloride (AF), was investigated. The presence of a dye resulted in the development of PPy nanofibers with the conductivity enhanced up to 14 S cm^{-1}. The structural analysis by Fourier-transform infrared and Raman spectroscopies confirmed the interaction of the AF with PPy. As far as the electrochemical activity of PPy is concerned, the gravimetric capacitance increased up to 85 F g^{-1} with the help of a AF. Additionally, a substantial improvement in the antibacterial activity against *Staphylococcus aureus* and *Escherichia coli* bacteria for all the PPy-containing organic dye was achieved. The conductivity, morphology, capacitance, and remarkable antibacterial properties of PPy tuned by an organic dye enable applications wherever the electroconductivity and antibacterial activity should meet requirements, for example, wound healing, electrochemical sensors, bioactuators, or even regenerative medicine.

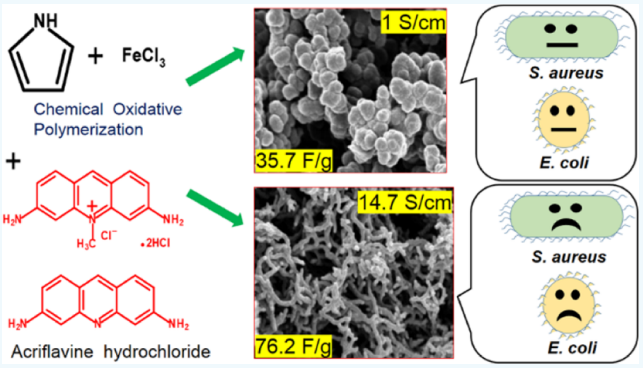

KEYWORDS: *acriflavine hydrochloride, polypyrrole, nanofibers, conductivity, capacitance, antibacterial activity*

1. INTRODUCTION

Considerable progress has been made in the field of conducting polymers due to their versatile applications, particularly in biosensors, electrochemical capacitors, and for employment in biomedical and health care sectors.[1,2] The cost-effective, easy synthesis, environmental stability, and tunable properties such as conductivity and morphology of polypyrrole (PPy), in addition to its biocompatibility, make it a high-ranking conducting polymer.[3] The combination of antibacterial properties and conductivity can be successfully utilized in various application fields, for example, in smart wearable equipment, where conductivity can be used for heating or sensing and antibacterial properties add to sustainable use.[4] Maráková et al. have demonstrated the enhanced antibacterial effect of PPy-embedded cotton along with lower cytotoxicity and further studied the effect of silver nanoparticles on the conductivity and antibacterial activity of PPy.[5] Liu et al. have successfully synthesized PPy−AgCl nanocomposites in the presence of methyl orange and obtained a conductivity of 17 S cm^{-1} with enhanced antibacterial properties.[6]

Efforts to improve the antimicrobial properties of PPy with the use of biopolymers such as cellulose,[7] dextrin,[8] chitosan,[9] and gelatin[10] have been made. Also, metals or metal oxides have been used for the preparation of PPy composites to achieve promising antibacterial properties; however, their high cost limits applications in biomedicine.[11−15] Moreover, abundant research work shows that high conductivity of PPy can be accomplished by introducing carbon nanotubes,[16] graphene,[17] or graphene oxide[18] in addition to its desirable capacitive properties.[19,20] Besides these, PPy with the cost-effective organic dyes have recently attracted interest of researchers for the high conductivity and easy tuning of morphology in the resulting composites.

In previous studies, our group has demonstrated the significance of various dyes such as methyl orange, ethyl orange, safranin and methyl red in improving the conductivity of PPy. Additionally, we successfully gained controlled

Received: July 2, 2021
Accepted: October 28, 2021
Published: November 10, 2021

https://doi.org/10.1021/acsapm.1c00775
ACS Appl. Polym. Mater. 2021, 3, 6063−6069

morphology of PPy such as nanorods, nanotubes, nanofibers, and so forth.[21−23] One of the recent studies has presented the cytotoxic activity of biocompatible PPy prepared in the presence of acid blue 25, signifying its potential biomedical applications.[24] However, regarding its antibacterial assessments, surprisingly, nothing is known, which thus encouraged our current research work.

The present study reports the effect of an organic dye, acriflavine hydrochloride (AF) (Figure 1a), not only on

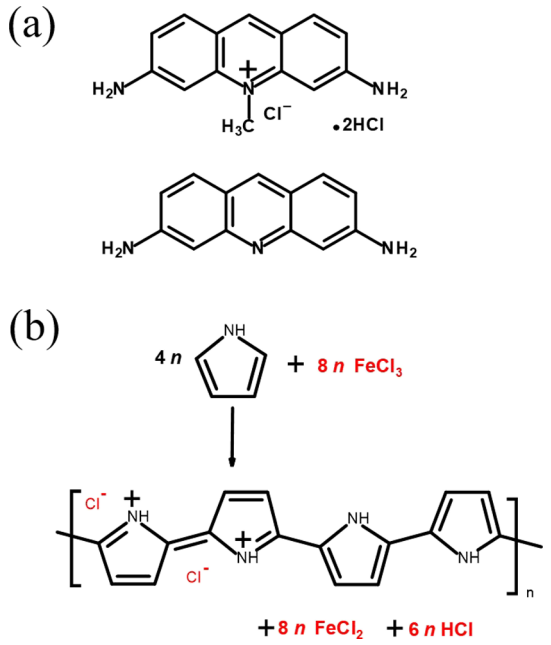

Figure 1. (a) Synthesis of PPy using iron(III) chloride as an oxidant and (b) structure of AF.

electrical conductivity and morphology but also on the electrochemical activity of PPy. The high capacitive behavior displayed by nanofibers compared to pristine globular PPy is also discussed. AF is well known for its antiseptic properties and ability to treat bacterial and fungal infections as well as is used in different biomedical applications.[25,26] For this purpose, the utmost emphasis has been made in investigating the antibacterial activity of conducting PPy prepared in the presence of AF. The enhanced capacitance of the conducting nanofibrous PPy with optimistic antibacterial activity is presented in this work.

2. EXPERIMENTAL SECTION

2.1. Chemicals and Reagents. Pyrrole (98%), iron(III) chloride hexahydrate, AF (mixture of 3,6-diamino-10-methylacridinium and 3,6-diaminoacridine), and Nafion 117 solution (lower aliphatic alcohols and water mixture) supplied from Sigma-Aldrich were employed without any further purification.

2.2. Preparation of PPy with or without the AF Dye. PPy was prepared by the oxidation of 0.15 M pyrrole using 0.3 M iron(III) chloride as an oxidant (Figure 1b). Both pyrrole and $FeCl_3{\cdot}6H_2O$ were dissolved separately in 50 mL of distilled water. Then, the reaction was started by fast mixing of the two solutions followed by vigorous shaking (1−2 min). The resultant 100 mL reaction mixture contained a fixed molar ratio of the oxidant to monomer, that is, [oxidant]/[pyrrole] = 2. Then, the polymerization was carried out by leaving the reaction mixture undisturbed overnight at room temperature. The obtained product was filtered and washed with excess of 0.2 M HCl and ethanol, and the black solid, PPy, was dried in a desiccator over silica gel to a constant weight. For the synthesis of PPy in the presence of a AF, a sequence of AF concentrations from 2.5 to 10 mM was selected. The dye was dissolved in 50 mL of distilled water along with pyrrole. The next step involved the addition of an oxidant to the solution of the monomer with the dye, and the reaction proceeded in a similar way as described above.

2.3. Characterization. The morphology of the PPy samples was examined with an MAIA3 TESCAN scanning electron microscope and TEC-NAI G2 SPIRIT transmission electron microscope.

DC conductivity was measured at room temperature by a van der Pauw method with spring-loaded electrodes on compressed pellets (diameter 13 mm, thickness 1.0 ± 0.3 mm) prepared under 530 MPa pressure using a hydraulic press TRYSTOM H-62 (Czech Republic). A Keithley 230 programmable voltage source in serial connection with a Keithley 196 System DMM was used as the current source, and the potential difference was measured with a Keithley 181 nanovoltmeter. The values were determined as an average from the measurements in two perpendicular directions taken from the linear part of the current−voltage curve.

Fourier-transform infrared (FTIR) spectra of the powders dispersed in potassium bromide pellets were registered using a Thermo Nicolet NEXUS 870 FTIR spectrometer with a DTGS TEC detector in the 400−4000 cm^{-1} wavenumber region.

Raman spectra were recorded on a Renishaw InVia Reflex Raman microspectrometer. The spectra were excited with HeNe 633 nm. A research-grade Leica DM LM microscope was used to focus the laser beam. The scattered light was analyzed with a spectrograph using holographic gratings of 1800 lines mm^{-1}. A Peltier-cooled charge-coupled device detector (576 × 384 pixels) registered the dispersed light.

Thermogravimetric analysis (TGA) of the PPy sample was performed on a PerkinElmer Pyris 1 thermogravimetric analyzer in a temperature range 35−800 °C at a rate of 10 °C min^{-1} with a fixed air flow rate at 25 mL min^{-1}.

Electrochemical studies were performed on a Metrohm AUTOLAB PGSTAT302N potentiostat in a three-electrode cell. Glassy carbon (diameter = 3 mm), Ag/Ag^+ wire, and Pt wire were used as the working, pseudoreference, and counter electrodes, respectively. As a supporting electrolyte, 0.2 M HCl was used. For each sample preparation, ∼5 mg of ground PPy with or without the dye was uniformly dispersed in 1 mL of a mixture containing 590 μL of Milli-Q water, 400 μL of isopropanol, and 10 μL of Nafion. Each measurement was carried out by drop-casting 1 μL of the dispersion onto a glassy carbon electrode under an inert atmosphere.

The gravimetric capacitance was calculated from the cyclic voltammograms (CVs) using the following equation

$$C = \frac{\int_{V_1}^{V_2} I \, dV}{2mv\Delta V}$$

where $\int I \, dV$ depicts the area under the CV, m (g) represents the mass of the active material drop-casted, v (V/s) is the scan rate, and ΔV is the potential window from V_1 to V_2.

For antibacterial testing, each sample was ground in a porcelain mortar to a fine powder and then weighed to prepare a stock concentrated suspension. From each sample, the stock concentrated suspension was prepared in sterile Mueller−Hinton broth (MHB) medium at a concentration of 64 mg mL^{-1}, and the stock suspension was further diluted to concentrations of 32, 16, 8, 4, 2, 1, 0.5, 0.25, 0.12, 0.062, and 0.031 mg mL^{-1}.[27] An equal amount of the bacterial suspension (inoculum) in MHB was added to each concentration, and after thorough homogenization, the tubes were incubated for 24 h at 35 °C. Then, 0.1 mL was taken from each tube and spread on the surface of tryptone soya agar (in duplicate for each concentration). After incubation at 35 °C for 18−24 h, the growth of the test bacteria on the surface of the plates was evaluated and the minimum inhibitory concentration (MIC) was determined accordingly. The tests were performed with Gram-positive *Staphylococcus aureus* (*S. aureus*) CCM 4516 (inoculum concentration 2.2 × 10^6 cfu mL^{-1}) and Gram-negative *Escherichia coli* (*E. coli*) CCM 4517 (inoculum concentration

https://doi.org/10.1021/acsapm.1c00775
ACS Appl. Polym. Mater. 2021, 3, 6063−6069

8.4 × 10^5 cfu mL^{-1}). The experimental setup was performed according to the procedure described in Nature Protocols.[27]

3. RESULTS AND DISCUSSION

3.1. Morphology. In general, pristine PPy shows a globular morphology which could be tuned to nanorods, nanotubes, nanofibers, or irregular patterns upon addition of organic dyes such as safranin, methyl orange, acid blue 25, or methyl red, respectively, to the polymerization mixture.[21−24] Herein, the conversion from globular PPy (Figures 2a and 3a) to

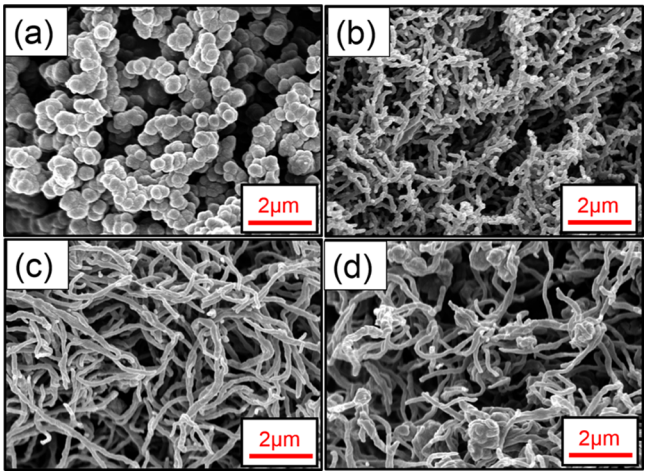

Figure 2. SEM micrographs of PPy prepared in the presence of (a) 0, (b) 2.5, (c) 7.5, and (d) 10 mM of AF.

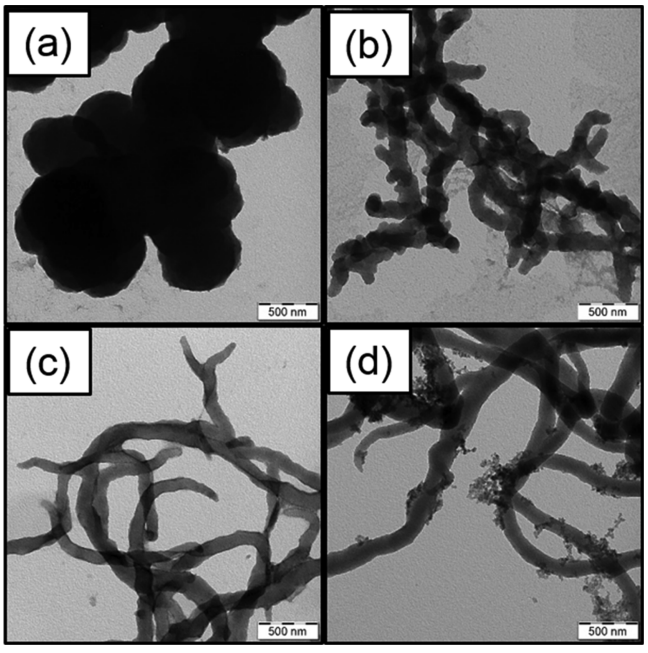

Figure 3. TEM micrographs of PPy prepared in the presence of (a) 0, (b) 2.5, (c) 7.5, and (d) 10 mM of AF.

nanofibers (Figures 2b and 3b) can be seen clearly upon introduction of even a small quantity of the AF dye. Upon increasing the dye concentration to 7.5 mM, PPy nanofibers show enlarged dimensions, signifying the role of concentration of the dye in determining the morphology (Figures 2c and 3c). However, the nanofibrous morphology of PPy is maintained even for the highest concentration of the dye, that is, 10 mM (excess of the dye in the polymerization mixture). The aggregate formation of undefined shape can also be noticed for this dye concentration (Figures 2d and 3d).

3.2. FTIR Spectra. Infrared spectra of the pristine PPy, AF dye, and PPy with various concentrations of the AF dye are displayed in Figure 4. In the spectrum of the AF dye, the band

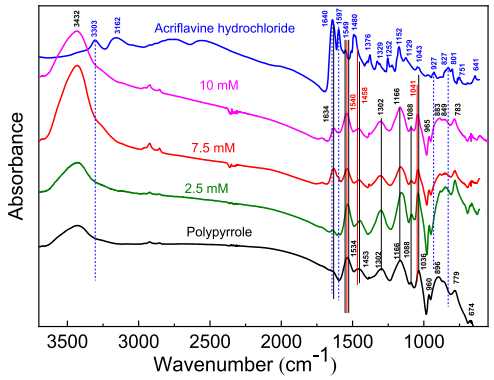

Figure 4. FTIR spectra of pristine PPy, acriflavine dye, and PPy prepared at various concentrations of AF. The peaks referring to AF are marked with dashed blue lines, PPy with black solid lines, and the peak shifts with red solid lines.

corresponding to the N−H^+ stretching vibration of amine hydrochloride (−NH_3^+) is observed at 3303 cm^{-1}. The C═C stretching vibrations in the aromatic ring show absorptions at 1597 cm^{-1}. In addition, the peak at 1480 cm^{-1} refers to the ring stretching vibration of the phenazine ring. The range, 1200−1400 cm^{-1}, represents the C−N stretching modes.[28] The peaks at 927 and 827 cm^{-1} represent out-of-plane C−H deformation on a trisubstituted aromatic ring structure present in the phenazine ring.

The spectra of PPy prepared in the presence of the dye reveal the main characteristic bands of PPy and a small shoulder at 1597 cm^{-1} that corresponds to the aromatic ring vibrations of AF. A weak absorption band is also observed at about 1634 cm^{-1} and can be related to AF ring-stretching vibrations (observed exactly at 1640 cm^{-1} in pure AF) or to the presence of the carbonyl group due to the nucleophilic attack of water during the polymerization.[29] The latter would indicate strong overoxidation of the sample induced by AF presence. The band observed at 1534 cm^{-1} (C−C stretching vibrations in the pyrrole ring) of the pristine PPy shifts to 1540 cm^{-1} after adding 10 mM of AF. The band of C−N stretching vibrations located at 1453 cm^{-1} shifts to 1458 cm^{-1}. The broad band at 1302 cm^{-1} corresponding to the C−H or C−N in-plane deformation vibration remains at the same position as well as the peak at 1166 cm^{-1} which refers to the C−H in-plane deformation vibration. The peak at 1036 cm^{-1} representing C−H out-of-plane bending shifts to 1041 cm^{-1} upon addition of AF. The small peak at 1597 cm^{-1} that appears in the spectra of PPy with various concentrations of the dye in addition to the peak shifts confirms the presence of the AF dye and its interaction with PPy. All mentioned shifts are in the direction to higher wavenumbers, indicating a slight stiffening of the pyrrole ring, most likely due to $\pi-\pi$ interactions with AF.

3.3. Raman Spectra. Raman spectra collected with a laser excitation wavelength of 633 nm as presented in Figure 5 provide information on the charge distribution on the PPy chains since both polarons and bipolarons are resonantly

https://doi.org/10.1021/acsapm.1c00775
ACS Appl. Polym. Mater. 2021, 3, 6063−6069

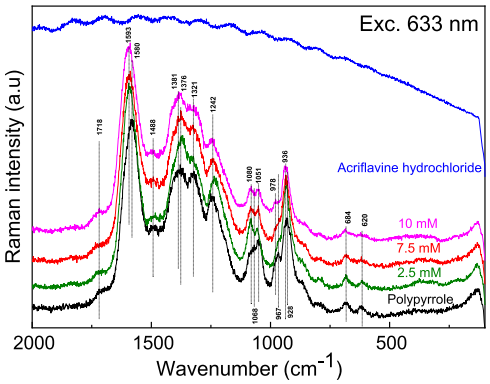

Figure 5. Raman spectra (excitation line 633 nm) of AF and PPy in the absence and presence of various concentrations of the AF.

enhanced with this excitation line. On the other hand, the AF dye is out of resonance with this excitation wavelength and thus is not observed.

In the recorded spectrum of pristine PPy, the typical band related to the backbone stretching of C=C bonds and the inter-ring C−C in the backbone of the polaron structure is located at 1580 cm^{-1}.[30−32] The band of C−N stretching vibrations in the pyrrole ring is located at 1488 cm^{-1}.[29,30] The doublet situated at 1376 and 1321 cm^{-1} corresponds to the ring stretching vibrations of PPy. The band located at higher wavenumbers is assigned to the vibrations of charged PPy, and the second one refers to the C−C ring stretching of neutral units.[30−32] The band maximum at about 1242 cm^{-1} is assigned to the C−H antisymmetric in-plane bending vibrations.[29,33] In the region 1090−1050 cm^{-1}, two peaks are detected: 1068 cm^{-1} is attributed to the C−H in-plane deformation vibrations of protonated species and 1051 cm^{-1} corresponds to the C−H in-plane deformations in the neutral units.[30,32,34] The bands at 967 and 928 cm^{-1} are assigned to the in-plane ring deformation related to the polaron and bipolaron states of PPy, respectively.[30,31,35] The small shoulder at 1718 cm^{-1}, observed in all samples, is connected to the carbonyl groups and overoxidation.

In the spectra of PPy in the presence of AF, we observe the same bands with blue shifts in comparison to the spectrum of pristine PPy. The C=C backbone stretching vibrations at 1580 cm^{-1} are moved to 1593 cm^{-1}, and the peaks at 1376, 1068, and 967 cm^{-1} corresponding to the bipolaron structure, observed in the spectrum of pristine PPy, are shifted, respectively, to 1381, 1080, and 978 cm^{-1} in the presence of the dye. This is connected to the interaction of PPy with the AF dye, as mentioned earlier in FTIR analysis.

The spectra of PPy with the dye exhibit an increase in the intensity of the band of C−H deformation in the bipolaron structure situated at 1080 cm^{-1} compared to the band at 1068 cm^{-1} in the pristine PPy. The intensity of the peak at 1080 cm^{-1} observed for the lowest dye concentration of 2.5 mM in PPy subsequently decreases upon further addition of the dye. As the bipolarons are dominant charge carriers in PPy, higher bipolaron content can be correlated with the higher conductivity of PPy.[29,36]

3.4. Yield and Conductivity. The yield is calculated with respect to the monomer used in the polymerization reaction. Theoretically, 1 g of pyrrole provides 1.23 g of PPy chloride (Figure 1a). Herein, we observe that the yield in the synthesis of globular PPy is lower, which, however, increases with the use of the dye and thus shows the incorporation of the dye (Table 1).

Table 1. Yield and Conductivity of the PPy Prepared at Different Molar Concentrations of AF with a Fixed Molar Ratio of the Oxidant to Pyrrole, *i.e.*, [Oxidant]/[Pyrrole] = 2

[AF] (mM)	yield (g g^{-1})	conductivity (S cm^{-1})
0	0.90	1.1 ± 0.2
2.5	1.54	14.7 ± 0.5
7.5	1.62	8.2 ± 0.3
10.0	1.46	5.3 ± 0.3

Globular PPy possesses a conductivity of 1.1 S cm^{-1} (Table 1), which is in good agreement with previously published results.[37] As presented in Table 1, the conductivity of PPy increases up to 14.7 S cm^{-1} for the PPy nanofibers prepared in the presence of 2.5 mM AF dye. The increase in the conductivity can be attributed to the higher content of charge carriers, bipolarons, in the nanofibrillar PPy, as evidenced by Raman spectroscopy (see Section 3.3). It can be observed that the further increase in the dye concentration lowers the conductivity; however, it is still greater in all cases compared to globular PPy. As visible in SEM (Figure 2d) and TEM (Figure 3d) images, increase in the dye concentration to 10 mM invokes the formation of dye aggregates (nonconducting islands) on the surface of nanofibers, leading to the inhomogeneity of the material; as a result, a decrease in the conductivity was observed, and hence, the further increase in dye concentration was not studied. It is previously well reported that the conductivity of globular PPy can increase up to 2 orders of magnitude[22,23] when organic dyes are added to the preparation procedure, depending on the nanostructure obtained.

3.5. Thermal Studies. TGA was carried out to study the thermal stability of globular and nanofibrous PPy (Figure 6).

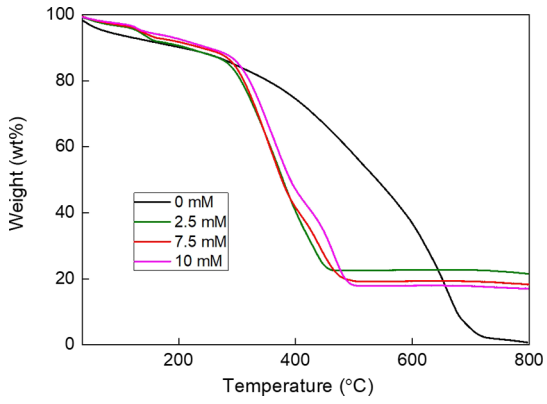

Figure 6. TGA of PPy prepared with different AF concentrations.

In all the cases, PPy shows stability up to nearly 200 °C, whereas a small weight loss is observed, which might be due to the removal of moisture. The thermal stability of PPy composites with the dye is higher than that of the pristine PPy. PPy nanofibers leave a residue of ∼20 wt % as compared to globular PPy with no residual weight.

3.6. Electrochemical Studies. In order to examine the potential in electrochemical capacitors, CV was performed for the prepared PPy, without and with the AF dye. Figure 7

https://doi.org/10.1021/acsapm.1c00775
ACS Appl. Polym. Mater. 2021, 3, 6063−6069

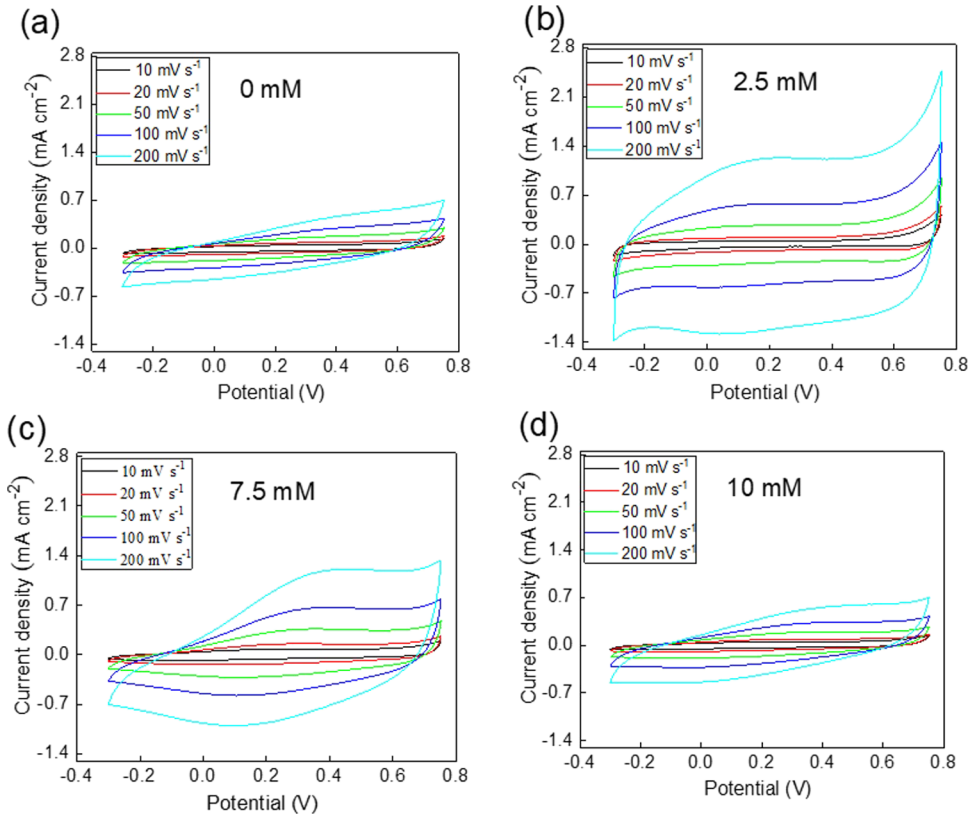

Figure 7. Cyclic voltammograms of PPy prepared in the presence of (a) 0, (b) 2.5, (c) 7.5, and (d) 10 mM AF.

presents the CV, carried out by the drop-casting method as explained above in the Experimental Section. Different scan rates of 10, 20, 50, 100, and 200 mV s^{-1} were used over the potential range from −0.35 to 0.75 V in 0.2 M HCl.

Globular PPy shows oxidation and reduction peaks (Figure 7a) similar to previously reported studies.[38,39] The cyclic voltammograms evidently display the influence of the dye on the current densities of PPy, which further affect their redox behavior. Herein, for the lowest dye concentration of 2.5 mM, a sudden increase in the current density was observed, resulting in an enhanced redox peak and provided with a quasi-rectangular shaped curve, thus signifying better capacitive properties. For higher dye concentrations, 7.5 or 10 mM (Figure 7c,d), however, a gradual decrease in the redox behavior, still better or similar to PPy alone, was observed, respectively. These cyclic voltammograms were further studied to evaluate the gravimetric capacitances based on their integral areas, as presented in Table 2. PPy itself is believed to have good capacitive behavior. The highest gravimetric capacitance was observed for the lowest dye concentration, which is fairly stable even at high potential scan rates. The enhanced capacitive behavior is also in accordance with the highest conductivity value obtained (Table 2). However, for other dye concentrations, lower capacitances which decay upon increasing the sweep rates, one of the commonly seen behaviors, were observed. It can be summarized that the presence of a AF certainly increases the capacitive property of PPy with the maximum capacitance of 85 F g^{-1} for the lowest amount of the dye.

Table 2. Gravimetric Capacitances (F g^{-1}) of PPy with Different AF Concentrations at Various Scan Rates

	gravimetric capacitances (F g^{-1})			
	concentration of the dye			
scan rates (mV s^{-1})	0 mM	2.5 mM	7.5 mM	10 mM
10	62.1	85.6	78.2	60.3
20	47.5	78.4	70.1	47.3
50	35.7	76.2	61.7	38.2
100	28.2	74.9	54.7	32.0
200	22.2	75.2	47.4	26.3

3.7. Antibacterial Properties. The assessment of antimicrobial activity is commonly achieved either by the diffusion or by the dilution method. In the dilution method, the minimum concentration of the antibacterial material to inhibit the bacterial growth, in media such as agar or broth, is determined, termed as MIC, which is often expressed in mg mL^{-1} or μg mL^{-1}.[40] In the current study, the MIC was determined by the CLSI/EUCAST macrodilution method for the prepared PPy-containing AF dye. The PPy nanofibers show abrupt rise in the antibacterial activity against both bacteria, irrespective of the dye concentrations, as presented in Table 3. The antibacterial activity of PPy can be related to various effects which have been previously described by Silva Júnior et al.[41] The dye concentrations, 2.5 and 7.5 mM, show similar

Table 3. Results of the MIC of the PPy in the Presence of (a) 0, (b) 2.5, (c) 7.5, and (d) 10 mM AF

	minimal inhibitory concentration (mg mL^{-1})			
bacteria	0 mM	2.5 mM	7.5 mM	10 mM
S. aureus	16	2	2	4
E. coli	16	4	4	4

https://doi.org/10.1021/acsapm.1c00775
ACS Appl. Polym. Mater. 2021, 3, 6063−6069

decreased MIC values of 2 and 4 mg mL^{-1} against *S. aureus* and *E. coli*, respectively, compared to PPy alone, signifying the enhanced antibacterial activity with incorporation of the dye. However, for the highest concentration, the response of the Gram-positive bacterium is reduced as the MIC value is increased to 4 mg mL^{-1}, but against the Gram-negative bacterium, no changes were observed.

In recent years, the antibacterial activity of PPy has gained significant interest. For example, Salabat et al. demonstrated the influence of palladium on the antibacterial activity of PPy against *S. aureus* by the microdilution method and obtained an MIC of 5.78 mg mL^{-1}.[12] Using the broth dilution method, Maruthapandi et al. presented the effect of Zn/CuO on the antibacterial activity of PPy with an MIC of 1 mg mL^{-1}.[13] It is clear that PPy has lower antibacterial activity; however, it can be improved with the addition of a variety of metal or metal oxides; nevertheless, the complicated synthesis and high cost are the major disadvantages. Herein, with the support of an inexpensive organic dye, we have successfully enhanced the antibacterial effect against the two bacteria with the lowest MIC of 2 mg mL^{-1}.

4. CONCLUSIONS

The successful preparation of PPy nanofibers in the presence of the AF dye, using iron(III) chloride was achieved. A maximum conductivity of 14.7 S cm^{-1} for PPy with the lowest dye concentration was observed. The FTIR and Raman spectroscopy confirmed the structure of PPy and its interaction with the AF dye. The higher bipolaron fraction in the PPy-containing dye was also indicated through Raman spectroscopy at a 633 nm excitation. The highest gravimetric capacitance of 85 F g^{-1} was observed for PPy prepared with the 2.5 mM dye at a scan rate of 10 mV s^{-1}. Additionally, the PPy-containing AF dye demonstrated enhanced antibacterial activity against both *S. aureus* and *E. coli* bacteria. Therefore, the addition of AF during PPy synthesis offers improved materials with possible applications in biosensors, antimicrobial surfaces, and bioelectronic devices. The low cost and easy availability of an organic dye are additional advantages in making the overall process simple and cost-effective.

AUTHOR INFORMATION

Corresponding Author

Patrycja Bober − *Institute of Macromolecular Chemistry, Czech Academy of Sciences, 162 06 Prague 6, Czech Republic;* orcid.org/0000-0002-1667-8604; Email: bober@imc.cas.cz

Authors

Sonal Gupta − *Institute of Macromolecular Chemistry, Czech Academy of Sciences, 162 06 Prague 6, Czech Republic*

Udit Acharya − *Institute of Macromolecular Chemistry, Czech Academy of Sciences, 162 06 Prague 6, Czech Republic*

Hana Pištěková − *Centre of Polymer Systems, Tomas Bata University in Zlín, 760 01 Zlín, Czech Republic*

Oumayma Taboubi − *Institute of Macromolecular Chemistry, Czech Academy of Sciences, 162 06 Prague 6, Czech Republic*

Zuzana Morávková − *Institute of Macromolecular Chemistry, Czech Academy of Sciences, 162 06 Prague 6, Czech Republic;* orcid.org/0000-0001-8128-1040

Martina Kašparová − *Centre of Polymer Systems, Tomas Bata University in Zlín, 760 01 Zlín, Czech Republic*

Petr Humpolíček − *Centre of Polymer Systems and Faculty of Technology, Tomas Bata University in Zlín, 760 01 Zlín, Czech Republic;* orcid.org/0000-0002-6837-6878

Complete contact information is available at: https://pubs.acs.org/10.1021/acsapm.1c00775

Notes

The authors declare no competing financial interest.

ACKNOWLEDGMENTS

The authors wish to thank the Czech Science Foundation (19-04859S) for the financial support. This work was supported by the Ministry of Education, Youth and Sports of the Czech Republic—DKRVO (RP/CPS/2020/001 and RP/CPS/2020/002). J. Hromádková is acknowledged for providing SEM and TEM images.

REFERENCES

(1) Gerard, M.; Chaubey, A.; Malhotra, B. D. Application of conducting polymers to biosensors. *Biosens. Bioelectron.* **2002**, *17*, 345−359.

(2) Snook, G. A.; Kao, P.; Best, A. S. Conducting-polymer-based supercapacitor devices and electrodes. *J. Power Sources* **2011**, *196*, 1−12.

(3) Humpolíček, P.; Kašpárková, V.; Pacherník, J.; Stejskal, J.; Bober, P.; Capáková, Z.; Radazkiewicz, K. A.; Junkar, I.; Lehocký, M. The biocompatibility of polyaniline and polypyrrole: A comparative study of their cytotoxicity, embryotoxicity and impurity profile. *Mater. Sci. Eng., C* **2018**, *91*, 303−310.

(4) Mahat, M. M.; Sabere, A. S. M.; Azizi, J.; Amdan, N. A. N. Potential Applications of Conducting Polymers to Reduce Secondary Bacterial Infections among COVID-19 Patients: a Review. *Emergent Mater.* **2021**, *4*, 279−292.

(5) Maráková, N.; Humpolíček, P.; Kašpárková, V.; Capáková, Z.; Martinková, L.; Bober, P.; Trchová, M.; Stejskal, J. Antimicrobial activity and cytotoxicity of cotton fabric coated with conducting polymers, polyaniline or polypyrrole, and with deposited silver nanoparticles. *Appl. Surf. Sci.* **2017**, *396*, 169−176.

(6) Liu, J.; Wang, J.; Yu, X.; Li, L.; Shang, S. One-pot synthesis of polypyrrole/AgCl composite nanotubes and their antibacterial properties. *Micro & Nano Lett.* **2015**, *10*, 50−53.

(7) Bideau, B.; Bras, J.; Saini, S.; Daneault, C.; Loranger, E. Mechanical and antibacterial properties of a nanocellulose-polypyrrole multilayer composite. *Mater. Sci. Eng., C* **2016**, *69*, 977−984.

(8) Nazarzadeh Zare, E.; Mansour Lakouraj, M.; Mohseni, M. Biodegradable polypyrrole/dextrin conductive nanocomposite: synthesis, characterization, antioxidant and antibacterial activity. *Synth. Met.* **2014**, *187*, 9−16.

(9) Ahmad, N.; Sultana, S.; Faisal, S. M.; Ahmed, A.; Sabir, S.; Khan, M. Z. Zinc oxide-decorated polypyrrole/chitosan bionanocomposites with enhanced photocatalytic, antibacterial and anticancer performance. *RSC Adv.* **2019**, *9*, 41135−41150.

(10) Milakin, K. A.; Capáková, Z.; Acharya, U.; Vajdák, J.; Morávková, Z.; Hodan, J.; Humpolíček, P.; Bober, P. Biocompatible and antibacterial gelatin-based polypyrrole cryogels. *Polymer* **2020**, *197*, 122491:1-7.

(11) Xu, Y.; Ma, J.; Han, Y.; Xu, H.; Wang, Y.; Qi, D.; Wang, W. A simple and universal strategy to deposit Ag/polypyrrole on various substrates for enhanced interfacial solar evaporation and antibacterial activity. *Chem. Eng. J.* **2020**, *384*, 123379:1-9.

(12) Salabat, A.; Mirhoseini, F.; Mahdieh, M.; Saydi, H. A novel nanotube-shaped polypyrrole−Pd composite prepared using reverse microemulsion polymerization and its evaluation as an antibacterial agent. *New J. Chem.* **2015**, *39*, 4109−4114.

(13) Maruthapandi, M.; Sharma, K.; Luong, J. H. T.; Gedanken, A. Antibacterial activities of microwave-assisted synthesized polypyrrole/

chitosan and poly (pyrrole-N-(1-naphthyl) ethylenediamine) stimulated by C-dots. *Carbohydr. Polym.* **2020**, *243*, 116474.
(14) Zasońska, B. A.; Acharya, U.; Pfleger, J.; Humpolíček, P.; Vajdák, J.; Svoboda, J.; Petrovsky, E.; Hromádková, J.; Walterova, Z.; Bober, P. Multifunctional polypyrrole@ maghemite@ silver composites: synthesis, physico-chemical characterization and antibacterial properties. *Chem. Pap.* **2018**, *72*, 1789−1797.
(15) Bober, P.; Liu, J.; Mikkonen, K. S.; Ihalainen, P.; Pesonen, M.; Plumed-Ferrer, C.; von Wright, A.; Lindfors, T.; Xu, C.; Latonen, R.-M. Biocomposites of nanofibrillated cellulose, polypyrrole, and silver nanoparticles with electroconductive and antimicrobial properties. *Biomacromolecules* **2014**, *15*, 3655−3663.
(16) Wu, T.-M.; Chang, H.-L.; Lin, Y.-W. Synthesis and characterization of conductive polypyrrole/multi-walled carbon nanotubes composites with improved solubility and conductivity. *Compos. Sci. Technol.* **2009**, *69*, 639−644.
(17) Hsu, F.-H.; Wu, T.-M. In situ synthesis and characterization of conductive polypyrrole/graphene composites with improved solubility and conductivity. *Synth. Met.* **2012**, *162*, 682−687.
(18) Bose, S.; Kuila, T.; Uddin, M. E.; Kim, N. H.; Lau, A. K. T.; Lee, J. H. In-situ synthesis and characterization of electrically conductive polypyrrole/graphene nanocomposites. *Polymer* **2010**, *51*, 5921−5928.
(19) Jurewicz, K.; Delpeux, S.; Bertagna, V.; Béguin, F.; Frackowiak, E. Supercapacitors from nanotubes/polypyrrole composites. *Chem. Phys. Lett.* **2001**, *347*, 36−40.
(20) Biswas, S.; Drzal, L. T. Multilayered nanoarchitecture of graphene nanosheets and polypyrrole nanowires for high performance supercapacitor electrodes. *Chem. Mater.* **2010**, *22*, 5667−5671.
(21) Li, Y.; Bober, P.; Trchová, M.; Stejskal, J. Polypyrrole prepared in the presence of methyl orange and ethyl orange: nanotubes versus globules in conductivity enhancement. *J. Mater. Chem. C* **2017**, *5*, 4236−4245.
(22) Minisy, I. M.; Bober, P.; Acharya, U.; Trchová, M.; Hromádková, J.; Pfleger, J.; Stejskal, J. Cationic dyes as morphology-guiding agents for one-dimensional polypyrrole with improved conductivity. *Polymer* **2019**, *174*, 11−17.
(23) Minisy, I. M.; Bober, P.; Šeděnková, I.; Stejskal, J. Methyl red dye in the tuning of polypyrrole conductivity. *Polymer* **2020**, *207*, 122854:1-9.
(24) Bober, P.; Li, Y.; Acharya, U.; Panthi, Y.; Pfleger, J.; Humpolíček, P.; Trchová, M.; Stejskal, J. Acid Blue dyes in polypyrrole synthesis: the control of polymer morphology at nanoscale in the promotion of high conductivity and the reduction of cytotoxicity. *Synth. Met.* **2018**, *237*, 40−49.
(25) Dana, S.; Prusty, D.; Dhayal, D.; Gupta, M. K.; Dar, A.; Sen, S.; Mukhopadhyay, P.; Adak, T.; Dhar, S. K. Potent antimalarial activity of acriflavine in vitro and in vivo. *ACS Chem. Biol.* **2014**, *9*, 2366−2373.
(26) Lee, K.; Zhang, H.; Qian, D. Z.; Rey, S.; Liu, J. O.; Semenza, G. L. Acriflavine inhibits HIF-1 dimerization, tumor growth, and vascularization. *Proc. Natl. Acad. Sci. U.S.A.* **2009**, *106*, 17910−17915.
(27) Wiegand, I.; Hilpert, K.; Hancock, R. E. W. Agar and broth dilution methods to determine the minimal inhibitory concentration (MIC) of antimicrobial substances. *Nat. Protoc.* **2008**, *3*, 163−175.
(28) Marjanović, B.; Ćirić-Marjanović, G.; Radulović, A.; Juranić, I.; Holler, P. Synthesis and characterization of polyacriflavine. *Mater. Sci. Forum* **2007**, *555*, 503−508.
(29) Stejskal, J.; Trchová, M.; Bober, P.; Morávková, Z.; Kopecký, D.; Vrňata, M.; Prokeš, J.; Varga, M.; Watzlová, E. Polypyrrole salts and bases: superior conductivity of nanotubes and their stability towards the loss of conductivity by deprotonation. *RSC Adv.* **2016**, *6*, 88382−88391.
(30) Crowley, K.; Cassidy, J. In situ resonance Raman spectroelectrochemistry of polypyrrole doped with dodecylbenzenesulfonate. *J. Electroanal. Chem.* **2003**, *547*, 75−82.
(31) Gupta, S. Hydrogen bubble-assisted syntheses of polypyrrole micro/nanostructures using electrochemistry: structural and physical property characterization. *J. Raman Spectrosc.* **2008**, *39*, 1343−1355.
(32) Morávková, Z.; Taboubi, O.; Minisy, I. M.; Bober, P. The evolution of the molecular structure of polypyrrole during chemical polymerization. *Synth. Met.* **2021**, *271*, 116608:1-6.
(33) Minisy, I. M.; Acharya, U.; Kobera, L.; Trchová, M.; Unterweger, C.; Breitenbach, S.; Brus, J.; Pfleger, J.; Stejskal, J.; Bober, P. Highly conducting 1-D polypyrrole prepared in the presence of safranin. *J. Mater. Chem. C* **2020**, *8*, 12140−12147.
(34) Ishpal; Kaur, A. Spectroscopic and electrical sensing mechanism in oxidant-mediated polypyrrole nanofibers/nanoparticles for ammonia gas. *J. Nanopart. Res.* **2013**, *15*, 1637:1-14.
(35) Liu, Y.-C. Characteristics of vibration modes of polypyrrole on surface-enhanced Raman scattering spectra. *J. Electroanal. Chem.* **2004**, *571*, 255−264.
(36) Varga, M.; Kopecká, J.; Morávková, Z.; Křivka, I.; Trchová, M.; Stejskal, J.; Prokeš, J. Effect of oxidant on electronic transport in polypyrrole nanotubes synthesized in the presence of methyl orange. *J. Polym. Sci., Part B: Polym. Phys.* **2015**, *53*, 1147−1159.
(37) Acharya, U.; Bober, P.; Trchová, M.; Zhigunov, A.; Stejskal, J.; Pfleger, J. Synergistic conductivity increase in polypyrrole/molybdenum disulfide composite. *Polymer* **2018**, *150*, 130−137.
(38) Fan, X.; Yang, Z.; He, N. Hierarchical nanostructured polypyrrole/graphene composites as supercapacitor electrode. *RSC Adv.* **2015**, *5*, 15096−15102.
(39) Liu, Y.; Wang, H.; Zhou, J.; Bian, L.; Zhu, E.; Hai, J.; Tang, J.; Tang, W. Graphene/polypyrrole intercalating nanocomposites as supercapacitors electrode. *Electrochim. Acta* **2013**, *112*, 44−52.
(40) Balouiri, M.; Sadiki, M.; Ibnsouda, S. K. Methods for in vitro evaluating antimicrobial activity: A review. *J. Pharm. Anal.* **2016**, *6*, 71−79.
(41) Silva Júnior, F. A. G. d.; Vieira, S. A.; Botton, S. D. A.; Costa, M. M. D.; Oliveira, H. P. D. Antibacterial activity of polypyrrole-based nanocomposites: a mini-review. *Polímeros* **2020**, *30*, No. E2020048:1-9.

https://doi.org/10.1021/acsapm.1c00775
ACS Appl. Polym. Mater. 2021, 3, 6063−6069

ARTICLE 4

Milakin K.A., Morávková Z., Acharya U., **Kašparová M.**, Breitenbach S., Taboubi O., Hodan J., Hromádková J., Unterweger C., Humpolíček P., Bober P., 2021. *Enhancement of conductivity, mechanical and biological properties of polyaniline-poly(N-vinylpyrrolidone) cryogels by phytic acid.* Polymer 217, 123450. DOI 10.1016/j.polymer. 2021.123450

Polymer 217 (2021) 123450

Contents lists available at ScienceDirect

Polymer

journal homepage: http://www.elsevier.com/locate/polymer

Enhancement of conductivity, mechanical and biological properties of polyaniline-poly(*N*-vinylpyrrolidone) cryogels by phytic acid

Konstantin A. Milakin [a], Zuzana Morávková [a], Udit Acharya [a,b], Martina Kašparová [c], Stefan Breitenbach [d], Oumayma Taboubi [a], Jiří Hodan [a], Jiřina Hromádková [a], Christoph Unterweger [d], Petr Humpolíček [c,e], Patrycja Bober [a,*]

[a] Institute of Macromolecular Chemistry, Czech Academy of Sciences, 162 06, Prague 6, Czech Republic
[b] Faculty of Mathematics and Physics, Charles University, 182 00, Prague, Czech Republic
[c] Centre of Polymer Systems, Tomas Bata University in Zlin, 760 01, Zlin, Czech Republic
[d] Wood K Plus – Kompetenzzentrum Holz GmbH, 4040, Linz, Austria
[e] Faculty of Technology, Tomas Bata University in Zlin, 760 01, Zlin, Czech Republic

ARTICLE INFO

Keywords:
Polyaniline
Cryogel
Conductivity
Biocompatibility

ABSTRACT

Polyaniline-based cryogels were prepared by oxidative cryopolymerization in the presence of various concentrations of poly(*N*-vinylpyrrolidone) and phytic acid used as a polymer support and a dopant, respectively. Mechanical strength and handling stability of the resulting macroporous materials (pore size up to 70 μm) were significantly improved by the addition of poly(*N*-vinylpyrrolidone) into the polymerization system compared to the cryogels crosslinked only by phytic acid. Increase of poly(*N*-vinylpyrrolidone) concentration in the reaction medium above 5 wt%, while not noticeably changing mechanical properties, was found to lead to a decrease of conductivity and specific surface area. Introduction of optimal amount of phytic acid (0.2 M) as an additional codopant, in opposite, allowed enhancement of the material conductivity and specific surface area as well as increase of their tensile modulus. Polyaniline-poly(*N*-vinylpyrrolidone) cryogels containing phytic acid also showed better cytocompatibility due to lower cytotoxicity and improved cell adhesion and proliferation.

1. Introduction

Polyaniline (PANI)-based cryogels are composite materials which consist of the conducting polymer and a water-soluble polymer support forming a three-dimensional macroporous network [1]. They are designed to combine intrinsic physicochemical characteristics of PANI with mechanical and chemical properties of the supporting polymer to overcome inherent brittleness of the conducting polymer for improved handling properties and opening new potential application options. Being a subclass of conducting polymer hydrogels, cryogels can be used in similar ways, for example, as sensors [2–4], supercapacitors [5,6], antibacterial materials [7,8], in tissue engineering [9,10] and drug-delivery [11,12]. Polyaniline cryogels are prepared by oxidative polymerization of aniline in a frozen medium containing a water-soluble polymer [1]. The prefix "cryo" in the term cryogel, therefore, refers to the cryogelation process which is a crucial step in the preparation procedure. Freezing of the reaction medium and subsequent formation of ice crystals acting as pore-forming agents, around which a conducting polymer network is formed, are stages, which define macroporous morphology and properties of the resulting materials [13]. Influencing the balance between the polymerization rate and the rates of ice crystal formation and growth by variation of the reaction medium composition (copolymerization approach) or freezing temperature allows tuning pore size, mechanical properties and specific surface area of the cryogels for a required application [14,15].

Choosing an appropriate polymer support for a conducting polymer gel preparation allows tailoring the material properties for the specific purpose. For instance, using poly(*N*-isopropylacrylamide) leads to thermoresponsive materials [4], poly(vinyl alcohol) is suitable for the preparation of the cryogels with superelasticity [16] or gelatin [17] can serve as a sacrificial template for the preparation of a cryogel derived macroporous conducting polymer. Poly(*N*-vinylpyrrolidone) (PVP) being an inert and biocompatible polymer, widely used for various biomedical purposes [18], can be a promising support for cryogels for

* Corresponding author.
E-mail address: bober@imc.cas.cz (P. Bober).

https://doi.org/10.1016/j.polymer.2021.123450
Received 1 September 2020; Received in revised form 7 January 2021; Accepted 17 January 2021
Available online 20 January 2021

bio-applications. It was shown [19] to be used in a PANI-based hydrogel. However, to the best of our knowledge, cryopolymerization of similar systems has not been reported yet.

Phytic acid is an organic acid, which is abundant in natural sources such as legumes, cereals and nuts, and represents up to 85% of phosphorus supply in plants [20]. Being a polybasic acid, which contains twelve acidic protons, phytic acid can be used as a dopant and crosslinker for PANI chains. The latter allows preparation of PANI hydrogels without additional polymer supports or matrices, where phytic acid serves as the only gelating agent [21,22]. The resulting macroporous materials show high surface area and specific capacitance, and can be used as supercapacitors [21], sensors [21] or adsorbents [22]. A combined approach involving cryogelation together with crosslinking by phytic acid for preparation of PANI–phytic acid cryogels was also reported [23]. Directed freezing and freeze-drying applied in the work [23] resulted in aerogels with anisotropic conductivity, high specific surface area and specific capacitance. Moreover, the cryogelation approach coupled with introduction of additional polymer support was also described [3,24]. In the mentioned works [3,24], however, freezing of polymerization mixture inducing gelation of poly(vinyl alcohol) was performed after PANI–phytic acid hydrogels had formed. This fact might affect morphology and mechanical properties of the materials compared to simultaneous formation of the hydrogel and the supporting polymer matrix.

It should be additionally noted that using phytic acid as the only dopant results in PANI of lower conductivity compared to the one doped by conventional hydrochloric acid [25]. Therefore, it was suggested [25,26] to use chloride and phytate in a mixed dopant approach for achieving both high conductivity and desired morphology.

In the present work, we have prepared PANI cryogels supported by PVP by a previously unreported combination of cryopolymerization and a mixed dopant approach with chloride, sulfate and phytate ions as codopants and studied influence of polymerization mixture composition on the morphology, mechanical and physicochemical properties of resulting materials. In contrast to the published works, flash-freezing of the reaction mixture has been utilized to ensure simultaneous formation of PVP and PANI–phytic acid hydrogel networks to minimize potential interference of growing ice crystals on the formed conducting polymer phase.

2. Experimental

2.1. Chemicals

Aniline (Penta, Czech Republic), aniline hydrochloride (Penta, Czech Republic), ammonium peroxydisulfate (Lach-Ner, Czech Republic), poly (*N*-vinylpyrrolidone) (PVP) (molecular weight 360000, Sigma-Aldrich, China) and phytic acid (50 wt% solution, Sigma-Aldrich, Japan) were used as received.

2.2. Synthesis of cryogels

Polyaniline-poly(*N*-vinylpyrrolidone) cryogels were prepared by oxidative cryopolymerization of aniline hydrochloride (0.2 M) by ammonium peroxydisulfate (0.25 M) in aqueous solution of PVP (5–8 wt %) containing various concentrations of phytic acid (0.04 M, 0.2 M, 1 M). After mixing of precooled monomer and oxidant solutions, the polymerization mixture was quickly sucked into plastic syringes, frozen in dry ice/ethanol bath at −78 °C and left to polymerize in a freezer at −24 °C for 7 days. After thawing, the cryogels were removed from the syringes, washed with excess of water and freeze-dried. Similar procedure was applied for preparation of reference cryogels in the absence of phytic acid (6 wt% PVP) or in the absence of PVP (0.2 M phytic acid). The latter material was prepared using aniline as a monomer instead of aniline hydrochloride.

2.3. Characterization

Morphology of freeze-dried PANI–PVP cryogels was studied by a scanning electron microscope (SEM) MAIA3 (Tescan, Czech Republic). Static mechanical properties of water-swollen PANI–PVP cryogels (cylindrical specimens – diameter 3 mm, length 60 mm) were investigated using electromechanical testing machine Instron 6025/5800R (Instron, USA) equipped with a 10 N load cell at room temperature in deionized water and with a cross-head speed of 10 mm min^{-1}. The values reported in the manuscript are averages of at least three measurements.

The DC electrical conductivity of freeze-dried cryogels was determined by a van der Pauw method on compressed pellets (diameter 13 mm, thickness 1.0 ± 0.3 mm) placed in sample holder fitted with gold plated spring loaded electrodes. A Keithley 230 Programmable Voltage Source in serial connection with a Keithley 196 System DMM served as a current source, the potential difference between the potential probes was measured with a Keithley 181 Nanovoltmeter (Keithley, USA). Measurements were carried out at constant ambient conditions at 24 ± 1 °C and relative humidity 35 ± 5%. The electrical conductivity σ was calculated from the applied current I and the measured potential difference U in the linear part of the current-voltage characteristics.

Specific surface area of cryogels was calculated from physisorption measurements on a volumetric sorption analyzer Autosorb-iQ (Anton Paar QuantaTec Inc., USA) using the Brunauer-Emmet-Teller (BET) method. 50 mg of the samples were outgassed for 2 h at 120 °C. The measurements were performed with nitrogen at 77 K at a relative pressure of 0.1–0.4.

Raman spectra of freeze-dried materials were measured with a InVia Reflex Raman microspectrometer (Renishaw, United Kingdom). The spectra were excited with a diode 785 nm laser. The scattered light was registered with a Peltier-cooled CCD detector (576 × 384 pixels) and analyzed by the spectrograph with holographic grating 1200 lines mm^{-1}. The spectra were obtained at several spots of the sample, and the samples were found to be inhomogeneous, average spectra are thus presented.

PANI–PVP cryogels (6 wt% PVP, 0.2 M and no phytic acid) were tested for cytotoxicity and proliferation of cells on the surface. The mouse embryonic fibroblast cell line (ATCC CRL-1658 NIH/3T3, USA) was used for all experiments. The cultivation medium consisted of Dulbecco's Modifed Eagle's Medium (PAA Laboratories GmbH, Austria) containing 10% bovine calf serum (BioSera, France) and 1% of Penicillin/Streptomycin (GE Healthcare HyClone, United Kingdom).

The cytotoxicity determination was performed according to ISO standard 10993–12; concretely the 0.1 g of PANI–PVP cryogel per 1 mL of media were used for extract preparation. The samples were disintegrated in culture medium and incubated for 24 h at 37 °C with stirring. The extracts were subsequently filtered using Syringe filter 0.22 μm. The parent extracts (100%) were then diluted in fresh culture medium to obtain a series of dilutions with concentrations of 75, 50, 25, 10, and 5% of extracts. All extracts dilutions were used immediately for testing. The cytotoxicity testing was done as follows: cells were seeded to pre-cultivate in the 96 well microtitration test plates dishes (TPP, Switzerland) in seeding concentration 1×10^5 cells per mL. After 24 h of pre-cultivation, the extracts were added to pre-cultivated cells. All assays were performed in quadruplets. After another 24 h, when the cells were cultivated in the presence of diluted extracts, the extracts were sucked up, replaced by fresh medium, and cell viability was determined.

The cell viability was evaluated by MTT assay (MTT cell proliferation kit, Duchefa Biochemie, Netherlands). Infinite M200 Pro NanoQuant (Tecan, Switzerland) was used for measuring the absorbance at 570 nm. The reference wavelength was adjusted on 690 nm. The results are presented as reduction of cell viability in percentage when compared to those cultivated in medium without the extracts of tested materials (reference cell viability corresponds to 1).

Before cell proliferation testing, the samples were sterilized by 70% ethanol for 24 h and washed four times (after 12 h) with ultra-pure

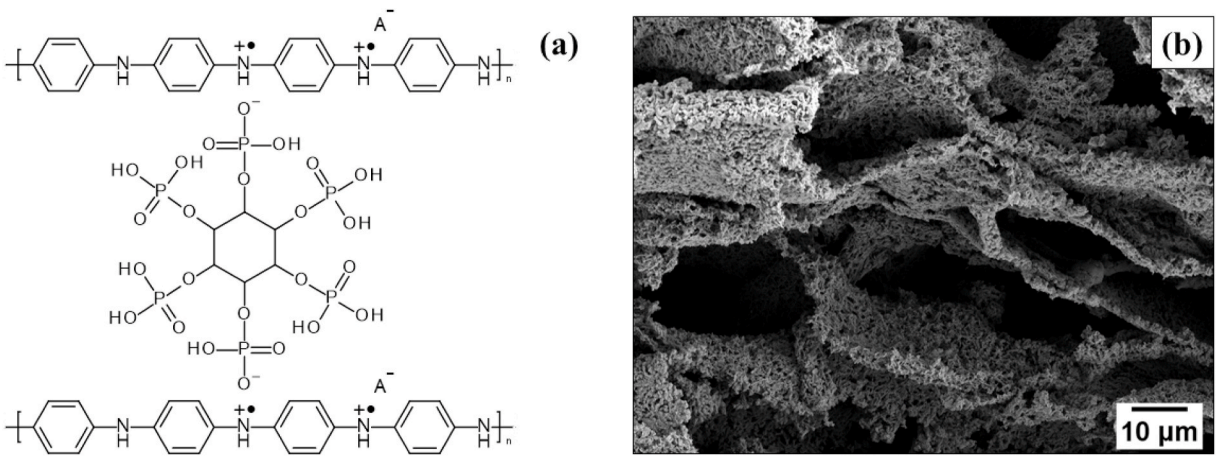

Fig. 1. (a) Scheme of PANI and phytic acid interaction; (b) SEM image of PANI–phytic acid cryogel prepared in aqueous solution of phytic acid (0.2 M) in the absence of PVP.

water to remove the residual ethanol. Then the samples were immersed into medium for next 24 h. The surface of PANI–PVP cryogels, approximately 0.79 cm^2, was overflowed with 0.5 mL of cell suspension in a concentration of 1×10^6 cells per mL. After 48 h of cultivation, staining of DNA and F-actin was used to determine the amount of cells and their cytoskeleton. Before staining, cells were fixed and permeabilized. Firstly, the cells were fixed using 4% formaldehyde (Penta, Czech Republic) for 15 min, then washed by phosphate buffered saline (PBS, Invitrogen, USA) and subsequently poured with 0.5% Triton X-100 (Sigma-Aldrich, USA) for 5 min to permeabilization. After this time cells were washed 3 times by PBS. Then Hoechst 33258 (Invitrogen, USA) at a concentration of 5 μg per mL was added to the new PBS to stain DNA. At the same time two drops of ActinRed™ 555 (Thermo Fisher Scientific, USA) per 1 mL of PBS were used for visualization of F-actin cytoskeleton and left to incubate for 30 min in the dark. The morphology of cells was observed using an inverted Olympus phase contrast microscope IX 81 (Olympus, Germany) and also confocal laser scanning microscope Olympus FV 3000.

3. Results and discussion

3.1. Polyaniline-phytic acid cryogel

Due to the fact that phytic acid can perform not only as a dopant for PANI but also as a gelator during formation of hydrogels (Fig. 1a) without additional supporting polymers [21], a reference synthesis was performed, in which oxidative cryopolymerization of aniline was carried out without PVP in an aqueous solution of phytic acid (0.2 M).

Fig. 1b shows that PANI–phytic acid cryogel is a double-porous material which consists of porous (pore size up to 2 μm) two-

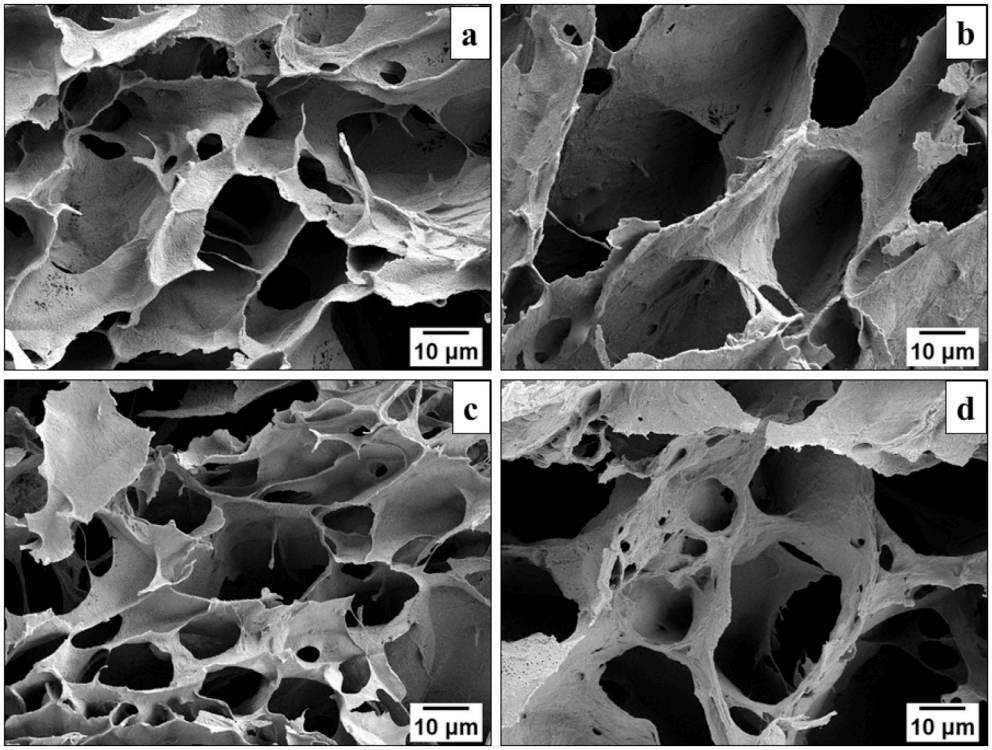

Fig. 2. SEM micrographs of PANI–PVP cryogels prepared in 0.2 M phytic acid solution containing following concentrations of PVP: (a) 5 wt%, (b) 6 wt%, (c) 7 wt%, (d) 8 wt%.

Table 1
Mechanical properties, conductivity and specific surface area of PANI–PVP cryogels prepared using various concentrations of PVP in polymerization mixture containing 0.2 M of phytic acid.

PVP concentration, wt%	Tensile strain at break, %	Tensile stress at break, kPa	Tensile modulus, kPa	Conductivity, S cm^{-1}	BET surface area, m^2 g^{-1}
5%	41 ± 6	3.5 ± 0.4	96 ± 13	2×10^{-1}	38.7
6%	63 ± 7	4.2 ± 0.7	112 ± 25	1×10^{-1}	28.0
7%	59 ± 10	3.9 ± 0.3	108 ± 60	8×10^{-2}	22.2
8%	70 ± 19	4.0 ± 0.3	88 ± 14	7×10^{-2}	11.0

dimensional conducting polymer layers forming a 3D structure with much larger pores (up to 30 μm). Double-porous morphology was previously described in the literature [21] for similar materials prepared without freezing the reaction medium. However, the largest reported pores were around units of micrometers. That value is similar to pore size in the individual polymer layers in our PANI–phytic acid cryogels but considerably smaller than the one for the pores between the layers. Thus, in the case of the cryogelated materials, significantly larger pores can be observed due to formation of ice crystals upon freezing of the reaction medium.

One of the main motivations for preparation of free-standing PANI-based hydrogels is enhancement of the conducting polymer processibility and applicability. Therefore, mechanical strength of the resulting materials is a crucial parameter for assessment. In the case of PANI–phytic acid cryogels mechanical integrity was found to be very low, the gels were difficult to handle and most of them were destroyed during the washing procedure. Thus, it was concluded that using of phytic acid as the only gelator is not enough for ensuring handling stability of the materials and all further experiments were performed with cryogels additionally containing PVP as a supporting polymer.

3.2. Polyaniline-poly(N-vinylpyrrolidone) cryogels doped by phytic acid: effect of the supporting polymer concentration

Polyaniline-poly(*N*-vinylpyrrolidone) cryogels were prepared by oxidative cryopolymerization of aniline hydrochloride in the aqueous solution of PVP containing phytic acid. In order to study the influence of the reaction medium composition on the morphology, mechanical strength and conductivity of the cryogels, the synthesis was carried out using various concentrations of the supporting polymer and the dopant. In the first step, the cryopolymerization was performed varying a concentration of PVP from 5 wt% to 8 wt% with a constant concentration of phytic acid (0.2 M).

SEM images of the resulting cryogels (Fig. 2) prepared using all studied concentrations of PVP show similar macroporous structure with pore sizes 10–40 μm typical for conducting polymer hydrogels prepared by cryopolymerization technique in the presence of a polymer support [1,14]. The porous structure of cryogelated materials is determined by size and distribution of ice crystals, which are formed upon freezing of the reaction medium and serve as pore-forming agents [13]. It was recently shown [15] that it is possible to influence the pore size of PANI-based cryogels by shifting the balance between growth of ice crystals and formation of polymer network around them. In the present case, when PVP concentration is the only variable in the composition of the polymerization mixture there is no observed variation in the pore sizes in the cryogels with the change of the parameter. Therefore, we can assume that the mentioned shift of balance does not occur.

The main role of a water-soluble polymer, such as PVP, in the preparation of conducting polymer-based cryogels is enhancement of material's mechanical strength and overcoming inherent brittleness of conducting polymers. It can be expected that changing the ratio between a conducting polymer and a polymer support in the cryogel might influence mechanical characteristics of the material. However, according to assessment of mechanical properties of PANI–PVP prepared using different concentrations of PVP (Table 1), changing the strengthening agent concentration from 5 wt% to 8 wt% does not lead to noticeable

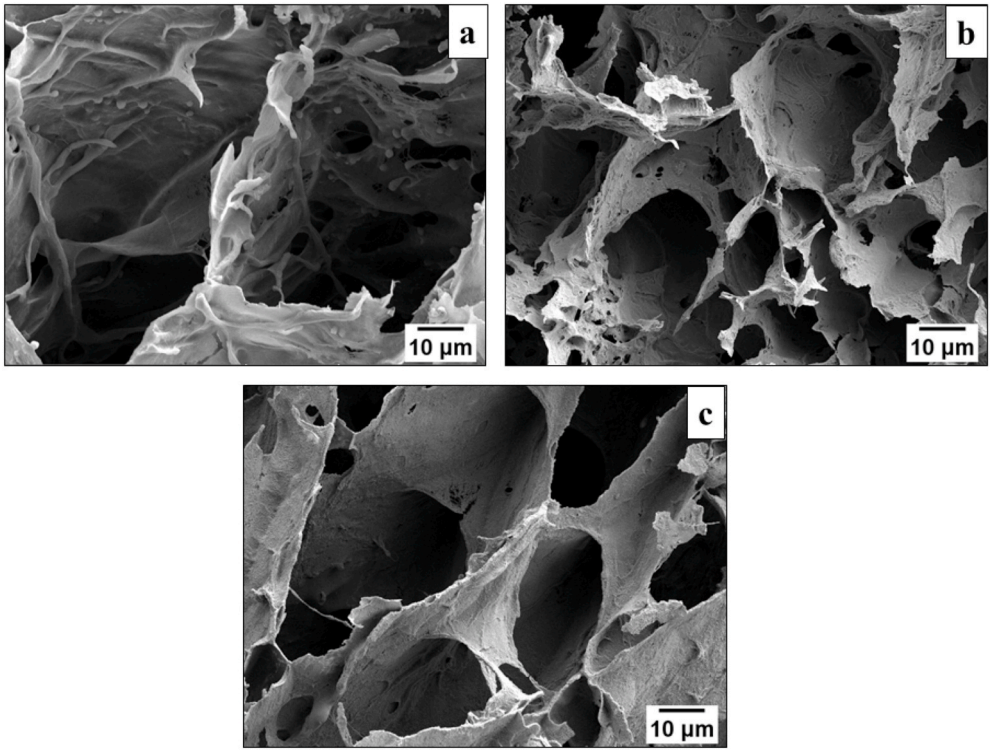

Fig. 3. SEM images of PANI–PVP cryogels prepared in 6 wt% solution of PVP in (a) the absence of phytic acid or containing following concentrations of phytic acid: (b) 0.04 M, (c) 0.2 M.

Table 2
Mechanical properties, conductivity and specific surface area of PANI–PVP cryogels prepared in 6 wt% solution of PVP containing various concentrations of phytic acid or in the absence of phytic acid.

Phytic acid concentration, M	Tensile strain at break, %	Tensile stress at break, kPa	Tensile modulus, kPa	Conductivity, S cm^{-1}	BET surface area, m^2 g^{-1}
0.2	63 ± 7	4.2 ± 0.7	112 ± 25	1×10^{-1}	28.0
0.04	55 ± 28	0.3 ± 0.2	16 ± 4	2×10^{-2}	5.8
0	196 ± 52	3 ± 1	15 ± 3	1×10^{-2}	9.3

change of tensile characteristics of the cryogels, while showing significant improvement compared to the reference PANI–phytic acid cryogels prepared in the absence of PVP, for which mechanical characteristics could not be measured due to the poor handling stability. The strengthening effect of addition of PVP into the polymerization system might be connected with the absence of pores in the PANI–PVP cryogel walls (Fig. 2), which were present in the structure of the material containing phytic acid as the only gelating agent (Fig. 1b) and could act as microdefects.

Influence of PVP content in the initial polymerization solution on conductivity of PANI–PVP cryogels is shown in Table 1. Increasing PVP concentration from 5 wt% to 8 wt% leads to a slight conductivity decrease from 2×10^{-1} S cm^{-1} to 7×10^{-2} S cm^{-1} which can possibly be explained by higher fraction of a non-conducting polymer component (PVP) in the resulting cryogels.

Specific surface area of PANI–PVP cryogels was found to decrease from 38.7 m^2 g^{-1} to 11.0 m^2 g^{-1} with increasing of PVP concentration from 5 wt% to 8 wt%. This is probably concerned with PVP interference with formation of pores, which can be assumed to take place based on the difference between porous structure of a reference cryogel prepared in the absence of PVP (Fig. 1b) and morphology of PVP-containing materials (Fig. 2).

3.3. Polyaniline-poly(N-vinylpyrrolidone) cryogels: effect of phytic acid concentration

The next step for optimization of the PANI–PVP cryogel preparation procedure was studying the influence of phytic acid concentration on the morphology, mechanical properties and conductivity of the materials. The cryogels were synthesized by the cryopolymerization technique in aqueous solution of PVP (6 wt%) in the presence of various concentrations of phytic acid (0.04 M, 0.2 M, 1 M) or in the absence of phytic acid. It should be noted that PANI–PVP cryogels prepared using 1 M phytic acid showed low mechanical strength and poor handling stability and were destroyed upon removal from plastic syringes immediately after preparation. Therefore, they were excluded from further studies.

Fig. 3 shows that all studied PANI–PVP cryogels prepared using various concentrations of phytic acid or in the absence of phytic acid have similar macroporous morphology typical for the cryogelation approach. However, the material obtained in the absence of phytic acid has notably larger pores with pore sizes reaching 70 μm while for the composites synthesized in the phytic acid containing solutions these values are lower (up to 40 μm). This effect might be attributed to the presence of additional type of ions (phytic acid) and difference in ionic strength in the system which can influence ice crystal formation [27] leading to the change in pore sizes of the resulting composites.

Influence of phytic acid concentration in the initial reaction mixture on mechanical properties of PANI–PVP cryogels is shown in Table 2. It can be seen that introduction of 0.2 M phytic acid into the polymerization medium results in higher tensile modulus and lower tensile strain

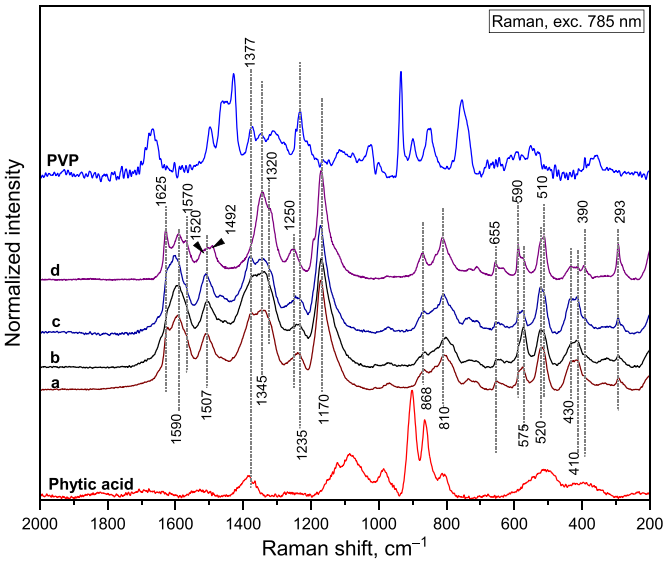

Fig. 4. Average Raman spectra of (a) PANI–phytic acid (0.2 M) cryogel synthesized without PVP; PANI–PVP (6 wt%) cryogel prepared (b) in the presence of 0.2 M phytic acid and (c) in the absence of phytic acid; (d) PANI–PVP (5 wt %) cryogel prepared in the presence of 0.2 M phytic acid (a typical spectrum of an inhomogeneity) and reference spectra of PVP and phytic acid. The spectra were excited with 785 nm laser line, normalized and shifted for clarity.

at break of the cryogels compared to the reference ones without phytic acid. This can possibly be explained by the fact that phytic acid can act as a crosslinker in the system and its presence leads to obtaining materials with lower elasticity. Increasing the phytic acid concentration further (to 1 M), as was mentioned before, led to mechanically weak cryogels, which were impossible to handle.

Conductivity of PANI–PVP cryogels (Table 2) was found to be in the same order of magnitude as observed for PANI-based cryogels containing dopants other than phytic acid (sulfate and chloride ions) [14]. However, addition of 0.2 M phytic acid into the polymerization medium resulted in a slight increase of the measured values: 1×10^{-2} S cm^{-1} for the material obtained in the absence of phytic acid, 1×10^{-1} S cm^{-1} for the cryogel prepared in 0.2 M solution of phytic acid. This can be attributed to higher resistance to deprotonation [28] of a phytic acid doped PANI which occurs during washing of the resulting cryogels with water.

Addition of 0.2 M phytic acid into the polymerization mixture was also found to increase specific surface area of resulting PANI–PVP cryogels up to 28.0 m^2 g^{-1} compared to the reference cryogel prepared in the absence of phytic acid (9.3 m^2 g^{-1}) (Table 2). This effect might be related to the morphology changes induced by the presence of phytic acid, which can be seen in Fig. 3. To summarize, 0.2 M is the optimal concentration of phytic acid in the polymerization mixture which leads to the noticeable improvement of mechanical strength, conductivity and specific surface area of PANI–PVP cryogels. Using 0.04 M phytic acid does not affect tensile modulus, conductivity and BET surface area compared to the reference cryogel without phytic acid and 1 M phytic acid leads to the dramatic reduction of the cryogel mechanical strength.

3.4. Spectroscopic study

To analyze chemical structure of PANI in the cryogels, Raman spectra excited with 785 nm laser line were obtained (Fig. 4). This excitation resonantly enhances various polaronic structures, allowing to study the protonation and oxidation states of the conducting polymer.

The samples were quite heterogeneous, polaron delocalization changed from spot to spot. Raman spectra were obtained at several spots of the sample and average spectra are presented (Fig. 4). Raman spectra

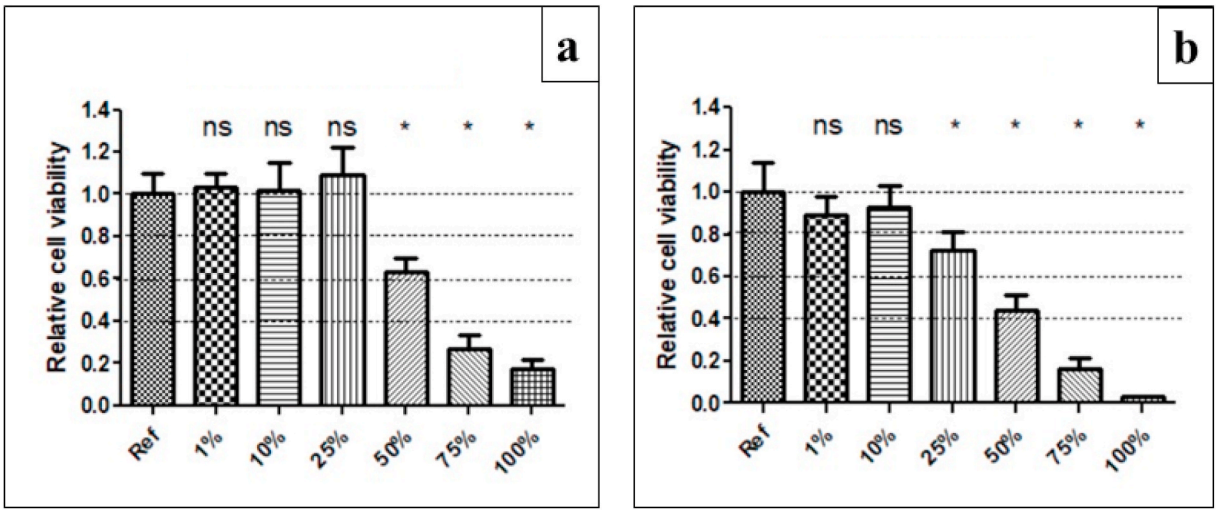

Fig. 5. Cell viability of extracts of PANI–PVP cryogels synthesized using 6 wt% of PVP in the presence of (a) 0.2 M phytic acid and (b) without it. Statistical significance was determined by ANOVA with post hoc Tukey's Multiple Comparison test; *P < 0.0001. (*) mark statistically significant difference compared to reference.

display the features of protonated PANI [29–34]: semiquinonoid ring stretching of emeraldine salt structure at 1590 cm^{-1}, N–H deformation vibration at 1507 cm^{-1}, C~$N^{\bullet+}$ stretching vibration of delocalized 1340 cm^{-1} and localized 1377 cm^{-1} polaronic structures, C–N stretching vibration at 1250 and 1235 cm^{-1}, C–H deformation vibrations at 1170 cm^{-1}, and various skeletal deformation vibrations below 1000 cm^{-1}.

A group of additional bands connected with overoxidation [29] appear in the spectra of some areas in the cryogels (Fig. 4d): ring stretching of the quinonoid ring in a pernigraniline-like or benzoquinone-like structure at 1625 cm^{-1}, benzenoid ring stretching at 1590 and 1575 cm^{-1}, N^{+}—H stretching in quinonoid structure at 1520 cm^{-1}, C═N stretching at 1492 cm^{-1}, bipolaron C~$N^{\bullet+}$ stretching at 1320 cm^{-1}, and skeletal deformation peaks at 590, 510, 390 and 293 cm^{-1}.

3.5. Biological properties

Influence of phytic acid presence on biocompatibility of PANI–PVP cryogels was studied by cytotoxicity and cell proliferation tests. The cryogels prepared at 6 wt% of PVP in the presence of 0.2 M phytic acid and without it were compared. The results of cytotoxicity evaluation are presented in Fig. 5. To determine any statistical differences between the reference and samples extracts, the ANOVA with post hoc Tukey's multiple comparison test was applied. The P values of < 0.0001 were considered statistically significant. Extracts from both type of cryogels proved no cytotoxicity for concentration 1% and 10% in cultivation medium. The first difference occurs in 25% of extracts, when the sample with phytic acid shows statistically non-significant difference from the reference, while the sample without phytic acid shows a mild cytotoxicity. Statistically significant differences were noted for both types of extracts with 50% and over. Overall, the cytotoxicity effect for PANI–PVP cryogel containing phytic acid was slightly lower than without phytic acid. Previously cryogels of PANI with poly(vinyl alcohol) were studied in context of cytotoxicity by Humpolicek et al. [35] Compared to the material reported in the present manuscript, the PANI–poly(vinyl alcohol) cryogel has slightly lower cytotoxicity as only 100% extracts show mild cytotoxicity while all other concentrations were non-cytotoxic. The results of these two studies are, however, not fully comparable as different cell lines were used in there. On the other hand, the cytotoxicity of the presented PANI–PVP material is comparable to the one determined for polypyrrole-poly(vinyl alcohol) cryogel which

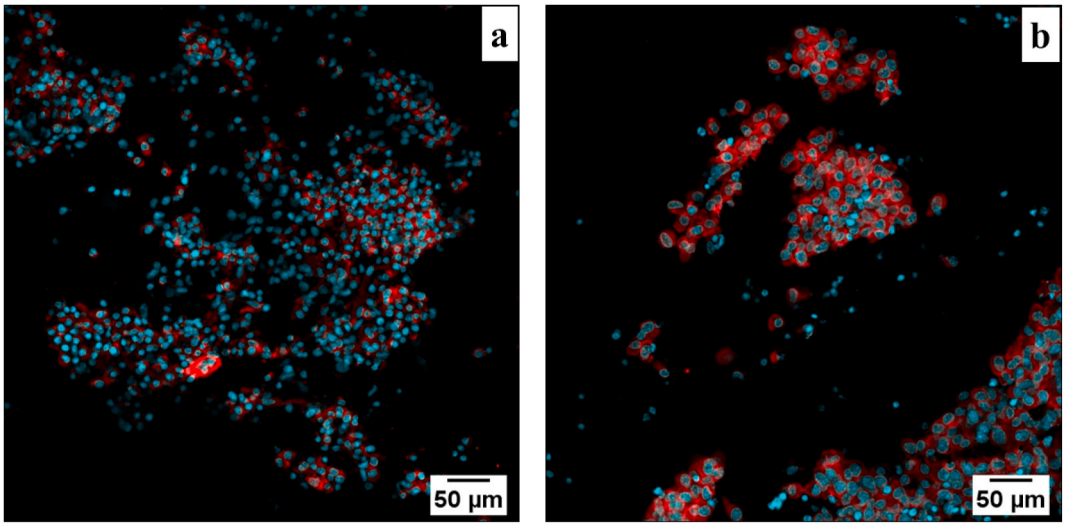

Fig. 6. Cell proliferation on surface of PANI–PVP cryogels synthesized using 6 wt% of PVP in the presence of (a) 0.2 M phytic acid and (b) without it.

was published in the study of Bober et al. [36], and where the same cell line was used. It is, therefore, obvious that cytotoxicity of PANI–PVP cryogels is common to those type of materials.

The cytotoxicity is just the first prerequisite for application of any biomaterial. Here another parameter, the cell adhesion and their subsequent growth and proliferation, was determined. For the cell proliferation testing, the cells were seeded on PANI–PVP cryogel surface and allowed to grow for 2 days. It is clear (Fig. 6), that cells were able to adhere on the surface. On the other hand, the cells form clusters and, thus, the surface was not covered homogeneously. Moreover, the morphology of cells shows limited spreading of cells on the material surface which can be connected to porous structure of the cryogel. Generally, there were more adhered cells on PANI–PVP cryogel prepared in the presence of phytic acid, than on the cryogel without one. This is an important improvement of cryogel properties in context of its practical application. To summarize, in terms of toxicity and proliferation, addition of phytic acid into PANI–PVP cryogels allows higher biocompatibility of PANI–PVP based cryogels.

4. Conclusions

Polyaniline-based macroporous conducting cryogels supported with PVP were synthesized by *in situ* one-step procedure in the presence of phytic acid as a codopant and a crosslinker for PANI. The presence of PVP was shown to be crucial for mechanical integrity of the materials, despite having phytic acid in the system as a crosslinker. The introduction of optimal amount of phytic acid, in addition to improvement of mechanical strength of the composites, enhanced conductivity, specific surface area and biocompatibility of the cryogels, shown by cytotoxicity and cell proliferation tests.

Declaration of competing interest

The authors declare that they have no known competing financial interests or personal relationships that could have appeared to influence the work reported in this paper.

Acknowledgment

The authors K.A.M., Z.M., U.A., P.B. wish to thank the Czech Science Foundation (18-04669S) for the financial support. The authors P.H. and M.K. thank the project of Czech Science Foundation (19-16861S) for the financial support. Part of this work was carried out within the project BioCarb-K, co-financed by the European Regional Development Fund (EFRE) and the province of Upper Austria through the programme IWB 2014–2020.

References

[1] J. Stejskal, P. Bober, M. Trchová, A. Kovalcik, J. Hodan, J. Hromádková, J. Prokeš, Polyaniline cryogels supported with poly(vinyl alcohol): soft and conducting, Macromolecules 50 (2017) 972–978, https://doi.org/10.1021/acs.macromol.6b02526.

[2] H. Al-Sagur, K.S. Sundaram, E.N. Kaya, M. Durmus, T.V. Basova, A. Hassan, Amperometric glucose biosensing performance of a novel graphene nanoplatelets-iron phthalocyanine incorporated conducting hydrogel, Biosens. Bioelectron. 139 (2019) 111323, https://doi.org/10.1016/j.bios.2019.111323.

[3] C.X. Hu, Y.L. Zhang, X.D. Wang, L. Xing, L.Y. Shi, R. Ran, Stable, strain-sensitive conductive hydrogel with antifreezing capability, remoldability, and reusability, ACS Appl. Mater. Interfaces 10 (2018) 44000–44010, https://doi.org/10.1021/acsami.8b15287.

[4] Z.X. Deng, Y. Guo, P.X. Ma, B.L. Guo, Rapid thermal responsive conductive hybrid cryogels with shape memory properties, photothermal properties and pressure dependent conductivity, J. Colloid Interface Sci. 526 (2018) 281–294, https://doi.org/10.1016/j.jcis.2018.04.093.

[5] H.B. Huang, R.P. Chen, S.Y. Yang, L. Li, Y.L. Liu, J. Huang, Facile fabrication of MnO2-embedded 3-D porous polyaniline composite hydrogel for supercapacitor electrode with high loading, High Perform. Polym. 32 (2019) 286–295, https://doi.org/10.1177/0954008319860893.

[6] Z.Q. Niu, W.Y. Zhou, X.D. Chen, J. Chen, S.S. Xie, Highly compressible and all-solid-state supercapacitors based on nanostructured composite sponge, Adv. Mater. 27 (2015) 6002–6008, https://doi.org/10.1002/adma.201502263.

[7] Y. Zhao, Z.H. Li, S.L. Song, K.R. Yang, H. Liu, Z. Yang, J.C. Wang, B. Yang, Q. Lin, Skin-inspired antibacterial conductive hydrogels for epidermal sensors and diabetic foot wound dressings, Adv. Funct. Mater. 29 (2019) 1901474, https://doi.org/10.1002/adfm.201901474.

[8] H. Hosseinzadeh, A. Barghi, Synthesis of poly(AN)/poly(AA-co-AM) hydrogel nanocomposite with electrical conductivity and antibacterial properties, Polym. Compos. 40 (2019) 2724–2733, https://doi.org/10.1002/pc.25080.

[9] M. Talikowska, X. Fu, G. Lisak, Application of conducting polymers to wound care and skin tissue engineering: a review, Biosens. Bioelectron. 135 (2019) 50–63, https://doi.org/10.1016/j.bios.2019.04.001.

[10] N. Alegret, A. Dominguez-Alfaro, D. Mecerreyes, 3D scaffolds based on conductive polymers for biomedical applications, Biomacromolecules 20 (2019) 73–89, https://doi.org/10.1021/acs.biomac.8b01382.

[11] K. Sharma, V. Kumar, B. Chaudhary, B.S. Kaith, S. Kalia, Application of biodegradable superabsorbent hydrogel composite based on gum ghatti-co-poly (acrylic acid-aniline) for controlled drug delivery, Polym. Degrad. Stab. 124 (2016) 101–111, https://doi.org/10.1016/j.polymdegradstab.2015.12.021.

[12] J. Qu, X. Zhao, P.X. Ma, B.L. Guo, Injectable antibacterial conductive hydrogels with dual response to an electric field and pH for localized "smart" drug release, Acta Biomater. 72 (2018) 55–69, https://doi.org/10.1016/j.actbio.2018.03.018.

[13] V.I. Lozinsky, I.Y. Galaev, F.M. Plieva, I.N. Savinal, H. Jungvid, B. Mattiasson, Polymeric cryogels as promising materials of biotechnological interest, Trends Biotechnol. 21 (2003) 445–451, https://doi.org/10.1016/j.tibtech.2003.08.002.

[14] K.A. Milakin, M. Trchová, U. Acharya, J. Hodan, J. Hromádková, J. Pfleger, B. A. Zasońska, J. Stejskal, P. Bober, Conducting composite cryogels based on poly (aniline-co-p-phenylenediamine) supported by poly(vinyl alcohol), Synth. Met. 246 (2018) 144–149, https://doi.org/10.1016/j.synthmet.2018.10.008.

[15] K.A. Milakin, M. Trchová, U. Acharya, S. Breitenbach, C. Unterweger, J. Hodan, J. Hromádková, J. Pfleger, J. Stejskal, P. Bober, Effect of initial freezing temperature and comonomer concentration on the properties of poly(aniline-co-m-phenylenediamine) cryogels supported by poly(vinyl alcohol), Colloid Polym. Sci. 298 (2020) 293–301, https://doi.org/10.1007/s00396-020-04608-5.

[16] L. Li, Y. Zhang, H.Y. Lu, Y.F. Wang, J.S. Xu, J.X. Zhu, C. Zhang, T.X. Liu, Cryopolymerization enables anisotropic polyaniline hybrid hydrogels with superelasticity and highly deformation-tolerant electrochemical energy storage, Nat. Commun. 11 (2020) 62, https://doi.org/10.1038/s41467-019-13959-9.

[17] K.A. Milakin, U. Acharya, M. Trchová, B.A. Zasońska, J. Stejskal, Polypyrrole/gelatin cryogel as a precursor for a macroporous conducting polymer, React. Funct. Polym. 157 (2020) 104751, https://doi.org/10.1016/j.reactfunctpolym.2020.104751.

[18] M. Kurakula, G.S.N.K. Rao, Pharmaceutical assessment of polyvinylpyrrolidone (PVP): as excipient from conventional to controlled delivery systems with a spotlight on COVID-19 inhibition, J. Drug Deliv. Sci. Technol. 60 (2020) 102046, https://doi.org/10.1016/j.jddst.2020.102046.

[19] C. Dispenza, C. Lo Presti, C. Belfiore, G. Spadaro, S. Piazza, Electrically conductive hydrogel composites made of polyaniline nanoparticles and poly(N-vinyl-2-pyrrolidone), Polymer 47 (2006) 961–971, https://doi.org/10.1016/j.polymer.2005.12.071.

[20] R.K. Gupta, S.S. Gangoliya, N.K. Singh, Reduction of phytic acid and enhancement of bioavailable micronutrients in food grains, J. Food Sci. Technol. 52 (2015) 676–684, https://doi.org/10.1007/s13197-013-0978-y.

[21] L.J. Pan, G.H. Yu, D.Y. Zhai, H.R. Lee, W.T. Zhao, N. Liu, H.L. Wang, B.C.K. Tee, Y. Shi, Y. Cui, Z.N. Bao, Hierarchical nanostructured conducting polymer hydrogel with high electrochemical activity, Proc. Natl. Acad. Sci. U.S.A. 109 (2012) 9287–9292, https://doi.org/10.1073/pnas.1202636109.

[22] H.J. Kim, S. Im, J.C. Kim, W.G. Hong, K. Shin, H.Y. Jeong, Y.J. Hong, Phytic acid doped polyaniline nanofibers for enhanced aqueous copper(II) adsorption capability, ACS Sustain. Chem. Eng. 5 (2017) 6654–6664, https://doi.org/10.1021/acssuschemeng.7b00898.

[23] R. Yao, Z.J. Yao, J.T. Zhou, Novel multi-configuration aniline/phytic acid based aerogel with directed higher performance, Mater. Lett. 198 (2017) 206–209, https://doi.org/10.1016/j.matlet.2017.03.032.

[24] J. Ye, D.J. Shi, Z.K. Yang, M.Q. Chen, Interpenetrating network hydrogels based on nanostructured conductive polymers for flexible supercapacitor, Polym. Sci. 60 (2018) 647–654, https://doi.org/10.1134/S0965545X18050164.

[25] Y. Gawli, A. Banerjee, D. Dhakras, M. Deo, D. Bulani, P. Wadgaonkar, M. Shelke, S. Ogale, 3D polyaniline architecture by concurrent inorganic and organic acid doping for superior and robust high rate supercapacitor performance, Sci. Rep. 6 (2016) 21002, https://doi.org/10.1038/srep21002.

[26] H.H. Wu, C.W. Chang, D.L. Lu, K. Maeda, C.C. Hu, Synergistic effect of hydrochloric acid and phytic acid doping on polyaniline-coupled g-C3N4 nanosheets for photocatalytic Cr(VI) reduction and dye degradation, ACS Appl. Mater. Interfaces 11 (2019) 35702–35712, https://doi.org/10.1021/acsami.9b10555.

[27] S.W. Wu, C.Q. Zhu, Z.Y. He, H. Xue, Q.R. Fan, Y.L. Song, J.S. Francisco, X.C. Zeng, J.J. Wang, Ion-specific ice recrystallization provides a facile approach for the fabrication of porous materials, Nat. Commun. 8 (2017) 15154, https://doi.org/10.1038/ncomms15154.

[28] D. Mawad, C. Mansfield, A. Lauto, F. Perbellini, G.W. Nelson, J. Tonkin, S.O. Bello, D.J. Carrad, A.P. Micolich, M.M. Mahat, J. Furman, D.J. Payne, A.R. Lyon, J. J. Gooding, S.E. Harding, C.M. Terracciano, M.M. Stevens, A conducting polymer with enhanced electronic stability applied in cardiac models, Sci. Adv. 2 (2016), e1601007, https://doi.org/10.1126/sciadv.1601007.

[29] Z. Morávková, E. Dmitrieva, Structural changes in polyaniline near the middle oxidation peak studied by in situ Raman spectroelectrochemistry, J. Raman Spectrosc. 48 (2017) 1229–1234, https://doi.org/10.1002/jrs.5197.
[30] S. Quillard, G. Louarn, J.P. Buisson, M. Boyer, M. Lapkowski, A. Pron, S. Lefrant, Vibrational spectroscopic studies of the isotope effects in polyaniline, Synth. Met. 84 (1997) 805–806, https://doi.org/10.1016/S0379-6779(96)04155-0.
[31] M.I. Boyer, S. Quillard, E. Rebourt, G. Louarn, J.P. Buisson, A. Monkman, S. Lefrant, Vibrational analysis of polyaniline: a model compound approach, J. Phys. Chem. B 102 (1998) 7382–7392, https://doi.org/10.1021/jp972652o.
[32] M. Cochet, G. Louarn, S. Quillard, J.P. Buisson, S.J. Lefrant, Theoretical and experimental vibrational study of emeraldine in salt form. Part II, Raman Spectrosc 31 (2000) 1041–1049, https://doi.org/10.1002/1097-4555(200012)31:12<1041::AID-JRS641>3.0.CO;2-R.
[33] M.I. Boyer, S. Quillard, G. Louarn, G. Froyer, S. Lefrant, Vibrational study of the FeCl3-doped dimer of polyaniline; A good model compound of emeraldine salt, J. Phys. Chem. B 104 (2000) 8952–8961, https://doi.org/10.1021/jp000946v.
[34] G. Ćirić-Marjanović, M. Trchová, J. Stejskal, The oxidative polymerization of aniline in water: Raman spectroscopy, J. Raman Spectrosc. 39 (2008) 1375–1387, https://doi.org/10.1002/jrs.2007.
[35] P. Humpolíček, K.A. Radaszkiewicz, Z. Capáková, J. Pacherník, P. Bober, V. Kašpárková, P. Rejmontová, M. Lehocký, P. Ponížil, J. Stejskal, Polyaniline cryogels: biocompatibility of novel conducting macroporous material, Sci. Rep. 8 (2018) 135, https://doi.org/10.1038/s41598-017-18290-1.
[36] P. Bober, Z. Capáková, U. Acharya, B.A. Zasońska, P. Humpolíček, J. Hodan, J. Hromádková, J. Stejskal, Highly conducting and biocompatible polypyrrole/poly (vinyl alcohol) cryogels, Synth. Met. 252 (2019) 122–126, https://doi.org/10.1016/j.synthmet.2019.04.015.

ARTICLE 5

Musilová L., Achbergerová E., Vítková L., Kolařík R., **Martínková M.**, Minařík A., Mráček A., Humpolíček P., Pecha J., 2022. *Cross-Linked Gelatine by Modified Dextran as a Potential Bioink Prepared by a Simple and Non-Toxic Process.* Polymers 14, 391. DOI 10.3390/polym14030391

polymers

MDPI

Article

Cross-Linked Gelatine by Modified Dextran as a Potential Bioink Prepared by a Simple and Non-Toxic Process

Lenka Musilová [1,2], Eva Achbergerová [3], Lenka Vítková [1], Roman Kolařík [2], Martina Martínková [2], Antonín Minařík [1,2], Aleš Mráček [1,2,*], Petr Humpolíček [1,2] and Jiří Pecha [3]

[1] Department of Physics and Materials Engineering, Faculty of Technology, Tomas Bata University in Zlin, Vavreckova 275, 760 01 Zlín, Czech Republic; lmusilova@utb.cz (L.M.); vitkova@utb.cz (L.V.); minarik@utb.cz (A.M.)

[2] Centre of Polymer Systems, Tomas Bata University in Zlín, tř. Tomáše Bati 5678, 760 01 Zlín, Czech Republic; rkolarik@utb.cz (R.K.); martinkova@utb.cz (M.M.); humpolicek@utb.cz (P.H.)

[3] CEBIA-Tech, Faculty of Applied Informatics, Tomas Bata University in Zlín, Nad Stráněmi 4511, 760 05 Zlín, Czech Republic; achbergerova@utb.cz (E.A.); pecha@utb.cz (J.P.)

* Correspondence: mracek@utb.cz

Abstract: Essential features of well-designed materials intended for 3D bioprinting via microextrusion are the appropriate rheological behavior and cell-friendly environment. Despite the rapid development, few materials are utilizable as bioinks. The aim of our work was to design a novel cytocompatible material facilitating extrusion-based 3D printing while maintaining a relatively simple and straightforward preparation process without the need for harsh chemicals or radiation. Specifically, hydrogels were prepared from gelatines coming from three sources—bovine, rabbit, and chicken—cross-linked by dextran polyaldehyde. The influence of dextran concentration on the properties of hydrogels was studied. Rheological measurements not only confirmed the strong shear-thinning behavior of prepared inks but were also used for capturing cross-linking reaction kinetics and demonstrated quick achievement of gelation point (in most cases < 3 min). Their viscoelastic properties allowed satisfactory extrusion, forming a self-supported multi-layered uniformly porous structure. All gelatin-based hydrogels were non-cytototoxic. Homogeneous cells distribution within the printed scaffold was confirmed by fluorescence confocal microscopy. In addition, no disruption of cells structure was observed. The results demonstrate the great potential of the presented hydrogels for applications related to 3D bioprinting.

Keywords: gelatine-dextran; hydrogel; 3D printing; microextrusion; rheology; cell distribution

Citation: Musilová, L.; Achbergerová, E.; Vítková, L.; Kolařík, R.; Martínková, M.; Minařík, A.; Mráček, A.; Humpolíček, P.; Pecha, J. Cross-Linked Gelatine by Modified Dextran as a Potential Bioink Prepared by a Simple and Non-Toxic Process. *Polymers* **2022**, *1*, 391. https://doi.org/10.3390/polym14030391

Academic Editor: Sidi A. Bencherif

Received: 20 December 2021
Accepted: 14 January 2022
Published: 19 January 2022

1. Introduction

Nowadays, 3D bioprinting has become one of the lead technologies in tissue engineering. Compared to the traditional preparation of cell-seeded scaffolds, the 3D bioprinting via microextrusion process enables the incorporation of selected cells within the printed material prior to or directly during the printing process. The major advantage of this technology is that cells, biomaterials, and biomolecules can be spatially defined. Therefore, more homogeneous cell distribution through the material could be achieved using this technique [1]. In addition, 3D bioprinting is more straightforward, less prone to human error, and gives an opportunity to precisely fabricate complex structures [2,3]. The technique relies on well-designed materials, so-called bioinks, which are essential for 3D-bioprinted scaffolds in tissue engineering [4]. Despite the rapid development, the discipline still has a shortage of materials utilizable as bioinks [5–7].

Materials for microextrusion in biological applications need to fulfill several criteria, concerning both cellular response to the ink and mechanical response to printing-induced stress. Good cytocompatibility and a suitable micro- and nanostructure serve to facilitate cell proliferation and growth [8–10]. Regarding the physical behavior during printing, their

rheological properties present the main contribution. They have to be tailored in a way that allows uninterrupted flow of the material in the nozzle and provides stability to the printed structure at the same time. In addition, the bioink should help minimize the shear stress during printing in order to avoid the risk of cell destruction [11,12]. In addition to suitable rheology, sufficient layer adhesion is needed to ensure stable structures [13,14]. From the described point of view, hydrogels hold a great promise as potential bioinks [15]. Those formed from biopolymers such as hyaluronan (HA), collagen, or gelatine (Gel) are especially useful due to their ability to mimic the cellular environment [16].

Hydrogels generally consist of a cross-linked polymer network. The cross-linking can be facilitated either by non-covalent interactions or covalent (chemical) interactions. A typical feature of the former is the reversibility of bonds under specific conditions, which offers an opportunity in terms of rheology tuning [17,18]. The downside to this characteristic is the sensitivity to changes of thermodynamic conditions. It can also result in poor mechanical properties of the hydrogels [13,19,20]. In contrast, covalent bonds are less dynamic, but they provide the material with long-term stability in various environments. Furthermore, hydrogels cross-linked by this type of bond show superior durability under mechanical stress compared to non-covalent ones [17,21,22], which is desired for printed products [20].

To date, several chemically cross-linked hydrogels based on biopolymers for 3D bioprinting have been reported. Photocross-linking using UV irradiation was performed for modified natural polymers, such as HA [23] or in combination with modified polypeptides [16,24]. Although UV-initiated polymerization is popular due to its effectivity and predictability, this approach is also associated with the potential risk of inducing chromosomal and genetic instabilities in cells and subsequent cell mortality. The weaknesses of UV light were omitted when HA and Gel, both modified by phenolic hydroxyl moieties, were photocross-linked by irradiation from a visible spectrum. However, a disadvantage of this hydrogel preparation was the employment of a ruthenium/ammonium persulfate system [25]. Regarding other methods of bioink preparation, Gel–norbornene hydrogels were synthesized by two-photon polymerization [26], or modified HA, Gel, and acrylate cross-linked via radical polymerization [27] have been reported. Nevertheless, both mentioned methods required the complex chemical modification of used biopolymers before hydrogels preparation.

In a different approach, a dual cross-linking mechanism employing enzymatic reaction and photocross-linking [28,29] or photo- with chemical cross-linking [30] was utilised for bioink preparation [28–30]. Although the dual cross-linking strategies were developed to improve the mechanical and degradation properties of bioink while maintaining their printability and cell viability, this approach involves multi-step bioink preparation processes, especially when it is compared to much more straightforward simple methods utilizing UV irradiation [16,23,24]. On the other hand, the combined methods may allow avoiding the harmful effect of high-energy light by shifting the UV irradiation prior to embedding the cells in the material [29].

The aim of our work was to design a novel bipolymer-based hydrogel using chemical cross-linking hydrogels that allows microextrusion printing while maintaining a relatively simple and straightforward preparation process. Specifically, three types of Gel were examined: bovine (Gel-B)—a source of Gel often used in biomedical application—and two promising alternative sources—rabbit (Gel-R) and chicken (Gel-C) gelatines. The advantages of Gel-R and Gel-C are that they do not suffer from concerns about bovine spongiform encephalopathy or religious limitations [31,32]. All three gelatines were combined with dextran polyaldehyde (Dex-Ox) providing firm hydrogels. To the best of our knowledge, this presents a unique approach to using the described hydrogels (Gel-Dex-Ox) as a convenient material for 3D printing bearing the potential to be combined with living cells in a direct and simple procedure, thus creating a bioink.

Prepared printing materials were thoroughly investigated, and their performance in microextrusion-based 3D printing was evaluated. The study comprises hydrogels reaction kinetics, a detailed characterization of hydrogel rheological and swelling behavior, porosity,

and printability, which are discussed with respect to Gel origin and the amount of cross-linking agent used throughout the study.

Die swell, a parameter closely connected to printing precision in microextrusion [14,33], is, to our best knowledge, underrepresented in case of biopolymer-based hydrogel 3D printing. Die swell is a result of normal stress induced by the sudden change in diameter of the flow channel [34]. Although the mechanical stress-induced cell mortality is primarily connected to tangential forces [35], evidence of normal stress affecting cell viability during printing have been found as well [36]. Consequently, the performed analysis also includes the issue of die swell.

Regarding the hydrogels performance in biomedical application, cytotoxicity assay was performed on the materials. Finally, fluorescently labeled mouse fibroblasts were added to the gels and printed so that the cell distribution could be evaluated. The prepared hydrogels proved to be shear thinning and suitable for 3D printing applications as well as showing good cytocompatibility and negligible deformation of cells during printing.

2. Materials and Methods

2.1. Chemicals

Gel-B (dry content 91.3%, M_w = 209,600 g·mol^{-1}) and Gel-R (dry content 86.5%, M_w = 157,800 g·mol^{-1}) were obtained from Tanex Vladislav, a.s. Gel-C (dry content 92.7%, M_w = 190,900 g·mol^{-1}) was prepared according to a patented biotechnological process [37], which is described in detail in Mokrejš et al., 2019 [38] and Gál et al., 2020 [39]. Dextran (Dex) M_w = 40,400 g·mol^{-1}, sodium periodate, and phosphate-buffered saline sterile solution (PBS), pH 7.4, were obtained from Sigma Aldrich. Demineralized (DEMI) water was prepared using Milipore Q System. Ammonia solution, 30 vol% was purchased from Penta and diluted to 25 vol%. $Na_2HPO_4.12H_2O$ and $NaH_2PO_4.2H_2O$, used for the preparation of PBS pH 7, were obtained form Lach-Ner.

2.2. Dextran Oxidation

The oxidation of Dex was performed according to the previously described method [40]. Briefly, to the 13 wt % water solution of Dex and a 0.4 molar fold of $NaIO_4$ pre-dissolved in 5 mL of DEMI water was added. The reaction was stirred for 4 h at room temperature. Subsequently, the reaction mixture was diluted with DEMI water and put into a dialysis tube (membrane cut-off 12,000 g·mol^{-1}). The crude product was purified via dialysis against DEMI water for 3 days. Then, the solution was casted in a glass mold and frozen first at −18 °C for 24 h followed by freeze drying in a freeze-dryer (ALPHA1-2 LD plus, M. Christ, Osterode am Harz, Germany). The pure product was obtained in yield 90%, and its M_w was 7700 g·mol^{-1}. The number of aldehyde groups per 100 glucose subunits was determined using hydroxylamine hydrochloride method [41]. Automatic titrator T50 (Metler Tolledo, Greifensee, Switzerland) was used for the measurements.

2.3. Polymers Characterisation

Proton Nuclear Magnetic Resonance (^{1}H NMR) spectra were recorded on a machine JEOL ECZ 400 (JEOL Ltd., Tokyo, Japan) operating at ^{1}H frequency of 399.78 MHz at 60 °C. The samples were dissolved in D_2O at concentration of 10 mg·mL^{-1} for the analysis. The water signal was used as reference and was set at 4.75 ppm.

The average molecular weight and distribution curve of the initial biopolymers were determined by means of the size exclusion chromatography (SEC) method performed on a high-performance liquid chromatograph (HPLC) system Shimadzu Prominence equipped with UV-Vis and RI detectors (Shimadzu Prominence, LC-20 series, Shimadzu corporation, Kyoto, Japan). The conditions for analysis of polysaccharides were following: 0.1M PBS solution of pH equal to 7.4, flow 0.8 mL·min^{-1}, oven temperature 30 °C, columns PL aquagel-OH 60 8 µm, 300 × 7.5 mm and PL aquagel-OH 40 8 µm, 300 × 7.5 mm were connected in series. Pullulan standards were used for molecular weight calibration, analysis was based on RI data. Conditions for analysis of proteins were as follows: 0.15 M PBS

solution of pH equal to 7.0, flow 0.35 mL·min^{-1}, oven temperature 30 °C, column Agilent Bio SEC-5, 5 µm, 150 Å, 300 × 4.6 mm. Protein standards were used for molecular weight calibration; analysis was based on UV data gained at 210 nm.

2.4. Hydrogels Preparation and Characterization

Hydrogels were prepared in the following manner: 2 wt % solution of Dex-Ox in PBS (0.1 M, pH 7.4) was mixed with 15 wt % solution of Gel dissolved in PBS (0.1 M, pH 7.4). Three volume ratios of the solutions were examined—Gel:Dex-Ox 1:1, 2:1, and 3:1. After that, 25 vol % ammonia solution was added in concentration 50 µL per 1 mL of Gel solution, and all the reactants were mixed.

Rheological measurements of the prepared fresh mixture of biopolymer solutions (2 mL) were performed on a rotational rheometer Anton-Paar MCR 502 (Graz, Austria) at 30 °C under normal pressure in an air atmosphere. In case of the reaction kinetics measurement, time sweep experiments were performed using a 50 mm parallel-plate measuring system oscillating at constant 10% deformation with a constant angular frequency of 10 rad·s^{-1}. Fundamental rheological data, i.e., complex viscosity η, storage (G′), and loss (G″) moduli, were followed in a 40 min time sweep. It should be noted that the sample preparation caused a 1 min delay between the reaction start and first data obtained.

On the other hand, the rheology of fully cross-linked hydrogels was performed using a 25 mm parallel-plate measuring system oscillating at constant 10% deformation with angular frequency sweep increasing from 0.1 to 10 rad·s^{-1} at 35 °C. The frequency sweep measurement in a descending direction was carried out as well, without any change in rheological behavior. It is important to note that before such measurement was started, the hydrogel samples were prepared 12 h before in the form of circular plates with a diameter of 30 mm and a thickness of 2 mm.

As a 3D Printing instrument, Cellink BioX (Gothemburg, Sweden) was used with the following specifications: a polypropylene conical nozzle—0.41 mm diameter, 3 mL polypropylene syringe, microextrusion syringe pump printhead, and microscope glass slide printbed. The printhead speed was 2 mm·s^{-1}, and the extrusion rate was 1.5 µL·s^{-1}. During printing, both the printhead and printbed were kept at room temperature. Optical analysis of the printing performance was carried out using a Dino-Lite AM4815ZT optical microscope and evaluated with the aid of ImageJ software. The shape fidelity was characterized using the method described by Ouyang et al. [42], i.e., determining the printability (Pr) as the similitude of a gap between printed strands to a square in the top layer of a multi-layered 10x10 mm rectilinear patterned grid. The distance between strand centers in a single layer had to be adjusted to 3.3 mm due to the strong die swell of the material. The layer height was set to 0.6 mm in order to account for the die swell as well as to ensure good adhesion between layers. To calculate Pr, the following formula was used: $Pr = L^2/16A$, where L denotes the perimeter (mm) and A the area of a gap (mm^2). Moreover, an uninterrupted flow of material was recorded, and the die swell was measured at the perceived distance between the printbed and nozzle, i.e., 0.5 mm. Additionally, a model specifically designed for the materials examined in the current study was developed in the following way: The overall dimensions were 10 × 10 × 5 mm, the layer height was 1 mm, the material extrusion was continuous, and the speed of the printhead was monotonous throughout the printing.

The shape and porosity of printed structures before and after freeze drying was analyzed using X-ray computed micro-tomography (CT) with the help of SkyScan (Model 1174, Bruker, Billerica, MA, USA). The printed structures were obtained using the material-specific model described earlier. The device was equipped with the X-ray source, (voltage of 20–50 kV, maximum power of 40 W) and the X-ray detector. The CCD 1.3 Mpix was coupled to the scintillator by a lens with 1:6 zoom range. The projection images were recorded at angular increments of 0.5° or 1° using tube voltage and tube current of 35 kV and 585 µA, respectively. The exposure time was set to 15 s without using any filter. The 3D reconstructions, surface, and volume analysis were performed via built-in CT image

analysis software (version 1.16.4.1, Bruker, USA). The results, in terms of images with different X-ray adsorption, 2D cross-sections, and 3D models were exported from DataViewer and CTvox software. Prior to CT characterization, the printed hydrogels were placed in a closed sample holder with increased humidity so that the analyzed scaffold does not dry out.

The inner porosity of the material was assessed via scanning electron microscopy (SEM) imaging of freeze-dried samples in vertical sections using a Phenom Pro instrument at an accelerating voltage of 10 kV. The samples were sputtered with a gold/palladium layer prior to imaging. The pore size and total pore area were statistically evaluated with the aid of ImageJ software.

The swelling behavior of hydrogels was determined gravimetrically as follows: weighed lyophilized samples were immersed in PBS (0.1 M pH 7.4) to gradually reach swelling equilibrium. The equilibrium buffer uptake, S(e)(%), of hydrogels was determined by taking the swollen samples from buffer solutions at selected time intervals of 1, 2, 6, 15, 30, 60, 120, 240, 360, and 1440 min, wiping with tissue paper and weighing. The presented results are expressed as an average values of 4 measurements. The samples were conditioned to 37 °C throughout the measurement in order to meet the requirements of testing for biological use.

2.5. Cytotoxicity

Cytotoxicity was tested using a mouse embryonic fibroblast cell line (ATCC CRL-1658 NIH/3T3). Testing was performed according to ISO 10-993 standard concretely by testing of extracts from freeze-dried hydrogel samples. Extracts were prepared according to ISO standard 10993-12 with modifications; the extraction ratio was 0.02 g per 1 mL of culture medium (which is a lower amount than according to the ISO, which is due to the swelling properties of lyophilized samples). The ATCC-formulated Dulbecco's Modified Eagle's Medium (PAA Laboratories, Inc., Etobicoke, ON, Canada) containing 10% of calf serum (BioSera, Nuaille, France) and 100 U mL^{-1} penicillin/streptomycin (GE 209 Healthcare HyClone, Hyclone Ltd., Cramlington, UK) was used as the culture medium. Tested samples were extracted in culture medium for 24 h at 37 °C under stirring. Subsequently, the extracts were filtered using a syringe filter with a pore size of 0.22 μm. Then, the parent extracts (100%) were diluted in culture medium to obtain a series of dilutions with concentrations of 75, 50, 25, 10, and 5%. Cells were proceeded in concentration of 10^5 per 1 mL and cultivated for 24 h at 37 °C in 5% CO_2 in humidified air. Then, the medium was removed after the pre-cultivation and replaced by individual extracts. Cell viability was evaluated after 24 h of exposure using ATP assay (ATP Determination Kit A22066, ThermoFisher Scientific, Waltham, MA, USA). The results are presented as the relative cell viability compared to the reference (cells cultivated without extracts), where the reference corresponding to 1 means 100% cell viability. The presented data are from three experiments, each performed in triplicate.

2.6. Cell Distribution within 3D-Printed Structure

Before the test, the cells were fixed and counterstained. The 4% formaldehyde (Penta chemicals, Prague, Czech Republic) was used to fix the cells within the suspension. After 15 min of exposure, the cell suspension was centrifugated (1.5 RPM for 2 min) and supernatant was aspirated. Then, the cells were washed with PBS, and after centrifugation (1.5 RPM for 2 min), 0.5% Triton x-100 (Merck Group, Darmstadt, Germany) was added for 5 min followed by centrifugation and three washes with PBS. Then, the cells nuclei were counterstained by Hoechst 3325 (λ_{ex} = 355 nm, λ_{em} = 465 nm) and the cytoskeleton was counterstained by ActinRed 555 (λ_{ex} = 540 nm and λ_{em} = 665 nm) according to the protocol of the producer (both Sigma Aldrich). The stained fibroblasts were mixed with hydrogel in concentration of $5{\cdot}10^5$ cells per 1 mL of hydrogel. These mixtures were printed (using the same procedure as describe before) and observed by the means of confocal microscopy using an Olympus FLUOVIEW FV3000 (Olympus corporation, Laser Scanning

Confocal Microscope (LSCM) in order to determine the homogeneity of cells distribution. The Plan-Apochromat objective with magnification 10× and numerical aperture NA = 0.8 or 4× and NA = 0.4, respectively, were used for analysis. The figures were obtained as three-dimensional reconstruction from confocal images in the z-axis (4× magnification—10 images with 10 µm steps, 10× magnification—10 images with 5 µm steps).

3. Results and Discussion

3.1. Polysaccharide Oxidation and Hydrogel Formation

In order to develop printable hydrogels as potential bioinks based on a chemically cross-linked polymeric matrix, modified Dex and Gels were utilized. Bovine, rabbit, and chicken gelatines, hydrolyzed forms of collagens, were chosen in order to achieve close resemblance of the scaffold to extracellular matrix [43], thus maximizing the potential to produce material which may ensure sufficient viability, adhesion, and proliferation of fibroblasts [44]. Note that the source of gelatine and method of its preparation affect the ultimate mechanical and functional properties of final hydrogels [45], and consequently, the present study shall facilitate comparison of these Gel sources as a matrix of printable hydrogel.

Oxidized dextran (Dex-Ox) was used as a cross-linking agent so that high-energy light irradiation, toxic chemicals [46–48], or free radicals formation [29] was avoided. Initially, Dex was oxidized by sodium periodate [40,49], forming Dex-Ox with approximately 50 aldehyde groups per 100 units of the biopolymer chain. Comparing the ^{1}H NMR spectrum of unmodified Dex to the spectrum of Dex-Ox (see Figure S1 in Supplement), in ^{1}H NMR of Dex-Ox, several characteristic peaks were observed in the region of 6.0–4.4 ppm. These signals, which were assigned to protons of hemiacetals formed from aldehyde groups, confirmed the successful oxidation of Dex [40]. Subsequently, the hydrogels were obtained when Gels of bovine, rabbit, or chicken origin were chemically cross-linked by Dex-Ox, expecting Schiff base formation between Dex-Ox and amino groups present in Gel [50], as presented in Figure 1. The chosen manner of hydrogel preparation is characterized by mild conditions, avoiding the presence of harmful chemicals or radiation, which could be favorable for the intended application with respect to cell compatibility and viability.

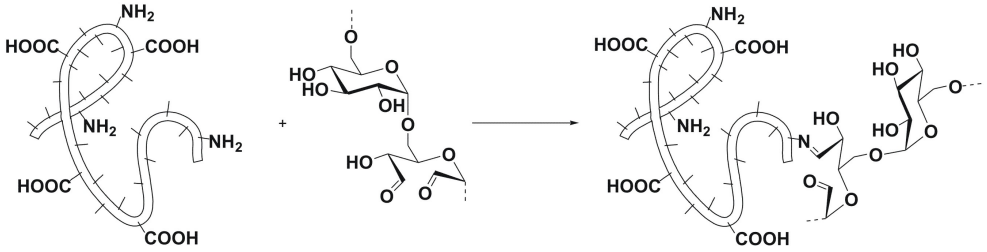

Figure 1. Schematic illustration of the cross-linking reaction between Dex-Ox and Gel.

3.2. Reaction Kinetics

Rheological experiments were designed to determine the kinetics of cross-linking reaction of Gels with Dex-Ox and a time of sol–gel transition, i.e., gelation point. A basic kinetics model of the first order was employed to fit the experimental rheological data and determine the reaction rates in order to facilitate reasonable kinetic data comparison (details of the data processing procedure are given in Supplementary Information). Table 1 summarizes the evaluated reaction rate coefficients together with the corresponding coefficients of determination. As can be seen, the reaction rates of a cross-linking reaction of Gel-B and Gel-R with Dex-Ox are similar; all were found to be in the range of 7–12 h^{-1}. In contrast, the cross-linking reaction of Gel-C was significantly slower with reaction rates in the range of 1.0–2.5 h^{-1}. The differences in reaction rates between Gel-B and Gel-R versus Gel-C can be most probably attributed to the different manufacturing procedures of the gelatines and resulting different properties of the used protein material. The rate coefficients show that conversion of cross-linking reaction equal to 75% is achieved in a time shorter than 10 min in case of Gel-B and Gel-R, while it took more than 30 min to

reach this conversion in case of Gel-C. From a practical point of view, it is advantageous to print the hydrogel after reaching such conversion of cross-linking reaction in order to ensure the relatively stable properties of ink during printing.

Table 1. Dependence of reaction rate coefficient on reaction mixture composition

Gel:Dex-Ox Solution Ratio	Reaction Rate Coefficient (h^{-1})	Coefficient of Determination (1)	Gelation Point (min)
	Gel-B		
1:1	11.6	0.998	<1
2:1	8.3	0.990	2
3:1	10.6	0.986	2
	Gel-R		
1:1	11.1	0.993	<1
2:1	7.6	0.994	2
3:1	8.7	0.990	2.5
	Gel-C		
1:1	2.0	0.997	2
2:1	1.2	0.999	13
3:1	2.4	0.994	>30

We should note that in some cases, a short initial "lag" period was observed. This lag period can be attributed to the cross-linking reaction complexity. Despite this not being described by a first-order kinetic model, the overall fit was good, as is documented by the values of coefficients of determination and similar values of reaction rate coefficients of each type of Gel. As a result, even a simple model of the first order was able to acceptably describe the course of this reaction.

Another significant characteristic obtained in this measurement is the gelation point, which describes the solidification of the material and therefore can be found as the time when the crossing of storage and loss moduli occurs [51]. From that point, elastic forces begin to overcome the viscous ones, and the substance is defined as solid. The gelation point was not recorded in case of 1:1 polymer solution ratio for neither Gel-B nor Gel-R-based hydrogel (see Table 1) as the storage modulus is higher than the loss modulus; therefore, it is safe to assume that it is lower than 1 min, and gelation took place during the sample preparation. In case of Gel-C, the gelation point was detected after 2 min of reaction. When the proportion of Gel was increased, the gelation point increased as well to approximately 2 min. Curiously, no difference was detected between the Gel-B:Dex 2:1 and 3:1 solution ratios. However, Gel-R exhibits an additional 30 s increase in gelation time with each decrease of Dex-Ox content. Gel-C based gels exhibit the highest increase in gelation time. Despite this, all of the hydrogels solidify within 1 hour, which is rapid enough for their utilization in practice.

3.3. Rheology

Knowledge of hydrogels' rheological behavior is of great importance in terms of printability and shape fidelity [52]. Cell viability can be ensured by minimizing the shear stress arising from the process [12]. A typical means of achieving this goal is to utilize a wider flow geometry [11]. However, this approach directly opposes precise positioning of the materials, which is the great advantage of 3D printing. Another way to reduce the shear stress during an ink flow is to reduce the viscosity [52]. However, during printing, a material with high viscosity and a significant difference between the loss and storage moduli is desirable due to the quickly achievable solid state. Other characteristics, such as brittleness of the extruded strand, also play an important role in the final appearance of the printed structure [42,52]. The above-mentioned requirements regarding the rheological behavior of gels indicate that the objectives of this work are to prepare a highly shear-thinning material with a fast sol–gel transition at various angular frequencies. For this

purpose, the rheological properties of fully cross-linked hydrogels were characterized in the region of increasing angular frequency, simulating 3D-printing conditions.

To this end, the linear viscoelastic region (LVE) on a fully formed gel-like structure was checked at 35 °C. Thus, strain sweep oscillatory measurements were performed with a constant angular frequency of 10 rad·s^{-1} for Gel:Dex-Ox 1:1 and 3:1 hydrogels (see Supplementary Information Figure S2). The LVE region was identified in the range where modulus G′ or G″ is independent of the applied deformation from 0.1% to 100%. Thus, 10% deformation was used for the following frequency sweep oscillatory measurements. It is clear that besides Gel-R:Dex-Ox 3:1 and Gel-B:Dex-Ox 3:1, the storage modulus, G′, is the significant one describing a gel-like state.

This fact is also followed in the case of performed frequency sweep oscillatory measurements describing loss and storage modulus dependence on printing speed expressed by angular frequency. As can be seen in Figure 2, a strong shear-thinning behavior of the prepared hydrogels is observed. In case of all Gel-C:Dex-Ox solutions, the highest viscosities are reached as well as gel-like structure. It is clear that Gel-R:Dex-Ox solutions reach the lowest viscosity values. Moreover, in case of Gel-R:Dex-Ox 2:1; 3:1, and Gel-B:Dex-Ox 3:1 when the gelation point is taken into account, the sol-like structure is observed when complex viscosity is lower than 0.3 Pa·s. This means that the angular frequency at which the gelation point occurs depends on both Gel origin and biopolymer ratio. It should be mentioned that reverse measurements (from 10 to 0.1 rad·s^{-1}) performed on the same sample achieved identical results as in the original measurements. Thus, any changes occurring in the material are reversible, even though such behavior is atypical in chemical hydrogels. Nevertheless, Khorsidi et al. [53] have found a growing number of amine-aldehyde cross-links to correlate with the increased shear-thinning character of hydrogels. Another research found that similar material compositions to the ones examined in the current study can be printed by microextrusion; therefore, a certain level of shear-thinning behavior can be assumed [54].

This described rheological characterization proves that the prepared hydrogels are suitable materials for 3D printing by microextrusion due to their shear flow and stability after stress relaxation. Based on experiments performed from prepared hydrogels composed of different gels and biopolymer ratios, it should be noted that these materials can be used in a variety of applications for 3D printing with specific rheological properties.

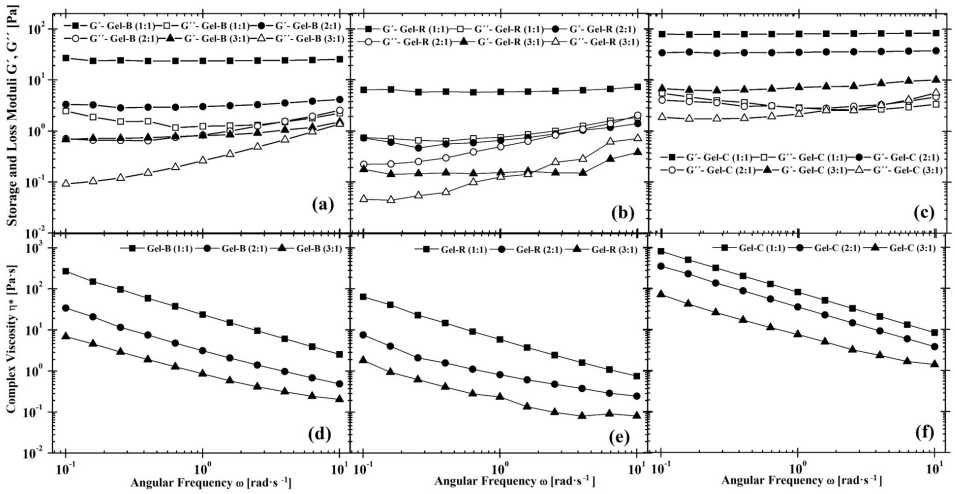

Figure 2. The angular frequency-dependent viscoelastic moduli (**a–c**) and complex viscosity (**d–f**) for Gel-based hydrogels: (**a**,**d**) Gel-B, (**b**,**e**) Gel-R, and (**c**,**f**) Gel-C for all examined Gel:Dex-Ox ratios.

3.4. 3D Printing

Printability of the materials was practically assessed in microextrusion printing experiments. Two contributions to printing precision were measured—die swell and shape

fidelity. Die swell is a parameter that affects the printing resolution, pore size, and layer height [14,55]. Several studies, both theoretical and experimental, have confirmed the significance of the phenomenon on the process of 3D printing [33,56–61]. Nevertheless, it is often omitted in the research of biopolymer based hydrogels as materials for microextrusion.

As is apparent from Table 2, all hydrogels examined in the current study experience a non-negligible die swell, reaching up to 3.3 times increase of the strand diameter. That is a clear indication of significant normal stress being built up in the material during shearing [14]. The die swell is notably lower in case of Gel-C:Dex-Ox 1:1 hydrogel. Some differences are found in the relative standard deviation (RSD) of die swell corresponding to different origins of Gel. The higher RSD suggests fluctuations in strand diameter, which are especially prominent in Gel-B-based materials and would consequently lead to lower printing precision. It can also indicate the phenomenon of over-gelation being present [42]. Based on this information, the highest printing precision is expected from Gel-C-based hydrogel. No significant difference caused by variation in Dex-Ox content was found, regardless of the Gel origin. It is possible that large fluctuations masked the influence of cross-linking agent amount on die swell.

The shape fidelity was characterized using the so-called printability (Pr) parameter, which was evaluated following a simple procedure described in [42]. This parameter reflects the precision of printing square-shaped pores. It is closely connected to the phenomenon of under- and over-gelation, and to a certain extend, it is able to describe the smoothness of the strand as well as hydrogel stability after removal of shear stress. The Pr values of most hydrogels are close to 1, as can be seen in Table 2, which encourages the possibility of using these materials for precise printing. Only Gel-B:Dex-Ox 3:1 exhibited insufficient mechanical strength of the strand, which caused the material to be completely fused and prevented the measurement. No significant difference in Pr with respect to neither Dex-Ox content nor Gel origin was observed.

Table 2. Printing characteristics of Gel-based hydrogels.

Gel:Dex-Ox Solution Ratio	Die Swell (1)	Relative Standard Deviation (RSD) of Die Swell (%)	Printability (Pr) (1)
	Gel-B		
1:1	3.0	13	1.0 ± 0.2
2:1	3.2	11	1.0 ± 0.2
3:1	3.0	14	/
	Gel-R		
1:1	2.9	10	0.90 ± 0.09
2:1	3.3	6	0.873 ± 0.009
3:1	3.2	10	0.90 ± 0.07
	Gel-C		
1:1	2.4	7	1.0 ± 0.1
2:1	2.6	9	1.0 ± 0.2
3:1	2.7	8	0.92 ± 0.09

Moreover, the printing of 5 layers of material proved that hydrogels presented in the current study provide self-supporting structures, i.e., those that do not collapse due to their own weight, in the 3D printing process. These structures were further used in the study of printing-induced porosity and hydrogel inner porosity.

To investigate the shape and pore distribution in the printed scaffold, the selected sample (Gel-C:Dex-Ox 1:1) was analyzed using CT (Figure 3). Due to the limited resolution of the CT used—SkyScan 1174 (6–30 µm per voxel), a special printing model was created for these purposes (Figure 3a left). In addition, it was necessary to create a special closed box for the hydrogel to prevent it from drying out during a 60-min CT scan (Figure 3a right). Figure 3b,c compares the scaffold in the hydrated state and after freeze drying. A

comparison of these figures shows that the shape of the printed structure corresponds to the desired model both in the hydrated and dry state. The hydrated structure is larger than the freeze-dried structure and does not contain pores inside printed layers, detectable air bubbles, or other large defects. The printed hydrogel occupies 59% of the volume (299 mm^3) with a surface area of 722 mm^2. After lyophilization, the volume of the printed structure decreases to 63 mm^3 (13% of space), while its surface increases to 1061 mm^2 due to the formation of open pores. The analyzed space was 11.1 × 11.1 × 4.1 mm^3 (505 mm^3). From X-ray adsorption images for two different angles (0° and 90°), it is clear that the printed material is accumulating in accordance with the printing model.

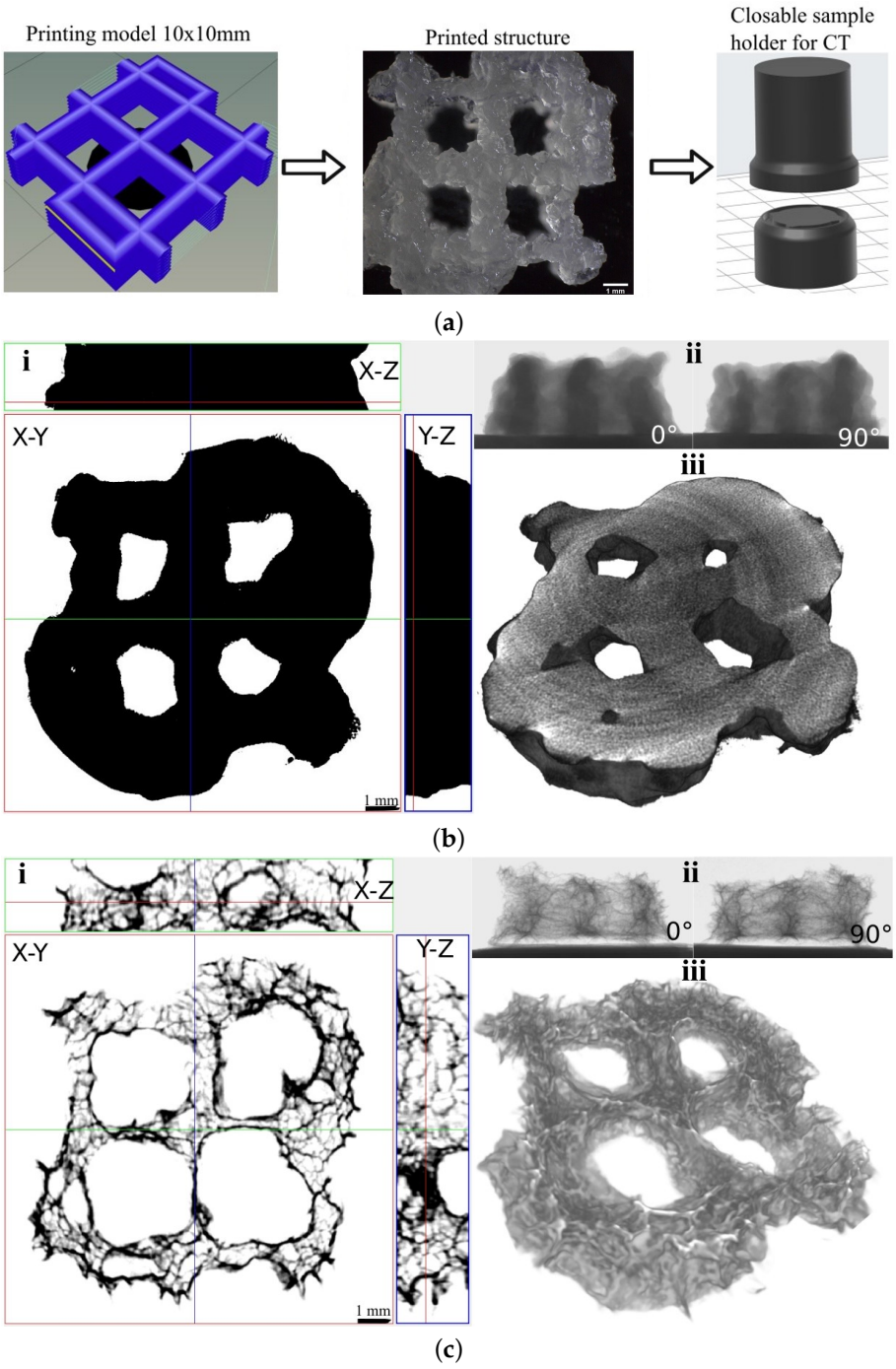

Figure 3. CT analysis of printed structures; (**a**) Scheme of sample preparation, (**b**) As-printed structure, (**c**) Lyophilized structure: **i**—2D cross-sections in respective planes, **ii**—X-ray adsorption for either 0° or 90°, and **iii**—3D model.

3.5. Swelling Tests

Swelling is defined as the amount of buffer or water bound into a hydrogel. It is considered to be a crucial characteristic of hydrogels, as it gives an initial view of their hydrophilicity and cross-linking density. In general, rigid networks lead to lower water uptake [62]. Moreover, the swelling characterization is useful in the hydrogel preparation procedure as an insight into the possibility of cell proliferation or to determine hydrogel stability over time. Figure 4 shows the equilibrium swelling of prepared hydrogels at different ratios of Gel and Dex-Ox. The only observed difference between used Gels is the speed of PBS uptake, being notably lower in the case of Gel-C in comparison. Meanwhile, both Gel-B and Gel-R displayed similar swelling behavior. These results could refer to different network rigidity. This assumption was supported by rheology results (see Figure 2). Statistical analysis of the swelling test results proved that the concentration of the cross-linking agent has a minimal impact on swelling, and the observed differences correspond to the measurement deviation. Thus, the mechanical characteristics and rheology of the prepared hydrogel can be tailored without any impact on swelling, which is advantageous in the case of the cell proliferation.

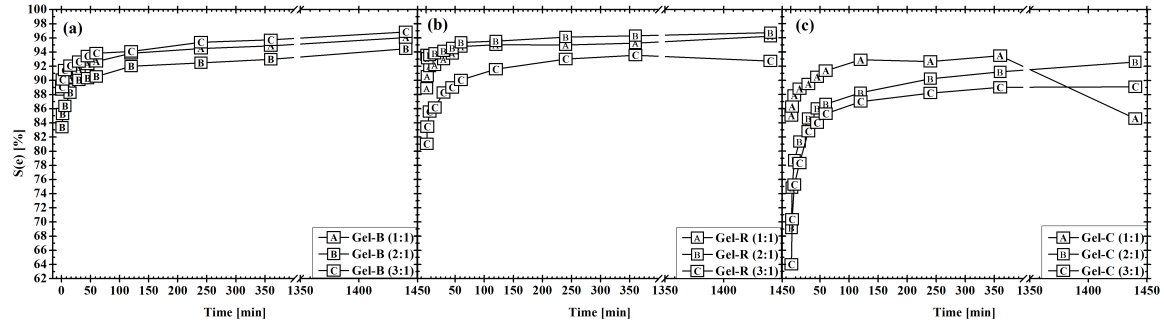

Figure 4. Swelling of Gel-based hydrogels: (**a**) Gel-B, (**b**) Gel-R, and (**c**) Gel-C.

3.6. Inner Porosity

SEM micrographs of the printed products after freeze drying revealed the highly porous inner structure of the materials. Table 3 presents the results of the average pore diameter in the cross-section. In addition, the relative pore area was determined in the cross-section in order to assess the porosity of the hydrogel. The pores are interconnected (see Supplementary Information Figure S2) and fall approximately in the range 50–100 µm in diameter [63]. The pore size remains practically constant regardless of both the Gel origin and the amount of Dex-Ox.

Table 3. Evaluation of pore size and porosity of hydrogels after shear strain and subsequent lyophylization.

Gel:Dex-Ox Solution Ratio	Average Pore Size (mm^2)	Relative Pore Area (%)
	Gel-B	
1:1	0.014 ± 0.009	40–70
2:1	0.017 ± 0.005	45–80
3:1	0.020 ± 0.009	60–75
	Gel-R	
1:1	0.017 ± 0.006	40–80
2:1	0.011 ± 0.003	35–65
3:1	0.009 ± 0.004	35–50
	Gel-C	
1:1	0.010 ± 0.004	35–45
2:1	0.036 ± 0.008	45–50
3:1	0.04 ± 0.02	30–50

3.7. Cytotoxicity

Due to their natural origin, the chosen biopolymers—Gel and Dex—are generally characterized by low toxicity [26,64–66], which makes them especially advantageous for scaffold preparation. However, the presence of highly reactive aldehyde groups raises the concerns over the biocompatibility of Dex-Ox [66,67]. Additionally, the cytotoxicity of Dex-Ox has been observed to increase with the decrease of M_w [68]. In order to address this issue, the cytotoxicity of the here-prepared hydrogels was tested. Samples with the highest amount of potentially cytotoxic component, i.e., those with a solution ratio of 1:1, were chosen for the test. The results are presented in Figure 5. As can be seen, Gel-B and Gel-C were non-cytotoxic in a whole range of concentrations. A non-significant decrease in cell viability in observed in the case of Gel-R for a concentration of extract above 50%. However, the viability does not decrease below 70%, which is the limit of cytotoxicity potential. It can be concluded that all tested hydrogels do not express cytotoxicity potential. These results are highly encouraging in terms of using the proposed hydrogels, especially Gel-B and Gel-C-based ones, as bioinks for the preparation of scaffolds.

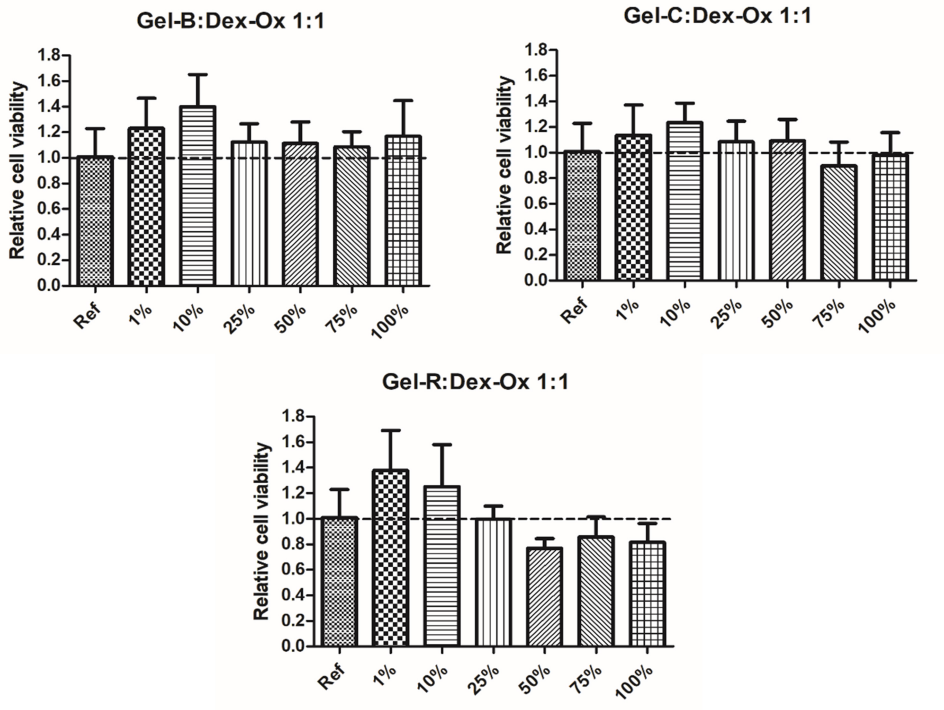

Figure 5. Cell viability determined by ATP assay performed on extracts from Gel:Dex-Ox 1:1 hydrogels.

3.8. Cell Distribution within 3D-Printed Structure Evaluation

The homogeneity of cell distribution within the structure of scaffolds is a critical parameter for their applicability. This parameter is not ideal in case of the standard procedure of cell seeding into the scaffolds (e.g., by forcing the cells through a scaffold by either internal pressure or external vacuum pressure). The direct printing of cells within the material allows overcoming this problem. Thus, the effect of microextrusion on mouse fibroblasts distribution was observed by the means of LSCM. As can be seen in Figure 6, 3D printing ensured a homogeneous distribution of cells within the printed material. In addition, the overlay (Figure 6) demonstrated that cell nuclei were located inside undisturbed cells; thus, fibroblasts were not destroyed during 3D printing. The results are promising in terms of considering the presented biopolymers-based hydrogels as bioinks.

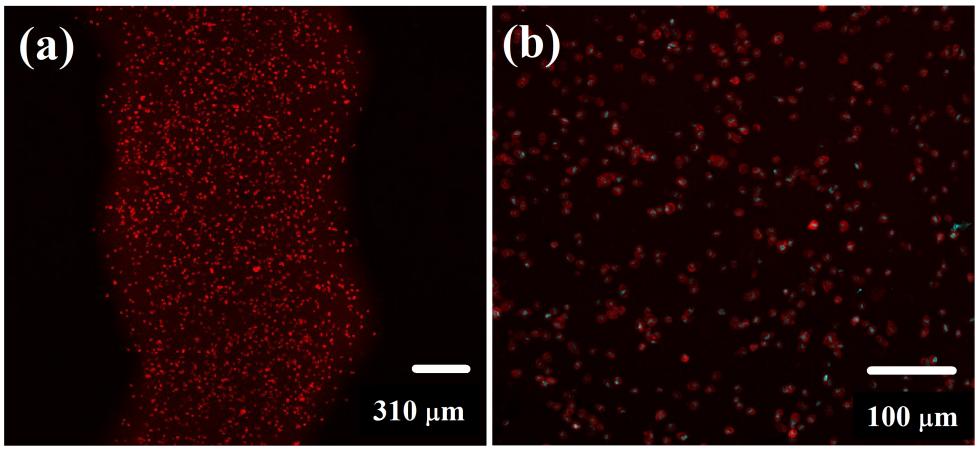

Figure 6. Microextruded Gel-B:Dex-Ox strand with incorporated mouse fibroblasts observed by the means of fluorescence confocal microscopy—(**a**) 4× magnification—image of cytoskeleton and (**b**) 10× magnification—overlay of cell nuclei and cytoskeleton images.

4. Conclusions

A series of hydrogels, which may potentially serve as bioinks, formed from Gel of different origin (bovine, rabbit, and chicken) cross-linked with various ratios of Dex-Ox were prepared by means of a simple and rapid method. Even though there are differences in Gel behavior depending on its origin, 3D-printing studies usually focus on bovine or porcine Gel, while research of rabbit and chicken Gel is rather scarce in this field. Study of the rheological behavior of the materials upon application of shear stress proved that the all investigated hydrogels were able to flow in shear, while they remain stable after stress relaxation and consequently are well suited for utilization in microextrusion. Additionally, die swell was significant, reaching a threefold increase in strand diameter in case of Gel-R and Gel-B samples. From the printing precision point of view, Gel-C was the most promising with the lowest die swell. Measurements confirmed that the complex viscosity of the hydrogels increased with the higher amount of cross-linking agent—Dex-Ox. In addition, rheology facilitated the study of reaction kinetics. This confirmed that the cross-linking reaction followed kinetics of the first order, and the gelation point was reached later as the amount of Dex-Ox solution decreased.

All the investigated hydrogels were able to form self-supporting structures in several layers, despite their various rheological properties. Moreover, the CT analysis confirmed that it is possible to produce constructs with continuous macroscopic pores throughout the structure via microextrusion processing of the hydrogels. In addition, the constructs remained stable even after freeze drying, and their highly porous inner structure was proved by means of CT and SEM measurements.

Optical imaging revealed that fluorescent-labeled mouse fibroblasts encapsulated within the polymeric matrix were of uniform distribution throughout the printed materials, and no cell disruption was observed. Finally, the printed constructs displayed no cytotoxicity in case of all tested materials. Thus, 3D-printable hydrogels with a potential to serve as bioinks have been successfully developed in the current study.

Supplementary Materials: The following are available at https://www.mdpi.com/article/10.3390/polym1010391/s1, Figure S1: 1H NMR spektra of dextran (Dex) and dextran after oxidation (Dex-Ox), Figure S2: Linearity sweep for hydrogels with different amount of cross-linking agent, Figure S3: SEM micrograph of lyophilized hydrogels in cross section

Author Contributions: Conceptualization, L.M., E.A., L.V., J.P. and A.M. (Aleš Mráček); methodology, L.M., E.A., L.V., J.P., P.H., M.M., A.M. (Anotnín Minařík) and R.K.; validation, L.M., E.A., L.V., J.P., P.H., M.M., A.M. (Anotnín Minařík) and R.K.; formal analysis, L.M., E.A., L.V., J.P., P.H., M.K, A.M. (Anotnín Minařík) and R.K.; investigation, L.M., E.A., L.V., J.P., P.H., M.M., A.M. (Aleš Mráček) and

R.K.; writing—original draft preparation, L.M., J.P., E.A., P.H. and L.V.; writing—review and editing, L.M., J.P., E.A., L.V., A.M. (Aleš Mráček); visualization L.M., E.A., L.V., J.P., M.M., A.M. (Anotnín Minařík) and R.K.; supervision, A.M. (Aleš Mráček); project administration, A.M. (Aleš Mráček); funding acquisition, A.M. (Aleš Mráček). All authors have read and agreed to the published version of the manuscript.

Funding: The work of authors L.M., A.M. (Aleš Mráček), A.M. (Anotnín Minařík) and R.K. was financially supported by the Ministry of Education, Youth and Sports of the Czech republic—DKRVO (RP/CPS/2022/003). Author LV gratefully acknowledge the project OP RDE Junior Grants of TBU in Zlín, Reg. No. CZ.02.2.69/0.0/0.0/19_073/0016941. Authors EA and JP received financial supports from CEBIA-Tech Instrumentation (Project No. CZ.1.05/2.1.00/19.0376). Authors PH and MM thank the project funded by Czech Science Foundation (Project No. 20-28732S) and project funded by Ministry of Education, Youth and Sports of the Czech Republic – DKRVO (RP/CPS/2022/001).

Institutional Review Board Statement: Not applicable.

Informed Consent Statement: Not applicable.

Data Availability Statement: The data presented in this study are available on request from the corresponding author.

Conflicts of Interest: The authors declare no conflict of interest.

References

1. Wei, L.; Jovina, T.; Wai, Y.; May, W. Proof-of-concept: 3D bioprinting of pigmented human skin constructs. *Biofabrication* **2018**, *10*, 1758–5090. [CrossRef]
2. Billiet, T.; Vandenhaute, M.; Schelfhout, J.; Vlierberghe, S.V.; Dubruel, P. A review of trends and limitations in hydrogel-rapid prototyping for tissue engineering. *Biomaterials* **2012**, *33*, 6020–6041. [CrossRef] [PubMed]
3. Gopinathan, J.; Noh, I. Recent trends in bioinks for 3D printing. *Biomater. Res.* **2018**, *22*, 11. [CrossRef] [PubMed]
4. Ashammakhi, N.; Ahadian, S.; Xu, C.; Montazerian, H.; Ko, H.; Nasiri, R.; Barros, N.; Khademhosseini, A. Bioinks and bioprinting technologies to make heterogeneous and biomimetic tissue constructs. *Mater. Today Bio* **2019**, *1*, 100008. [CrossRef] [PubMed]
5. Gungor-Ozkerim, P.; Inci, I.; Zhang, Y.; Khademhosseini, S.; Dokmeci, M. Bioinks for 3D bioprinting: An overview. *Biomater. Sci.* **2018**, *6*, 915–946. [CrossRef] [PubMed]
6. Dorishetty, P.; Dutta, N.; Choudhury, N. Bioprintable tough hydrogels for tissue engineering applications. *Adv. Colloid Interface Sci.* **2020**, *281*, 102163. [CrossRef] [PubMed]
7. Chimene, D.; Kaunas, R.; Gaharwar, A. Hydrogel Bioink Reinforcement for Additive Manufacturing: A Focused Review of Emerging Strategies. *Adv. Mater.* **2020**, *32*, 1902026–1902048. [CrossRef]
8. Chung, S.H.; Son, S.; Min, J. The nanostructure effect on the adhesion and growth rates of epithelial cells with well-defined nanoporous alumina substrates. *Nanotechnology* **2010**, *21*, 125104. [CrossRef]
9. Ermis, M.; Antmen, E.; Hasirci, V. Micro and Nanofabrication methods to control cell-substrate interactions and cell behavior: A review from the tissue engineering perspective. *Bioact. Mater.* **2018**, *3*, 355–369. [CrossRef]
10. Buskermolen, A.; Suresh, H.; Shishvan, S.; Vigliotti, A.; DeSimone, A.; Kurniawan, N.; Bouten, C.; Deshpande, V. Entropic Forces Drive Cellular Contact Guidance. *Biophys. J.* **2019**, *116*, 1994–2008. [CrossRef]
11. Smith, C.; Stone, A.; Parkhill, R.; Stewart, R.; Simpkins, M.; Kachurin, A.; Warren, W.; Williams, S. Three-Dimensional BioAssembly Tool for Generating Viable Tissue-Engineered Constructs. *Tissue Eng.* **2004**, *10*, 1566–1576. [CrossRef]
12. Blaeser, A.; Campos, D.D.; Puster, U.; Richtering, W.; Stevens, M.; Fischer, H. Controlling Shear Stress in 3D Bioprinting is a Key Factor to Balance Printing Resolution and Stem Cell Integrity. *Adv. Healthc. Mater.* **2016**, *5*, 326–333. [CrossRef]
13. Hölzl, K.; Lin, S.; Tytgat, L.; Vlierberghe, S.V.; Gu, L.; Ovsianikov, A. Bioink properties before, during and after 3D bioprinting. *Biofabrication* **2016**, *8*, 032002–032020. [CrossRef]
14. Mackay, M. The importance of rheological behavior in the additive manufacturing technique material extrusion. *J. Rheol.* **2018**, *62*, 1549–1561. [CrossRef]
15. Mori, A.D.; Fernández, M.P.; Blunn, G.; Tozzi, G.; Roldo, M. 3D Printing and Electrospinning of Composite Hydrogels for Cartilage and Bone Tissue Engineering. *Polymers* **2018**, *10*, 285. [CrossRef] [PubMed]
16. Mazzocchi, A.; Devarasetty, M.; Huntwork, R.; Soker, S.; Skardal, A. Optimization of collagen type I-hyaluronan hybrid bioink for 3D bioprinted liver microenvironments. *Biofabrication* **2019**, *11*, 015003–015014. [CrossRef] [PubMed]
17. Caló, E.; Khutoryanskiy, V. Biomedical applications of hydrogels: A review of patents and commercial products. *Eur. Polym. J.* **2015**, *65*, 252–267. [CrossRef]
18. Gřundělová, L.; Gregorova, A.; Mráček, A.; Vícha, R.; Smolka, P.; Minařík, A. Viscoelastic and mechanical properties of hyaluronan films and hydrogels modified by carbodiimide. *Carbohydr. Polym.* **2015**, *119*, 142–148. [CrossRef]
19. Dababneh, A.; Ozbolat, I. Bioprinting Technology: A Current State-of-the-Art Review. *J. Manuf. Sci. Eng.* **2014**, *136*, 061016. [CrossRef]

20. Jungst, T.; Smolan, W.; Schacht, K.; Scheibel, T.; Groll, J. Strategies and Molecular Design Criteria for 3D Printable Hydrogels. *Chem. Rev.* **2016**, *116*, 1496–1539. [CrossRef]
21. Khunmanee, S.; Jeong, Y.; Park, H. Crosslinking method of hyaluronic-based hydrogel for biomedical applications. *J. Tissue Eng.* **2017**, *8*, 2041731417726464–2041731417726479. [CrossRef] [PubMed]
22. Musilová, L.; Mráček, A.; Kovalcik, A.; Smolka, P.; Minařík, A.; Humpolíček, P.; Vícha, R.; Ponížil, P. Hyaluronan hydrogels modified by glycinated Kraft lignin: Morphology, swelling, viscoelastic properties and biocompatibility. *Carbohydr. Polym.* **2018**, *181*, 394–403. [CrossRef] [PubMed]
23. Poldervaart, M.; Goversen, B.; de Ruijter, M.; Abbadessa, A.; Melchels, F.; Öner, F.; Dhert, W.; Vermonden, T.; Alblas, J.; Yamamoto, M. 3D bioprinting of methacrylated hyaluronic acid (MeHA) hydrogel with intrinsic osteogenicity. *PLoS ONE* **2017**, *12*, e0177628. [CrossRef]
24. Skardal, A.; Zhang, J.; McCoard, L.; Xu, X.; Oottamasathien, S.; Prestwich, G. Photocrosslinkable Hyaluronan-Gelatin Hydrogels for Two-Step Bioprinting. *Tissue Eng. Part A* **2010**, *16*, 2675–2685. [CrossRef] [PubMed]
25. Sakai, S.; Ohi, H.; Taya, M. Gelatin/Hyaluronic Acid Content in Hydrogels Obtained through Blue Light-Induced Gelation Affects Hydrogel Properties and Adipose Stem Cell Behaviors. *Biomolecules* **2019**, *9*, 342. [CrossRef]
26. Dobos, A.; Hoorick, J.V.; Steiger, W.; Gruber, P.; Markovic, M.; Andriotis, O.; Rohatschek, A.; Dubruel, P.; Thurner, P.; Vlierberghe, S.V.; et al. Thiol–Gelatin–Norbornene Bioink for Laser-Based High-Definition Bioprinting. *Adv. Healthc. Mater.* **2019**, *9*, 1900752–1900761. [CrossRef] [PubMed]
27. Noh, I.; Kim, N.; Tran, H.; Lee, J.; Lee, C. 3D printable hyaluronic acid-based hydrogel for its potential application as a bioink in tissue engineering. *Biomater. Res.* **2019**, *23*, 3. [CrossRef]
28. Mehrotra, S.; Melo, B.; Hirano, M.; Keung, W.; Li, R.; Mandal, B.; Shin, S. Nonmulberry Silk Based Ink for Fabricating Mechanically Robust Cardiac Patches and Endothelialized Myocardium-on-a-Chip Application. *Adv. Funct. Mater.* **2020**, *30*, 1907436. [CrossRef] [PubMed]
29. Petta, D.; Armiento, A.; Grijpma, D.; Alini, M.; Eglin, D.; D'Este, M. 3D bioprinting of a hyaluronan bioink through enzymatic-and visible light-crosslinking. *Biofabrication* **2018**, *10*, 044104–044114. [CrossRef] [PubMed]
30. Kajave, N.; Schmitt, T.; Nguyen, T.U.; Kishore, V. Dual crosslinking strategy to generate mechanically viable cell-laden printable constructs using methacrylated collagen bioinks. *Mater. Sci. Eng. C* **2020**, *107*, 110290–110301. [CrossRef]
31. Yu, J.H.; Fridrikh, S.V.; Rutledge, G.C. The role of elasticity in the formation of electrospun fibers. *Polymer* **2006**, *47*, 4789–4797. [CrossRef]
32. Angel Martinez-Ortiz, M.; Delia Hernandez-Fuentes, A.; Pimentel-Gonzalez, D.J.; Campos-Montiel, R.G.; Vargas-Torres, A.; Aguirre-Alvarez, G. Extraction and characterization of collagen from rabbit skin: partial characterization. *CYTA-J. Food* **2015**, *13*, 253–258. [CrossRef]
33. Yousefi, A.M.; Smucker, B.; Naber, A.; Wyrick, C.; Shaw, C.; Bennett, K.; Szekely, S.; Focke, C.; Wood, K. Controlling the extrudate swell in melt extrusion additive manufacturing of 3D scaffolds: A designed experiment. *J. Biomater. Sci.* **2017**, *29*, 195–216. [CrossRef]
34. Tanner, R. A theory of die-swell. *J. Polym. Sci. Part A-2 Polym. Phys.* **1970**, *8*, 2067–2078. [CrossRef]
35. Emmermacher, J.; Spura, D.; Cziommer, J.; Kilian, D.; Wollborn, T.; Fritsching, U.; Steingroewer, J.; Walther, T.; Gelinsky, M.; Lode, A. Engineering considerations on extrusion-based bioprinting: interactions of material behavior, mechanical forces and cells in the printing needle. *Biofabrication* **2020**, *12*, 025022. [CrossRef] [PubMed]
36. Ning, L.; Yang, B.; Mohabatpour, F.; Betancourt, N.; Sarker, M.; Papagerakis, P.; Chen, X. Process-induced cell damage: Pneumatic versus screw-driven bioprinting. *Biofabrication* **2020**, *12*, 025011. [CrossRef] [PubMed]
37. Mokrejš, P.; Gál, R.; Mrázek, P. Biotechnology-Based Production of Food Gelatine from Poultry by-Products. Patent number: CZ 307665, 16 May 2019.
38. Mokrejš, P.; Mrázek, P.; Robert, R.G.; Pavlačková, J. Biotechnological Preparation of Gelatines from Chicken Feet. *Polymers* **2019**, *11*, 1060. [CrossRef]
39. Gál, R.; Mokrejš, P.; Mrázek, P.; Pavlačková, J.; Janáčová, D.; Orsavová, J. Chicken Heads as a Promising By-Product for Preparation of Food Gelatins. *Molecules* **2020**, *25*, 494. [CrossRef]
40. Maia, J.; Carvalho, R.; Coelho, J.; Simoes, P.; Gil, M. Insight on the Periodate Oxidation of Dextran and Its Structural Vicissitudes. *Polymer* **2011**, *52*, 258–265. [CrossRef]
41. Zhao, H.; Heindel, N. Determination of Degree of Substitution of Formyl Groups in Polyaldehyde Dextran by the Hydroxylamine Hydrochloride Method. *Pharm. Res.* **1991**, *8*, 400–402. [CrossRef]
42. Ouyang, L.; Yao, R.; Zhao, Y.; Sun, W. Effect of bioink properties on printability and cell viability for 3D bioplotting of embryonic stem cells. *Biofabrication* **2016**, *8*, 035020–035033. [CrossRef] [PubMed]
43. Chattopadhyay, S.; Raines, R. Collagen-based biomaterilas for wound healing. *Biopolymers* **2014**, *8*, 821–830. [CrossRef] [PubMed]
44. Eisenbarth, E. Biomaterials for Tissue Engineering. *Adv. Eng. Mater.* **2007**, *9*, 1051–1060. [CrossRef]
45. Young, A.T.; White, O.C.; Daniele, M.A. Rheological Properties of Coordinated Physical Gelation and Chemical Crosslinking in Gelatin Methacryloyl (GelMA) Hydrogels. *Macromol. Biosci.* **2020**, *20*, 2000183. [CrossRef] [PubMed]
46. Draye, J.P.; Delaey, B.; de Voorde, A.V.; Bulcke, A.V.D.; Reu, B.D.; Schacht, E. In vitro and in vivo biocompatibility of dextran dialdehyde cross-linked gelatin hydrogel films. *Biomaterials* **1998**, *19*, 1677–1687. [CrossRef]

47. Balakrishnan, B.; Jayakrishnan, A. Self-cross-linking biopolymers as injectable in situ forming biodegradable scaffolds. *Biomaterials* **2005**, *26*, 3941–3951. [CrossRef]
48. Kristiansen, K.; Potthast, A.; Christensen, B. Periodate oxidation of polysaccharides for modification of chemical and physical properties. *Carbohydr. Res.* **2010**, *345*, 1264–1271. [CrossRef] [PubMed]
49. Liu, Z.; Li, Y.; Li, W.; Lian, W.; Kemell, M.; Hietala, S.; Figueiredo, P.; Li, L.; Mäkilä, E.; Ma, M.; et al. Close-loop dynamic nanohybrids on collagen-ark with in situ gelling transformation capability for biomimetic stage-specific diabetic wound healing. *Mater. Horiz.* **2019**, *6*, 385–393. [CrossRef]
50. Nonsuwan, P.; Matsugami, A.; Hayashi, F.; Hyon, S.H.; Matsumura, K. Controlling the degradation of an oxidized dextran-based hydrogel independent of the mechanical properties. *Carbohydr. Polym.* **2019**, *204*, 131–141. [CrossRef]
51. Winter, H. Chapter Physical and Chemical Gelation. In *Encyclopedia of Materials: Science and Technology*; Elsevier: Amsterdam, The Netherlands, 2001.
52. Wu, D.; Yu, Y.; Tan, J.; Huang, L.; Luo, B.; Lu, L.; Zhou, C. 3D bioprinting of gellan gum and poly (ethylene glycol) diacrylate based hydrogels to produce human-scale constructs with high-fidelity. *Mater. Des.* **2018**, *160*, 486–495. [CrossRef]
53. Khorshidi, S.; Karkhaneh, A.; Bonakdar, S.; Omidian, M. High-strength functionalized pectin/fibroin hydrogel with tunable properties: A structure–property relationship study. *J. Appl. Polym. Sci.* **2019**, *137*, 48859–48872. [CrossRef]
54. Zehnder, T.; Freund, T.; Demir, M.; Detsch, R.; Boccaccini, A. Fabrication of Cell-Loaded Two-Phase 3D Constructs for Tissue Engineering. *Materials* **2016**, *9*, 887. [CrossRef]
55. McIlroy, C.; Olmsted, P. Deformation of an amorphous polymer during the fused-filament-fabrication method for additive manufacturing. *J. Rheol.* **2017**, *61*, 379–397. [CrossRef]
56. Comminal, R.; Serdeczny, M.; Pedersen, D.; Spangenberg, J. Numerical modeling of the strand deposition flow in extrusion-based additive manufacturing. *Addit. Manuf.* **2018**, *20*, 68–76. [CrossRef]
57. Serdeczny, M.; Comminal, R.; Pedersen, D.; Spangenberg, J. Experimental validation of a numerical model for the strand shape in material extrusion additive manufacturing. *Addit. Manuf.* **2018**, *24*, 145–153. [CrossRef]
58. Xia, H.; Lu, J.; Tryggvason, G. A numerical study of the effect of viscoelastic stresses in fused filament fabrication. *Comput. Methods Appl. Mech. Eng.* **2019**, *346*, 242–259. [CrossRef]
59. Hebda, M.; McIlroy, C.; Whiteside, B.; Caton-Rose, F.; Coates, P. A method for predicting geometric characteristics of polymer deposition during fused-filament-fabrication. *Addit. Manuf.* **2019**, *27*, 99–108. [CrossRef]
60. Coogan, T.; Kazmer, D. Modeling of interlayer contact and contact pressure during fused filament fabrication. *J. Rheol.* **2019**, *63*, 655–672. [CrossRef]
61. Gopi, S.; Kontopoulou, M. Investigation of thermoplastic melt flow and dimensionless groups in 3D bioplotting. *Rheol. Acta* **2020**, *59*, 83–93. [CrossRef]
62. Ahmed, E. Hydrogel: Preparation, characterization, and applications. *J. Adv. Res.* **2015**, *6*, 105–121. [CrossRef]
63. Trautmann, A.; Rüth, M.; Lemke, H.D.; Walther, T.; Hellmann, R. Two-photon polymerization based large scaffolds for adhesion and proliferation studies of human primary fibroblasts. *Opt. Laser Technol.* **2018**, *106*, 474–480. [CrossRef]
64. Choksakulnimitr, S.; Masuda, S.; Tokuda, H.; Takakura, Y.; Hashida, M. In vitro cytotoxicity of macromolecules in different cell culture systems. *J. Control. Release* **1995**, *34*, 233–241. [CrossRef]
65. Groot, C.D.; Luyn, M.V.; Dijk-Wolthuis, W.V.; Cadee, J.; Plantinga, J.; Otter, W.D.; Hennink, W. In vitro biocompatibility of biodegradable dextran-based hydrogels tested with human fibroblasts. *Biomaterials* **2001**, *22*, 1197–1203. [CrossRef]
66. Poursamar, S.; Hatami, J.; Lehner, A.; da Silva, C.; Ferreira, F.; Antunes, A. Gelatin porous scaffolds fabricated using a modified gas foaming technique: Characterisation and cytotoxicity assessment. *Mater. Sci. Eng. C* **2015**, *48*, 63–70. [CrossRef] [PubMed]
67. Pronina, E.; Vorotnikov, Y.; Pozmogova, T.; Solovieva, A.; Miroshnichenko, S.; Plyusnin, P.; Pishchur, D.; Eltsov, I.; Edeleva, M.; Efremova, M.S.O. No Catalyst Added Hydrogen Peroxide Oxidation of Dextran: An Environmentally Friendly Route to Multifunctional Polymers. *ACS Sustain. Chem. Eng.* **2020**, *8*, 5371–5379. [CrossRef]
68. Artzi, N.; Shazly, T.; Crespo, C.; Ramos, A.; Chenault, H.; Edelman, E. Characterization of Star Adhesive Sealants Based on PEG/Dextran Hydrogels. *Macromol. Biosci.* **2009**, *9*, 754–765. [CrossRef]